CHEMICAL AND ISOTOPIC STUDIES OF DECCAN TRAPS DIKES (INDIA) AND LOUISVILLE SEAMOUNTS (SOUTH PACIFIC): ASPECTS OF THE YOUTH AND MATURITY OF HOTSPOTS

A DISSERTATION SUBMITTED TO THE GRADUATE DIVISION OF THE UNIVERSITY OF HAWAI'I IN PARTIAL FULFILLMENT OF THE REQUIREMENTS FOR THE DEGREE OF

DOCTOR OF PHILOSOPHY

IN

GEOLOGY AND GEOPHYSICS

DECEMBER 2008

By
Loÿc Vanderkluysen

Dissertation Committee:

John J. Mahoney, Chairperson
Garrett Apuzen-Ito
Stephen J. Martel
Douglas G. Pyle
Yuan-Hui Li

We certify that we have read this dissertation and that, in our opinion, it is satisfactory in scope and quality as a dissertation for the degree of Doctor of Philosophy in Geology and Geophysics.

DISSERTATION COMMITTEE

_____
Chairperson

_____

_____

_____

_____

DEDICATION

To Stéphanie, without whom I would never have worked on the Deccan Traps.

ACKNOWLEDGMENTS

It was as a young geology undergraduate, around 1997, that I became fascinated by large igneous provinces and began fostering the dream to one day work on the Deccan Traps, a dream that I never thought would one day become reality. That is, until June 13, 2003. On that day, during a late night of work in my office at the University of Lausanne, I received an e-mail from John Mahoney regarding the possibility of working on the famed volcanic province. I turned to a friend for advice, and she confirmed my gut-feeling: "it's a no-brainer", she said; and this is how it started. Her name was Stéphanie Chemin, former mineralogy student turned igneous petrologist, coworker, and friend, whom I miss dearly. She can never be thanked enough.

As with any Ph.D. research, this work proved to be more than a single man can chew; thankfully, I was not alone in this endeavor and my thanks go to all who provided time, help, comments and support. John Mahoney, chairman of my committee, is where all begins and ends. I thank him for being a mentor, relentless editor of manuscripts, and purveyor of guidance, ideas, advice, and funds. He got me to work on the Deccan Traps and supported a season of field work, fulfilling a decade-long dream, for which I am ever grateful. My gratitude is extended to Jean Hernandez, my mentor in Lausanne, who inspired me to enter the field of igneous geochemistry and petrology.

To Doug Pyle goes an enormous mahalo, for his patience, understanding, for training me in lab techniques and practices and for providing advice and counsel every step of the way. The ultimate problem-solver, Doug went above and beyond the call of duty, for which he needs to be thanked a hundred times over. I thank Steve Martel for providing help and insights in interpreting dike patterns in the Deccan, Garrett Ito for his comments and suggestions regarding, in particular, the Louisville hotspot and mantle melting in plume environments, and Telu Li for teaching me a thing or two about multivariate statistical analyses.

This work would not have been possible without those who shared their samples and analyses: Peter Hooper, and through him John Beane and K. V. Subbarao, whose collection of dike samples and analyses offered solid foundations to chapter 2, and whose comments and advice helped tremendously; Hetu Sheth, who sampled many of the Narmada-Tapi dikes and whose expertise of the Deccan was invaluable; Leo Melluso, who shared samples from the Nandurbar area and was ever-opened to discussion; and Mike Widdowson, who provided us with his Goan dike samples. Hetu is thanked doubly for taking me under his wing during my trip to India, as are those who shared my life for those few weeks atop the Deccan plateau: Jyotirmoy Mallik, Ranjini Ray, Avanti Shirke, Raymond Duraiswami and our unfaltering pilot, Deepak Gosain. I also wish to show my appreciation to those who shared my life at sea during the 42 days of cruise AMAT02RR, who made the trip a life-changing experience and ensured our safe return: Peter Lonsdale, indefatigable chief-scientist and bottomless well of knowledge; Anthony Koppers, endless supplier of good counsel (and good humor, and wit); fellow science party members Jeff Gee and Barry Eakins, for making the expedition a success; Ron Comer

and Jim Dorrance, for getting us samples; and Captain Dave Murline and the cooks, technicians, mates, seamen and engineers on the R.V. *Revelle*.

I extend my gratitude to all who shared the expertise and knowledge of analytical procedures: Denys VonderHaar first and foremost, who often knew how to get me out of trouble; Ken Rubin, for his help with U-Th separation procedures; Kent Ross, John Sinton, Eric Hellebrand and Chuck Fraley at the XRF; Greg Ravizza at the Element2; and Eric De Carlo at the Quadrupole. My appreciation goes to my fellow lab rats, Chris Russo, Iris van der Zander, Eric Bergmanis, Bill Chazey, Georg Zellmer and Rhea Workman (to name a few), whose presence in the clean lab kept me from surrendering to insanity. Stephanie Ingle and Mike Garcia deserve special mention for providing helpful comments and ideas regarding aspects of hotspot geochemistry.

Finally, my deepest thanks go to my friends, classmates, officemates, too numerous to name, and family who supported and aided me in all possible manners. I am particularly grateful to my parents, who compiled and verified the bibliography and spellchecked large sections of the text, Meryl McDowell who drew some of the figures and helped me where my foreign knowledge of the English language failed me, and my brother who knows a thing or two about graphic design. I thank Eric Mittelstaedt and Todd Bianco for showing such enthusiasm about my research, Rebecca Carey for being my partner in crime, and finally fellow expatriates Alain Volentik and Martin Jutzeler, who know how to raise my spirit when no one else can.

The US National Science Foundation supported this research through grants EAR02-29824 and OCE04-52127. I also wish to thank the University of Hawai‘i Graduate Students Organization, which supported travel to attend the IAVCEI general assembly in Iceland.

ABSTRACT

The source of intraplate volcanism is commonly postulated to be melting anomalies, referred to as hotspots, relatively fixed in the Earth's mantle and fed by deep-seated thermal plumes. In plume models, flood basalts are thought to form when a rising mantle plume-head breaches the lithosphere, and age-progressive volcanic chains represent the trace of these mantle plume "tails" as lithospheric plates move over the melting anomaly. In this dissertation, I studied both aspects: the Deccan Traps (India), representing volcanism related to a plume-head, and the Louisville Seamount Chain (Southwest Pacific) tracking plume-tail activity, to gain insights into aspects of hotspot initiation and maturity.

The Deccan Traps of India is one of the Earth's largest flood basalt province. Using elemental and Pb-Nd-Sr isotope characteristics, feeder dikes for Deccan flow formations were identified and dike strikes were measured to inferred tectonic conditions at the time of their emplacement. Lower and middle lava formations were fed by E-W or N-S striking dikes. Feeder dikes for upper lava formations displayed no clear preferred strike. The absence of a preferred dike orientation for the voluminous upper formation lavas favors a plume-head origin for the Deccan Traps.

The Louisville Seamount Chain is the second longest hotspot track in the Pacific. This geochemical study was undertaken to characterize the mantle source evolution of a hotspot that has been active for ~80 Myr and compare those findings with generic models of hotspot volcanism. I focused on lavas dredged from scarps and steep slopes of seamounts along the chain between 72 Ma and 24 Ma. I found little evidence of chemical

variations that would be caused by mantle source heterogeneity. In fact, age-corrected Sr, Nd and Pb isotope ratios are extraordinarily homogeneous. The small variations that do exist, do not correlate with the age of the seamounts, degree of partial melting or age of the lithosphere at the time of seamount emplacement.

TABLE OF CONTENTS

Acknowledgements…… iv
Abstract…… vi
List of Tables…… x
List of Figures…… xi
Chapter 1: Introduction…… 1
The Deccan Traps…… 4
Geography and physical features…… 4
Stratigraphy and origin of isotopic variability…… 8
Age of the Deccan Traps…… 9
The Louisville Seamount Chain……11
Analytical methods…… 13
XRF……14
ICP-MS…… 14
Isotopic analyses…… 16
Chapter 2: Geochemical signatures of Deccan Traps (India) dikes: implications for the evolution of the flood basalt province and feeder system…… 17
Introduction……17
Background……20
The timing of lithospheric extension…… 26
Samples and methods…… 28
Samples and definition of dike swarms…… 28
Chemical and isotopic analyses…… 31
Data evaluation procedures and statistical methods…… 32
Results…… 34
Within-dike chemical variation…… 34
Isotopic compositions of Western Ghats flow members…… 37
The coastal dike swarm…… 43
Elemental signature and DFA…… 43
Isotopic signature…… 47
The Nasik-Pune swarm…… 50
Elemental signature and DFA…… 50
Isotopic signature…… 54
The Narmada-Tapi swarm…… 55
Elemental signature and DFA……55
Isotopic signature…… 56
Discussion…… 60
Implications of results for models of Deccan emplacement…… 66
The plume-head model…… 67
Models involving rifting above a plume……68
The triple junction model…… 69
Non-plume models…… 70
Conclusions……74
Acknowledgements……76

Chapter 3: Alkalic dikes of the Narmada-Tapi swarm and India's west coast..... 78
Introduction.....78
Samples and methods..... 81
Results.....83
Discussion..... 89
Conclusions.....92
Chapter 4: Petrogenetic processes of the Louisville Seamount Chain and geochemical evolution of its mantle source.....94
Introduction.....94
Sampling..... 100
Methods.....101
Results..... 102
Effects of alteration..... 102
Major and trace elements..... 111
Isotopic composition.....117
Discussion.....119
Lithospheric thickness at the time of volcanism..... 125
Modeling melting..... 127
Systematic geochemical variations..... 137
The Louisville hotspot as the source of the Greater Ontong Java Plateau..... 142
Conclusions..... 145
Acknowledgements..... 148
Chapter 5: Conclusions.....149
Dikes of the Deccan Traps..... 149
The Louisville Seamount Chain..... 153
Appendix A: Major and trace element compositions of Deccan dikes.....157
Appendix B: Parameters used to model melting in the Louisville seamounts' mantle source 184
Appendix C: Principles of discriminant function analyses..... 185
Appendix D: Major and trace element compositions of Deccan dikes.....187
References.....192

LIST OF TABLES

Table Page

2.1 Stratigraphic nomenclature and thickness of the western Deccan basalt formations…… 21

2.2 Isotopic and isotope-dilution data for members of the Western Ghats previously uncharacterized isotopically…… 40

2.3 Isotopic and isotope-dilution data for Deccan dikes…… 57

3.1 Major and trace element compositions of alkalic and lamprophyric Deccan dikes…… 85

3.2 Isotopic data for Deccan alkalic dikes…… 87

4.1 Major and trace element compositions of Louisville lavas…… 104

4.2 Isotopic and isotope-dilution data of Louisville lavas……128

LIST OF FIGURES

Figure Page

1.1 Structure of a thermo-chemical plume…… 2

1.2 General map of the Deccan Traps…… 5

1.3 Map of the Indian Ocean and the Réunion hotspot track…… 7

1.4 Pb-Nd-Sr isotopic data of Deccan flow formations…… 10

1.5 Map of the Pacific Ocean and location of the Louisville Seamount Chain…….12

2.1 Map of the Deccan Traps and its three major recognized dike swarms…… 18

2.2 Sketch map of published Deccan stratigraphic sections…… 22

2.3 Cross sections across the Deccan province…… 23

2.4 Sample location maps of the Dediapada and Dhadgaon areas……29

2.5 Comparative primitive mantle-normalized incompatible trace element patterns of Deccan dikes and flow formations…… 36

2.6 New Pb-Nd-Sr isotopic data for Deccan flow members and chemical types… 39

2.7 Harker diagrams of discriminative major and trace elements and ratios of Deccan Traps dikes…… 44

2.8 Values of the first two canonical discriminant functions for Deccan dikes……45

2.9 Comparative primitive mantle-normalized incompatible trace element patterns of Deccan dikes and flow formations…… 46

2.10 Pb-Nd-Sr isotopic data of Deccan tholeiitic dikes…… 48

2.11 Histogram of formational matches determined by DFA for each dike swarm…51

2.12 Statistical analysis of dike directional data for each dike swarm……52

2.13 Location map, strike and formational affinity of Deccan dikes……. 62

2.14 Location map, strike and formational affinity of Deccan dikes……. 63

Figure Page

3.1 Map of important acidic and alkalic complexes of the Deccan Traps..... 79

3.2 Schematic map of dikes in the Rangpur area..... 82

3.3 Total alkali vs. silica classification diagram of studied acidic and alkalic dikes..... 84

3.4 Pb-Nd-Sr isotopic data of Deccan lamprophyric and other alkalic dikes.....88

4.1 Map of the Louisville Seamount Chain and location of dredge sites..... 95

4.2 Primitive mantle-normalized incompatible trace element patterns of Louisville lavas.....103

4.3 Total alkali vs. silica classification diagram of Louisville volcanic samples... 112

4.4 Harker variation diagrams of selected major and trace elements and ratios... 114

4.5 Nb/Y vs. Zr/Y diagram for Louisville seamounts..... 116

4.6 Age-corrected Pb-Nd-Sr isotopic data of Louisville seamounts..... 118

4.7 Variation in isotopic composition of Louisville rocks as a function of key petrogenetic parameters.....120

4.8 Variation in Pb and Nd isotopic composition of Louisville rocks as a function of La/Yb, Pb and Nd..... 122

4.9 Principle component analysis of some LSC major and trace element compositions.....124

4.10 Aggregated fractional melt model of $(Dy/Yb)_N$ and $(Yb/Sm)_N$..... 135

4.11 Isotopic and trace element variation of Louisville rocks as a function of lithospheric thickness and age at the time of seamount emplacement.....140

4.12 Comparison of Louisville $^{207}Pb/^{204}Pb$-$^{206}Pb/^{204}Pb$ values with age-adjusted fields for basalts of the Greater Ontong Java Plateau..... 144

CHAPTER 1

INTRODUCTION

The hotspot theory, proposed by Wilson (1963), was designed to explain the pattern of long-lived intraplate volcanism that leaves linear chains of seamounts observed on the ocean floor and appear to track the motion of lithospheric plates. The model proposed the existence of hot and fixed melting anomalies beneath the lithosphere: literally, hot spots. Morgan (1971) elaborated on this model by ascribing the stability of hotspots to deep mantle plumes seated in the lower mantle. Subsequent developments in the production of model mantle plumes through scaled experiments (e.g., Richards *et al*., 1989; Campbell & Griffiths, 1990) and numerical modeling intricately linked the origin of large igneous provinces and hotspot tracks to the head and tail phases of mantle plumes, respectively (Fig. 1.1).

The term "intraplate volcanism" refers to volcanism unrelated to plate boundaries, while "hotspot" was defined as a hot and fixed melting anomaly in the mantle that can produce volcanism, and "mantle plume" is an upwelling of mantellic material rising from thermal boundary layers. Despite these differences, these three terms have often been used interchangeably, essentially blurring the boundary between observations, causes and effects. However, some authors have proposed that hotspots may not be hot (e.g., Schilling *et al*., 1980; Bonatti, 1990; Herzberg, 2004), but may be wet instead, and that some presumed hotspot tracks do not show a systematic (or at least, not linear) progression in age (e.g., Davis *et al*., 2002; Koppers *et al*., 2007a). As a result, in the past few years, the mantle plume theory has come under scrutiny and sometimes under

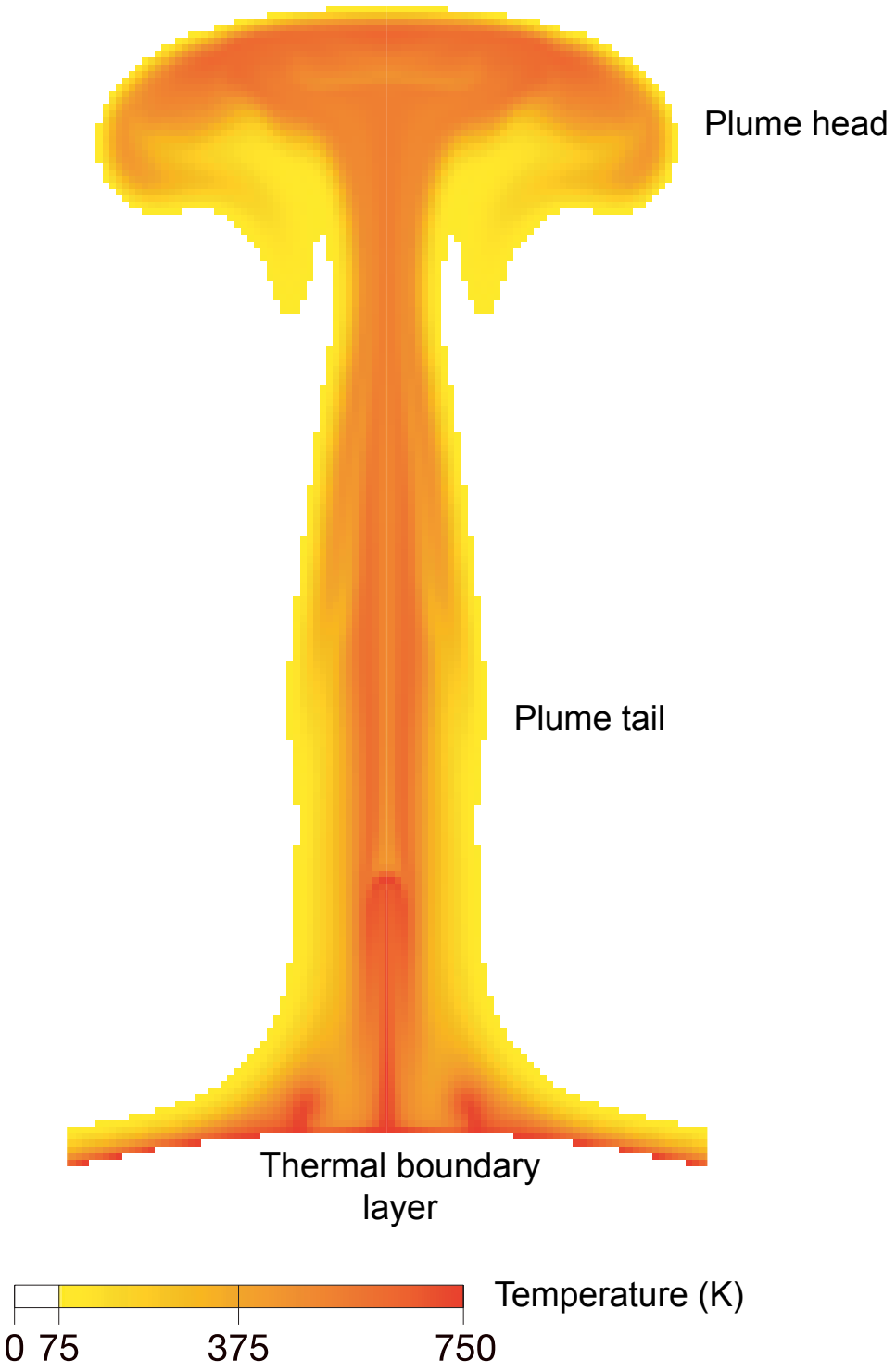

Fig. 1.1: Thermal structure of a numerically modeled thermo-chemical plume. Temperatures are given (in K) in excess of ambient mantle. After Lin & van Keken (2005).

vigorous assault (e.g., Smith, 1993; Anderson, 1994; King & Anderson, 1995; Smith & Lewis, 1999; Sheth, 1999; 2005; Foulger & Anderson, 2005).

The present research was carried out during years of intense debate regarding the plume hypothesis, which saw numerous authors (ibid.) dispute the existence of mantle plumes and point to features of intraplate volcanism that the plume model typically fails to explain (e.g., the lack of evidence for uplift above mantle plumes in some large igneous provinces, such as the Deccan; e.g., Sheth, 2007). This dissertation focuses on two localities commonly proposed to be the products of mantle plume volcanism: the Deccan Traps of India (assumed to be the plume head of the Réunion plume; e.g., Morgan, 1972) and the Louisville Seamount Chain in the South Pacific (assumed to be the plume tail of an unknown plume head; e.g., Hawkins, 1973; Clague & Jarrard, 1973; Lonsdale, 1988). The goals of the Deccan study were to: (1) determine the association of feeder dikes to the lava pile by comparing the chemical and isotopic compositions of dikes with those of the lava flow formations defined in the central western Deccan; (2) use the feeders' strike to infer the timing of rifting along the west coast and the grabens of the northern Deccan relative to the main phases of volcanism; and (3) assess the plume-head and alternative (rifting-plus-plume, and non-plume) models for the origin of the Deccan province. The purpose of the Louisville study was to determine the geochemical composition of the Louisville seamounts and guyots and assess the evolution of their mantle source(s). As the only other long-lived seamount chain besides the Hawai'i-Emperor chain located on the Pacific plate, the Louisville chain offers a unique opportunity to compare models for the origin of hotspot ocean island magmatism in the Pacific Ocean.

THE DECCAN TRAPS

Geography and physical features

The Deccan Traps – the name "Traps" deriving from the step-like morphology of the exposed pile of lava flows – is one of the world's larger continental flood basalt provinces, covering ~0.5 x 10^6 km^2 of west-central India, an area roughly equal to the size of Spain or Texas (Fig. 1.2). Accounting for erosion (≥50%), the estimated volume of lava ranges from ~1 to 3 x 10^6 km^3 (e.g., Wadia, 1975; Eldholm & Coffin, 2000; Sen, 2001). In its thickest part along the Western Ghats escarpment (Fig. 1.2), the Deccan Traps reach a stratigraphic thickness of ~3400 m, the largest continuous exposed section, ~1500 m, being located at Kalsubai Peak. At the eastern, northern and southern fringes of the province, the Traps thin to a few flows and total exposures of 200 m or less. The Rajahmundry Traps, possibly representing the southeasternmost edge of the province, are just a handful of flows thought to be related to the Deccan, located on India's eastern coast some ~350 km from the main province. To the north, magmatic precursors to the Deccan event have been found near Barmer (Basu *et al*., 1993; Simonetti *et al*., 1995), and perhaps as far north as the South Tethyan suture zone of Pakistan, near Zhob (Fig. 1.2; Mahoney *et al*., 2002). Seaward dipping reflectors have also been imaged by seismic reflection off the west coast and are thought to represent the offshore expression of Deccan volcanism as the Seychelles Bank was rifting away from the Indian mainland (e.g., Collier *et al*., 2008). Morgan (1972) proposed that the hotspot at the source of the Deccan Traps can be linked to the source of volcanism on Réunion Island; this link was strengthened by Duncan (1990) who showed age-progressive volcanism

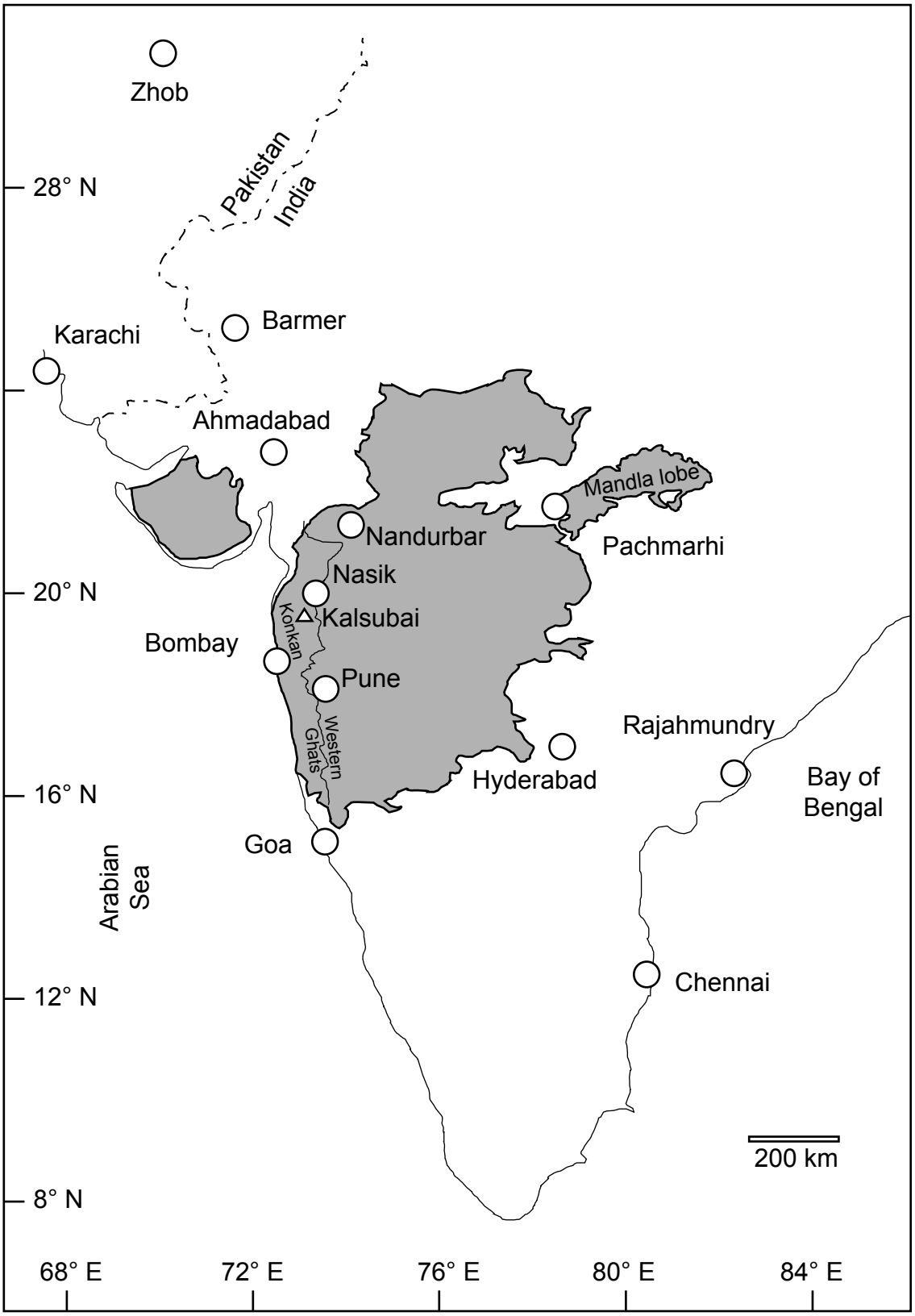

Fig. 1.2: Map of the Deccan Traps (in gray) showing important localities mentioned in the text.

along a path following the archipelagos of Lakshadweep, Maldives, Chagos, Mauritius and the Mascarene Plateau (Fig. 1.3).

Flows of the Deccan Traps generally are nearly flat-lying with dips of 1° or less (e.g., West, 1959; Raja Rao *et al*., 1978). Compound flows predominate in the central western Deccan, whereas simple flows appear to be more common on the periphery of the province (e.g., Walker, 1971; Raja Rao *et al*.,1978). Raja Rao *et al*. (1978) interpreted this flow pattern distribution as indicating the proximity of the province's main eruptive vents. However, unambiguous eruptive vents have not been found, Crookshank (1936) describing perhaps the sole example of a sill feeding a flow in the western Mandla lobe. Three large dike swarm systems have been recognized in the province (Beane *et al*., 1986; Deshmukh & Sehgal, 1988; Hooper, 1990; 1999), which will be introduced in more detail in Chapter 2: the Narmada-Tapi swarm system comprises dikes running preferentially E-W and parallel to the Narmada and Tapi grabens; the coastal swarm is composed of dikes striking N-S, parallel to the west coast; and the Nasik-Pune swarm of the central western Deccan displays only a weakly defined NNE-SSW trend. On the basis of preliminary chemical analyses of dikes, it has commonly been assumed that the Nasik-Pune dike swarm (roughly located between the cities of Nasik and Pune; Fig. 1.2) represents the main locus of feeder dikes for the province (Beane *et al*., 1986; Hooper, 1990). Hooper (1990, 1999) interpreted the near-absence of preferred orientation in the Nasik-Pune system as strong evidence that the main phase of Deccan eruptive activity was not accompanied by significant directed extension of the regional lithosphere. This conclusion, in turn, has been used as a key argument in favor of a plume-head origin for

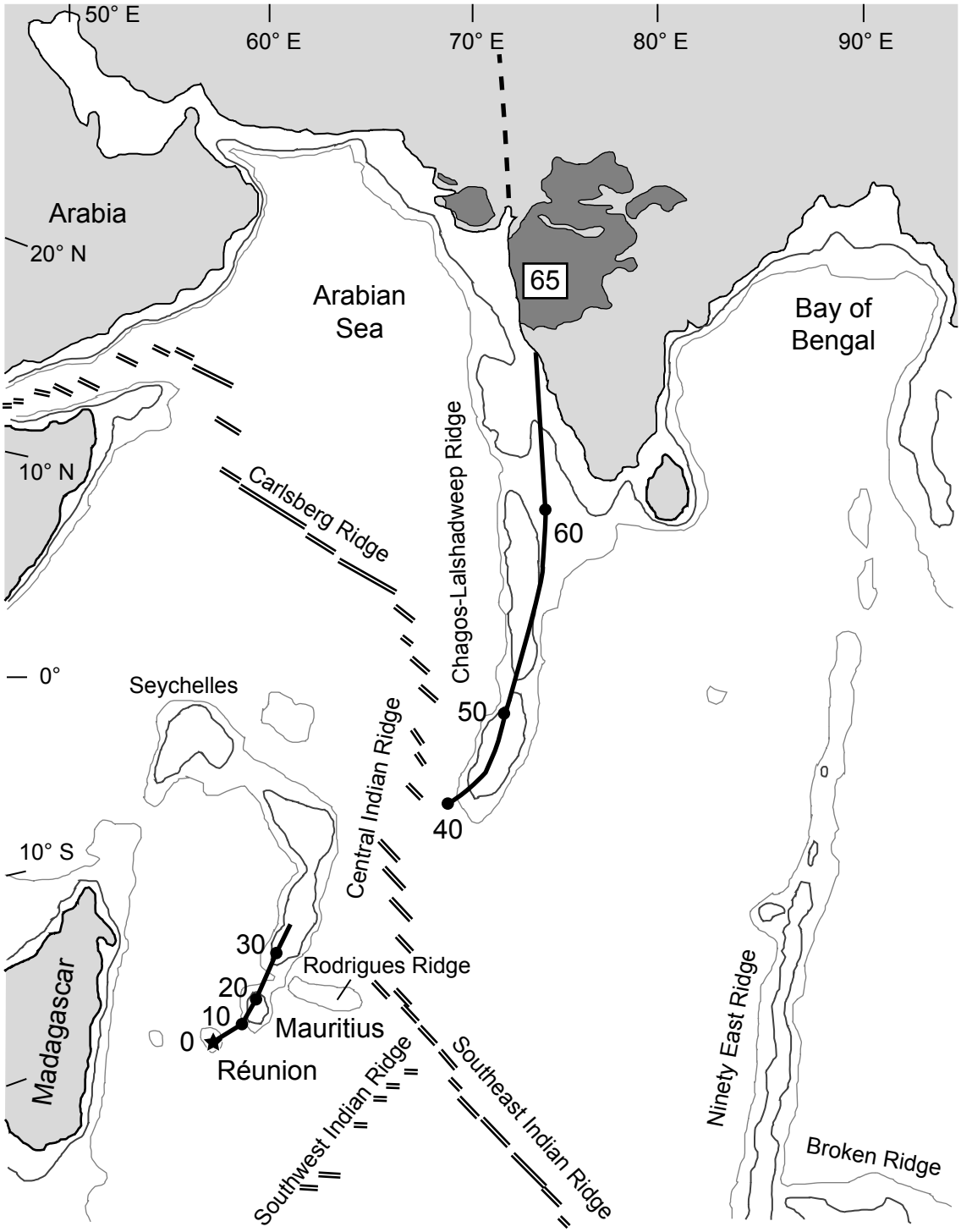

Fig. 1.3: Map of the Indian Ocean, modified after Mahoney *et al*. (2002), showing the Deccan Traps (dark gray) and a model 0-65 Ma track of the Réunion hotspot (heavy line), after Duncan (1990), and 83.5-95 Ma (dotted heavy line), after the plate reconstruction of Kent *et al*. (2002). Dots mark model hotspot positions in 10 Ma increments. Black star represents the currently active Piton de la Fournaise volcano on Réunion Island.

the Deccan Traps, as opposed to a rifting-controlled origin (e.g., Hooper, 1990; Campbell, 1998).

Stratigraphy and origin of isotopic variability

Eleven lava formations (Table 2.1, in chapter 2) have been defined in the southwestern Deccan on the basis of their major and trace element compositions and their Pb, Nd and Sr isotopic ratios (e.g., Mahoney *et al*., 1982; Cox & Hawkesworth, 1985; Beane *et al*., 1986; Beane, 1988; Devey & Lightfoot, 1986; Lightfoot *et al*., 1990; Mitchell & Widdowson, 1991; Peng *et al*., 1994; Subbarao *et al*., 1994). Most formations have been subdivided into chemical types and members of relatively homogeneous chemical composition. In the absence of geological markers (paleosols, discontinuities such as ash or sediment beds) that can be traced over large distances, the basalt compositional stratigraphy has proven to be the most useful tool to correlate lava sequences separated by hundreds of kilometers. Over the last decade, substantial progress has also been made in correlating the geochemically dissimilar exposures of the northern, northeastern, northwestern and southeastern Deccan with the better-studied sections of the Western Ghats (e.g., Mitchell & Widdowson, 1991; Peng & Mahoney, 1995; Melluso *et al*., 1995; Peng *et al*., 1998; Mahoney *et al*., 2000; Jay & Widdowson, 2008).

The chemical and isotopic differences between formations are distinctive and are thought to arise from variable mixing and assimilation of products from different mantle sources and/or crustal end-members (e.g., Mahoney *et al*., 1982; Cox & Hawkesworth, 1985; Mahoney, 1988; Matsuhisa *et al*., 1986; Lightfoot & Hawkesworth, 1988; Lightfoot *et al*., 1990; Peng *et al.*, 1994; 1998). Peng *et al*. (1994) proposed a two-stage

mixing model to account for the isotopic variations observed among Deccan lava formations (Fig. 1.4). They postulated that the first stage of mixing involved melts of an Ambenali-formation-like end-member (thought to represent a chemically transitional-mid-ocean ridge basalt (MORB)-like source) and lower-crustal or lithospheric mantle material with a distinct high-$^{206}Pb/^{204}Pb$, high-$^{87}Sr/^{86}Sr$ and low-ε_{Nd} signature. The first stage of mixing would explain the isotopic array observed between the Ambenali formation and high-$^{206}Pb/^{204}Pb$ regions of the Poladpur, Khandala, Neral, Bhimashankar, Igatpuri, Jawhar, Thakurvadi and Bushe formations, and an isotopic array displayed by lavas in the northeastern Deccan or Mandla lobe. Products of variable amounts of first-stage mixing were proposed to have then mixed with a variety of low-$^{206}Pb/^{204}Pb$ continental (possibly granulitic) end-members to produce the observed arrays of most of the formations.

Age of the Deccan Traps

Although some debate remains as to the exact age of the main volcanic event (e.g., Venkatesan *et al*., 1993; Hofmann *et al*., 2000), most lavas of the Deccan have been dated between 64 and 66 Ma (Courtillot *et al*., 1988; Duncan & Pyle, 1988; Vandamme *et al*., 1991; Baksi, 1994; Allègre *et al*., 1999; Pande *et al*., 2004). Radiometric ^{40}Ar-^{39}Ar and ^{187}Re-^{187}Os age data show no statistically significant difference between the top and bottom of the sequence. More recently, Chenet *et al*. (2007; 2008) isolated two paleomagnetic stages in the formation of the Deccan, a precursory event at ~67 Ma and a main phase of volcanism at ~65 Ma. The latter phase encompasses the bulk of the Western Ghats formations, at least from the Jawhar to the Mahabaleshwar. These authors

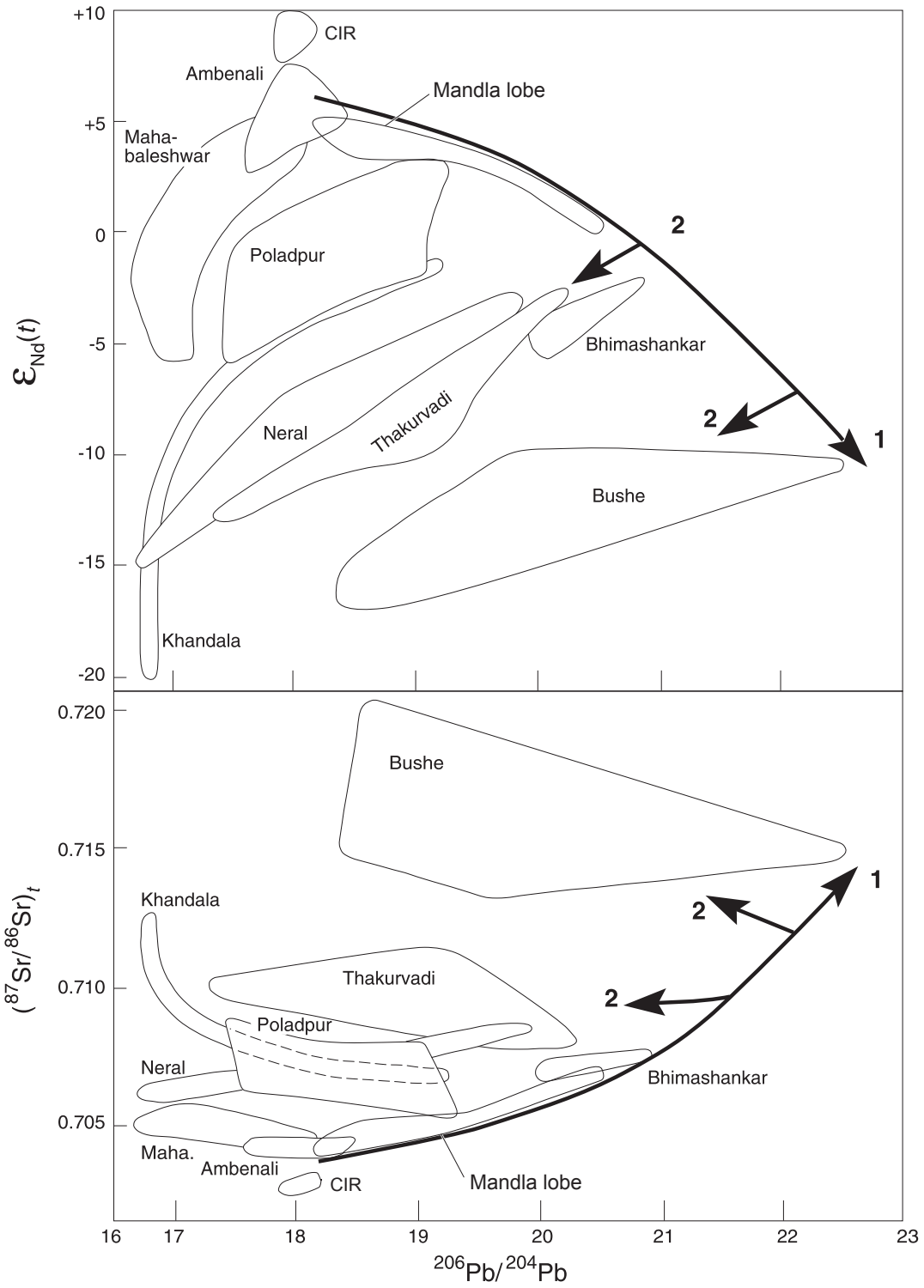

Fig. 1.4: Pb-Nd-Sr isotopic data of Deccan flow formations. Fields represent the southwestern Deccan formations, as well as data for the northeastern Deccan (Mandla lobe), modified after Mahoney *et al*. (2000). Central Indian Ridge (CIR) field after Mahoney et al. (1989). Some fields are not shown to avoid cluttering. Arrows represent the two-stages model of Peng *et al*. (1994).

also present strong paleomagnetic secular variation evidence that lavas of the Poladpur through Ambenali formations in the Mahabaleshwar area were formed by major short-lived eruptive events or pulses, each lasting but a few decades. The same authors thus estimate eruption rates of ~100 km^3/yr being sustained for decades during these pulses, three order of magnitudes more than those of the Pu‘u ‘Ō‘ō eruption of Kilauea (Sutton *et al*., 2003)

THE LOUISVILLE SEAMOUNT CHAIN

The Louisville Seamount Chain (LSC), historically termed “Louisville Ridge”, is a ~4300 km long chain of extinct submarine volcanoes located in the southwestern Pacific Ocean, second only to the Hawai‘i-Emperor chain in terms of length (Lonsdale, 1988). Comprising over 70 guyots and seamounts of varying sizes, it extends from 138.1° W, 50.9° S at its eastern end to the Kermadec Trench (175.3° W, 25.7° S), where it is currently being subducted (Fig. 1.5). Although not perfectly linearly progressive, ages of seamounts have been shown to get younger to the east (Watts *et al*., 1988; Koppers *et al*., 2004), spanning an age range of 79-1.1 Ma. As a result, the LSC has commonly been interpreted as a hotspot trail recording the passing of the Pacific plate over a mantle melting anomaly that has been fixed over 79 Myr (e.g., Hawkins, 1973; Epp, 1978; Jurdy, 1978; Lonsdale, 1988; Clague & Jarrard, 1973; Molnar *et al*., 1975; Vogt *et al*., 1976; Cheng *et al*., 1987; Koppers *et al*., 2004). This hypothesis is further supported by the apparent synchronicity of bends in the LSC and Hawai‘i-Emperor chain, that are thought to record changes in Pacific plate motion. As the only other long-lived hotspot trail located on the Pacific plate, the LSC presents a premium opportunity for evaluating

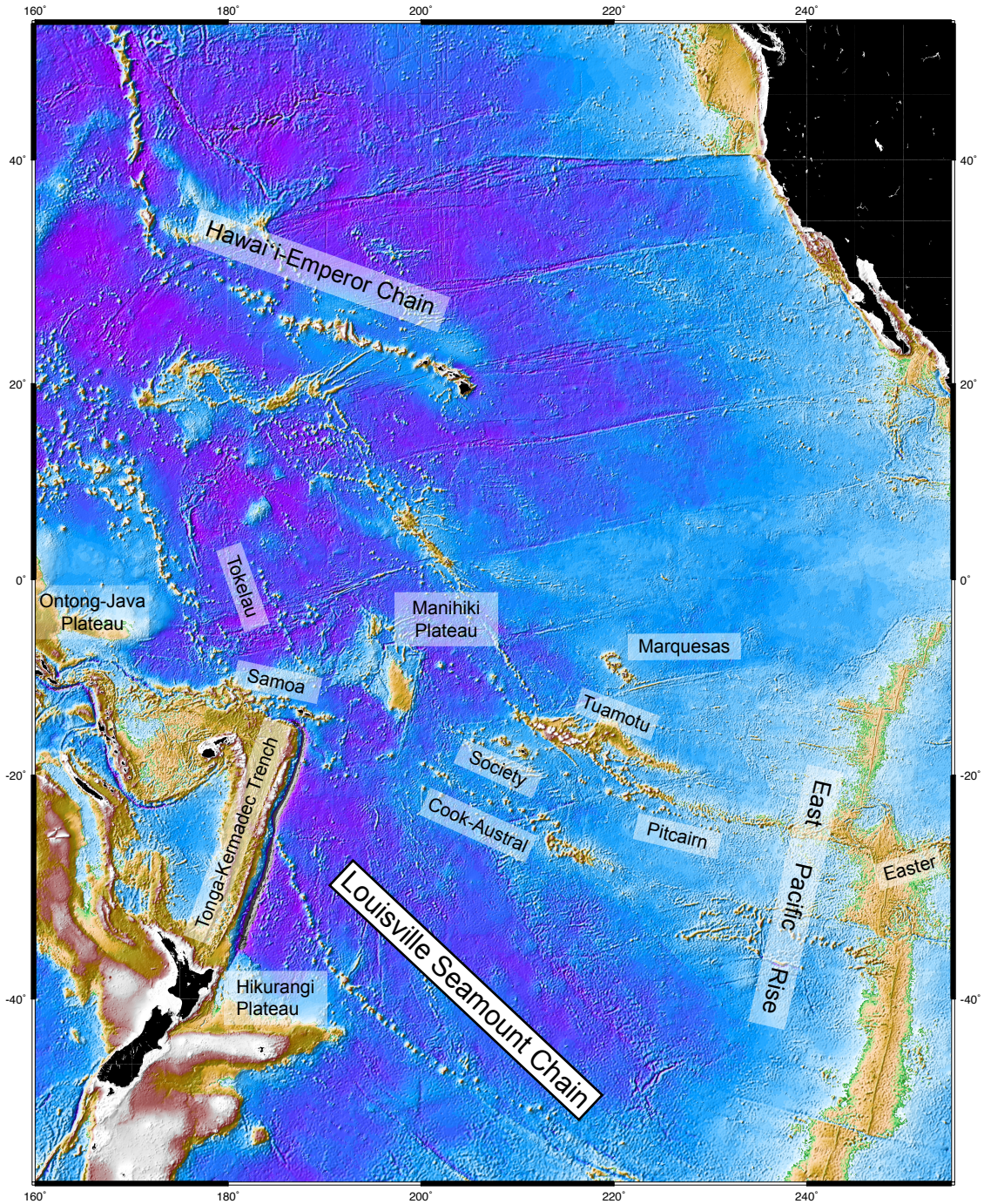

Fig. 1.5: Location of the Louisville Seamount Chain in the Pacific Ocean relative to other important features mentioned in the text (modified after Lonsdale, 1988).

geochemical and geodynamical models for the origin of hotspot volcanism, which have largely been developed from the study of Hawai‘i and its volcanic chain. However, the LSC also presents its own set of characteristics that set it apart from its North Pacific counterpart. Published geochemical data for a small collection of dredged LSC samples hint that, unlike their Hawai‘ian counterparts, Louisville seamounts are dominantly alkalic and result from smaller degrees of partial melting of a much more homogeneous mantle source (Hawkins *et al*., 1987; Cheng *et al*., 1987). Lonsdale (1988), using estimates of seamount volumes, showed that magma productivity at the LSC has been an order of magnitude smaller than that of the Hawai‘ian hotspot, and has declined sharply over the past 25 Myr, sparking hypotheses that the Louisville hotspot is dying. The scarcity and degree of alteration of available samples emphasized the need for more-detailed sampling and study of Louisville seamounts and their geochemistry, which will be presented in chapter 4.

ANALYTICAL METHODS

Major and trace element concentrations and Pb, Nd and Sr isotopic analyses of samples used in this dissertation were measured using a variety of instruments at several facilities. Major and trace element concentrations of many Deccan samples were already available from previous analyses carried out at the X-ray fluorescence (XRF) and inductively coupled plasma mass spectrometry (ICP-MS) facilities of Washington State University (Knaack *et al*., 1994; Johnson *et al*., 1999) and at the inductively coupled plasma-atomic emission spectrometry (ICP-AES) laboratory of Royal Holloway College (UK) (after Walsh, 1992). A few isotopic analyses had also been conducted on the

Deccan dike samples at the University of Alberta's (Canada) thermal ionization mass spectrometry (TIMS) facility (following Creaser *et al*., 1997). Major and trace element concentrations of LSC samples were also measured at the XRF and ICP-MS laboratory of Washington State University. These methods and laboratory procedures are presented in the following chapters. Below, I will detail the laboratory procedures of XRF, ICP-MS and isotopic analyses carried out at the University of Hawai'i in order to keep the description of analytical procedures succinct in upcoming chapters.

XRF

Major elements in our recently collected suite of Deccan Traps dike samples were measured by XRF on fused disks at the University of Hawai'i, following Eason & Sinton (2006). Whole rock powders were prepared from ~40 g of cleaned and picked ~5 mm rock chips in an alumina swing mill and disks were fused using a $Li_2B_4O_7$ flux. Major element concentration data were collected on the fused disks on a Siemens 303 AS XRF spectrometer using a Rh-target, end-window x-ray tube, following Norrish & Hutton (1977). Corrected intensities were calibrated against a wide range of natural rock standards (AGV-1, BHVO-1, BIR-1, G-2, JA-2, JA-3, JB-1, JB-2, JB-3, NIMG, NIMN, W-1, W-2). Accuracy and precision data for this system are reported by Sinton *et al*. (2005) and in legends of the relevant tables in Chapters 2-4.

ICP-MS

Concentrations of trace elements were determined by ICP-MS following a procedure similar to that of Pyle *et al*. (1995) and Neal (2001). Chips or slabs of rocks

were crushed to a 1-2 mm size, hand-picked, and powdered with an agate mortar and pestle. For each sample, ~50 mg of powder was weighed and subsequently digested with an HF-HNO_3 (1:2) solution. Samples then underwent four successive evaporation and redissolution steps, the first with 6N HCl, followed by three redissolutions in ~8N HNO_3. Samples were then diluted with 4N HNO_3, from which subsequent dilutions were made for analysis on the ICP-MS instrument. A range of trace elements was analyzed using the University of Hawai‘i Thermo-Finnigan Element2 and VG Elemental PlasmaQuad II+ machines. Trace element concentrations were determined by external calibration with USGS standards AGV-1, BIR-1, W-2, BHVO-1 and BCR-1. Two dilutions of each standard were analyzed at the beginning and end of each analytical run, resulting in a 20-point calibration curve (Pyle *et al.*, 1995). A University of Hawai‘i in-house standard, K1919 (from the same lava flow as BHVO-1), was analyzed after every fifth sample to monitor possible instrument drift not accounted for by the 1 ppb internal standards (Be, In, Tl, Bi) added to each sample and standard. Repeat analyses of K1919 are good indicators of analytical uncertainty and run-to-run precision. Separate dissolutions of BHVO-1 and BIR-1 were also treated as unknowns (i.e., not used in the standard calibration) as a further assessment of accuracy. Two samples were picked, dissolved and analyzed in duplicate to assess procedural error and variation in glass picking procedure. All tests show the data reported here to be within analytical error. Relative errors as two standard deviations range from 1.4% (for Sr) to 7.0% (for Gd).

Isotopic analyses

Sample preparation and mass spectrometry for Sr, Nd and Pb isotopic and isotope-dilution measurements were carried out following Mahoney *et al*. (1991, 2005). Analyses were performed on splits prepared from small (1-2 mm) rock chips that were picked to avoid alteration, acetone- and acid-cleaned and sonicated and rinsed with quartz-distilled water prior to powdering and dissolution. We prepared ~200 mg of powder from the picked and cleaned grains with a boron carbide mortar and pestle that was cleaned with ~6N HCl in a sonic bath for 30 min and pre-contaminated in between each sample to avoid cross-contamination. About 40 mg of powder was then digested with a HF-HNO_3 (1:2) solution, followed by eight evaporation and redissolution steps (the first three in ~8N HNO_3, the fourth in ~6N HCl, the fifth in ~2N HCl and the last three in ~4N HBr in preparation of Pb extraction). Finally, Pb, Sr, Rb, Nd and Sm, as well as U and Th for the LSC samples, were separated by routine ion-exchange chromatography techniques and analyzed on a VG Sector multi-collector thermal ionization mass spectrometer (TIMS) or a VG/Micromass Sector 54 in the case of Th and U. Deccan Pb isotope analyses were carried out using conventional multi-collector static analyses, whereas the LSC data were acquired by double-spike measurements in multi-collector dynamic mode.

CHAPTER 2

GEOCHEMICAL SIGNATURES OF DECCAN TRAPS (INDIA) DIKES:

IMPLICATIONS FOR THE EVOLUTION OF THE FLOOD BASALT PROVINCE AND FEEDER SYSTEM

Loÿc Vanderkluysen[1], John J. Mahoney[1], Peter R Hooper[2], Hetu C. Sheth[3], Ranjini Ray[3]

1. Department of Geology and Geophysics, School of Ocean and Earth Science and Technology, University of Hawai‘i, Honolulu, HI 96822, U.S.A.

2. School of Earth and Environmental Sciences, Washington State University, Pullman, WA 99164, U.S.A.

3. Department of Earth Sciences, Indian Institute of Technology Bombay, Powai, Mumbai 400 076, India

INTRODUCTION

The Deccan Traps is a flood basalt province presently covering 500,000 km^2 of west-central India (Fig. 2.1), and is one of the larger continental large igneous provinces (e.g., Eldholm & Coffin, 2000). With an estimated original lava volume of approximately 1.5 to 3 x 10^6 km^3 (Wadia, 1975; Eldholm & Coffin, 2000; Sen, 2001), it is mainly

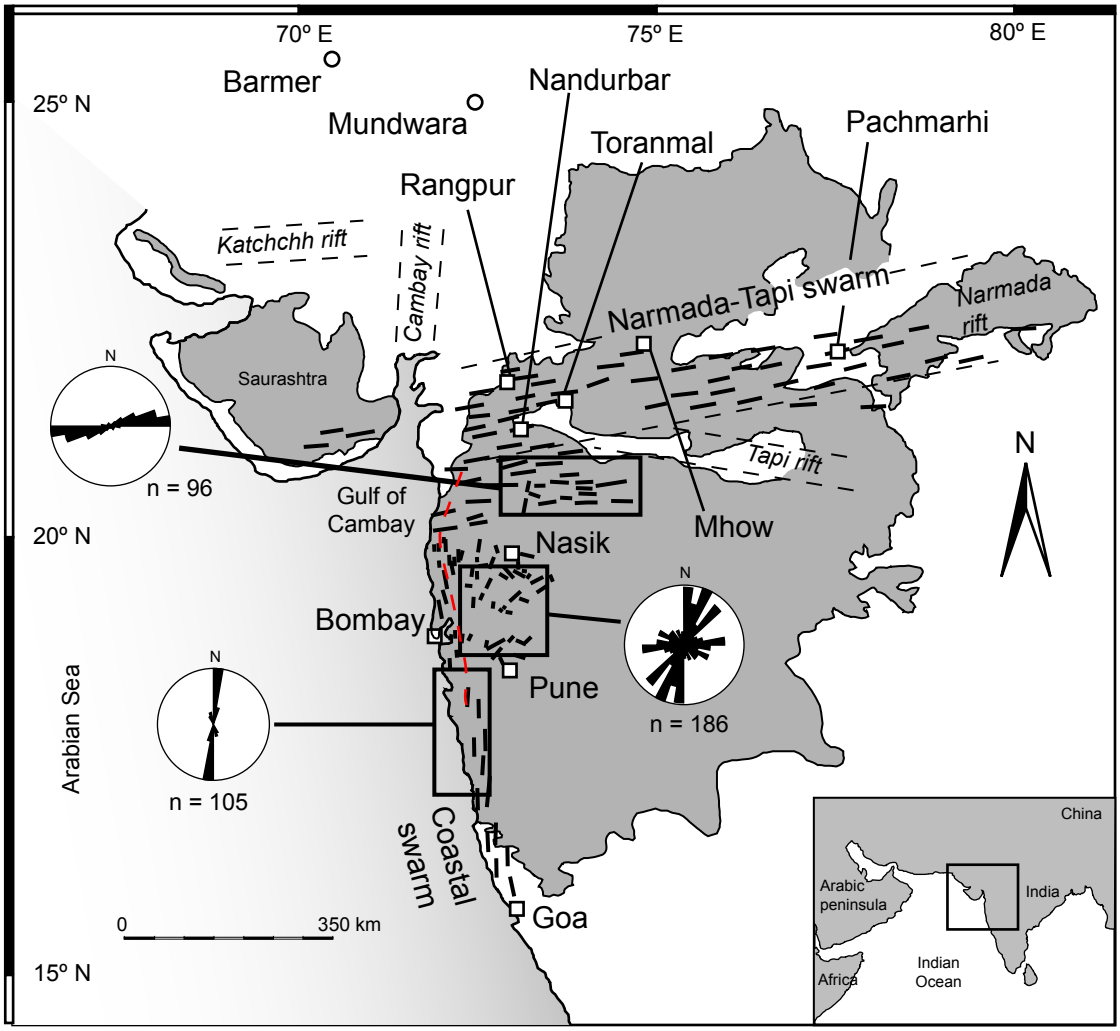

Fig. 2.1: Map of the Deccan Traps (in gray), important localities mentioned in the text (white squares), the intrusions of Mundwara and Barmer (white circles) and the three major dike swarms (shown schematically). Boxes delimit the areas of each swarm for which we have made substantial numbers (indicated by n) of dike-strike measurements, with associated rose diagrams. The red dashed line along the west coast represents the Panvel flexure (after Subrahmanya, 1998).

composed of nearly flat-lying tholeiitic lava flows (e.g., West, 1959; Raja Rao *et al.*, 1978), with notable picritic and alkalic occurrences in the northwestern Deccan (e.g., Krishnamurthy & Cox, 1977). Several scattered alkalic, acidic and carbonatitic complexes cut through or overlie tholeiitic lavas elsewhere (see review of Mahoney, 1988).

Raja Rao *et al*. (1978) noted a predominance of compound flows in the central western Deccan that they interpreted as indicating the relative proximity of the province's main eruptive vents. However, eruptive vents have not been found. In the absence of vent location, the study of dikes is crucial for determining the source area(s) of the lava flows (and therefore, the length of the flows), the architecture of the volcanic edifice, and its evolution during the flood basalt event (e.g., Beane *et al*., 1986; Devey & Lightfoot, 1986; Watts & Cox, 1989; Hooper, 1990; Mitchell & Widdowson, 1991; Jerram & Widdowson, 1995; Hooper, 1997). In turn, these factors bear strongly on models of the environmental impact of Deccan emplacement (e.g., Ravizza & Peucker-Ehrenbrink, 2003; Self *et al*., 2006; Chenet *et al*., 2008), which is of particular importance considering that the Deccan event straddled the Cretaceous-Tertiary (K-T) boundary (65 Ma) and the controversy surrounding the origin of the K-T mass extinction (e.g., Courtillot *et al*., 2000, and references therein).

In the present paper, we report major and trace element and Pb-Sr-Nd isotopic compositions of dikes sampled from the three principal dike systems in the province. We use the data to compare the dikes with the compositions of major lava packets (using lava data from the literature), with the goals of determining the major loci of feeder dikes and how feeder dike locations may have changed or migrated. Finally, we combine the

geochemical comparisons with data on dike trends to explore the evolution of the Traps' feeder system and to evaluate the viability of plume-head and rifting-based models for the province.

BACKGROUND

Previous authors have divided the lava stratigraphy in the southwestern part of the province into eleven flow formations (Table 2.1) on the basis of major and trace element compositions and Pb, Nd and Sr isotope ratios (e.g., Cox & Hawkesworth, 1985; Beane *et al.*, 1986; Lightfoot *et al.*, 1990; Peng *et al.*, 1994; Subbarao *et al*., 1994). These studies have mostly focused on the ~3400-m-thick pile (stratigraphic thickness) of lava exposed in the type-sections of the Western Ghats range (Fig. 2.2), an escarpment that separates the western coastal plain (or Konkan plain) from the Deccan Plateau (Fig. 2.2 and 2.3). Several of these formations have been shown to extend far to the southeast, east, and/or northeast, although their chemical and isotopic variability in distant locations is somewhat greater than seen in the Western Ghats sections (e.g., Mitchell & Widdowson, 1991; Peng *et al*., 1998; Mahoney *et al*., 2000; Jay & Widdowson, 2008). These eleven formations have been divided further into three sub-groups (from bottom to top: Kalsubai, Lonavala and Wai subgroups) on the basis of field characteristics, which also correspond to breaks in chemical and isotopic characteristics. Transitions from one sub-group to the next typically are accompanied by a shift from massive amygdaloidal compound flows to individual simple flows (e.g., Beane *et al*., 1986). This transition is typically thought to result from shifts in lava effusion rates (e.g., Walker, 1971).

Table 2.1: Stratigraphic nomenclature and thickness of the western Deccan basalt formations (after Peng *et al*., 1994 and references therein), in stratigraphic order according to the type sequences of the Western Ghats. Values in bold represent data from this study, with the associated sample name reported in the far right column. CT: chemical type; GPB: giant plagioclase basalt; KCG: Khandala coarse-grained; KA: Khandala aphyric; HFS: high field-strength.

Subgroup	Formation (Max. Thickness)	Member or Chemical Type	$(^{87}Sr/^{86}Sr)_t$	Avg. Mg#	TiO_2 %	Avg. Ba/Zr	Samples (this study)
Wai	Panhala (>175 m)	Desur	0.7072-0.7080	48	1.6-1.9	11.4	
		Panhala	0.7046-0.7055	52	1.6-2.3	14.8	
	Mahabaleshwar (280 m)		0.7040-0.7055	47	2.5-4.3	11.4	
	Ambenali (500 m)	Ambenali CT	0.7038-0.7044	49	1.9-3.1	14.4	
	Poladpur (375 m)	Upper	0.7061-0.7083	52	1.8-2.3	12.7	
		Lower	0.7053-0.7110	56	1.5-2.0	14.0	
		Sambarkada	**0.7075**	43	2.2-2.3	12.6	JEB-300
		Valvhan	0.7068	42	2.5-2.6	12.3	
		Ambavne	**0.7056**	45	2.0-2.1	14.0	BEL-13
Lonavala	Bushe (325 m)	Pingalvadi	**0.7127**	61	1.1-1.2	17.2	JEB-353
		Bushe CT	0.713-0.720	55	1.0-1.3	15.3	
		Shingi Hill	0.718-**0.7181**	49	1.3-1.4	16.2	JEB-211
		Hari.	0.7078-0.7079	46	2.0-2.1	12.9	
		Karla Picrite	0.7147-**0.7150**	68	1.1-1.2	19.7	JEB-136
		Bhaja	0.712-**0.7164**	58	1.3-1.5	18.2	JEB-185
	Khandala (140 m)	Rajmachi	**0.7093**-0.7102	44	2.1-2.5	14.6	JEB-297
		Khandala Phyric CT	**0.7085**	41	2.4-2.8	13.6	JEB-134
		KA3	0.7107	49	1.7	12.9	
		Madh	**0.7095**	58	1.6	14.0	DDW-13
		Boyhare	0.7102	63	1.2-1.3	13.7	
		KA2	0.7124	57	1.2	13.5	
		Khandala Phyric CT	0.7077	41	2.5-2.8	13.6	
		KA1	0.7094	61	1.0-1.1	15.4	
		Dhak Dongar	0.7071-0.7072	40	2.9-3.1	13.1	BOR-4
		KCG	0.7098	48	1.4-1.6	18.7	
		Monkey Hill GPB	0.7073-**0.7075**	41	3.1-3.4	12.2	KOP-21
		Giravli GPB	0.7068-0.7074	45	2.8-3.1	12.1	
Kalsubai	Bhimashankar (140 m)	Bhimashankar CT	0.7067-**0.7077**	47	1.9-2.6	11.7	CH-24
		Manchar GPB	**0.7075-0.7077**	42	2.9-3.1	13.2	M-12, M-13
	Thakurvadi (650 m)	Thakurvadi CT	0.7073-0.7080	58	1.8-2.2	12.0	
		Water Pipe Member	0.7099-0.7112	59	1.4-1.6	12.3	
				71	1.0-1.1	12.0	
		Paten Basalt	**0.7224**	58	1.0	15.2	JEB-434
		Thakurvadi CT	0.7067-0.7070	58	1.8-2.2	12.4	
		Ashane	0.7068	62	2.0-2.1	9.6	
		Thakurvadi CT	0.7080-**0.7088**	58	1.8-2.2	11.6	M-8
		Jammu Upper	0.7112	34	2.7	9.8	
		Patti Middle	0.7099	46	2.2-2.3	8.4	
		Member Lower	0.7066-0.7067	56	1.7-2.0	11.2	
	Neral (100 m)	Tunnel Five GPB	0.7082-0.7083	36	3.3-3.5	10.8	
		Tembre Basalt	**0.7084**	43	2.8-3.0	10.6	Tem-04
		Neral CT	0.7062-0.7073	62	1.5-1.7	12.3	
		Ambivli Picrite	0.7104	67	1.4-1.5	18.6	
	Igatpuri - Jawhar (>700 m)	Kashele GPB	0.7102-0.7122	40	2.6-3.1	11.5	
		Mg-Rich Igatpuri		59	1.4-1.9	13.3	
		Igatpuri Phyric	0.7107-0.7124	49	1.9-2.2	14.3	
		Thal Ghat GPB	0.7108	36	3.6	10.7	
		HFS-Poor Jawhar		51	1.3-1.6	13.0	
		Plag. Phyric	0.7085	38	3.0	11.7	
		Mg-Rich Jawhar	0.7128	59	1.4-1.9	12.7	
		Kasara Phyric	0.7091	39	2.8-3.0	10.8	

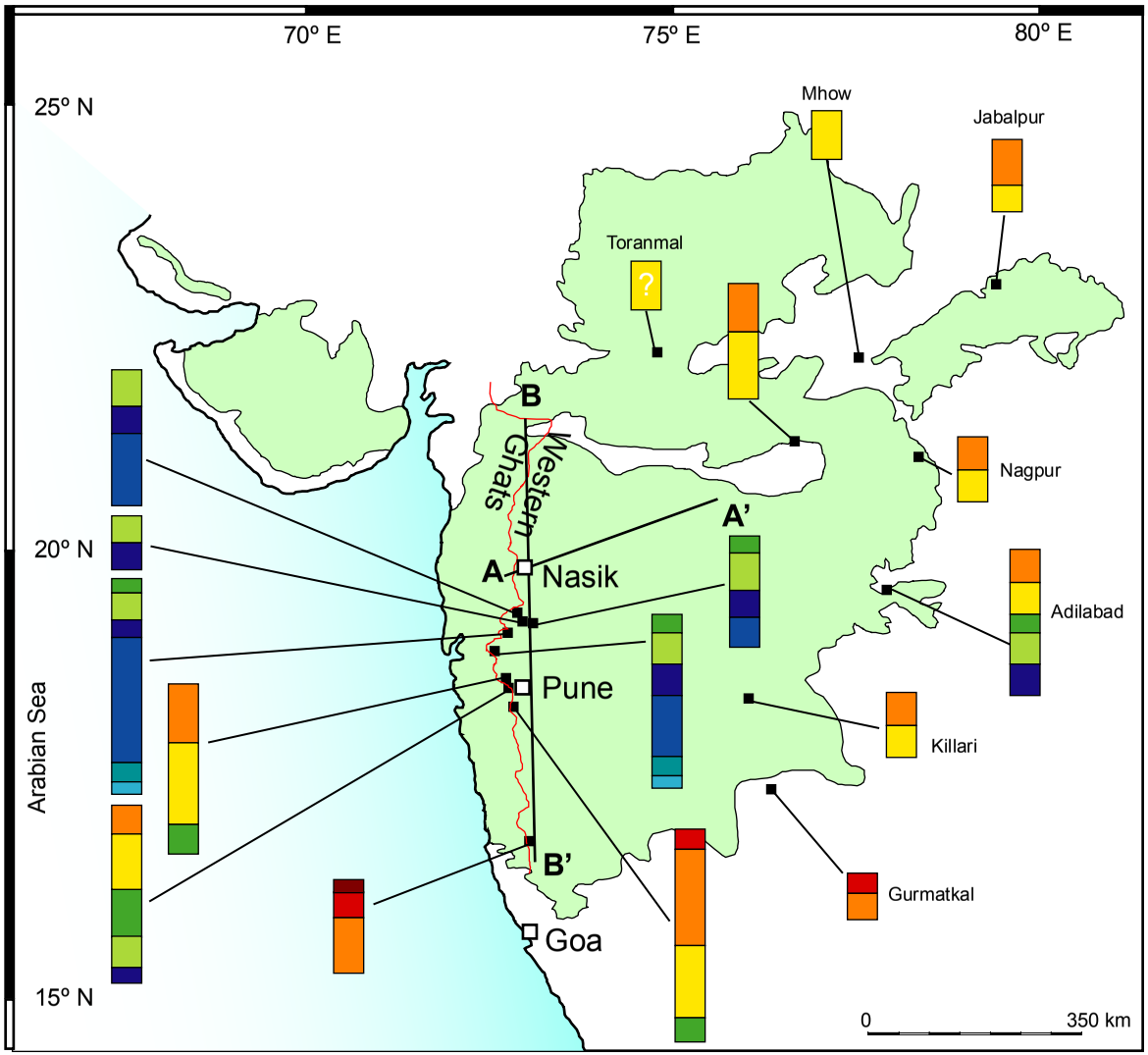

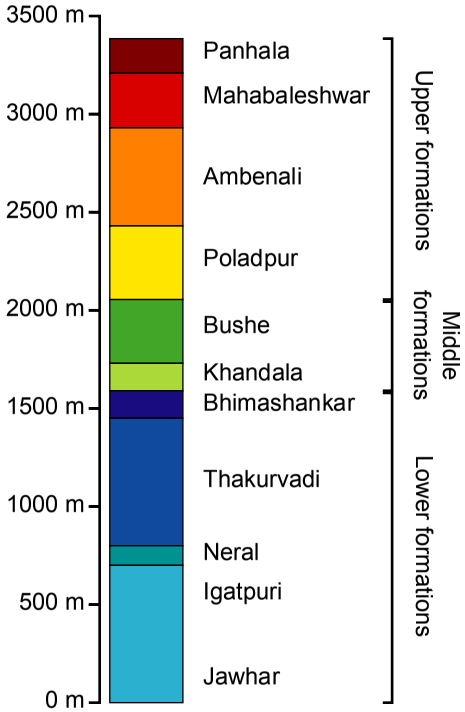

Fig. 2.2: Sketch map of stratigraphic sections across the Deccan Traps and simplified stratigraphic type section. Compiled after Devey & Lightfoot (1986), Subbarao *et al*. (1994), Mitchell & Widdowson (1991), Peng *et al*. (1998), Mahoney *et al*. (2000) and Jay & Widdowson (2008).

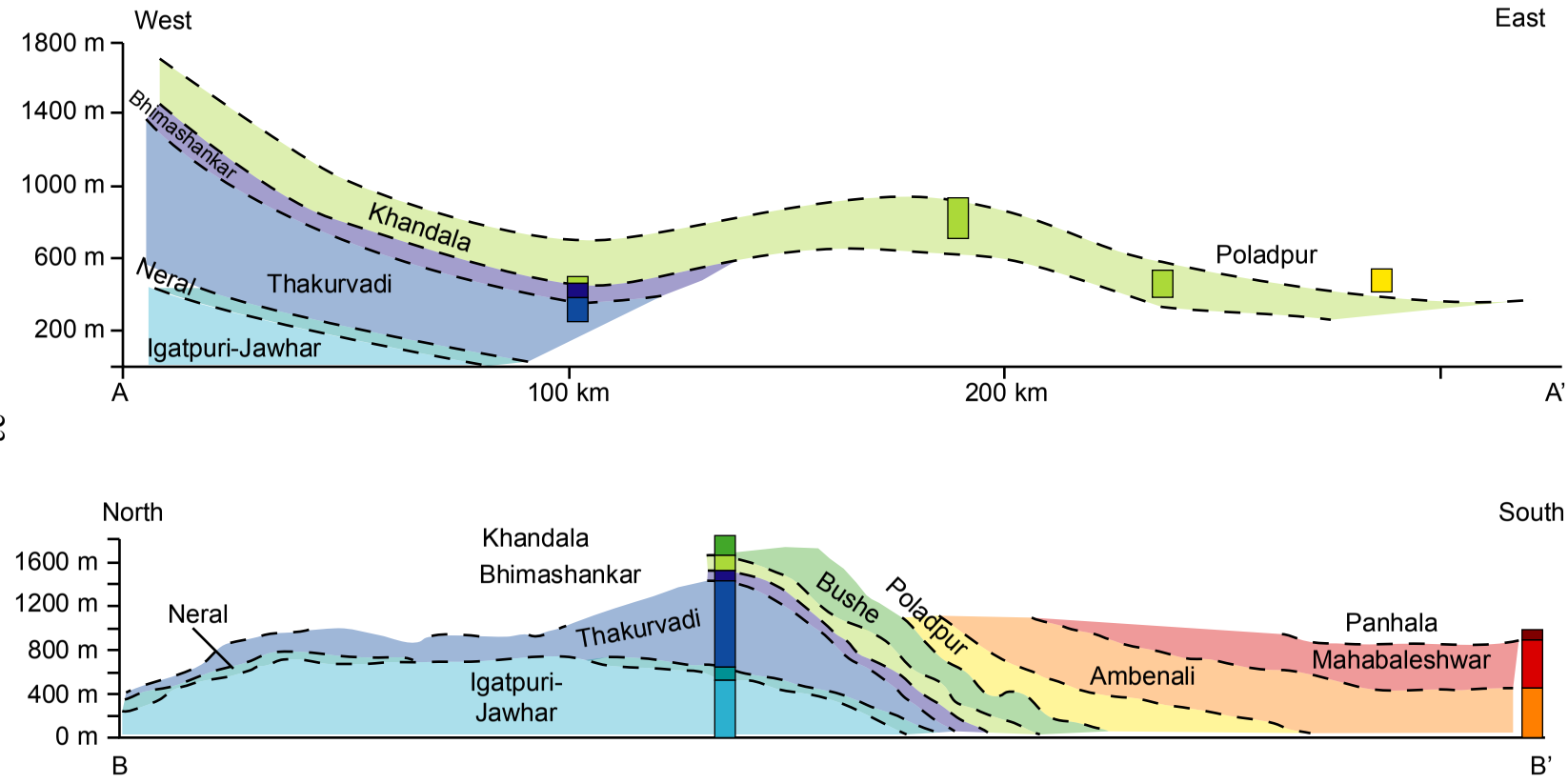

Fig. 2.3: Schematic cross sections of the central Deccan Traps, along (A-A') and (B-B') lines of Fig. 2.2. Modified after Kaila (1988), Mahoney (1988) and Peng (1998).

The chemical and isotopic differences between formations are distinctive and are thought to arise from variable mixing and assimilation of products from different mantle sources and/or crustal end-members (e.g., Mahoney *et al*., 1982; Cox & Hawkesworth, 1985; Mahoney, 1988; Matsuhisa *et al*., 1986; Lightfoot & Hawkesworth, 1988; Lightfoot *et al*., 1990; Peng *et al.*, 1994; 1998). Peng *et al*. (1994) proposed a two-stage mixing model to account for the isotopic variations observed among Deccan lava formations. They postulated that the first stage of mixing involved melts of an Ambenali-formation-like end-member (thought to represent a chemically transitional-MORB-like source) and lower-crustal or lithospheric mantle material with a distinct high-$^{206}Pb/^{204}Pb$, high-$^{87}Sr/^{86}Sr$ and low-ε_{Nd} signature. Products of variable amounts of first-stage mixing were proposed to have then mixed with a variety of low-$^{206}Pb/^{204}Pb$ continental (possibly granulitic) end-members to produce the observed arrays of most of the formations.

Dikes from across the province have been described and studied (e.g., Auden, 1949; Agashe & Gupte, 1972; Agrawal & Rama, 1976; Powar, 1981; Sinha-Roy & Radhakrishna, 1983; Sreenivasa Rao *et al*., 1985; Beane *et al*., 1986; Dessai & Viegas, 1995; Bhattacharji *et al*., 1996; Sethna *et al*., 1996; Chandrasekharam *et al*., 1999; Melluso *et al*., 1999; Mahoney *et al*., 2000; Widdowson *et al*., 2000; Paul *et al*., 2008), and previous researchers have recognized three main dike systems (Beane *et al*., 1986; Deshmukh & Sehgal, 1988; Hooper, 1990; 1999): (1) the Narmada-Tapi swarm, in which dikes strike roughly E-W, paralleling the grabens of the Narmada and Tapi rivers; (2) the coastal swarm, which is approximately parallel to the west coast and composed largely of N-S striking dikes; and (3) the Nasik-Pune swarm, in which dikes exhibit a weakly expressed NNE preferred strike (Beane *et al*., 1986) (Fig. 2.1). Tholeiitic dikes are the

most abundant; they are overwhelmingly vertical or nearly so. Dikes (both alkalic and tholeiitic) with a noticeable dip (10-30° from vertical) have been found among the dikes cropping out along the coast north and south of Bombay. These may have been tilted after their emplacement.

Despite a lack of systematic geochemical studies, the Narmada-Tapi swarm and coastal swarm have previously been discounted as major feeder systems, because many of these dikes appear to cut flows at all levels of outcrop (e.g., Auden, 1949; Beane *et al*., 1986; Hooper, 1990). On the basis of reconnaissance major and trace element analysis of 42 Nasik-Pune dikes, Beane *et al*. (1986) postulated that the Nasik-Pune swarm served as the principal locus of feeders for the lava pile. Hooper (1990, 1999) interpreted the near-absence of preferred orientation in the Nasik-Pune system as strong evidence that the main phase of eruptive activity was not accompanied by significant directed extension of the regional lithosphere. This conclusion, in turn, has been used as a key argument in favor of a plume-head origin for the Deccan Traps, as opposed to a rifting-controlled origin (e.g., Hooper, 1990; Campbell, 1998).

One caveat that must be kept in mind is that, with the exception of the Western Ghats escarpment, there are few deep incisions exposing the deeper parts of the stratigraphy. The Deccan Plateau, east of the Western Ghats, covers the majority of the province. On the plateau, only the topmost flows of the local stratigraphy are exposed, in general, and access to lower portions of the stratigraphy is very limited. This situation implies that outcrops of feeder dikes will be biased toward feeders of the upper formations. To help minimize this problem, we devoted particular attention to dikes in areas offering windows into deeper parts of the stratigraphy in the Konkan plain

(Fig. 1.2) north and northeast of Bombay, and in the Narmada-Tapi grabens (Fig. 2.2), where the lower formations are exposed (e.g., Devey & Lightfoot, 1986; Watts & Cox, 1989; Jerram & Widdowson, 2005). Nevertheless, the bias cannot be removed entirely.

The timing of lithospheric extension

Dike orientation at the time of emplacement results from local stresses and pre-existing zones of weakness within the fracturing rock (e.g., Delaney *et al*., 1986). In a homogeneous medium, dikes form perpendicular to the minimum principal compressive stress (e.g., Ida, 1999; Ernst *et al*., 2001; Gudmundsson & Marinoni, 2002; Jourdan *et al*., 2006). The existence of two large swarms of well-oriented dikes in the Deccan indicates that these dikes were either emplaced during two episodes of regional extension or within zones that had previously been fractured. The tectonic history of western India during the Cretaceous and Paleocene is marked by a succession of rifting events following the breakup of Gondwana. The first of these events resulted in the breakup of Madagascar from Greater India (completed around 84 Ma; Storey *et al*., 1995), followed by the separation of the Seychelles Bank from the west coast of India at ~62 Ma (e.g., Dyment, 1998; Collier *et al*., 2008). The Cambay graben, Katchchh rift and Narmada-Tapi rift zones (Fig. 2.1) are also thought (e.g., Sheth, 1999 and references therein) to have been active around the time of the Deccan event, although the timing of rifting in these zones relative to Deccan volcanism is not well constrained. This issue is of critical importance when studying dike emplacement in these regions.

The Narmada-Son lineament, a structure where the Narmada graben (Fig. 2.1) developed, is thought to be a continental transform fault active since the Jurassic (Sen,

1991), and may have reactivated even older structures (e.g., Raval & Veeraswamy, 2003). Pal & Bhimasankaran (1976) indicated that the lineament possibly offsets the lower Deccan volcanic sequence. Kaila (1988) reported seismic evidence of an extensional sedimentary basin under the Deccan flows in the Narmada area, and Ray *et al*. (2007) presented dike length and thickness measurements indicating that N-S extension was taking place in the area during emplacement of the Narmada-Tapi dike swarm.

Of the two other major extensional structures in the Deccan area (Fig. 2.1), rifting in the Cambay graben might have begun in the Early Cretaceous but was pronounced during the Tertiary (Biswas, 1987; Sheth, 1999), whereas the Katchchh rift is thought to have initiated in the Late Triassic and remained active until the Late Cretaceous-Early Paleocene (ibid.). The Panvel "flexure" is a monocline that formed along the west coast of India as a consequence of the post-Deccan E-W rifting of the Seychelles microcontinent and whose mechanism of formation is disputed (Devey & Lightfoot, 1986; Watts & Cox, 1989; Dessai & Bertrand, 1995; Sheth, 1998). Various authors have argued, however, that rifting along the west coast occurred near the end of Deccan volcanism or soon afterward (Hooper, 1990; Devey & Stephens, 1991; Sheth, 1998). In summary, although there is abundant evidence of extension shortly before the onset of Deccan volcanism in the Cambay and Narmada-Tapi rift zones, evidence of pre-flood-basalt extension along the west coast is lacking.

SAMPLES AND METHODS

Samples and definition of dike swarms

Most of the dike samples from the coastal and Nasik-Pune swarms were taken from the collections of Mahoney (1984), Beane (1988), Widdowson *et al*. (2000), Hooper & Widdowson (submitted) and Hooper's other coworkers. Data for the major elements and a group of trace elements analyzed by X-ray fluorescence spectrometry (XRF) were already available for these samples. Supplemental data for a wider array of trace elements, determined by inductively coupled plasma mass spectrometry (ICP-MS), existed for some of them. For three samples (BO-31, BO-32 and DH-27), data were available for several trace elements analyzed by ICP-AES (inductively coupled plasma-atomic emission spectrometry) at Royal Holloway College, UK. These XRF, ICP-MS, and ICP-AES data are listed in Appendix A, together with information on precision and accuracy.

The samples we studied from the Narmada-Tapi swarm included several described by Melluso *et al*. (1999). In addition, we collected samples from the Narmada-Tapi swarm, the Nasik-Pune swarm and the coastal swarm in the northern Konkan plain between 2003 and 2005. Descriptions of some of these samples are given by Ray *et al*. (2007, 2008), and location maps are presented in Fig. 2.4 here and by Ray *et al*. (2007).

Samples used in this study were dominantly fine- to medium-grained aphyric or sparsely phyric basaltic rocks with mm-size phenocrysts of plagioclase, clinopyroxene and olivine. Rare dikes with cm-size plagioclase are also present, particularly in the Narmada-Tapi swarm. As already noted by previous authors (e.g., Sethna *et al*., 1996; Hooper & Widdowson, submitted), lamprophyric and other alkalic dikes are present in

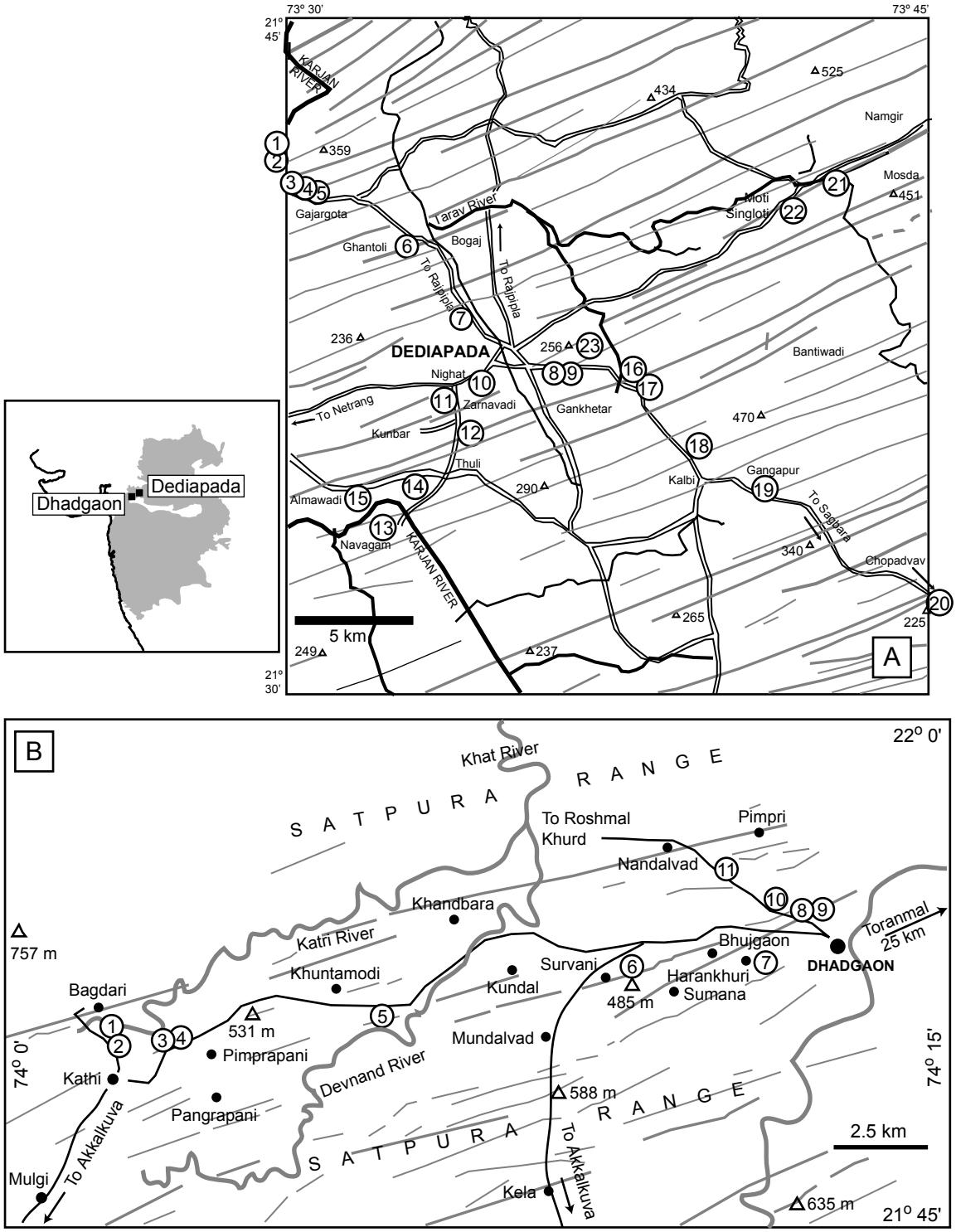

Fig. 2.4: Sample location maps of (A) the Dediapada and (B) Dhadgaon areas. Gray lines in (A) represent recognized dikes (modified after Krishnamacharlu, 1972), whereas we drew gray lines in (B) on the basis of satellite imagery. Sample numbers are indicated. The DD and DHD sample prefixes have been omitted for clarity.

the Narmada-Tapi swarm (in particular, near the locality of Rangpur; Fig. 2.1) and the coastal swarm (most notably near Bombay and along the coast to the south), although tholeiitic dikes are the norm. These alkalic dikes cannot represent feeder dikes to the tholeiitic lava pile; geochemical data for them are presented in chapter 3.

Unlike the dikes, the southwestern Deccan flow formations are generally well-characterized isotopically; however, combined Nd-Pb-Sr isotopic data were lacking for one or more members of several formations. To characterize these formations more fully, we measured the Nd, Sr, and Pb isotope ratios of samples of these members that remained in the collection of Beane (1988). Samples of two other members without isotope data (the HFS-Poor member of the Jawhar formation and the Mg-Rich member of the Igatpuri formation) were either missing or contained too little remaining material for analysis.

Although the three main dike swarms have long been recognized, their boundaries have been defined rather loosely. Because these swarms overlap substantially in some areas (e.g., the coastal and Nasik-Pune swarms overlap in the Konkan plain north of Bombay, though cross-cutting relationships are scarcely observed), we apply strict criteria to categorize the swarm to which each dike belongs. In this study, dikes of the Narmada-Tapi swarm only include those dikes observed and sampled north of latitude 20º30' N. We define the coastal swarm as comprising only dikes located to the west of the Panvel flexure that trend N-S ± 20º. The Nasik-Pune swarm is defined as all the dikes east of the Panvel flexure, plus all the dikes west of the flexure that have an orientation departing from N-S by more than 20º. The potential drawback of these criteria is that, for example, dikes that were emplaced as part of the Nasik-Pune swarm and that strike

roughly N-S and are located near the coast are considered as part of the coastal swarm. Similarly, dikes emplaced in the coastal swarm but whose orientation deviates from N-S by > 20º will erroneously be classified as Nasik-Pune dikes. Because of such overlap, no set of classification criteria can be completely satisfying. The criteria used here were designed in the spirit of the original definition of the swarms (Beane *et al*., 1986). In any event, the small number (< 20) of contentious cases is offset by the large size of the data set and is unlikely to affect overall interpretations.

Chemical and isotopic analyses

Major elements in our recently collected samples were measured by XRF on fused disks at the University of Hawai‘i, following Eason & Sinton (2006). Concentrations of trace elements were determined by ICP-MS following a procedure similar to that of Pyle *et al*. (1995) and Neal (2001). Relative errors as two standard deviations range from 1.4% (for Sr) to 7.0% (for Gd). Sample preparation and mass spectrometry for Sr, Nd and Pb isotopic and isotope-dilution measurements were principally carried out at the University of Hawai‘i following Mahoney *et al*. (1991). Analyses were performed on splits prepared from small (1-2 mm) rock chips that were picked to avoid alteration, and acid-cleaned prior to dissolution. Although concentrations of Pb, Sr, Nd and Sm determined by isotope-dilution are generally in good (within 10% or less) agreement with those obtained by other methods on the bulk samples (Rb shows greater variation), the isotope-dilution values are used only for age correction (to 65 Ma) of the Sr and Nd isotope ratios because these concentrations are not strictly representative of the whole-rock concentrations (e.g., as a result of picking). Isotope ratios of a smaller

group of samples were analyzed at the University of Alberta, following Creaser *et al.* (1997); for age-correcting these, we have used the corresponding XRF and ICP-MS concentration data for parent and daughter elements.

Data evaluation procedures and statistical methods

Comparisons of the dikes with the flow formations of the Western Ghats were made combining four different approaches, following Peng *et al*. (1998), Mahoney *et al*. (2000) and Bondre *et al*. (2006): 1) element vs. element and element ratio vs. element ratio plots (involving >850 lava flow analyses for comparison with the dike data), 2) mantle-normalized patterns of selected incompatible element abundances, 3) discriminant-function analysis (DFA) using several major and trace elements and 4) combined Nd, Sr and Pb isotope ratios.

Element plots and mantle-normalized incompatible element patterns were particularly useful when studying the chemical composition of individual samples, but a statistical approach proved more practical to treat our large number of samples in a systematic way. Discriminant-function analysis has proven to be a powerful classification tool for treating large flood-basalt data sets, particularly for working out regional lava chemostratigraphy (e.g., Beane *et al*., 1986; Beane, 1988; Peng *et al*., 1998; Mahoney *et al*., 2000). DFA is a multivariate statistical technique that calculates discriminant functions, group centroids and the Mahalanobis distance of each sample composition to the nearest centroids (e.g., Davis, 2002), concepts that are explained in more detail in Appendix C. In essence, it computes the affinity of an unknown sample to a standard set of known sample groups. The technique, however, has been found to be somewhat

unreliable for samples with transitional chemical characteristics (such as flows near some boundaries between formations; Peng *et al*., 1998). Also, processes such as alteration and, particularly, variable fractional crystallization or flowage differentiation in both flows and dikes can substantially affect the results of a classification. The effects of these processes can be greatly reduced by a careful selection of the variables used in the statistical analysis (Peng *et al*., 1998). Despite of this, DFA and isotopic analyses can sometimes point to conflicting results. Isotope ratios provide the ultimate test for comparing Deccan dike samples with the flow formations because of the limited overlap between the isotopic fields for most of the individual formations in multi-isotope space and because these ratios tend not to be affected much by near-surface magmatic processes or subaerial alteration. For this reason, we consider results of the isotopic analyses to provide more reliable matches than the DFA. However, many more chemical data are available for the Deccan basalts than Nd-Pb-Sr isotopic data.

Discriminant-function analysis was conducted with the SPSS 11.0.4 software for Macintosh (SPSS, Inc.), following the procedure detailed by Peng *et al*. (1998; see also Appendix C) and using an updated 624-sample standard set of major and trace element data for the lava formations. Elements used as variables included the same suite used by Mahoney *et al*. (2000), for repeatability, availability and internal consistency: SiO_2, Al_2O_3, TiO_2, CaO, K_2O, P_2O_5, Ni, Ba, Sr, Zr, Y and Nb. With these parameters, samples known to be from specific flow formations, when treated as unknowns, were correctly predicted (i.e. assigned to the correct formation) 87.8% of the time. The success rate rose to 96.6% when both the first *and* second closest formation matches were considered. Appendix A reports the closest formation match if the squared Mahalanobis distance to

the group centroid is ≤ 25; samples with no match listed are considered to be unclassified because the large Mahalanobis distance indicates an unreliable statistical match (conditional probability less than 1%).

In this study, the DFA standard set was divided into nine individual groups. A given formation is represented by one group, with the exception of the lowermost two formations, the Jawhar and Igatpuri, for which data were merged because of their substantial geochemical similarities (Peng *et al*., 1994). Data for the Panhala flow formation were not included in the standard set, because too few have been analyzed in the literature to be statistically significant in the DFA. To account for the absence of Panhala formation data in the DFA, samples found matching Ambenali, Poladpur or Mahabaleshwar formation (with which the Panhala has the most chemical affinity) compositions where checked individually for compatibility with the Panhala (e.g., Ba<90 ppm, Ba/Y<3, Zr/Nb>13; Lightfoot & Hawkesworth, 1988). Samples from several formation members considered anomalous within their formation (such as the Harischandrigad of the Bushe formation and the Paten Basalt of the Thakurvadi formation) were also not included in the DFA standard set.

RESULTS

Within-dike chemical variation

Although the majority of dikes appear homogeneous at the centimeter scale, a few that we sampled display some degree of macroscopic heterogeneity, most commonly in the form of vertical (i.e., top to bottom) stratification caused by varying amounts of plagioclase (cf. Melluso *et al*., 1999); in one case (the dike from which sample DND-3

came), an uneven distribution of xenoliths was observed (cf. Ray *et al*., 2008). For this reason, along-strike chemical variations were investigated in five localities. Sample NBD-1B was taken 15 km to the east of NBD-1 along the same dike and is nearly identical in chemical and mineralogical composition (Appendix A). Sample NBD-03B was taken 10 km east of sample NBD-03 along the same dike and, with the exception of Cr and Ni, the two have nearly identical mantle-normalized incompatible trace element patterns (Fig. 2.5A). Samples NBD-12 and NBD-21, separated by 11 km, probably belong to the same dike, although it does not crop out continuously between the two sites. The dike is 5.5 m wide, coarser grained, and rich in centimeter-size plagioclase at the site of NBD-21, in contrast to the fine-grained aphyric rock at the NBD-12 site (20 m wide). Despite these differences, these two samples are chemically nearly identical, with only minor variation in the large-ion lithophile elements (LILE) and heavy rare-earth elements consistent with different cooling and crystallization histories. SDPD-2 was sampled 38 km east of SDPD-1 along the same dike, and has a nearly identical chemical signature. UDD-7 is from the same dike as UDD-7B, but 3 km farther north; again, these two samples are almost indistinguishable. These results demonstrate that dikes can be geochemically homogeneous over considerable distances along strike.

Some of the wider dikes, such as the 62-m-thick NBD-24 dike, show signs of multiple injections as evidenced by the presence of multiple pairs of chilled margins within the dike. Samples NBD-37 and NBD-38 were taken from two markedly different (in terms of texture, grain size and crystal content) and adjacent sections across-strike of a single dike displaying signs of multiple injections. The NBD-37 section is 8 m thick; that of NBD-38 is 12 m. Even though they exhibit clear differences in some elements

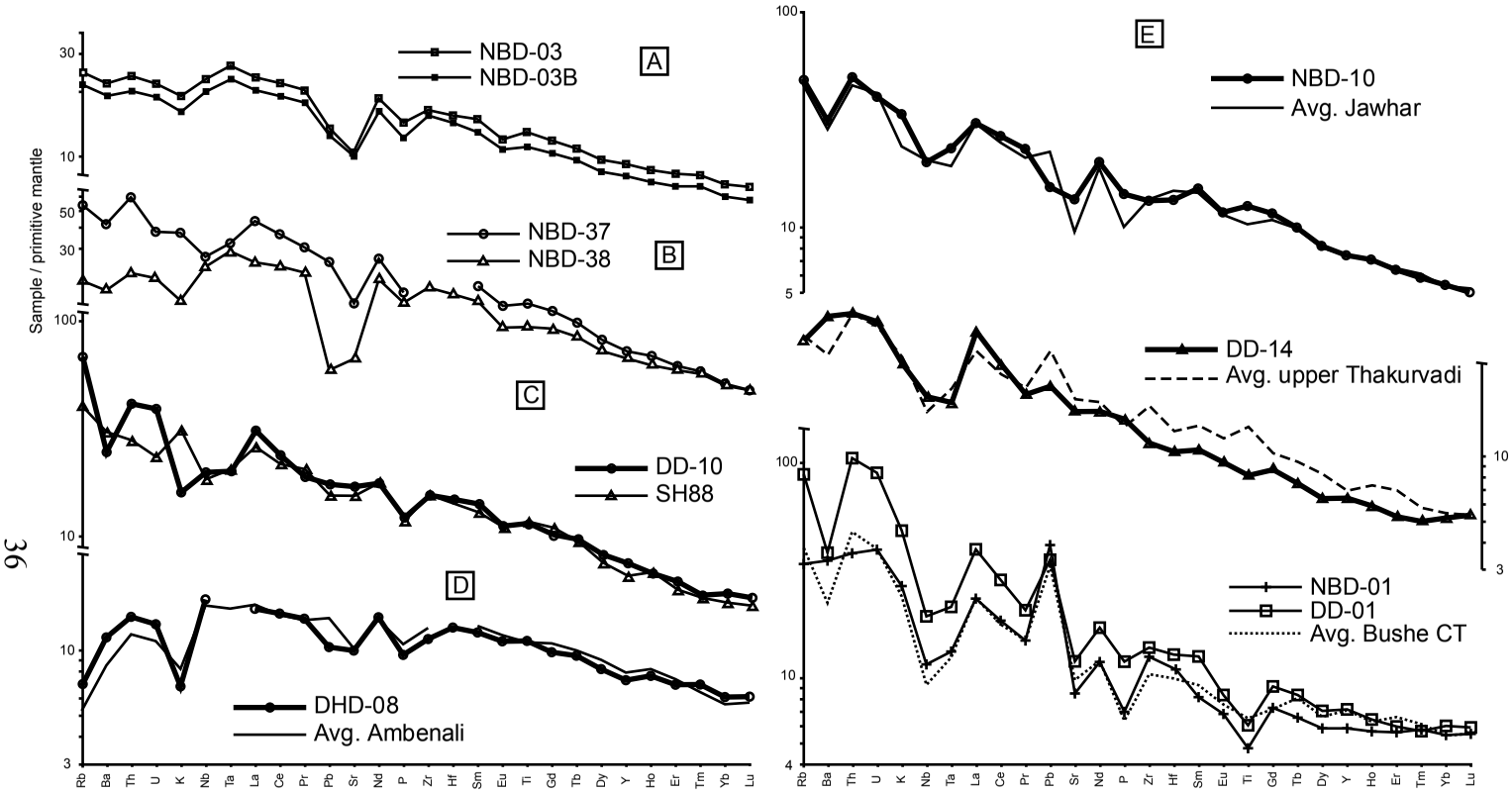

Fig. 2.5: Selected primitive-mantle-normalized patterns of incompatible elements, using the primitive-mantle estimate of Sun & McDonough (1989). Formation and member averages are from data of Beane (1988), Beane *et al*. (1986) and Peng *et al*. (1994). (A) Comparison of patterns of two samples collected along the same dike, 15 km apart. (B) Comparison between two injections in the same dike, normalized to the same Lu value. (C) Comparison between patterns of dike DD-10 of the Narmada-Tapi swarm and sample SH88 from a lava flow of the Toranmal section in the northern Deccan, some 100 km from the DD-10 sample location (Mahoney *et al*., 2000). (D) Comparison between Narmada-Tapi swarm dike DHD-08, which has an Ambenali-like isotopic signature, and the Ambenali formation average. (E) Patterns of dikes of the Narmada-Tapi swarm possessing lower and middle formation-like isotopic signatures are compared with the average pattern of the isotopically relevant formation. Formation averages have been normalized to the same Lu value as the samples for comparison.

(most notably Pb, Sr and LILE), the major and trace element compositions of the two samples are very similar overall, indicating that in this case two magma injections probably occurred close in time, such that similar magma types were injected, but with some differences in source composition and alteration history. Alternatively, dikes may branch and, at a different level, rejoin; the paths of ascent and the cooling histories of magma in different parts of a merged dike may be sufficiently different to generate multiple chilled margins, but the dike would consist of a single magma type (e.g., Pallister, 1981; Delaney & Gartner, 1997; Gudmundsson & Marinoni, 2002). Substantial differences in La/Ta, a ratio unaffected by fractional crystallization, discount the second phenomenon as a plausible explanation in the case of samples NBD-37 and NBD-38. Despite the strong similarities between the geochemical signatures of these two samples, differences in Ta/La (0.045 and 0.064, resp.) cannot be explained by minor differences in alteration and cooling history and require two different magma types to have been injected in the dike, either resulting from melting of slightly different sources or having undergone different degrees of crustal contamination.

Isotopic compositions of Western Ghats flow members

The Western Ghats represent the thickest and best-exposed part of the Deccan and, as a result, the most studied. Lavas of the upper five formations (i.e., Bushe, Poladpur, Ambenali, Mahabaleshwar and Panhala) have been the subject of several isotopic investigations (e.g., Mahoney *et al.* 1982; Cox & Hawkesworth, 1984; 1985; Lightfoot & Hawkesworth, 1988; Lightfoot *et al.*, 1990; Peng *et al.*, 1994). The lower six formations

(i.e., Jawhar, Igatpuri, Neral, Thakurvadi, Bhimashankar and Khandala) have received less attention (Peng *et al*., 1994) and their isotopic composition is less well known.

New Nd, Sr, and Pb isotope ratios were measured on previously uncharacterized flow formation members, as shown in Table 2.2. Fig. 2.6 shows how data for the new samples plot relative to the isotopic fields defined by previous studies. The new data for the Poladpur lie within the field of previous Poladpur data, whereas the boundaries of the Neral and Khandala fields are extended slightly. Those for the Bhimashankar extend the previous field to higher values of $\varepsilon_{Nd}(t)$ and slightly lower $^{206}Pb/^{204}Pb$. The new Bushe data extend the field of the Bushe formation even more, with the Pingalvadi sample displaying the highest $\varepsilon_{Nd(t)}$ measured for the formation (-7.9) and the Shingi Hill sample the lowest (-18.9). The Paten Basalt (thought to be a single flow; Beane, 1988) displays a chemical signature uncharacteristic of other Thakurvadi formation members, with many concentrations and inter-element ratios more typical of the Bushe formation (Beane, 1988); for instance, TiO_2 <1 wt% and Y/Zr >0.23 whereas values between 1.3 and 2.7 wt% and 0.15 and 0.23, respectively, are observed for other members of the Thakurvadi formation. Thus, we expected this member also might be isotopically distinct and, indeed, the isotope ratios of the Paten Basalt sample (JEB-434D) differ considerably from those of other Thakurvadi basalts, broadly resembling Bushe formation values, with $^{206}Pb/^{204}Pb$ = 20.938, $\varepsilon_{Nd(t)}$ = -15.4 and even higher $^{87}Sr/^{86}Sr_{(t)}$ (0.72235) than found among the Bushe basalts. To our knowledge, this $^{87}Sr/^{86}Sr_{(t)}$ ratio is the highest reported for a Deccan basalt. The intercalation of an anomalous Bushe-like flow within an older formation is reminiscent of the anomalously Poladpur-like Harischandrigad member

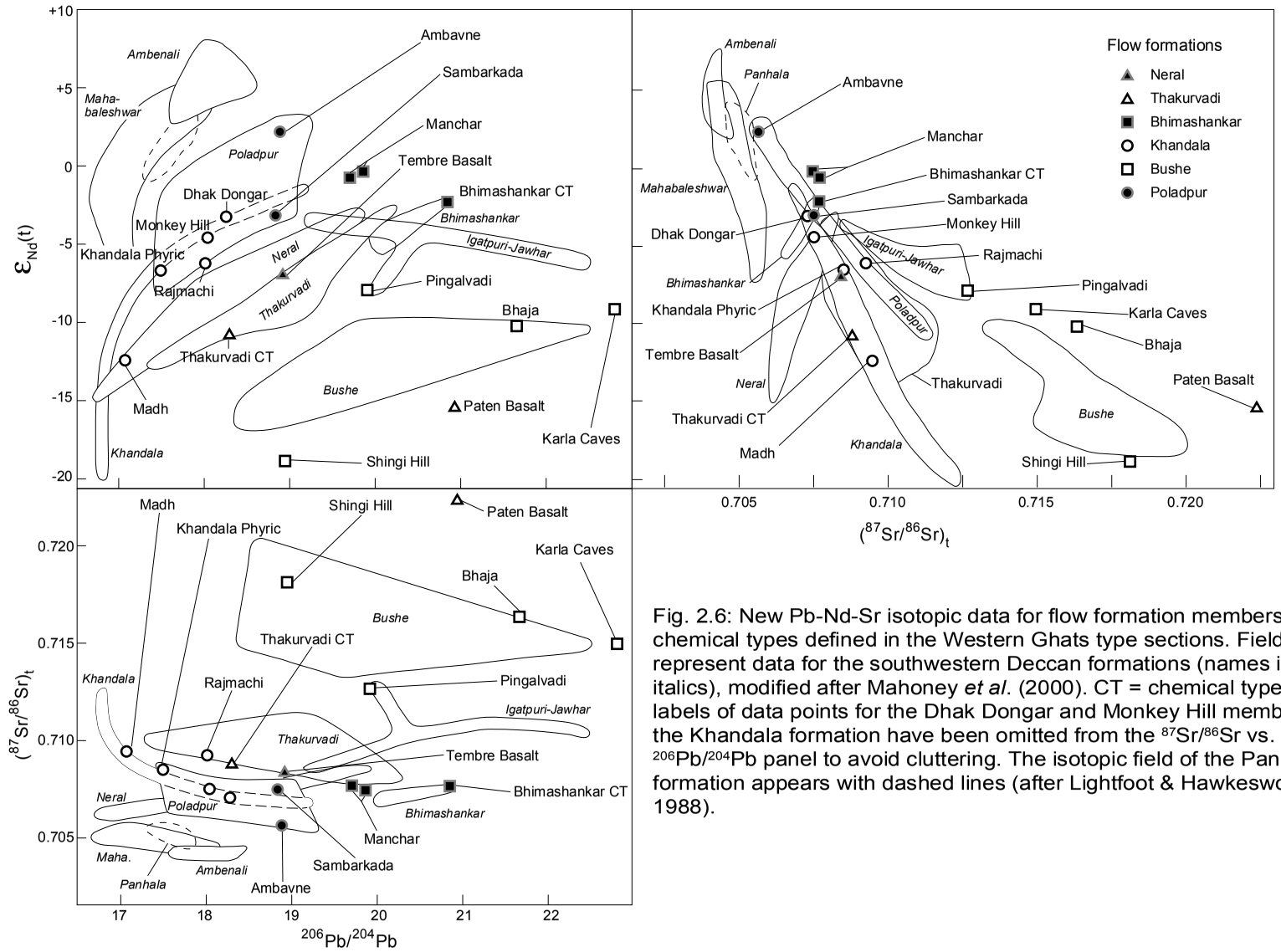

Fig. 2.6: New Pb-Nd-Sr isotopic data for flow formation members or chemical types defined in the Western Ghats type sections. Fields represent data for the southwestern Deccan formations (names in italics), modified after Mahoney *et al*. (2000). CT = chemical type. The labels of data points for the Dhak Dongar and Monkey Hill members of the Khandala formation have been omitted from the $^{87}Sr/^{86}Sr$ vs. $^{206}Pb/^{204}Pb$ panel to avoid cluttering. The isotopic field of the Panhala formation appears with dashed lines (after Lightfoot & Hawkesworth, 1988).

Table 2.2: Isotopic and isotope-dilution data for members of the Western Ghats previously uncharacterized isotopically. The ε_{Nd} and $^{87}Sr/^{86}Sr$ values have been age-corrected to t = 65 Ma. Pb isotope ratios are present-day values, as commonly reported in Deccan literature. Data are reported relative to values of $^{87}Sr/^{86}Sr = 0.710238 \pm 0.000016$ (2σ; n = 39) for standard NBS 987 Sr, $^{143}Nd/^{144}Nd = 0.511843 \pm 0.000009$ (n = 28; 0.2 ε_{Nd} units) for La Jolla Nd, and the Pb isotopic values of Todt *et al.* (1996) for NBS 981 Pb; the 2σ range measured for NBS 981 Pb (n = 44) was ±0.009 for $^{206}Pb/^{204}Pb$, ±0.011 for $^{207}Pb/^{204}Pb$ and ±0.028 for $^{208}Pb/^{204}Pb$. Within-run errors on the isotopic data are less than or equal to the external uncertainties on the standards. Isotope-dilution concentrations (in ppm) have uncertainties of 0.2% for Sm and Nd, 0.4% for Sr and 1% for Pb and Rb. Total procedural blanks were typically ≤25 pg for Pb, <60 pg for Sr, and <10 ng for Nd. Present day $\varepsilon_{Nd} = 0$ corresponds to 143Nd/144Nd = 0.512640; $\varepsilon_{Nd}(t) = 0$ at 65 Ma corresponds to $^{143}Nd/^{144}Nd = 0.512556$. All data were acquired at the University of Hawai‘i.

Table 2.2: Isotopic and isotope-dilution data for new flow members of the Western Ghats

Sample	Formation	Member	$^{87}Sr/^{86}Sr_{(0)}$	$^{87}Sr/^{86}Sr_{(t)}$	$^{143}Nd/^{144}Nd_{(0)}$	$^{143}Nd/^{144}Nd_{(t)}$	$\varepsilon_{Nd}(t)$
Tem-04	Neral	Tembre Basalt	0.70858	0.70844	0.512265	0.512199	-7.0
M-8	Thakurvadi	Thakurvadi CT	0.70903	0.70881	0.512066	0.512004	-10.8
JEB-434	Thakurvadi	Paten Basalt	0.72267	0.72236	0.511829	0.511766	-15.4
M-12	Bhimashankar	Manchar	0.70777	0.70768	0.512591	0.512518	-0.7
M-13	Bhimashankar	Manchar	0.70753	0.70746	0.512607	0.512539	-0.3
CH-24	Bhimashankar	Bhimashankar CT	0.70774	0.70768	0.512506	0.512439	-2.3
KOP-21	Khandala	Monkey Hill	0.70754	0.70751	0.512383	0.512324	-4.5
BOR-4	Khandala	Dhak Dongar	0.70732	0.70710	0.512462	0.512390	-3.2
DDW-13	Khandala	Madh	0.70967	0.70946	0.511981	0.511920	-12.4
JEB-134	Khandala	Khandala Phyric	0.70864	0.70850	0.512290	0.512216	-6.6
JEB-297	Khandala	Rajmachi	0.70948	0.70925	0.512289	0.512238	-6.2
JEB-136	Bushe	Karla Caves	0.71556	0.71496	0.512157	0.512088	-9.1
JEB-185	Bushe	Bhaja CT	0.71659	0.71636	0.512099	0.512032	-10.2
JEB-211	Bushe	Shingi Hill	0.71869	0.71813	0.511646	0.511590	-18.9
JEB-353	Bushe	Pingalvadi	0.71304	0.71268	0.512223	0.512150	-7.9
BEL-13	Poladpur	Ambavne	0.70571	0.70564	0.512742	0.512668	+2.2
JEB-300	Poladpur	Sambarkada	0.70769	0.70749	0.512463	0.512396	-3.1

Table 2.2 (Cont.): Isotopic and isotope-dilution data for new flow members of the Western Ghats

Sample	$^{206}Pb/^{204}Pb$	$^{207}Pb/^{204}Pb$	$^{208}Pb/^{204}Pb$	Pb	Sr	Rb	Nd	Sm	$^{147}Sm/^{144}Nd$	$^{87}Rb/^{86}Sr$
Tem-04	18.923	15.553	39.261	2.51	231.4	12.52	13.14	3.359	0.1545	0.1565
M-8	18.299	15.425	39.295		232.8	19.11	20.20	4.890	0.1464	0.2375
JEB-434	20.938	16.080	40.372	7.55	154.5	18.35	15.67	3.823	0.1474	0.3441
M-12	19.707	15.749	40.417		258.4	8.26	13.87	3.915	0.1706	0.0925
M-13	19.863	15.746	40.291		226.6	6.01	15.29	4.036	0.1596	0.0767
CH-24	20.851	15.922	41.407		244.7	5.96	19.65	5.087	0.1570	0.0702
KOP-21	18.041	15.479	38.647		267.1	3.23	21.70	5.007	0.1395	0.0350
BOR-4	18.263	15.517	38.968		261.0	21.89	16.68	4.640	0.1682	0.2426
DDW-13	17.076	15.439	38.550	3.87	262.7	20.64	19.21	4.526	0.1424	0.2273
JEB-134	17.497	15.46	38.586		260.5	13.46	15.34	4.416	0.1740	0.1495
JEB-297	18.015	15.545	39.281		349.0	39.51	21.74	4.310	0.1199	0.2447
JEB-136	22.807	16.169	41.407	3.12	136.6	31.35	16.38	4.399	0.1623	0.6624
JEB-185	21.663	16.055	40.034	4.65	166.2	14.46	15.44	4.032	0.1578	0.2519
JEB-211	18.949	15.682	40.899	5.86	210.4	44.19	22.92	5.017	0.1323	0.6084
JEB-353	19.915	15.806	39.547	2.76	120.3	16.14	10.89	3.081	0.1709	0.3882
BEL-13	18.890	15.637	39.195	1.75	208.4	6.07	15.18	4.389	0.1748	0.0842
JEB-300	18.837	15.632	39.004	3.62	172.2	12.81	14.57	3.805	0.1579	0.2151

within the Bushe itself (Beane, 1988; Peng *et al*., 1994); such flows pose special challenges in terms of petrogenetic models and stratigraphic correlations.

The coastal dike swarm

Elemental signature and DFA

The coastal dikes comprise two main categories: those of tholeiitic composition and those of lamprophyric and other alkalic compositions. The great majority of the tholeiitic dikes fall within the range of major and trace element compositions observed for flows of the Western Ghats (Fig. 2.7A) and cover most of the Western Ghats compositional spectrum. Along the coast south of Bombay, the lamprophyric dikes cross-cut both the tholeiitic dikes and local flows, indicating they are a late-stage feature (Hooper & Widdowson, submitted).

Results of the DFA (e.g., Fig. 2.8A) show that 43% of the coastal tholeiitic dikes have a strong chemical affinity with the Poladpur, Ambenali (two of the upper formations) or Thakurvadi (a lower formation) formations. Approximately 27% of dikes remain unclassified by the DFA. On the basis of DFA and element vs. element plots (e.g., Ba vs. TiO_2, MgO vs. TiO_2, Sr vs. Zr), Hooper & Widdowson (submitted) note that dikes of the coastal swarm with compositions indistinguishable from those of the Thakurvadi formation (a lower formation) cut across dikes with Poladpur-, Ambenali- and Mahabaleshwar-type (three upper formations) chemical signatures. As these chemically Thakurvadi-like dikes (Fig. 2.9A) cut through flows of the Poladpur, Ambenali and Mahabaleshwar formations, they cannot have been feeders to the Thakurvadi formation and must represent a post-Mahabaleshwar-formation phase of magmatism. It will be

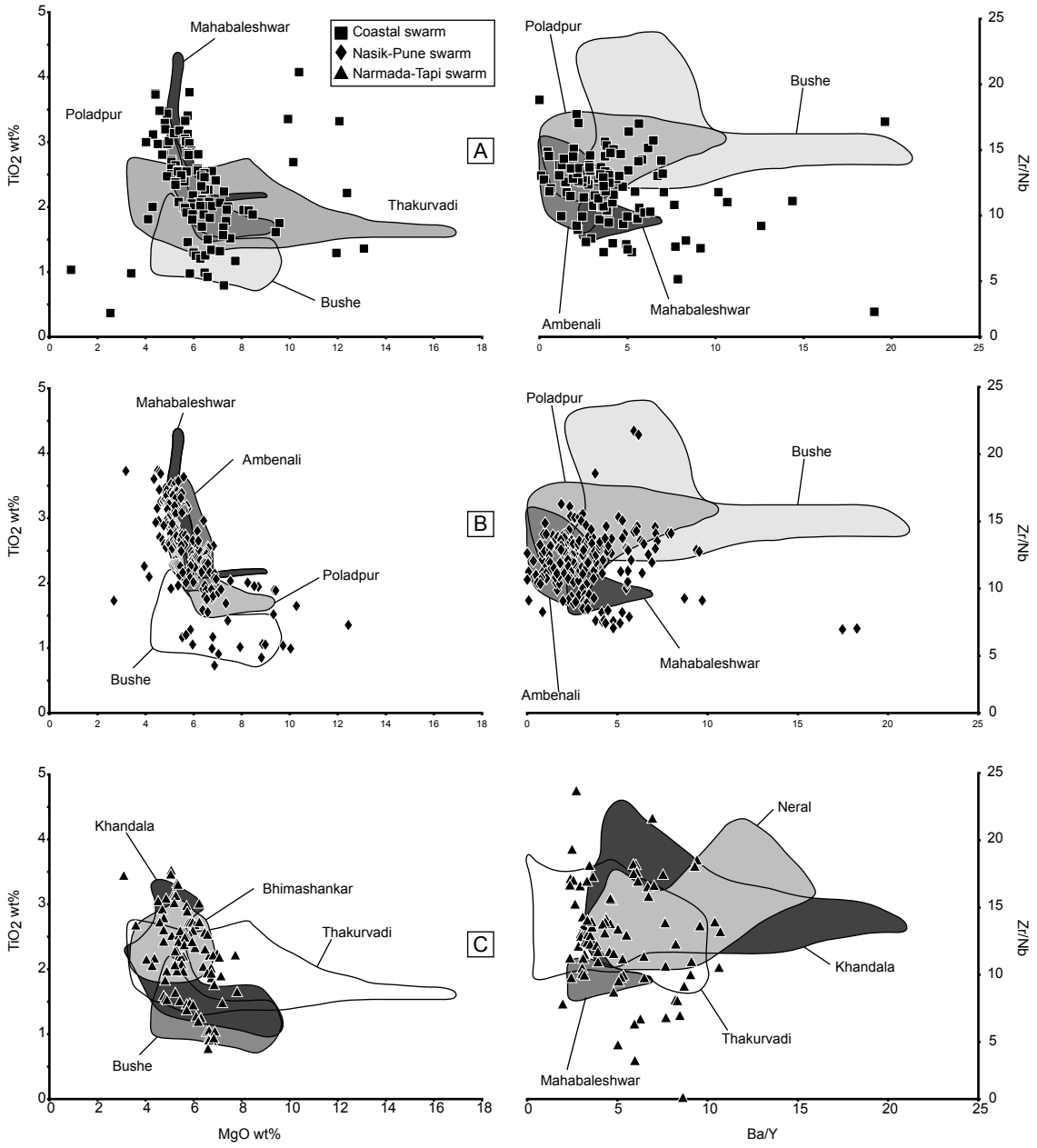

Fig. 2.7: Harker diagrams of some major and trace element ratios commonly used (e.g., Beane *et al*., 1986; Lightfoot & Hawkesworth, 1988) to help discriminate among Deccan flow formations of the Western Ghats. Fields enclose data of the respective formations (after Beane, 1988; Beane *et al*., 1986; Peng *et al*., 1994). (A) Dikes of the coastal swarm. (B) Dikes of the Nasik-Pune swarm. (C) Dikes of the Narmada-Tapi swarm. Some fields have been omitted for clarity.

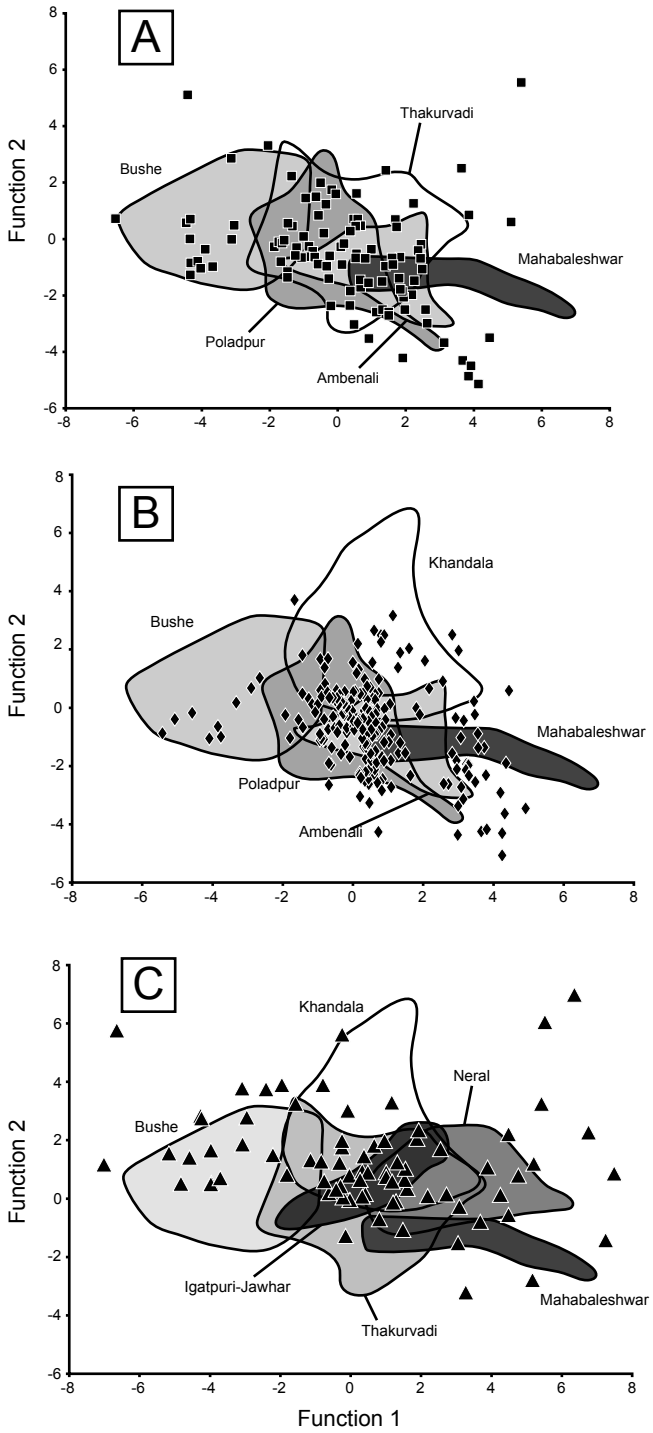

Fig. 2.8: Values of the first two canonical discriminant functions for Deccan dikes are shown with the fields of the Western Ghats lava formations (some fields have been omitted for clarity). Symbols as in Fig. 2.5. (A) Dikes of the coastal swarm; (B) dikes of the Nasik-Pune swarm; (C) dikes of the Narmada-Tapi swarm. Function 1 = $-0.48SiO_2 - 0.155Al_2O_3 + 1.289TiO_2 + 0.157CaO + 0.097K_2O + 1.397P_2O_5 - 0.048Ni + 0.462Ba + 0.301Sr - 1.707Zr - 0.744Y - 0.002Nb$. Function 2 = $0.145SiO_2 + 0.135Al_2O_3 - 0.141TiO_2 - 0.251CaO - 0.286K_2O + 0.439P_2O_5 + 0.058Ni + 0.953Ba - 0.247Sr + 0.815Zr + 0.039Y - 1.215Nb$.

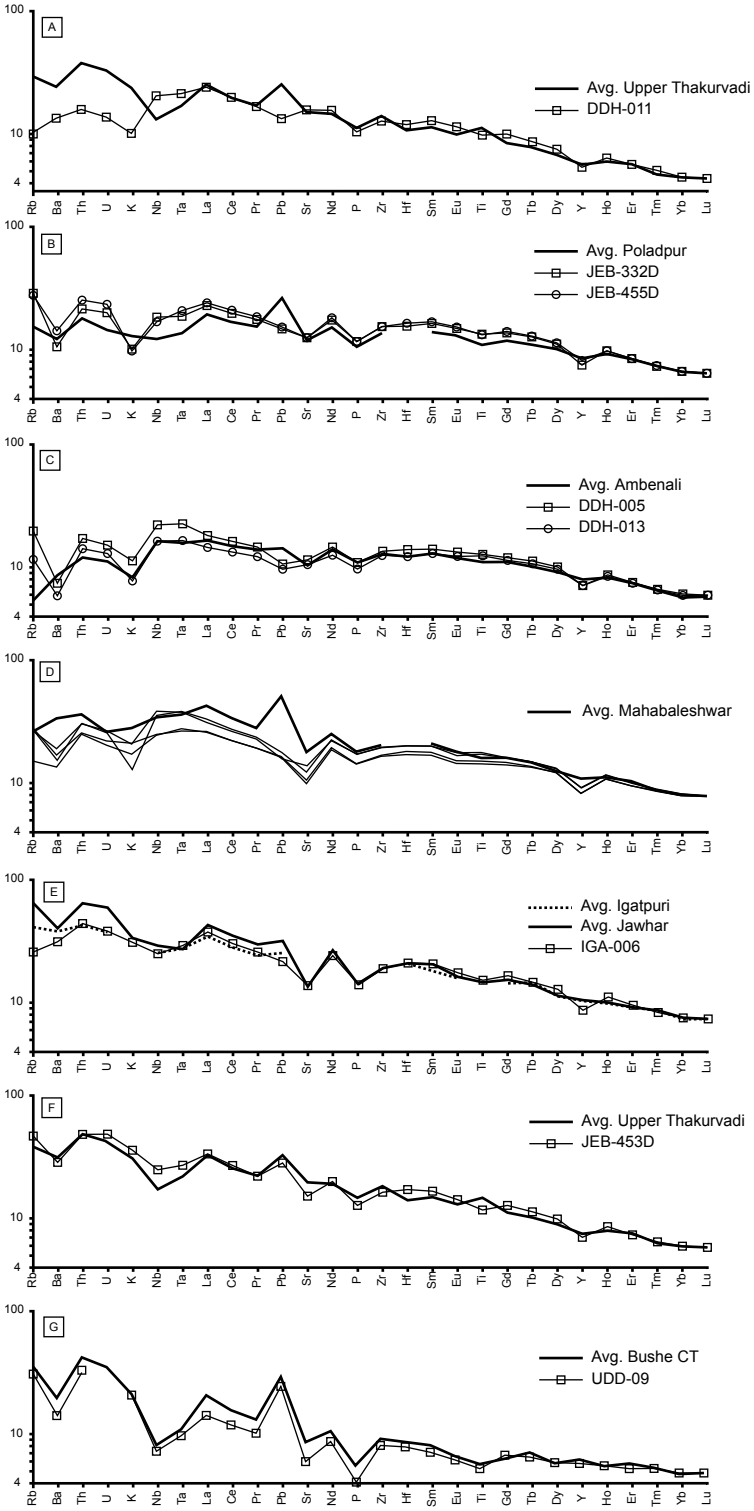

Fig. 2.9: Comparison between the primitive-mantle-normalized patterns of incompatible elements of dike samples geochemically similar to Deccan lava formations. Normalizing primitive-mantle values and formation member averages are as in Fig. 2.7. Formation averages and samples have been normalized to the same Lu value for comparison. In panel (D), the names of the Mahabaleshwar-like samples (BOR-20, DDH-030, DDH-039 and JEB-396D) have been omitted for clarity.

shown in the next section, however, that these dikes' chemical affinity for the Thakurvadi formation does not translate in the isotope space.

Our DFA also shows that dikes with affinities with the lower or middle formations (excluding the Thakurvadi formation matches mentioned above), although rarer (27%), tend to occur preferentially in the Konkan plain (Fig. 1.2) at some distance from the coast north-east of Bombay, whereas upper-formation-like dikes are generally found along the coast south of Bombay. The remaining 3% are classified as Mahabaleshwar by the DFA.

Isotopic signature

Sixteen tholeiitic samples from the coastal swarm were selected for isotopic analysis (Fig. 2.10). Two samples from the coast near Goa, ~70 km to the southwest of the current boundary of the flood basalts, were analyzed isotopically, to test Widdowson *et al.*'s (2000) hypothesis that some of these dikes might represent feeders of the upper lava formations. One sample, IND-005, is chemically similar to both the upper formations of Ambenali and Poladpur (with Ba, TiO_2 and MgO levels closer to those typical of the Poladpur, but Ba/Y and Zr/Nb closer to typical Ambenali values). Its isotope ratios, however, are unequivocally Poladpur-like. The other sample, ORL-005, has low Sr, Ba and Zr concentrations rarely observed in Deccan flows, except those of the Panhala formation (Lightfoot & Hawkesworth, 1988; Lightfoot *et al.*, 1990). Isotope ratios for this sample fall within the uppermost Panhala formation field (which is enclosed in the Mahabaleshwar field; Fig. 2.6), at the boundary with the field of the Ambenali formation. On the basis of these results, it is probable that dikes in the Goa region indeed acted as feeders to some of the flows of the Poladpur and Panhala

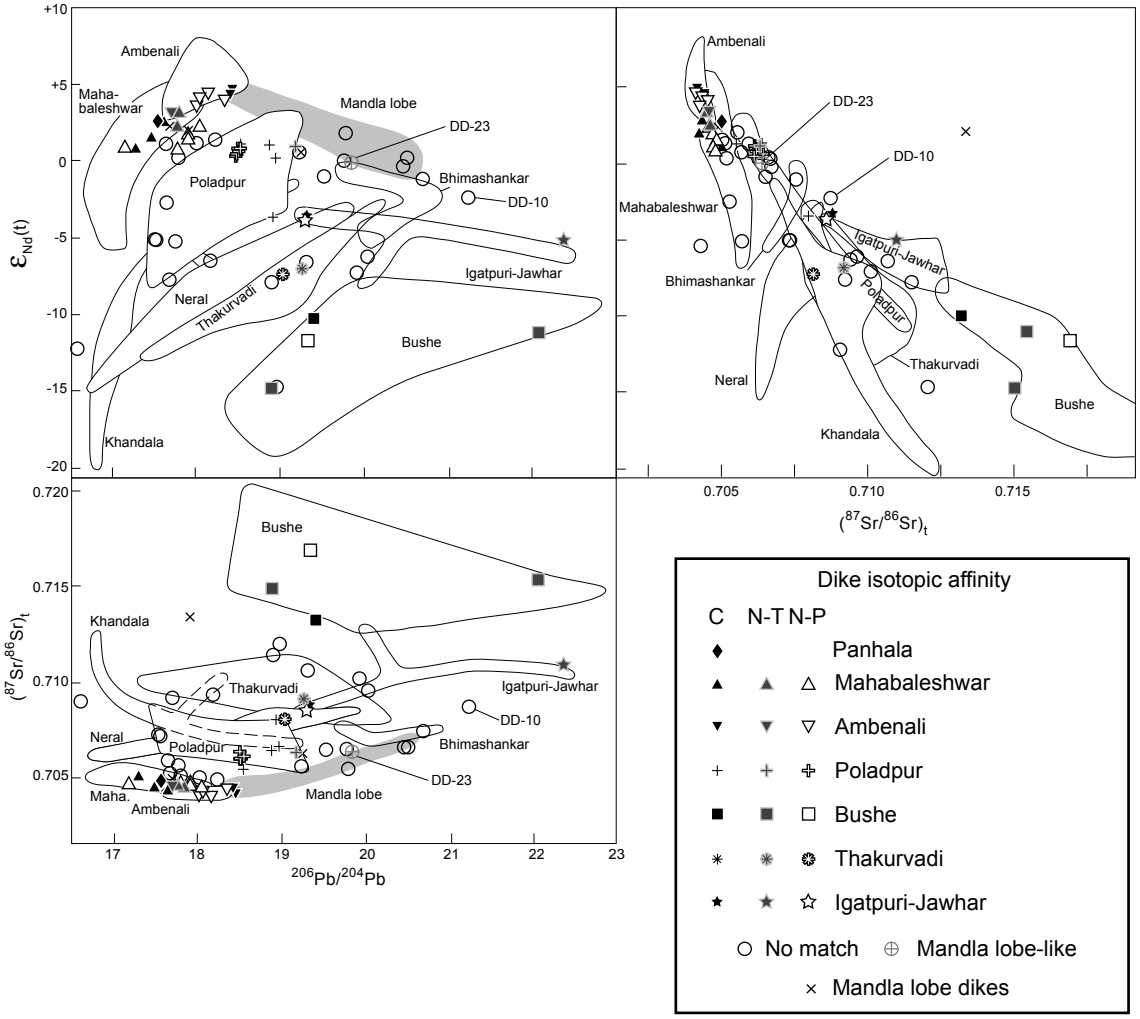

Fig. 2.10: Pb-Nd-Sr isotopic data for Deccan dikes. Fields represent data of the southwestern Deccan flow formations (after Peng *et al*., 1998; Mahoney *et al*., 2000) modified according to Fig. 2.6. Black symbols correspond to the coastal swarm (C), gray symbols to the Narmada-Tapi swarm (N-T), and open symbols to the Nasik-Pune swarm (N-P). The gray-shaded field encompasses data for the Mandla lobe (Peng *et al*., 1998). Data for dikes of the Mandla lobe (crosses) are from J. Mahoney (unpublished data).

formations. Lavas of the Panhala, in particular, are found only in the extreme southwestern Deccan, relatively near (~135 km) the Goa-area dikes.

The majority (eight) of the remaining coastal-swarm dikes that we analyzed isotopically can be matched with the three main upper lava formations (three with Poladpur, two with Ambenali, three with Mahabaleshwar), in good agreement with their major and trace element characteristics (Figs. 2.9C and 2.9D). These dikes are located along the coast north and south of Bombay and in the Konkan plain north-east of Bombay. We interpret them as probable feeders for the upper formations.

The Konkan plain (Fig. 1.2) east and north-east of Bombay exposes the lowermost known parts of the Deccan lava stratigraphy (Beane *et al*., 1986); thus, this area (~75 x 130 km^2) is one where feeders for the lower formations might be exposed. One coastal-swarm dike in this area (JW-32) was found to have a chemical and isotopic signature that closely resembles the signature of the lowermost Igatpuri-Jawhar formations (specifically, the Plagioclase Phyric member of the Jawhar formation). Another (DDH-036) has unmistakable Bushe-type (a middle formation) isotope ratios and major and trace element compositions. These two dikes are part of a set of a dozen sampled dikes in this area with major and trace element affinities to the lower and middle formations, particularly the Igatpuri-Jawhar, Thakurvadi and Bushe. Nevertheless, possible feeder dikes for the lower and middle formations remain rare, at least partly because younger-formation flows cover much of the oldest part of the stratigraphy.

Finally, four dikes, three of which have major and trace element patterns matching those of members of the Thakurvadi, Bushe and Poladpur formations, have isotope ratios unlike those of any formation. One such dike (DDH-11) belongs to the late-stage,

chemically Thakurvadi-like group mentioned above that cuts across dikes with upper-formation characteristics. The timing of emplacement of the other three dikes is currently unknown.

The Nasik-Pune swarm

Elemental signature and DFA

In contrast to the coastal and Narmada-Tapi swarms, all the dikes sampled in the Nasik-Pune swarm are tholeiitic. The great majority (88%) have major and trace element signatures similar to those of Western Ghats flows (Fig. 2.7B), as Beane *et al*. (1986) and Beane (1988) suggested from their reconnaissance study. Results of our DFA confirm that the chemical similarities are generally strong (Fig. 2.7B). The Nasik-Pune swarm also displays the smallest proportion of unclassified cases among the three swarms, with only 12% of 196 samples yielding Mahalanobis distances >25. Over 55% of the classified cases match the signatures of formations of the Wai subgroup (Fig. 2.11) of the upper lava stratigraphy. Thakurvadi- and Khandala-like (a lower and middle formation, respectively) signatures are also widely represented.

Beane *et al*. (1986) and Hooper (1990) noted that when treated as a whole, strikes of the Nasik-Pune swarm dikes are nearly random, showing only a weak preferred NNE orientation (Fig. 2.1). Deshmukh & Sehgal (1988) and Bondre *et al*. (2006) additionally pointed out that some portions of the Nasik-Pune swarm exhibit well-defined orientations at the local scale. Our results confirm Beane *et al*. (1986) and Hooper's (1990) observations (Figs. 2.12B and 2.12G), but also reveal an important difference in dike orientation with dike composition (Figs. 2.12D, E, F and G): the dikes with Wai-

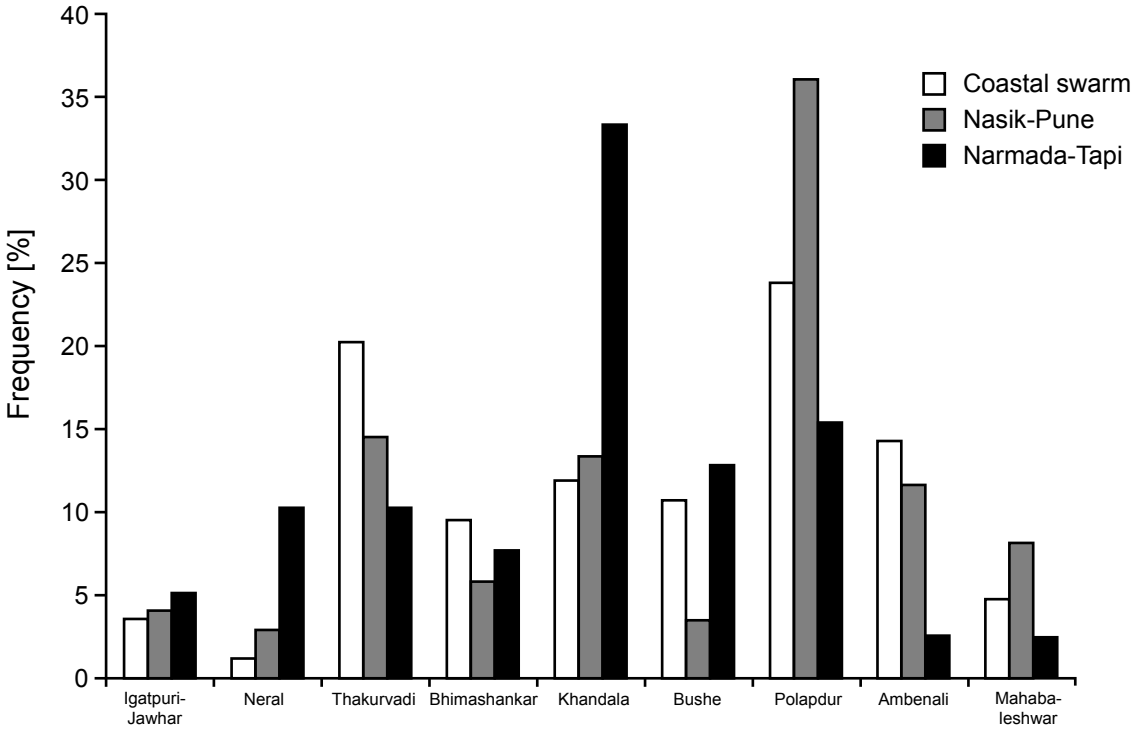

Fig. 2.11: Histogram of formational matches determined by DFA for each dike system, illustrating the affinity of each swarm for specific formations. Formations are in stratigraphic order from lower (left) to upper (right) formations from left to right. Note the chemical affinity for the upper formations of the coastal and Nasik-Puneswarms, which is not oberved in the Narmada-Tapi swarm. Unclassified cases are not included.

Fig. 2.12: (A-F) Rose histograms of dike strikes. The number of samples included in the histogram is indicated by n. (A) Dikes of the coastal swarm. (B) Dikes of the Nasik-Pune swarm. (C) Dikes of the Narmada-Tapi swarm. (D) Dikes of the Nasik-Pune swarm that are matched by DFA to formations of the Wai subgroup. (E) Dikes of the Nasik-Pune swarm matched by DFA to the Ambenali and Mahabaleshwar formations. (F) Dikes of the Nasik-Pune swarm matched by DFA to formations of the Kalsubai subgroup. (G) "Box and whiskers" diagram of dike strike data. All data are included between the short vertical lines, which represent the minimum and maximum values observed (whiskers), whereas the gray rectangles encompass data within the 25% and 75% percentiles; i.e., each box represents the median percentages of the dataset. Thick tick marks represent the averages. In the scale at the top of the figure, zero indicates due north; i.e., dikes striking N-S. Data are broken down by swarm and chemical affinity. From top to bottom: dikes of the coastal swarm; the Nasik-Pune swarm; the Narmada-Tapi swarm; dikes of the Nasik-Pune swarm matched by DFA with formations of the Wai subgroup, higher in the stratigraphy (Poladpur, Ambenali, Mahabaleshwar); dikes of the Nasik-Pune swarm matched by DFA with formations of the Kalsubai subgroup, lower in the stratigraphy (Jawhar, Igatpuri, Neral, Thakurvadi, Bhimashankar) ; dikes of the Nasik-Pune swarm unclassified by DFA; dikes of the Nasik-Pune swarm matched to the Ambenali and Mahabaleshwar formations by DFA; dikes in both the coastal and Nasik-Pune swarms matched to formations of the Wai subgroup by DFA.

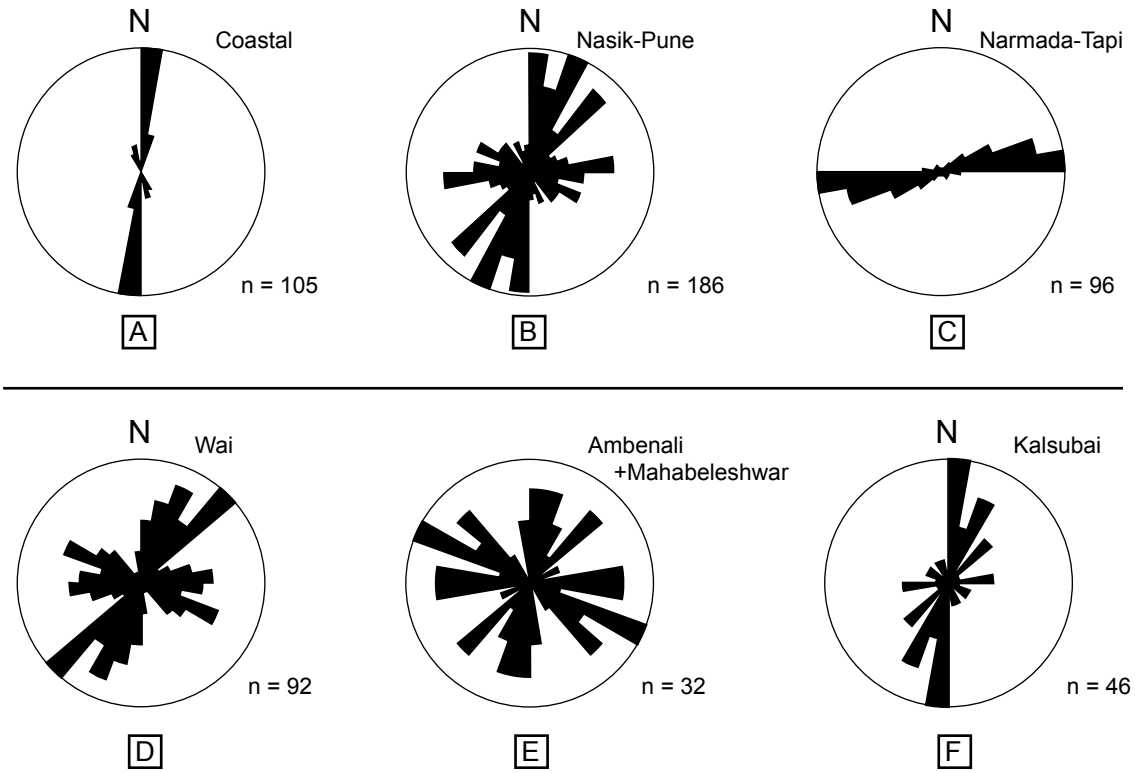
N
Coastal
n = 105
A
N
Nasik-Pune
n = 186
B
N
Narmada-Tapi
n = 96
C
N
Wai
n = 92
D
Ambenali
+Mahabeleshwar
n = 32
E
N
Kalsubai
n = 46
F

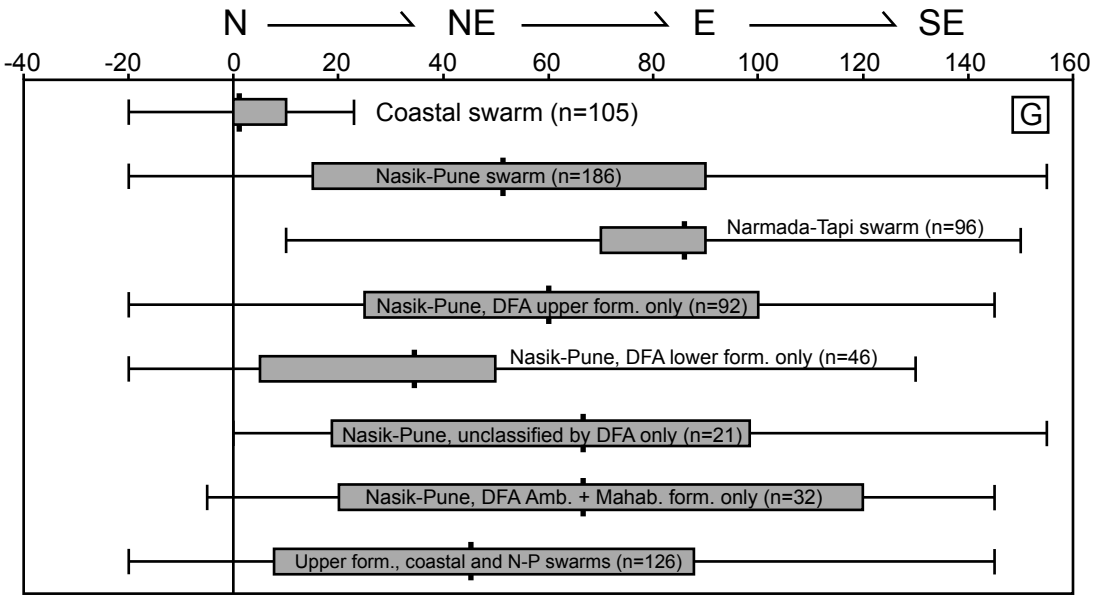
N
NE
E
SE
-40
-20
0
20
40
60
80
100
120
140
160
Coastal swarm (n=105)
G
Nasik-Pune swarm (n=186)
Narmada-Tapi swarm (n=96)
Nasik-Pune, DFA upper form. only (n=92)
Nasik-Pune, DFA lower form. only (n=46)
Nasik-Pune, unclassified by DFA only (n=21)
Nasik-Pune, DFA Amb. + Mahab. form. only (n=32)
Upper form., coastal and N-P swarms (n=126)

subgroup-like signatures display two or three dominant orientations (Figs. 2.12D and G); however, when considering only the dikes matched by the DFA to the Ambenali and Mahabaleshwar (i.e., upper) formations, the directional pattern appears roughly random (Figs. 2.12E and G). The Kalsubai-subgroup-like dikes in the swarm, on the other hand, display a strong N-S orientation (Figs. 2.12F and G).

Isotopic signature

We analyzed the Sr, Nd and Pb isotope ratios of 35 samples from the Nasik-Pune swarm (Fig. 2.10). Fourteen were found to fall within the isotopic fields of the Poladpur (5 matches), Ambenali (3 matches), or Mahabaleshwar (5 matches, and one sample that falls within the space where Mahabaleshwar and Ambenali data overlap) formations. These isotopic matches are generally in good agreement with the samples' elemental affinities (e.g., Figs. 2.9B, C and D). In two chemically borderline cases, BOR-013 and BOR-014, which share many characteristics with the Mahabaleshwar formation but also diverge from it (with Sr<250 ppm and Ba/Y<3.5, whereas most Mahabaleshwar lavas have Sr>250 ppm and Ba/Y>4), close isotopic matches to the Mahabaleshwar formation were found. Indeed, in all but three cases (JEB-182D, JEB-393D and JEB-438D), samples matched with the upper formations by the DFA also yielded the corresponding upper-formation-type isotope ratios. We conclude that the majority of dikes with upper-formation chemical affinities sampled in the Nasik-Pune swarm acted as feeders for these formations.

Fourteen of the 21 remaining samples analyzed isotopically exhibit a chemical resemblance (ranging from close to distant) to formations of the Kalsubai or Lonavala

subgroups. Interestingly, the isotopic characteristics of these dikes generally do not match those of any of the formations defined in the type sections of the Western Ghats. There are only three exceptions, for which both isotopic and elemental characteristics are in agreement: one dike has an Igatpuri-Jawhar-type signature (more specifically, it resembles the Plagioclase Phyric member of the Jawhar formation: IGA-006; Fig. 2.9E), one a Thakurvadi-type signature (JEB-453D; Fig. 2.9F), and one a Bushe-type signature (UDD-09; Fig. 2.9G). We infer that, despite dikes of the Nasik-Pune swarm possessing major and trace element characteristics resembling those of the lower and middle formations (i.e., from Jawhar to Bushe), they are unlikely to be feeders for these formations. Some of these dikes may have fed flows that are not exposed or have not yet been sampled; others may represent "dead-end" intrusions that did not result in eruptions.

The Narmada-Tapi swarm

Elemental signature and DFA

The Narmada-Tapi swarm shows greater chemical variability than observed in the other two swarms. This is due to the fairly fractionated nature of some of the dikes (e.g., DD-05, NBD-30; Melluso *et al*., 1999), to the abundant presence of basalts with low (<1.5 wt%) TiO_2 concentrations (typical of the Bushe formation and some members of the Khandala and Neral formations), and to a greater presence of alkalic dikes.

Because of these factors, Narmada-Tapi dike chemical compositions compare rather poorly as a group with those of the Western Ghats formations. The results of our DFA (Fig. 2.8C) show that 56% of cases have Mahalanobis distances >25 from the statistically closest formation match.

The remaining 44% of cases (39 out of 89) can be matched principally with the lower and middle formations (from Jawhar to Bushe) (Fig. 2.11); such dikes outnumber dikes matched with formations of the Wai subgroup (Poladpur through Panhala formations) by 4:1. This result is in sharp contrast to the coastal and Nasik-Pune swarms, for which most DFA matches are with the three main upper formations (Poladpur, Ambenali and Mahabaleshwar). The DFA also assigns twice as many Narmada-Tapi samples to the Khandala formation as to any other.

Sample DD-10 is worth special mention, as it is classified as Bhimashankar by the DFA but is rather distinct from the Bhimashankar formation in having higher Ba and Sr concentrations. However, it is chemically similar to broadly Bhimashankar-like flows near the locality of Mhow (Fig. 2.1) in the northern Deccan. (Peng *et al.*, 1998) and, for most of the incompatible elements, nearly identical (except for the mobile LILE) to a Bhimashankar-like flow in the northern Deccan near Toranmal (Mahoney *et al.*, 2000) (Figs. 2.1 and 2.5C).

Isotopic signature

Isotope ratios were measured for 14 samples from the Narmada-Tapi swarm (Table 2.3; Fig. 2.10). Of these, data for four fall outside the isotopic fields defined by the Western Ghats formations (Table 2.1). Four can be matched isotopically to one of the lower or middle formations (one to the Igatpuri-Jawhar, one to the Thakurvadi, two to the Bushe), and have trace element patterns that broadly support the affiliation based on the isotopic results (Fig. 2.5E), despite the failure of the DFA to match them with any Western Ghats formations. Four samples that share chemical similarities with the upper

Table 2.3: Isotopic and isotope-dilution data for dikes. Nasik-Pune is abbreviated as N-P and Narmada-Tapi as N-T. Most dike samples were analyzed in lab "UH" (University of Hawai'i); standard values and errors are the same as in Table 2.2. Analyses in lab "UA" were performed at the University of Alberta. Age-corrections for these samples use parent-daughter ratios determined from XRF and ICP-MS concentration values. Errors (2σ) on UA sample measurements are ±0.00002 for Sr, ±0.000009 (0.2 ε_{Nd} units) for Nd, ±0.011 for $^{206}Pb/^{204}Pb$, ±0.012 for $^{207}Pb/^{204}Pb$ and ±0.012 for $^{208}Pb/^{204}Pb$. "SIO" indicates a sample analyzed at the Scripps Institution of Oceanography, for which analytical methods are presented by Mahoney (1984) and Mahoney *et al*. (1982); errors for this sample are 0.00003 for $^{87}Sr/^{86}Sr$ and +0.3 ε_{Nd} units.

Sample	Lab	Swarm	$^{87}Sr/^{86}Sr_{(0)}$	$^{87}Sr/^{86}Sr_{(t)}$	$^{143}Nd/^{144}Nd_{(0)}$	$^{143}Nd/^{144}Nd_{(t)}$	$\varepsilon_{Nd}(t)$	$^{206}Pb/^{204}Pb$	$^{207}Pb/^{204}Pb$	$^{208}Pb/^{204}Pb$	Pb	Sr	Rb	Nd	Sm
AL82-12	SIO	Coast		0.70444		0.512794	+4.6					195.5	5.64	16.81	4.95
DDH-011	UA	Coast	0.70439	0.70434	0.512337	0.512269	-5.6	16.342	15.149	36.793					
DDH-015	UA	Coast	0.70538	0.70531	0.512461	0.512418	-2.7	17.640	15.366	38.010					
DDH-030	UH	Coast	0.70506	0.70505	0.512668	0.512600	+0.8	17.267	15.335	38.035	2.21	180.7	0.81	22.45	5.955
DDH-034	UH	Coast	0.70669	0.70665	0.512642	0.512567	+0.2	18.941	15.637	40.003	0.97	148.0	2.23	11.13	3.239
DDH-036	UH	Coast	0.71366	0.71327	0.512105	0.512036	-10.2	19.389	15.752	39.617	3.26	143.9	20.7	12.60	3.399
DDH-039	UH	Coast	0.70480	0.70455	0.512706	0.512638	+1.6	17.451	15.378	38.139	2.66	191.6	18.1	29.48	7.817
DDH-040	UH	Coast	0.70458	0.70437	0.512758	0.512690	+2.6	17.617	15.389	38.117	2.23	210.5	16.2	27.15	7.207
DDH-095	UH	Coast	0.70677	0.70650	0.512629	0.512561	+0.1	19.754	15.741	40.148	2.47	195.6	19.9	24.49	6.481
DDH-116	UH	Coast	0.70429	0.70423	0.512873	0.512798	+4.7	18.421	15.536	38.822	1.19	205.9	4.33	18.07	5.257
IND-005	UH	Coast	0.70560	0.70542	0.512684	0.512614	+1.1	18.526	15.594	39.012	1.87	176.1	11.8	19.39	5.282
JH-35	UH	Coast	0.70459	0.70452	0.512864	0.512783	+4.4	18.404	15.557	38.891	0.90	111.7	2.98	10.83	3.400
JH-40	UH	Coast	0.70665	0.70647	0.512688	0.512614	+1.1	18.861	15.638	39.104	2.95	152.8	10.7	17.93	5.168
JH-48	UH	Coast	0.70829	0.70803	0.512437	0.512371	-3.6	18.907	15.622	39.656	2.97	215.2	23.4	21.28	5.506
JH-72	UH	Coast	0.71059	0.71018	0.512254	0.512186	-7.2	19.902	15.835	40.598	2.58	113.5	17.3	12.42	3.270
JW-32	UH	Coast	0.70936	0.70886	0.512439	0.512376	-3.5	19.297	15.727	40.259	3.62	223.1	39.7	30.14	7.433
ORL-5	UH	Coast	0.70499	0.70496	0.512766	0.512691	+2.6	17.551	15.398	38.297	0.72	106.3	1.82	8.380	2.436
AM-2	UH	N-P	0.70414	0.70407	0.512861	0.512788	+4.5	18.142	15.467	38.509	0.91	203.4	4.75	18.35	5.214
AM-30	UA	N-P	0.70938	0.70920	0.512243	0.512164	-7.6	17.677	15.600	38.631					
BOR-13	UH	N-P	0.70486	0.70467	0.512713	0.512647	+1.8	17.898	15.446	38.335	2.65	228.9	16.4	30.38	7.799
BOR-14	UA	N-P	0.70489	0.70479	0.512704	0.512630	+1.4	17.898	15.454	38.369					
BOR-20	UA	N-P	0.70466	0.70452	0.512747	0.512671	+2.2	18.031	15.471	38.520					
BOR-29	UH	N-P	0.70620	0.70614	0.512669	0.512599	+0.8	18.528	15.59	39.218	2.13	226.9	4.6	22.80	6.198
DDH-5	UA	N-P	0.70435	0.70421	0.512828	0.512747	+3.7	18.000	15.465	38.502					

Table 2.3 (Cont.): Isotopic and isotope-dilution data for dikes.

Sample	Lab	Swarm	$^{87}Sr/^{86}Sr_{(0)}$	$^{87}Sr/^{86}Sr_{(t)}$	$^{143}Nd/^{144}Nd_{(0)}$	$^{143}Nd/^{144}Nd_{(t)}$	$\varepsilon_{Nd}(t)$	$^{206}Pb/^{204}Pb$	$^{207}Pb/^{204}Pb$	$^{208}Pb/^{204}Pb$	Pb	Sr	Rb	Nd	Sm
DDH-13	UH	N-P	0.70454	0.70451	0.512841	0.512767	+4.1	18.332	15.567	38.693	1.19	194.1	2.66	15.67	4.603
DDH-081	UH	N-P	0.70616	0.70608	0.512671	0.512601	+0.9	18.499	15.565	39.143	2.18	241.2	6.89	22.99	6.276
DDH-089	UH	N-P	0.70556	0.70550	0.512726	0.512655	+1.9	19.779	15.710	39.925	0.88	173.2	3.56	12.26	3.383
IGA-6	UH	N-P	0.70865	0.70854	0.512429	0.512364	-3.8	19.281	15.719	40.227	3.35	249.2	10.4	29.61	7.463
IGA-13	UH	N-P	0.70657	0.70647	0.512577	0.512508	-0.9	19.517	15.723	40.033	2.00	232.4	8.39	21.22	5.666
IGA-19	UA	N-P	0.71215	0.71204	0.511870	0.511804	-14.7	18.951	15.547	38.793					
JEB-008	UA	N-P	0.70480	0.70470	0.512681	0.512604	+0.9	17.152	15.314	37.785					
JEB-016	UA	N-P	0.70752	0.70728	0.512370	0.512297	-5.1	17.517	15.466	38.515					
JEB-182	UA	N-P	0.70516	0.70508	0.512693	0.512620	+1.2	18.007	15.470	38.372					
JEB-284	UA	N-P	0.70751	0.70729	0.512368	0.512295	-5.1	17.528	15.462	38.517					
JEB-327	UA	N-P	0.70759	0.70733	0.513675	0.513603	+20.4	17.521	15.475	38.591					
JEB-332	UA	N-P	0.70624	0.70608	0.512657	0.512579	+0.4	18.485	15.558	39.094					
JEB-333	UA	N-P	0.70914	0.70903	0.512005	0.511930	-12.2	16.580	15.405	37.911					
JEB-393	UA	N-P	0.70699	0.70668	0.512619	0.512544	-0.2	20.448	15.844	40.947					
JEB-396	UA	N-P	0.70490	0.70474	0.512668	0.512593	+0.7	17.775	15.344	38.075					
JEB-397	UH	N-P	0.70524	0.70514	0.512633	0.512572	+0.3	17.781	15.453	38.576	2.29	321.1	12.2	26.35	6.268
JEB-426	UH	N-P	0.70509	0.70496	0.512694	0.512632	+1.5	18.217	15.489	38.692	2.82	305.7	14.4	33.48	8.031
JEB-438	UH	N-P	0.70688	0.70665	0.512637	0.512570	+0.3	20.499	15.834	40.458	2.59	184.4	16.1	25.83	6.765
JEB-442	UH	N-P	0.70578	0.70565	0.512660	0.512591	+0.7	19.226	15.653	39.461	1.43	239.3	11.9	17.75	4.786
JEB-453	UA	N-P	0.70835	0.70809	0.512251	0.512181	-7.3	19.025	15.551	39.175					
JEB-455	UA	N-P	0.70642	0.70642	0.512662	0.512584	+0.5	18.493	15.576	39.163					
JH-20	UH	N-P	0.70821	0.70752	0.512562	0.512497	-1.2	20.683	15.893	41.129	4.20	203.1	52.0	40.46	10.225
JH-22	UH	N-P	0.70632	0.70612	0.512659	0.512589	+0.6	18.489	15.575	39.144	2.52	231.0	17.7	23.82	6.497
JH-25	UH	N-P	0.71166	0.71148	0.512217	0.512155	-7.8	18.893	15.722	40.272	3.81	247.1	16.6	24.08	5.844
JH-28	UH	N-P	0.70435	0.70432	0.512849	0.512774	+4.2	18.041	15.473	38.454	1.19	171.3	2.34	15.39	4.514
TRM-59	UH	N-P	0.70574	0.70566	0.512355	0.512292	-5.2	17.754	15.343	37.939	2.29	306.3	9.07	21.49	5.256
UDD-9	UH	N-P	0.71712	0.71691	0.512030	0.511960	-11.6	19.323	15.732	38.794	6.79	97.22	7.74	10.08	2.749
DD-1	UH	N - T	0.71606	0.71537	0.512047	0.511990	-11.1	22.066	16.113	43.612	4.64	163.6	42.0	20.53	4.580
DD-10	UH	N - T	0.70892	0.70870	0.512504	0.512438	-2.3	21.233	15.930	41.487	1.81	252.6	20.0	19.65	5.057
DD-14	UH	N - T	0.70941	0.70912	0.512260	0.512204	-6.9	19.260	15.759	40.224	2.54	250.5	12.2	19.94	4.352
DD-15	UH	N - T	0.71101	0.71064	0.512293	0.512224	-6.5	19.301	15.764	40.071	3.96	115.7	16.2	14.29	3.862

Table 2.3 (Cont.): Isotopic and isotope-dilution data for dikes.

Sample	Lab	Swarm	$^{87}Sr/^{86}Sr_{(0)}$	$^{87}Sr/^{86}Sr_{(t)}$	$^{143}Nd/^{144}Nd_{(0)}$	$^{143}Nd/^{144}Nd_{(t)}$	$\varepsilon_{Nd}(t)$	$^{206}Pb/^{204}Pb$	$^{207}Pb/^{204}Pb$	$^{208}Pb/^{204}Pb$	Pb	Sr	Rb	Nd	Sm
DD-23	UH	N - T	0.70642	0.70638	0.512670	0.512557	0.0	19.836	15.775	40.103	2.44	149.7	2.72	20.63	5.480
DHD-8	UH	N - T	0.70460	0.70454	0.512801	0.512729	+3.4	17.698	15.410	38.241	1.25	192.4	3.65	15.72	4.394
DHD-9	UH	N - T	0.70454	0.70448	0.512798	0.512727	+3.3	17.791	15.438	38.376	1.44	174.5	3.86	17.85	4.964
DHD-11	UH	N - T	0.70642	0.70630	0.512681	0.512611	+1.1	19.177	15.670	39.635		211.9	10.0	20.27	5.502
DND-2	UH	N - T	0.70954	0.70937	0.512297	0.512232	-6.3	18.168	15.563	39.529	3.32	240.3	15.1	20.30	5.158
NBD-1	UH	N - T	0.71526	0.71495	0.511859	0.511802	-14.7	18.883	15.800	39.090	5.11	159.8	18.3	15.06	3.340
NBD-4	UH	N - T	0.71007	0.70960	0.512310	0.512242	-6.1	20.031	15.863	40.640	2.60	118.6	20.9	12.07	3.176
NBD-10	UH	N - T	0.71119	0.71093	0.512360	0.512297	-5.1	22.360	16.085	43.163	2.81	255.9	24.3	28.01	6.884
TAP-001	UH	N - T	0.70639	0.70592	0.512682	0.512619	+1.2	17.637	15.556	37.639	7.38	181.7	32.0	21.80	5.325
TAP-002	UH	N - T	0.70473	0.70461	0.512748	0.512679	+2.4	17.764	15.415	38.411	2.03	209.7	9.56	20.19	5.434

formations (e.g., Fig. 2.5D) have Poladpur-, Ambenali-, or Mahabaleshwar-formation-type isotope ratios. Even though the DFA indicated that the Khandala might be the most abundantly represented formation in the swarm, no sample was found to be isotopically equivalent to any known Khandala member composition.

The chemically Bhimashankar-like sample DD-10 has no isotopic equivalent in the Deccan, although its data fall along an extension of the field defined by lavas of the Mandla lobe (Fig. 2.10). Unfortunately, it cannot be compared isotopically to the chemically Bhimashankar-like Toranmal or Mhow samples noted above, for which isotopic data are lacking.

Finally, DD-23 has an isotopic signature outside the range of the Western Ghats flows but within that for lavas of the northeastern Deccan (Mandla lobe field in Fig. 2.10) as defined by Peng *et al*. (1998) .

We infer that the Narmada-Tapi swarm may well have fed flows belonging to the lower and upper Western Ghats formations, as well as some flows cropping out in the northern and northeastern regions of the province. Although major and trace element correlations with the Western Ghats formations are weak for about half of the Narmada-Tapi dike samples, we have little evidence for this swarm contributing to flows of the southern sector of the province.

DISCUSSION

Our results combined with previous studies allow the reconstruction of a multi-stage history of emplacement of the Deccan's plumbing system.

(1) Early alkalic intrusive rocks were emplaced near the localities of Mundwara and Barmer (Fig. 2.1; Basu *et al*., 1993; Simonetti *et al*., 1995), and perhaps well north of these localities (e.g., Mahoney *et al*., 2002).

(2) Dikes formed striking E-W in the Narmada-Tapi region, and N-S in what is now the coastal plain. The chemical compositions of some of these dikes are consistent with them being feeders of the lower and middle formations, from the Jawhar to the Bushe.

(3) Dikes isotopically and chemically similar to the upper formations of Poladpur, Ambenali and Mahabaleshwar were emplaced in all three dike swarms, with the greatest number being in the latitudes between Nasik and Pune and west of Sangamner (Fig. 2.13B and 2.14B and C). These dikes as a group show no specific preferred orientation (Fig. 2.12G, bottom; Fig. 2.14C). This group includes coastal dikes as far as 350 km south of Pune, near Goa (Figs. 2.13B and C), although the timing of emplacement of these latter dikes (dated at ~62 Ma by Widdowson *et al*., 2000) is uncertain relative to the emplacement of geochemically similar lava flows of the Western Ghats, the southernmost exposures of which are >70 km to the northeast (Widdowson *et al*., 2000). In addition, some dikes of the Narmada-Tapi region may also have fed Wai-subgroup flows, as well as some Wai-like flows in the northern and northeastern Deccan.

(4) Dikes similar in major and trace element composition to, in particular, members of the Thakurvadi and Khandala formations, but with different isotopic characteristics, were emplaced in all three dike systems (Fig. 2.14D and E). These dikes show a strong preferred N-S orientation in the coastal and Nasik-Pune swarms. Although this set of dikes has not been dated radiometrically, field relationships clearly indicate that they cross-cut flows and potential feeder dikes of the upper formations in some areas (Dessai

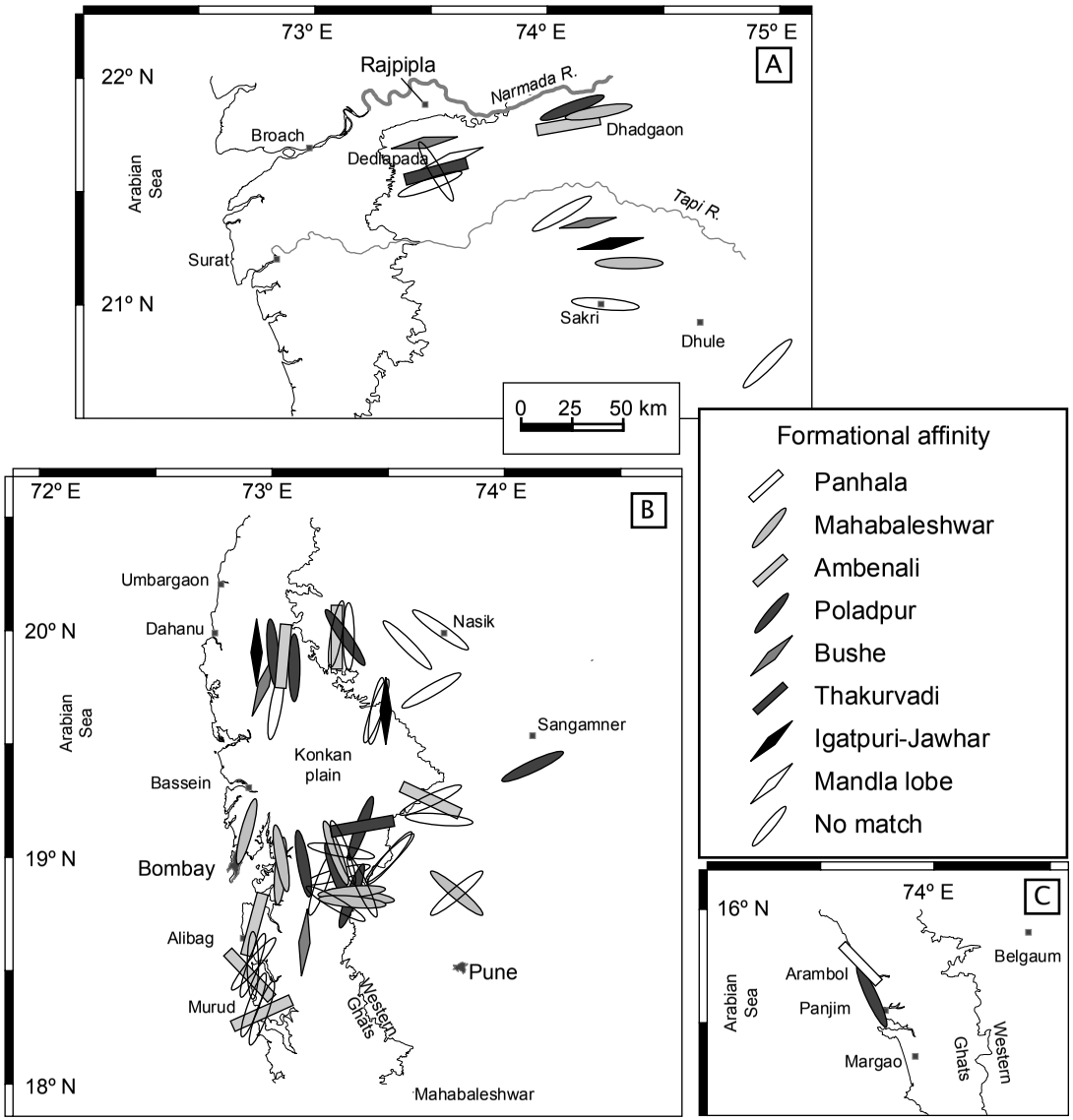

Fig. 2.13: Location and strike of dikes for which we have isotopic data. Formational affinity indicated by the combined isotopic and chemical data is shown.

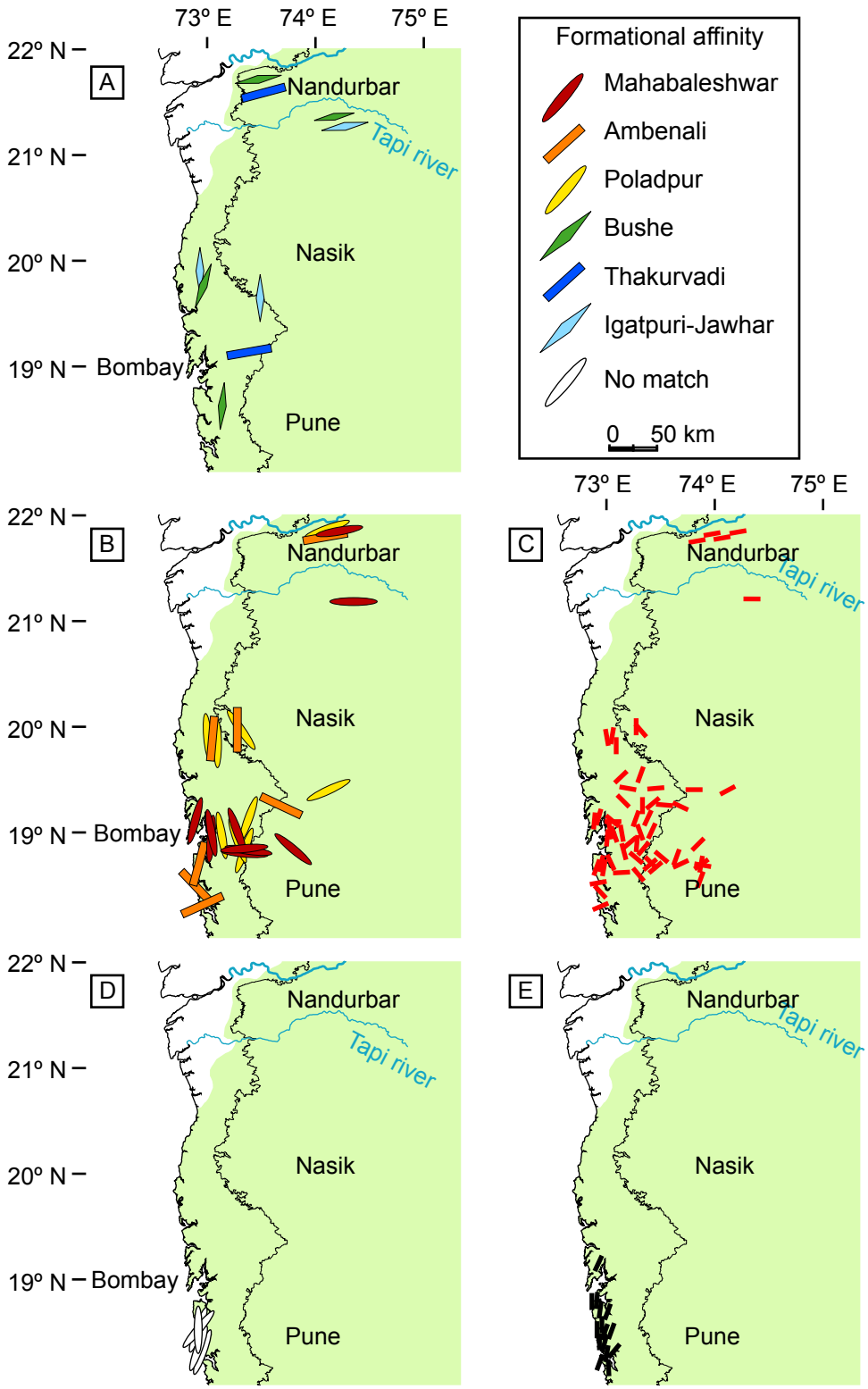

Fig. 2.14: Sketch map of the evolution of dike activity in the Deccan. Inferred feeders for the lower and middle formations (A), upper formations (B) and post-Deccan dikes (D) for which isotopic data is available. Feeders for the upper formations (C) and post-Deccan dikes (E) inferred from their chemical composition only.

& Viegas, 1995; Hooper & Widdowson, submitted). Lava flows with chemical and isotopic compositions corresponding to these dikes have not been found. Three hypotheses can account for this fact: (a) the dikes are hypabyssal; i.e., they did not reach the surface (e.g., Auden, 1949); (b) they fed flows higher up in the stratigraphy that have since then been eroded, although work by Widdowson & Cox (1996) argues against large amounts of erosion from the top of the lava pile, in general; (c) they fed late lavas that flowed to the west and that are now in the largely unknown portion of the Deccan province that has foundered in the Arabian Sea.

(5) In the last stages of magmatism, dikes of alkalic, including lamprophyric, composition were emplaced (Dessai & Viegas, 1995; Widdowson & Hooper, submitted) along the coast, from at least as far north of Bombay as Umbargaon to at least as far south as Murud (Fig. 2.13B and 2.14D and E) (e.g., Mahoney, 1984; Beane, 1988; see also chapter 3, this volume). Alkalic dikes also formed along the Narmada-Son lineament. Some of these dikes are possibly associated with some of the alkalic intrusions and flows of the Deccan, such as those observed in the Rajpipla area (e.g., Krishnamurthy & Cox, 1980; Mahoney *et al*., 1985; Gwalani *et al*., 1993; Sethna *et al*., 1996; Simonetti *et al*., 1998) and around Bombay (e.g., Sethna & D'Sa, 1991; Melluso *et al*., 2002).

Previous estimates of the timing of emplacement of the lava flows and feeder dikes relative to rifting and separation of the Seychelles Bank from western Greater India were largely based on observations in the coastal area between Bombay and Murud (e.g., Hooper, 1990; Dessai & Viegas, 1995; Hooper & Widdowson, submitted). We have determined that at least some possible feeder dikes for the lower and middle formations are present in the E-W-striking Narmada-Tapi swarm and, although rare, in the N-S

striking coastal swarm. Possible feeders of the upper formations in the Narmada-Tapi swarm strike E-W; in contrast, inferred feeders of the three main upper formations (in particular, the upper two of these, the Ambenali and Mahabaleshwar; Figs. 2.12E and G) in the Nasik-Pune swarm do not exhibit a dominant strike. Finally, dikes that are likely to, and in some cases clearly do, post-date the upper formations display a strong E-W strike in the Narmada-Tapi swarm and a N-S strike everywhere else.

The combined results indicate that broadly N-S crustal tension was prevalent in the Narmada-Tapi area throughout the period of Deccan volcanism. East-west extension may have occurred along the (future) west coast during emplacement of the lower and middle formations. However, signs of directed extension (i.e., rifting) during emplacement of the upper formations are lacking from the coast to at least as far inland as Sangamner (e.g., Fig. 2.13B), either because directed extension had greatly diminished, or because directed extensional stresses in this area were negated by more prevalent regional stresses, or stresses were more evenly distributed; e.g., radially above a plume head located below the Nasik-Pune area. East-west extension appears to have resumed along what would become the west coast shortly after eruption of the upper Deccan formations, leading to emplacement of the N-S striking, chemically Thakurvadi-like tholeiitic dikes in the coastal and Nasik-Pune swarms, followed by N-S oriented alkalic dikes along the coast. This well-expressed phase of E-W extension eventually led to the split-off of the Seychelles Bank, which was followed by full-fledged seafloor spreading at ~62 Ma (Dyment, 1998; Collier *et al*., 2008).

We can also rule out pre-existing structural weaknesses in the continental crust as a major control on emplacement of the Narmada-Tapi swarm. The length, spacing and

straightness of the dikes, as well as the absence of *en échelon* dike patterns (e.g., Delaney *et al*., 1986), suggest that the dikes of this system were emplaced under conditions of regional N-S, tension, and were not controlled predominantly by underlying geological structures, in agreement with conclusions reached by Ray *et al*. (2007) on the basis of magmatic overpressure calculations and dike aspect-ratio measurements.

The exact time interval over which this evolution took place remains a matter of debate. One body of geochronological work argues that emplacement of nearly all the Deccan flood basalts occurred in a million years or less (e.g., Courtillot *et al*., 1986; 1988; Duncan & Pyle, 1988; Vandamme *et al*., 1991; Hofmann *et al*., 2000; Sen, 2001; Chenet *et al*., 2007). Other workers hold that the flood basalt eruptions occurred over a few million years (Venkatesan *et al*., 1993; 1996; Baksi, 1994; 2007; Widdowson *et al*., 2000; Pande, 2002; Pande *et al*., 2004), and ended with the emplacement of alkalic rocks near Bombay at ~60 Ma (Sheth *et al*., 2001). However, recent studies of paleomagnetic secular variation in lavas of the Western Ghats by Chenet *et al*. (2008) offer strong evidence for major short-lived eruptive events, each lasting but a few decades, for the lavas of the Poladpur through Ambenali formations in the Mahabaleshwar area (Fig. 2.13B).

Implications of results for models of Deccan emplacement

The timing of magmatism relative to rifting, the orientation of dikes, and the migration of dike swarm activity provide important insights that can be used to help evaluate models for the province.

The plume-head model

The plume-head model (e.g., Richards *et al*., 1989; Campbell & Griffiths, 1990; Campbell, 1998) explains the large volumes of magma produced in continental flood basalts (and oceanic plateaus) by the impingement of the head of a new, deep-seated mantle plume upon the base of the lithosphere. Although rifting can develop as a consequence of the plume head's arrival, the main phase of volcanism is not associated with regional directed lithospheric extension. This model predicts random or radial feeder dike patterns in the main stage of volcanism, pre-eruptive lithospheric uplift shortly before flood volcanism, a short duration (less than about 5 Myr; Campbell, 1998) of peak eruptive activity accounting for the bulk of a province's volume, and an age progression of volcanism if the plate is moving rapidly relative to the hotspot.

Sheth (1999, 2007) has argued that evidence is lacking for either pre-eruptive uplift or a southward age progression in the Deccan. The 2.5 Myr difference in ^{40}Ar-^{39}Ar ages (though measured in different laboratories) between the upper formations in the Western Ghats and the dikes near Goa (Widdowson *et al*., 2000), on the other hand, is consistent with the 450 km the Indian plate would have traveled northward, assuming a plate velocity of 18 cm/yr (McKenzie & Sclater, 1971). The apparent southward off-lap (Fig. 2.3) of formations from Nasik south noted by numerous authors (e.g., Beane *et al*., 1986; Devey & Lightfoot, 1986; Watts & Cox, 1989; Mitchell & Widdowson, 1991) probably reflects this migration. However, a plume-head model involving a brief and intense episode of magmatism preceded by a short (<5 Ma) "incubation" period does not by itself predict directed extension and minor extension-related magmatism either before flood basalt volcanism (e.g., the Barmer and Mundwara alkalic complexes in the Cambay

graben, dated at 68.5 Ma; Basu *et al*., 1993) or during the main phase (as evidenced by the probable feeder-like dikes in the Narmada-Tapi swarm), or during the late stages of volcanism (e.g., the late-stage chemically Thakurvadi-like tholeiitic dikes, the alkalic dikes associated with the west coast rift [e.g., Sheth *et al*., 2001; Melluso *et al*., 2002], and the alkalic complexes of the Narmada graben [e.g., Mahoney *et al*., 1985; Simonetti *et al*., 1998]). Mahoney *et al*. (2002), however, noted that minor magmatic activity is not unexpected in the few million years preceding the outpouring of flood basalts, as the impacting plume head spreads at the base of still-thick lithosphere. The plume-head model also explains well the near-random overall pattern of probable upper-formation feeder dikes in the combined Nasik-Pune and coastal swarms. In particular, it can explain the apparent absence of directed extensional stress in the brief interval during which the upper formations were emplaced (Chenet *et al*., 2008) by having the plume head centered under the Nasik-Pune area at the apex (Hooper, 1990; Self *et al*. ,2006) of Deccan volcanism.

Models involving rifting above a plume

Another end-member of plume-related models was developed largely to account for the apparent syn- and post-rift nature of flood basalts in several provinces. It involves the arrival of a relatively small plume head that spreads and also grows in volume ("incubates") at the base of the lithosphere for as much as 50 Myr, causing dynamic uplift of the overlying lithosphere, which generates extension and melting (e.g., Courtney & White, 1986; White & McKenzie, 1989). Here, rifting is not a consequence of flood volcanism but triggers it; massive magmatism is a response to lithospheric extension over

hotter-than-average mantle. Besides a protracted period of pre-volcanic uplift during the incubation phase, this type of model also predicts that rifting will occur in the early stages of volcanism, and that the maximum amount of melting will occur at the time of crustal breakup.

In the Deccan case, this model is particularly successful at explaining the period of precursory volcanism along the western rift zones (Barmer and Mundwara in the Cambay graben, and possibly a suite of dikes along the west coast near the southern tip of India, in Kerala [Radhakrishna *et al*., 1994]). A long period of plume incubation (40-60 Ma) would also imply that lithospheric uplift began some, perhaps many, millions of years prior to the onset of volcanism, which would explain an absence of evidence of uplift shortly before the Deccan event (Sheth, 2007). What the model fails to explain is how a deep-sourced mantle plume could have grown at the base of the lithosphere for ~25 Myr (White & McKenzie, 1989) while the Indian plate was drifting at a very high rate of 18 cm/yr (McKenzie & Sclater, 1971). It also fails to account for the fact that the formations of the Wai subgroup, which may comprise 50% or more of the Deccan volume (Self *et al*., 2006), appear to have been fed without any dominant control by rifting. In addition, it does not account for the fact that the extensional phase leading to the break-off of the Seychelles Bank was only associated with dikes that do not seem to have fed any significant volume of lava flows, at least onshore.

The triple junction model

Burke & Dewey (1973) proposed the earliest form of the plume-head model, noting the coincidental occurrence of triple junctions, flood basalts, and in some cases persistent

subsequent basaltic volcanism, most notably in the Afar region of eastern Africa. In their compilation, they included the Deccan Traps, suggesting that a triple junction of the Cambay graben, Narmada-Tapi graben and west coast rift (two of which were later aborted) was generated by a rising plume. This and similar models (e.g., Ernst & Buchan, 1997) predict a radial feeder dike pattern surrounding the triple junction, which Burke & Dewey (1973) argued was located in what is now the Gulf of Cambay.

As noted by Sheth (1999), the presence of the often-disregarded Katchchh rift makes this area a quadruple junction, with the Katchchh (Late Triassic to Late Cretaceous), Cambay (Early Cretaceous to Tertiary), Narmada (Jurassic to Late Cretaceous) and West Coast (Late Cretaceous/Early Tertiary) branches not all actively rifting at the same times. However, patterns of pre-Deccan alkalic dikes in Katchchh (Paul *et al*., 2008) and of probable lower and middle formation feeders in the Narmada-Tapi and coastal swarms are not conflicting with a pattern of dikes radiating from the Gulf of Cambay. Nevertheless, this model fails to explain the near-absence of preferred orientation of the numerous probable upper-formation feeders in the Nasik-Pune swarm, which falls ~350-400 km south of the Cambay graben on or near an extrapolated Réunion hotspot track (Fig. 1.2) going through the Gulf of Cambay (Duncan, 1990).

Non-plume models

In recent years, an increasing number of non-plume models (e.g., Smith, 1993; Anderson, 1994; King & Anderson, 1995; Smith & Lewis, 1999; Sheth, 1999; 2005) have been proposed as alternatives to plume-based models of large igneous province generation. Most originate from attempts to address shortcomings of the various plume

models and what the authors have perceived as the indiscriminate application of a single type of model to a disparate worldwide set of provinces. Sheth (1999, 2005) proposed such a model for the Deccan Traps.

Rifting is a prerequisite to flood volcanism in most non-plume models. Although evidence exists of rifting in the early stages of Deccan volcanism, the extensive and voluminous upper formations appear to have been fed largely from dikes whose emplacement was not controlled by rifting, as they strike more or less randomly. This fact contradicts non-plume models. Such models are also unsuccessful at explaining why the peak rifting event – occurring along the west coast and culminating with break-off of the Seychelles microcontinent – post-dates the peak of volcanism and is associated, at least onshore, with only comparatively tiny volumes of magmatic rock. Furthermore, Collier *et al*. (2008) concluded that the rifting and breakup of the Seychelles Bank from India was caused by external plate-boundary forces and was unrelated to Deccan volcanism.

In summary, all existing models present serious weaknesses when applied to the Deccan. Objections by Sheth (1999; 2007) notwithstanding, the plume-head model of Campbell & Griffiths (1990) successfully accounts for the majority of observed characteristics of the dikes and must thus be preferred, assuming that some or all of the Cambay, Katchchh, Narmada and Tapi rifts and extension along parts of the western coastal zone (dating back to the break-up of Madagascar and earlier; Storey *et al.*, 1995; Raval & Veeraswamy, 2003) were already active at the time of plume head arrival. Minor melting would have occurred a few million years prior to the main melting event as a consequence of rising upper-mantle temperatures in regions of already thinned

lithosphere, such as the Katchchh and Cambay grabens. Minor precursory volcanism might also be expected in the regions affected by Precambrian tectonism as a result of pre-existing zones of weaknesses, as in southwestern India where the Kerala dikes were emplaced (Biswas, 1987; Sheth, 1999). The 4-5 Myr interval separating plume head arrival from the onset of the main phase of volcanism predicted by Campbell & Griffiths (1990) is similar to the gap separating the precursory 61 Ma phase from the 56 Ma main magmatic phase in the North Atlantic Tertiary province (e.g., Saunders *et al*., 1997) and fits rather well with the ~69 Ma ages measured for the alkalic rocks of the Cambay graben (Basu *et al*., 1993). It also fits with the (more controversial) ~69 Ma age of the Kerala dikes (Radhakrishna *et al*., 1994) and perhaps could also account for the ~73 Ma, possibly Deccan-related rocks of Pakistan without overstretching the model (Mahoney *et al*., 2002). In the plume-head model, voluminous melt generation and eruption could begin abruptly following this phase of precursory volcanism, as a consequence of adiabatic decompression as the plume-head reaches the top of the upper mantle (e.g., Campbell & Griffiths, 1990). Continued rifting in the region of the Narmada and Tapi grabens would favor the emplacement of E-W striking lower-, middle- and upper-formation feeder dikes. Likewise, existing trends in the Archean basement (e.g., Raju, 1968; Chandrasekharam, 1985; Biswas, 1987; Raval & Veeraswamy, 2003) along the west coast would have favored the emplacement of N-S trending feeder dikes of the middle and lower formations. By the time of the Poladpur formation, stresses related to the plume head could have overridden the effects of pre-existing structures, leading to emplacement of an important swarm of poorly oriented feeder dikes in the Nasik-Pune area feeding voluminous, widespread lava flows (e.g., Self *et al*., 2006) over very short

periods of time (Chenet *et al*., 2008). The transition between the middle and upper formations is also marked by important chemical and isotopic variations indicating changes in source processes and magma pathways to the surface (e.g., Lightfoot & Hawkesworth, 1988; Peng *et al*., 1994). The Ambenali formation's chemical characteristics, for instance, indicate that these magmas were formed by relatively high degrees of partial melting beneath relatively thin lithosphere (e.g., Peng & Mahoney, 1995; Melluso *et al*., 1995; Sen, 1995), consistent with the idea that the upper formations coincide with a surge in magmatic activity expressed in the form of very large flow volumes (Self *et al*., 2006), very high eruption rates during short-duration eruptions (Chenet *et al*., 2008) and a randomly oriented feeder system (Beane *et al*., 1986; this study).

In this view of the plume-head scenario, the main phase of volcanism can be followed by E-W rifting and sea-floor spreading as a result of lithospheric thinning and tensions caused by surface uplift above the plume head; stressed produced by the uplift are, by themselves, thought to be insufficient to produce runaway extension (Campbell & Griffiths, 1990), but can favor sea-floor spreading coupled with external plate-tectonic forces. Collier *et al.* (2008) proposed that E-W rifting occurred along the west coast as a result of external plate-boundary forces and was accompanied by minor magmatism along the rift zone. Alternatively, E-W rifting could have been favored as a consequence of N-S stretching or smearing of the plume head in response to the fast northward motion of the Indian plate; N-S stretching of the plume would lead to an elongate zone of uplift along a N-S axis, which in turn would favor E-W rifting, provided external stresses were sufficient to induce runaway extension and breakup. A late phase of magmatism would

also be observed in the Narmada-Tapi region, where ongoing N-S extension would still control dike orientation.

CONCLUSIONS

Study of the elemental and isotopic signatures of dikes of the Deccan Traps allows us to correlate a substantial subset of dikes with flow formations, and places important constraints on the location, geometry and evolution of the feeder systems to the lava pile. In particular, it provides the following information regarding the relative timing of dike emplacement with respect to regional directed lithospheric extension.

* Inferred feeders of the three main upper formations (Poladpur, Ambenali, and Mahabaleshwar) are found in all three dike swarms, their greatest concentration being between Nasik and Pune, where they do not show a marked preferred orientation.

* Multiple inferred feeder dikes of the lower and middle formations are found in the E-W oriented Narmada-Tapi swarm. Ray *et al*. (2007) suggest that this area was actively rifting N-S at the time, and that dike emplacement was not controlled significantly by pre-existing geological structures.

* Few probable feeder dikes to the lower and middle formations are found in the coastal and Nasik-Pune swarms. The few that are present display an overall preferred N-S strike.

* The inferred lower- and middle-formation feeder dikes remain few in comparison with upper formation feeders, possibly as a result of poor to nonexistent exposure in most areas and unfavorable exposure even in the northern Konkan plain.

* Geochemical similarities between several sampled dikes of the Narmada-Tapi swarm and lavas of the Mandla lobe (Fig. 1.2) and the northern Deccan near Toranmal suggest this swarm might have acted as a feeder system for flows spreading to the north and northeastern reaches of the province.

* Widespread tholeiitic feeder dikes with chemical affinities to the Western Ghats lava formations (the Thakurvadi and Khandala formations, in particular) cross-cut and thus post-date flows and probable feeders of stratigraphically higher formations. These dikes have isotopic signatures different than those observed in the Western Ghats formations. This group of dikes strikes E-W in the Narmada-Tapi swarm and N-S everywhere else, and does not seem to have fed significant volumes of lava. The strong N-S trend of these dikes outside the Narmada region indicates that they are contemporaneous with late-stage rifting along the west coast, which eventually led to the breakup of the Seychelles Bank from India.

* An even later phase of syn-rift magmatism is recognized in acidic, lamprophyric and other alkalic dikes in the coastal swarm. This phase may have persisted until ~60 Ma (Sheth *et al*., 2001).

Despite the apparent absence of pre-volcanic uplift (Sheth 1999; 2007), a plume-head model for the formation of the Deccan should be preferred. It best accounts for the observed feeder dike patterns: (1) the lack of preferred orientation of the inferred upper-formation feeder dikes and (2) the main phase of volcanism preceded the main phase of rifting along the Indian west coast. Rifting models fail to account for these observations. Although rift-related precursory magmatic events and a rifting-controlled emplacement of the inferred lower and middle formation feeder dikes seem to favor rifting models, they do not discount plume-head models, as rifting was active for millions of years prior to the onset of volcanism. Although the possibility that directed extension triggered large-scale volcanism cannot be ruled out, it appears that another mechanism(s) must be invoked to account for the voluminous upper formations. The fact that the graben regions of the northern Deccan had been tectonically active for 55-145 Myr prior to the onset of Deccan volcanism (i.e., since the Late Triassic for the Katchchh rift and the Early Cretaceous for the Cambay graben) and had not previously been the site of voluminous volcanism is another indication that rifting alone did not generate the flood basalt event. The most likely scenario involves the arrival of a plume head under a region already undergoing rifting.

ACKNOWLEDGMENTS

We thank J. Mallik, A. Shirke, D. Gosain and R. Duraiswami for help in the field, and D. Pyle, D. VonderHaar, G. Ravizza, C. Fraley, K. Ross, E. Hellebrand, J. Sinton and E. De Carlo for laboratory assistance. S. Ingle offered many helpful comments. The

authors gratefully acknowledge the support of the US National Science Foundation (grant EAR02-29824).

CHAPTER 3

ALKALIC DIKES OF THE NARMADA-TAPI SWARM AND INDIA'S WEST COAST

Loÿc Vanderkluysen[1], John J. Mahoney[1], Peter R Hooper[2], Hetu C. Sheth[3]

1. Department of Geology and Geophysics, School of Ocean and Earth Science and Technology, University of Hawai'i, Honolulu, HI 96822, U.S.A.

2. School of Earth and Environmental Sciences, Washington State University, Pullman, WA 99164, U.S.A.

3. Department of Earth Sciences, Indian Institute of Technology Bombay, Powai, Mumbai 400 076, India

INTRODUCTION

Despite the overwhelming predominance of tholeiitic lavas in the Deccan volcanic province, the volumetrically minor occurrences of acidic, lamprophyric and other alkalic lavas and intrusions have historically garnered disproportional scientific attention (Mahoney, 1988). These rocks (Fig. 3.1) have been known to occur both at the early Deccan stages, like the Mundwara and Barmer intrusions of the Cambay graben (e.g., Basu *et al*., 1993; Simonetti *et al*., 1995) and the alkalic rocks of Katchchh (alternatively spelled "Kutch", "Kutchchh", "Katch", "Kuch" or "Kachchh"; e.g., Paul *et al*., 2008; Sen

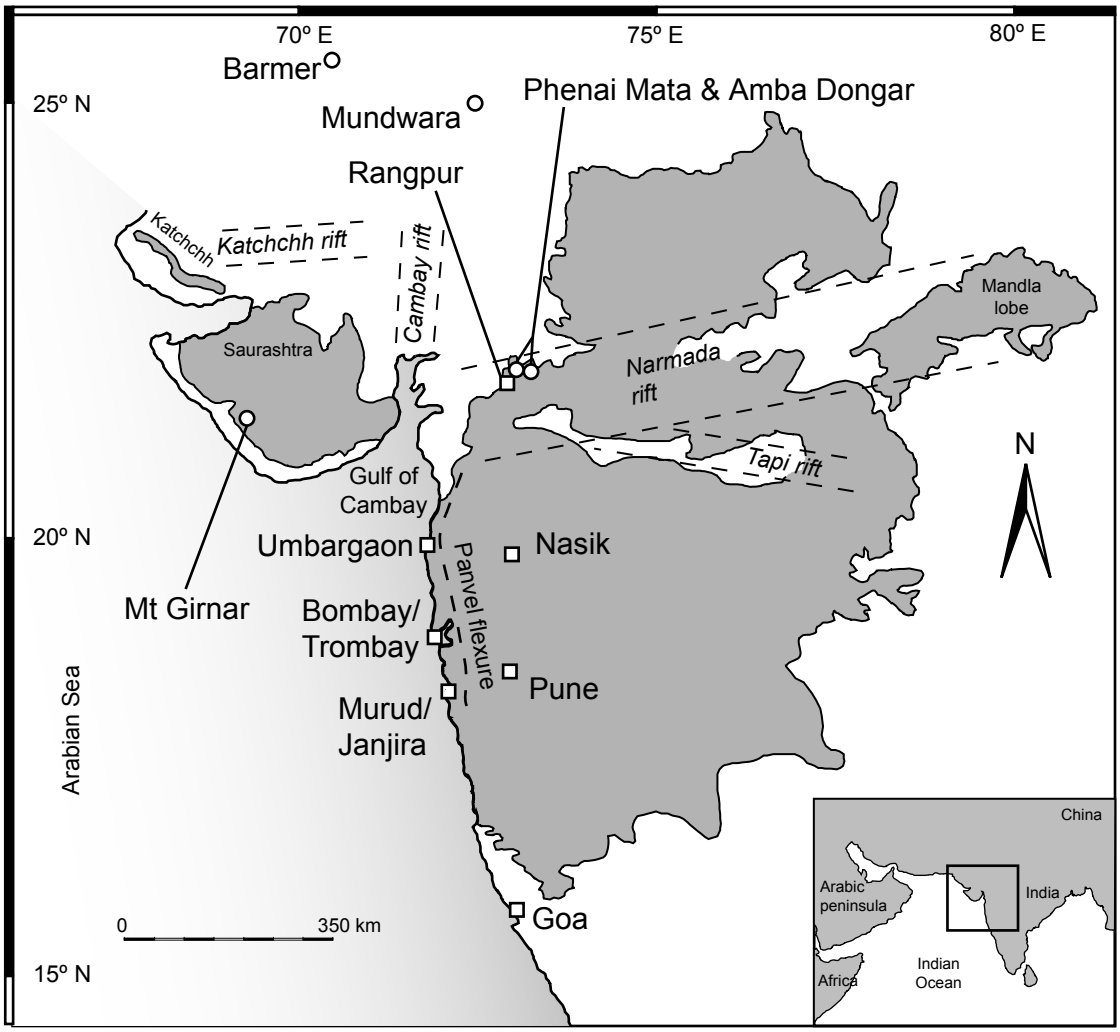

Fig. 3.1: Map of the Deccan Traps (in gray), with important localities mentioned in the text (white squares) and some notable alkalic Deccan-related intrusions (white circles). The dashed line along the west coast represents the Panvel flexure (after Subrahmanya, 1998).

et al., submitted), and in the Deccan's late stages, cross-cutting or overlying local flows, such as the intrusive complex of Mt. Girnar (e.g., Bose, 1973; Murali *et al*., 1976; Paul *et al*., 1977), the Rajpipla intrusive suite, 60 km west of Rangpur (e.g., Krishnamurthy & Cox, 1980; Mahoney *et al*., 1985), the alkalic, acidic and carbonatitic rocks of the Phenai Mata and Amba Dongar complexes of the Narmada graben (e.g., Sukheswala & Avasia, 1972; Simonetti *et al*., 1995; 1998) and the acidic, lamprophyric and other alkalic intrusive and extrusive rocks of the Bombay, Murud, Janjira and Trombay region, along India's west coast (e.g., Sethna & Battiwala, 1980; Mahoney *et al*., 1985; Melluso *et al*., 2002; Hooper & Widdowson, submitted). Although lamprophyres have been reported in the Murud-Janjira region (Melluso *et al*., 2002), they are much less common than melanephelinites and nephelinites found in the area.

Alkalic rocks occur in many continental large igneous provinces, typically at the early or late stages of volcanism (e.g., Paraná-Etendeka, Peate, 1997; Karoo, Eales *et al*., 1984; Siberian Traps, Sharma, 1997). In the Deccan, these occurrences are commonly explained by a combination of melting of metasomatized lithospheric mantle and low degrees of partial melting (e.g., at the edge of the hotspot) (e.g., Mahoney *et al*., 1984; Simonetti *et al*., 1998; Melluso *et al*., 2002).

During the course of our study of dikes of the Deccan Traps, we encountered numerous acidic, lamprophyric and other alkalic dikes of varying geochemistry and mineralogy. Because these dikes cannot be considered to be feeders to the voluminous tholeiitic lava pile, they do not receive nearly as much attention in our work as their tholeiitic counterparts. Nevertheless, we present here geochemical analyses of scattered

dikes from the west coast north and south of Bombay and from the Narmada-Tapi rift system and compare them to other acidic and alkalic rocks of the Deccan Traps.

SAMPLES AND METHODS

The dike samples from the coastal area south of Bombay were taken from the collections of Beane (1988), Hooper & Widdowson (submitted) and their coworkers. Data for the major elements and a group of trace elements analyzed by X-ray fluorescence spectrometry (XRF), and, for some samples, additional trace element data (determined by inductively coupled plasma mass spectrometry (ICP-MS)), were already available for these samples. In addition, we collected samples from the Narmada-Tapi swarm near Rangpur (Fig. 3.2) and Dediapada (Fig. 2.2) and the coastal swarm in the northern Konkan plain, near Umbargaon (Fig. 3.1), between 2003 and 2005. Although generally fine-grained and aphyric or sparsely phyric, one sample is porphyritic with biotite and cm-sized plagioclase (RD-1), and some other samples are plagioclase-phyric with trachytic textures (DDH-159; UDD-03). The lamprophyres, on the other hand, are dominated by assemblages of clinopyroxene (cm-sized), biotite and plagioclase.

Major elements in our recently collected samples (UDD-03, DD-04 and the RD sample suite) were measured by XRF on fused disks at the University of Hawai‘i, following Eason & Sinton (2006). Concentrations of trace elements were determined by ICP-MS following a procedure similar to that of Pyle *et al*. (1995) and Neal (2001). Detailed analytical procedures are described in chapters 1 and 2. Isotope ratios of three samples were analyzed at the University of Alberta, following Creaser *et al*. (1997); for

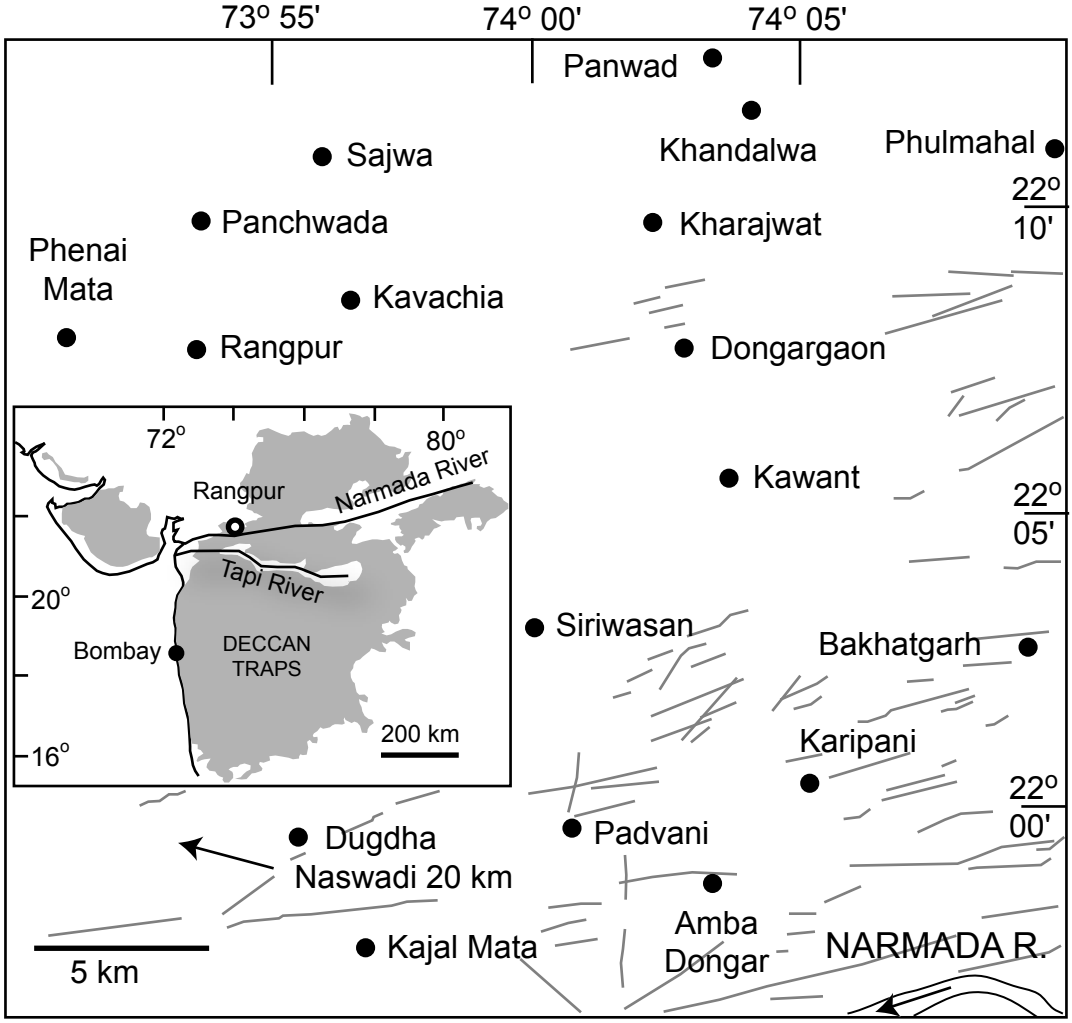

Fig. 3.2: Schematic map of dikes in the Rangpur area. Gray lines represent recognized dikes based on satellite imagery.

age-correcting these ratios, we have used the corresponding XRF and ICP-MS concentration data for parent and daughter elements.

RESULTS

The acidic, lamprophyric and other alkalic dikes encountered in the present study broadly fall in four geographic categories: (1) the mafic, intermediate and acidic dikes of the Rangpur area (Fig. 3.1 and 3.2), (2) lamprophyric dikes of the west coast south of Bombay, (3) other alkalic dikes of the west coast, from Murud to Umbargaon (Fig. 3.1), and (4) a single alkalic dike (DD-04) of the Narmada-Tapi graben, sampled near Dediapada (Fig. 2.2). Mineralogical observations and major and trace element concentrations (Table 3.1; Fig. 3.3) further subdivide these dikes into multiple categories. (1) The coastal lamprophyres are melanocratic with dominant biotite and clinopyroxene mafic phases. (2) The alkalic dikes of the west coast comprise both silica-oversaturated acidic rocks that have either a potassic affinity (DDH-159 and UDD-03), are barely silica-undersaturated (mugearite) with a sodic affinity (DDH-014), or are very silica-undersaturated phonotephrites (DDH-006A and -006B). (3) The alkalic dike near Dediapada is a trachybasalt with sodic affinity (i.e., hawaiite; DD-04). (4) The Rangpur dike suite is very diverse, including mafic, intermediate and acidic dikes that are subalkalic (RD-3, -5, -7 and -8) and belong to the high-K series of Peccerillo & Taylor (1976), as well as alkalic basalts, shoshonites and latites (i.e., with a potassic affinity; RD-1, -2, -4 and -6).

Three samples from dikes in the western coastal zone were analyzed for Sr, Nd and Pb isotopes at the University of Alberta (Table 3.2; Fig. 3.4). Data show that, not

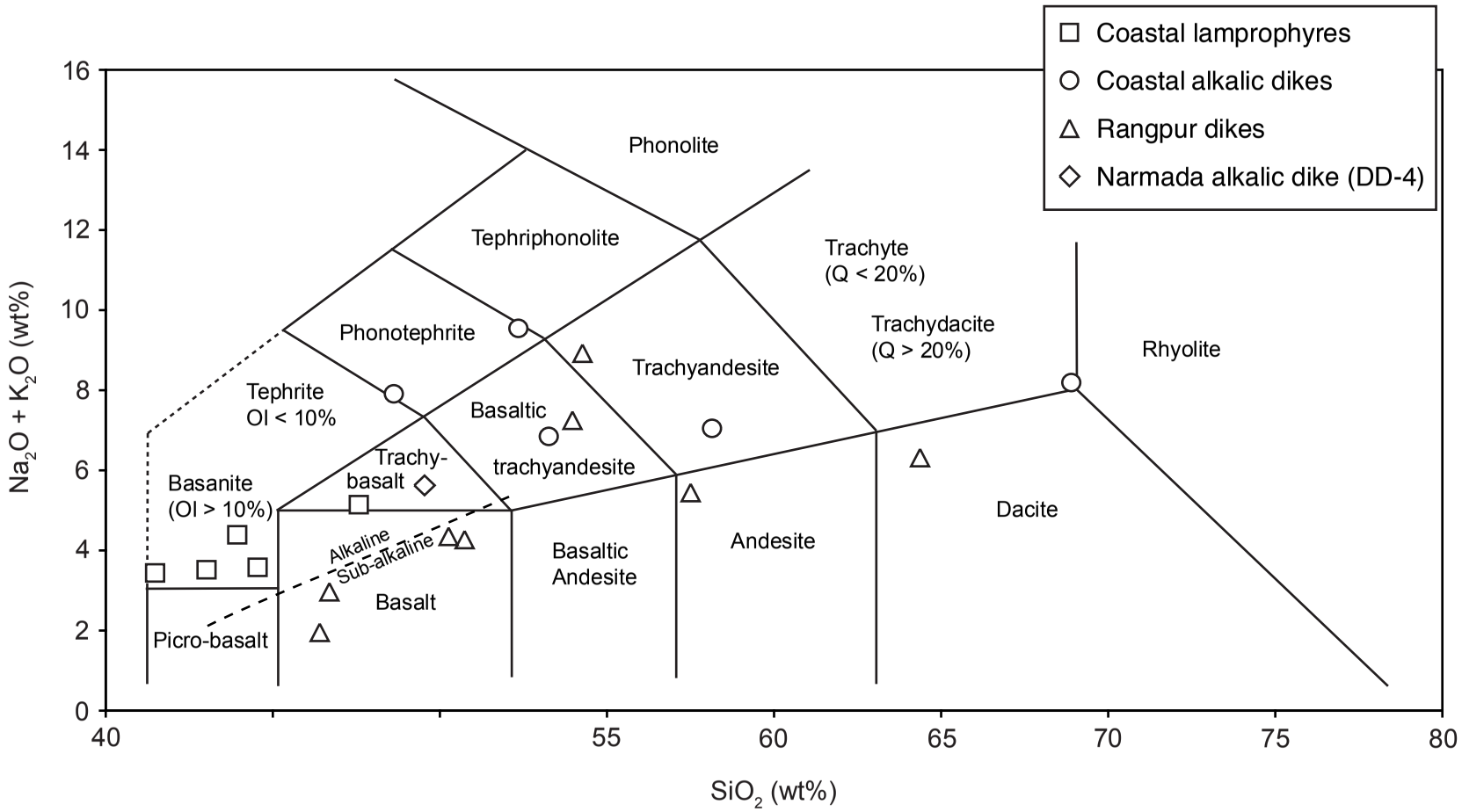

Fig. 3.3: Total alkali vs. silica (Le Bas *et al*., 1986) classification diagram for some acidic, alkalic and lamprophyric dikes of the Deccan Traps. Alkaline / sub-alkaline divide line (doted line) is after Irvine & Baragar (1971).

Table 3.1: Major element (wt%) and trace element (ppm) compositions of alkalic and lamprophyric Deccan dikes. Calculated CIPW normative mineral abundances (wt%) of major phases are reported at the bottom. Abbreviations are as in Appendix A.

Sample	DDH-004	DDH-007	DDH-012	DDH-020	DDH-021	DDH-006A	DDH-006B	DDH-014	DDH-159
Swarm	Coast	Coast	Coast	Coast	Coast	Coast	Coast	Coast	Coast
Strike	177	15	10	20	40?	20		20	160
Thickness (m)	1	1	1	0.5	1	20		25	3
Category	Lampro.	Lampro.	Lampro.	Lampro.	Lampro.	Phono-tephrite	Phono-tephrite	Mugearite	Trachyandes./ latite
Lab	WSU	WSU	WSU	WSU	WSU	WSU	WSU	WSU	WSU
SiO_2	44.58	41.51	47.61	43.97	43.05	52.39	48.66	53.30	58.19
TiO_2	4.09	5.51	3.34	5.09	5.30	0.35	0.99	3.00	0.98
Al_2O_3	8.97	7.82	11.16	8.73	9.09	20.59	14.88	14.37	17.82
FeO (t)	14.38	16.47	12.18	15.24	15.76	6.27	13.16	11.90	6.55
MnO	0.34	0.36	0.20	0.38	0.30	0.21	0.20	0.17	0.08
MgO	10.38	11.40	9.93	9.12	9.69	2.53	6.47	4.02	3.41
CaO	12.82	12.76	9.70	12.22	12.37	7.15	7.30	5.91	5.68
Na_2O	2.11	1.75	2.85	2.68	2.47	4.97	3.96	5.48	4.42
K_2O	1.50	1.72	2.32	1.74	1.08	4.59	3.97	1.39	2.65
P_2O_5	0.82	0.71	0.72	0.82	0.87	0.95	0.41	0.46	0.22
Total									
LOI									
Sc	36	38	29	38	35	12	25	24	18
V	310	331	245	315	330	80	231	308	100
Cr	742	694	455	268	208	35	149	64	61
Co	49	57	44	48	48	12	28	32	
Ni	248	235	228	114	90	32	86	47	68
Cu	241	320	157	175	219	16	68	38	120
Zn	137	136	137	174	184	106	143	136	74
Ga	16	18	15	15	16	23	15	25	20
Rb	33	71	40	59	30	75	39	27	65
Sr	812	1184	1912	1547	873	3149	858	433	580
Y	29	28	25	32	34	21	20	39	15
Zr	398	360	367	535	485	362	131	238	174
Nb	152.8	222.6	151.1	260.2	252.1	84.1	20.4	23.7	21.9
Ba	8920	830	1056	1152	646	710	622	298	599
Li	28	14	32	43	24	26	12	9	
La					205	16		29	
Ce					378	31		61	
Pr					39.1	4.0		7.9	
Nd					142	17		36	
Sm					23.0	4.0		9.5	
Eu					6.1	1.2		3.1	
Gd					15.4	3.5		9.5	
Tb					1.90	0.59		1.52	
Dy					9.1	3.6		8.9	
Ho					1.47	0.69		1.69	
Er					3.3	2.0		4.2	
Tm					0.41	0.30		0.58	
Yb					2.2	1.9		3.3	
Lu					0.33	0.31		0.5	
Hf					12.8	6.1		6.5	
Ta					15.3	4.7		1.4	
Pb					12	16		4.2	
Th					23.1	3.4		2.9	
U					4.84	0.30		0.65	
Quartz									2.15
Plagioclase	15.79	8.40	25.32	11.20	17.11	40.06	19.15	55.85	58.36
Orthoclase	8.86	1.63	13.71	10.28	6.38	27.13	23.46	8.21	15.66
Nepheline	6.84	8.02	5.20	9.82	7.76	12.09	13.79	0.56	
Leucite		6.69							
Diopside	39.13	41.23	26.67	40.07	37.17	7.55	18.79	13.32	4.82
Hypersthene									16.65
Olivine	19.71	21.93	21.11	17.06	19.49	10.31	21.99	15.30	

Table 3.1 (Cont.): Major element (wt%) and trace element (ppm) compositions of alkalic and lamprophyric dikes.

Sample	UDD-03	DD-04	RD-1	RD-2	RD-3	RD-4	RD-5	RD-6	RD-7	RD-8
Swarm	Coast	Narm.-Tapi	Narm.-Tapi	Narm.-Tapi	Narm.-Tapi	Narm.-Tapi	Narm.-Tapi	Narm.-Tapi	Narm.-Tapi	Narm.-Tapi
Strike		90	20	100	60	80	130	80	80	75
Thickness (m)		2	1.4	0.7	0.4	0.35	1.5	0.9	1.8	2
Category	Trachy-dacite	Hawaiite	Trachyande s./ latite	Alkali basalt	Subalkalic high-K basalt	Alkali basalt	High-K dacite	Shoshonite	Subalkalic high K basalt	High-K andesite
Lab	UH	UH	UH	UH	UH	UH	UH	UH	UH	UH
SiO_2	69.28	50.39	54.27	46.89	50.52	46.58	64.36	54.17	50.01	57.32
TiO_2	1.03	2.95	1.16	1.12	1.29	1.14	1.07	1.74	1.34	1.12
Al_2O_3	14.14	13.13	19.33	15.82	15.18	12.36	13.88	14.60	16.79	15.13
FeO (t)	4.32	14.59	7.16	11.05	11.02	9.20	6.94	11.53	10.75	8.53
MnO	0.06	0.20	0.15	0.20	0.16	0.15	0.11	0.15	0.16	0.13
MgO	0.90	4.74	2.22	7.31	5.77	12.23	1.88	3.49	4.74	4.14
CaO	1.71	7.73	5.31	13.31	9.75	15.31	4.28	5.57	9.76	6.58
Na_2O	3.36	3.44	3.75	1.60	2.13	1.38	1.81	2.62	2.32	2.19
K_2O	4.90	2.30	5.19	1.41	2.15	.62	4.53	4.67	2.04	3.26
P_2O_5	0.28	0.40	0.62	0.42	0.30	0.32	0.30	0.47	0.32	0.27
Total	99.96	100.73	99.12	99.10	98.24	99.27	99.13	99.01	98.23	98.65
LOI			3.13	2.87	2.62	4.65	2.26	2.42	2.90	1.89
Sc	11	35								
V										
Cr	10	79								
Co	6	36								
Ni		42								
Cu		133								
Zn	54	123								
Ga										
Rb	188	61								
Sr	207	337								
Y	45	36								
Zr	390	121								
Nb	23.7	16.8								
Ba	888	298								
Li										
La	75	22								
Ce	132	48								
Pr	15.3	6.2								
Nd	54	27								
Sm	9.4	6.1								
Eu	2.3	1.9								
Gd	9.4	6.6								
Tb	1.29	1.04								
Dy	7.0	6.1								
Ho	1.32	1.16								
Er	3.8	3.								
Tm	0.58	0.41								
Yb	3.4	2.7								
Lu	0.51	0.39								
Hf	9.0	3.3								
Ta	1.5	1.0								
Pb	10	5.1								
Th	24.2	2.7								
U	3.34	0.59								
Quartz	23.89						22.24	0.89		9.64
Plagioclase	35.09	42.64	50.29	42.52	44.22	32.40	31.91	36.74	49.84	40.85
Orthoclase	28.96	13.59	30.91	8.39	12.88	3.66	26.95	27.83	12.23	19.50
Nepheline		0.06	1.34	1.75		2.82				
Leucite										
Diopside		18.71	1.51	26.30	17.60	38.99	2.46	8.76	14.30	7.64
Hypersthene	8.59				17.54		12.21	18.92	14.90	17.78
Olivine		18.46	12.30	17.91	2.23	17.26			3.09	

Table 3.2: Isotopic data for Deccan alkalic dikes. Analytical parameters and errors are as in tables 2.2 and 2.3.

Sample	Swarm	Category	Lab	$(^{87}Sr/^{86}Sr)_0$	$(^{87}Sr/^{86}Sr)_t$	$(^{143}Nd/^{144}Nd)_0$	$(^{143}Nd/^{144}Nd)_t$	$\varepsilon_{Nd}(t)$	$^{206}Pb/^{204}Pb$	$^{207}Pb/^{204}Pb$	$^{208}Pb/^{204}Pb$
DDH-6A	coast	Phonotephrite	UA	0.70553		0.511717	0.511656	-17.6	18.269	15.448	38.430
DDH-14	coast	Mugearite	UA	0.70637	0.70622	0.512281	0.512213	-6.7	16.575	15.226	37.732
DDH-21	coast	Lamprophyre	UA	0.70436	0.70427	0.512687	0.512646	+1.7	18.894	15.524	39.167

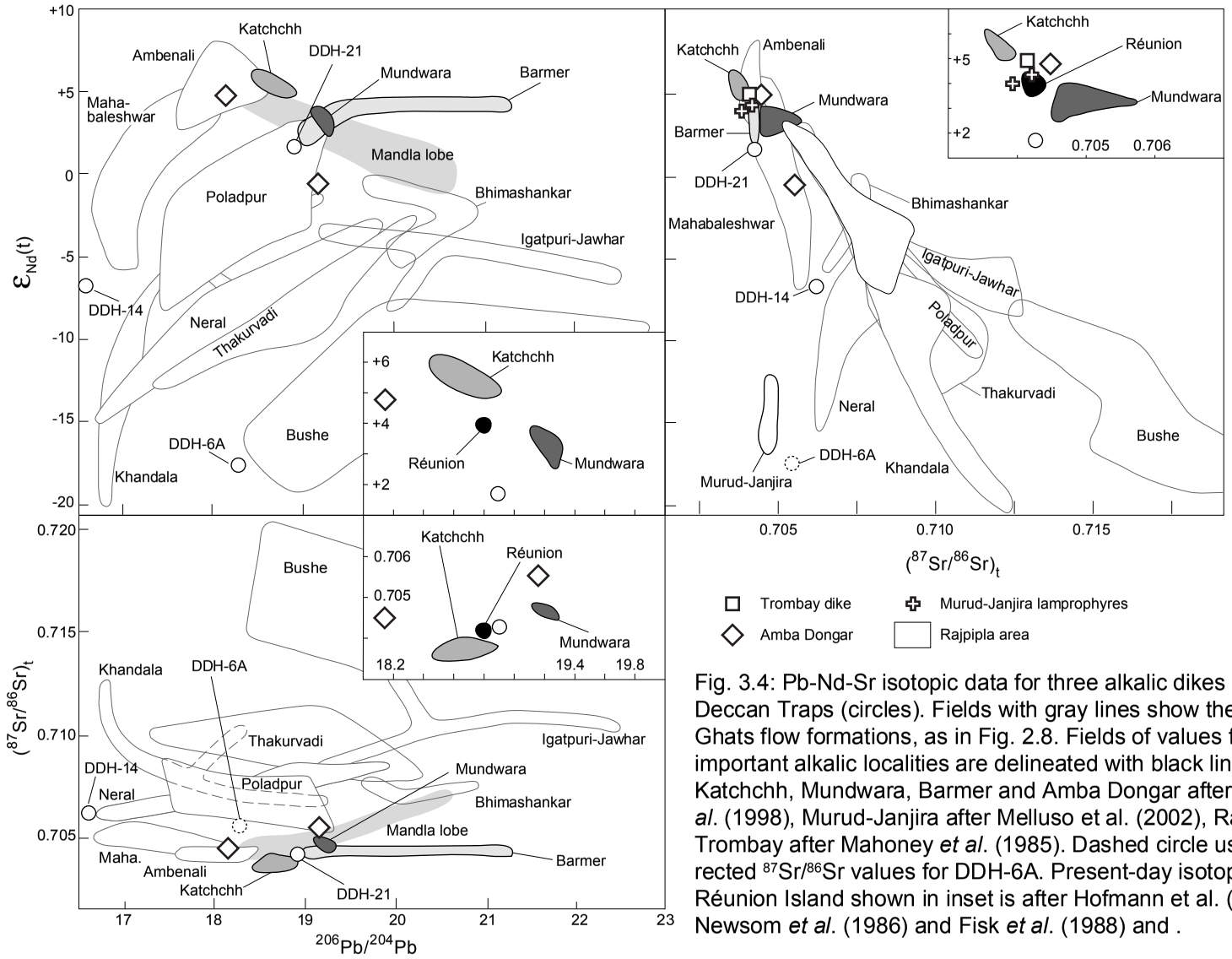

Fig. 3.4: Pb-Nd-Sr isotopic data for three alkalic dikes of the Deccan Traps (circles). Fields with gray lines show the Western Ghats flow formations, as in Fig. 2.8. Fields of values for some important alkalic localities are delineated with black lines: Katchchh, Mundwara, Barmer and Amba Dongar after Simonetti *et al*. (1998), Murud-Janjira after Melluso et al. (2002), Rajpipla and Trombay after Mahoney *et al*. (1985). Dashed circle uses uncorrected $^{87}Sr/^{86}Sr$ values for DDH-6A. Present-day isotopic field of Réunion Island shown in inset is after Hofmann et al. (1986), Newsom *et al*. (1986) and Fisk *et al*. (1988) and .

surprisingly, all three dikes are isotopically distinct from any of the Western Ghats flow formations. Although the majority of published data for alkalic complexes (Barmer, Mundwara, Katchchh, Amba Dongar, Trombay and two samples from Murud-Janjira; Mahoney *et al*., 1985; Simonetti *et al*., 1998; Melluso *et al*., 2002) fall on or near Trend 1 of Peng *et al.* (1994) (see Ch. 2), only lamprophyre DDH-021 comes close to that trend among the present group of samples. The other two samples (DDH-006A and -014) have noticeably low ε_{Nd} (-17.6 and -6.7, respectively). Among Deccan-related alkalic rocks, such low ε_{Nd} values have only been observed in nearby nephelinites of Murud and Janjira island (Melluso *et al*., 2002). The very low $^{206}Pb/^{204}Pb$ for DDH-014 (16.575) is also uncharacteristic of other alkalic samples of the Deccan. Pb isotope data are not available for the Murud-Janjira rocks studied by Melluso *et al*. (2002), unfortunately.

DISCUSSION

Our analyses of lamprophyres of the west coast, south of Bombay in the vicinity of Murud, show that they are distinct from previously studied alkalic rocks, including lamprophyres, from the same area (Melluso *et al*., 2002). Most notably, the lamprophyres of Murud-Janjira have a potassic affinity, whereas our samples are sodic. Isotopically, our lamprophyre analysis (DDH-021) falls close to that for a lamprophyre from Murud-Janjira (Melluso *et al*., 2002) and to a lamprophyric dike from Trombay Island (Mahoney *et al*., 1985) in $^{87}Sr/^{86}Sr$, but are distinct in ε_{Nd}. However, the composition of DDH-021 conspicuously fall at the tip of the array defined by data for the Barmer intrusion (some 835 km farther north; Fig. 1.2 and 2.1). This array, which points toward low-$^{87}Sr/^{86}Sr$ and low-ε_{Nd}, is like other parallel isotopic data arrays defined by basalts interpreted to be

contaminated by Lewisian-like granulites (e.g., Peng *et al*., 1994). Although previous lamprophyre data showed that the rocks were more or less uncontaminated by crust and had isotopic ratios close to recent products of the Réunion hotspot (Fig. 3.4), lamprophyres studied here appear to be contaminated with the material that also affected the nephelinitic magmas of Murud-Janjira.

Other alkalic rocks from the Murud area are phonotephrites (DDH-006A and -006B). These differ from previously studied Murud-Janjira alkalic rocks, which are dominantly melanephelinites and nephelinites. The closest equivalent is a tephrite from Melluso *et al*. (1998), markedly different in its alumina and alkali content (9.66 wt% Al_2O_3 in the tephrite, ~14-20 wt% in the phonotephrites; 4.92 wt% total alkali in the tephrite, 8-9 wt% in the phonotephrites). Isotopic data for phonotephrite DDH-006A also differ from any other alkalic rock from Murud and other rocks from the Deccan plateau. Isotopically somewhat similar in Sr and Nd isotopes to the nephelinites of Murud, it falls well off any possible contamination path with granulites of Lewisian-like Pb isotopic composition. Further isotopic comparisons with other low-$^{87}Sr/^{86}Sr$, low-ε_{Nd} rocks (like the Murud-Janjira nephelinites) cannot be made until the Pb isotope ratios of the Murud-Janjira alkalic suite are available.

The mugearite sample DDH-014 also represent a rare rock type in this area. In terms of Pb isotope ratios, it is the most distinct sample of our study, having no equivalent near or far in the isotopic field of Deccan alkalic rocks. With very low $^{206}Pb/^{204}Pb$ values (16.575), its closest isotopic resemblance is to the (tholeiitic) lavas of the Mahabaleshwar formation, which has long been postulated to represent the mixing of an Ambenali-like isotopic end-member with either old granulitic crust (e.g., Mahoney *et*

al., 1982) or old continental lithospheric mantle (e.g., Lightfoot & Hawkesworth, 1988; Lightfoot *et al*., 1990). In either case, the isotopic composition of this mugearite records a contamination process involving a low-$^{206}Pb/^{204}Pb$ and low-$^{208}Pb/^{204}Pb$ component that had previously not been observed in the Deccan's alkalic rocks.

The trachyandesite (DDH-159, found just north of Bombay) and trachydacite (UDD-03, sampled near Umbargaon) are similar in composition to trachytes and rhyolites (though the terms now reflect outdated definitions of these rocks) of the Bombay volcanic series (Sethna & Battiwala, 1977; Lightfoot *et al*., 1987; Sheth & Ray, 2002). If these rocks are related, the Bombay acidic volcanic series would extend some ~100 km farther north than originally thought.

Sample DD-04, collected near Dediapada (Fig. 2.2), is also an oddity. To our knowledge, no other alkalic dike has been reported in the vicinity, and indeed, the great majority of dikes in the area are tholeiitic. This hawaiite is also sodic in nature, in stark contrast with the potassic suite of Rajpipla (Mahoney *et al*., 1985), located just 25 km farther north. It also stands in sharp contrast with the highly silica-undersaturated alkalic rocks and carbonatites of Phenai Mata and Amba Dongar (Simonetti *et al*., 1998), located only 70 km to the north-east.

The proximity of the Phenai Mata and Amba Dongar alkalic intrusions (e.g., Sukheswala & Avasia, 1972; Gwalani *et al*., 1995; Simonetti *et al*., 19995; 1998; Ray & Shukla, 2004) to the Rangpur dike suite may suggest a petrogenetic relationship between the alkalic dikes and these intrusions. However, these two intrusions are prominently carbonatitic and highly silica-undersaturated, unlike our dike samples, half of which are only mildly alkalic and half subalkalic. Our samples also have a strongly marked potassic

affinity, whereas existing data for the two intrusions (e.g., Gwalani *et al*., 1993; Simonetti *et al*., 1998) indicate a sodic affinity. The dikes certainly cannot be considered feeders to the carbonatitic complexes. Any petrological connection, let alone synchronicity, between the alkalic/acidic dikes and the subalkalic ones also needs to be established.

CONCLUSIONS

Dikes, lavas and intrusive complexes with alkalic affinities occur in the Deccan Traps and are closely associated with rift zones (Cambay graben, Narmada-Tapi rift, Panvel flexure and west coast rift, Katchchh rift). Besides their tectonic characteristic, these intrusive and extrusive rocks display little compositional similarities. Some (e.g., in the Katchchh rift, and in the Barmer and Mundwara intrusions of the Cambay graben) are thought to have been intruded in the Deccan's early stages (e.g., Basu *et al*., 1993; Simonetti *et al*., 1995). Others (like the Amba Dongar and Phenai Mata intrusions, others along the Narmada rift zone, and the alkalic dikes of the west coast south of Bombay) have been shown to have been emplaced in the late stages of volcanism (e.g., Sukheswala & Avasia, 1972; Simonetti *et al*., 1995; 1998). Our geochemical study shows that our acidic and alkalic samples cover nearly the whole spectrum of alkalic rocks, from mafic (alkalic basalts, hawaiites) to intermediate (mugearites, shoshonites, latites, andesites) to acidic (dacites, trachydacites) to strongly silica-undersaturated (phonotephrite) to lamprophyric.

Previous isotopic studies of the alkalic rocks of Mundwara, Barmer and Katchchh as well as of lamprophyres at Trombay and Murud-Janjira, showed that the sources of these magmas isotopically resembled the source of recent products of the Réunion

hotspot (Fig. 3.4) (e.g., Mahoney *et al*., 1985; Peng & Mahoney, 1995; Simonetti *et al*., 1998; Melluso *et al*., 2002), representing a narrow range of values compared to the much wider range of isotopic compositions observed in the tholeiitic lava pile. New isotopic data confirm that the Murud lamprophyres had a mantle source with limited isotopic variability, but also reveal a very wide range of isotopic values for our other alkalic dikes, unlike any seen in the Western Ghats flows and alkalic complexes.

The Rangpur dike suite, despite its close proximity to the carbonatitic complexes of Phenai Mata and Amba Dongar, is geochemically distinct, in that it is subalkalic to mildly alkalic, and dominantly potassic whereas the two intrusive complexes are sodic. Future efforts should involve the characterization of the Pb isotope ratios of the Murud-Janjira dikes, in order to constrain the nature of mantle and crustal components involved in the petrogenesis of the magmas and compare them with the end-members inferred to play a part in the evolution of the tholeiitic series. Furthermore, field, petrological, chemical and isotopic work is required to determine the relative timing of the subalkalic and alkalic dikes of Rangpur, and their timing and petrogenesis relative to the neighboring carbonatitic complexes.

CHAPTER 4

PETROGENETIC PROCESSES OF THE LOUISVILLE SEAMOUNT CHAIN AND GEOCHEMICAL EVOLUTION OF ITS MANTLE SOURCE

Loÿc Vanderkluysen[1], John J. Mahoney[1], Anthony A. P. Koppers[2,a], Peter F. Lonsdale[2] & Jeffrey S. Gee[2]

1. Department of Geology and Geophysics, School of Ocean and Earth Science and Technology, University of Hawai‘i, Honolulu, HI 96822, U.S.A.

2. Scripps Institution of Oceanography, University of California, San Diego, La Jolla, CA 92093, USA

a. Current address: College of Oceanic and Atmospheric Sciences, Oregon State University, Corvallis, OR 97331, USA

INTRODUCTION

The Louisville Seamount Chain (LSC) is a 4300 km long chain of seamounts and guyots (Lonsdale, 1988) in the South Pacific Ocean, extending from 138.1º W, 50.9° S at its eastern end, in the vicinity of the Heezen Fracture Zone, to the Tonga-Kermadec Trench at its western edge (175.3° W, 25.7° S), where it is subducted (Fig. 4.1). Menard

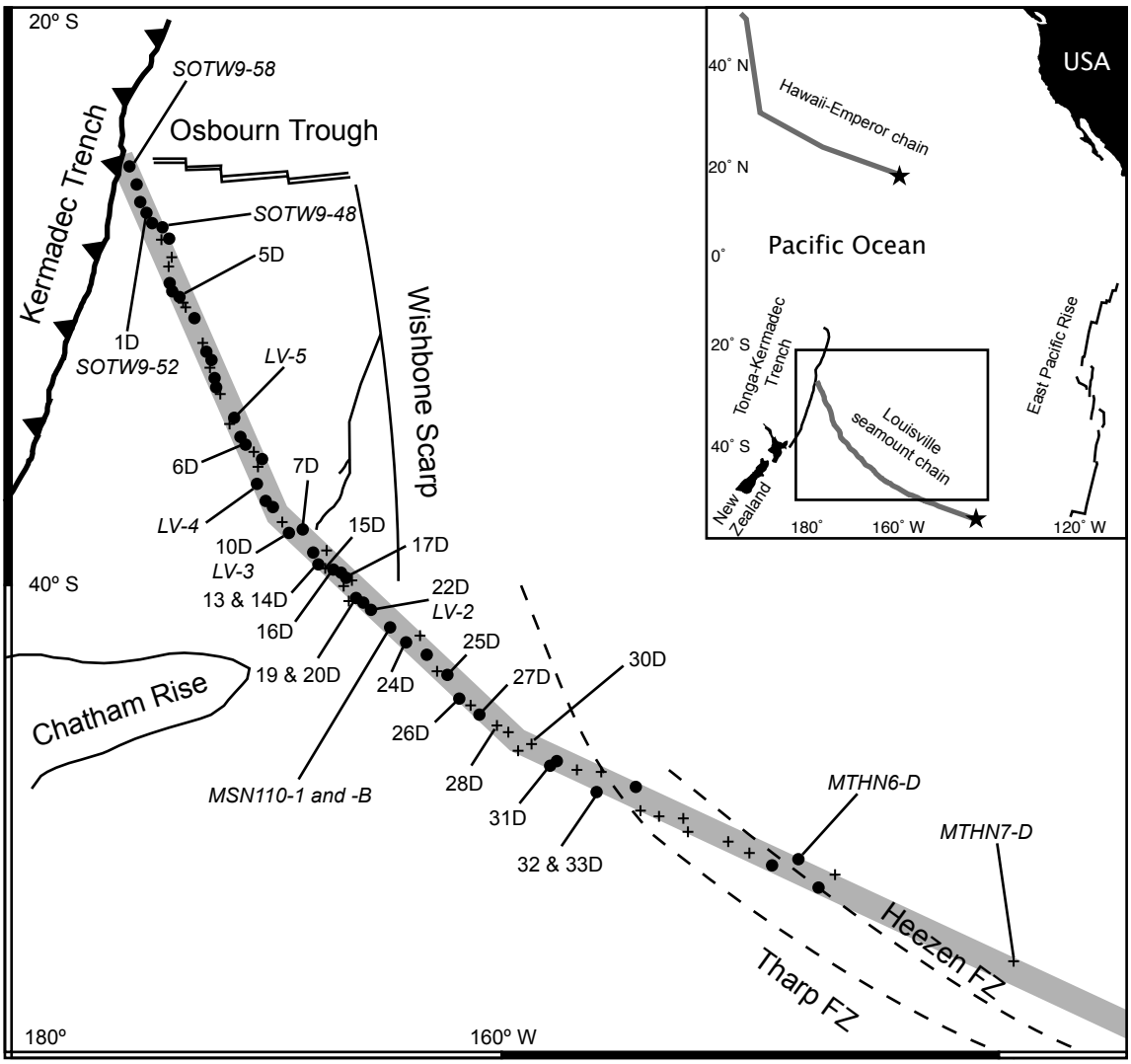

Fig. 4.1: Location of the Louisville Seamount Chain. Insert shows two other major geological features: the East Pacific Rise and the Hawai‘i-Emperor chain. The inferred Louisville (Lonsdale, 1988) and Hawai‘ian (Wessel & Kroenke, 2008) hotspot locations are indicated by black stars. Rectangle in insert indicates area displayed in main map. The Louisville Seamount Chain is indicated by gray-shading. Guyots are indicated by black circles, other seamounts by crosses. Dredge sites of cruise AMAT02RR for which volcanic samples were recovered are indicated by the dredge site number. Dredge sites of the Cheng *et al*. (1987) and Hawkins *et al*. (1987) studies are labeled in italics. F Z = fracture zone.

et al. (1964) first reported the existence of an 1100 km long section of the chain. Its origin was linked to the Eltanin transform fault system, which includes the Heezen and Tharp fracture zones (Fig. 4.1; Hayes & Ewing, 1971; Larson & Chase, 1972). Over the years, however, the hypothesis of a hotspot origin for the Louisville chain has become prevalent (e.g., Hawkins, 1973; Epp, 1978; Jurdy, 1978; Lonsdale, 1988; Clague & Jarrard, 1973; Molnar *et al*., 1975; Vogt *et al*., 1976; Cheng *et al*., 1987; Koppers *et al*., 2004). Geochronological studies (Watts *et al*., 1988; Koppers *et al*., 2004, Koppers *et al*., 2007b) have shown the existence of a progression, though not linear, in seamount ages, going from the oldest (78 Ma) at the northwestern, Tonga Trench end of the chain to the youngest dated seamount (1.1 Ma) at 139º 9' W. Two first-order bends (~47 and 25 Ma) have been recognized in the chain (at 169º W and 159º W; Lonsdale, 1988). These are coeval with similar bends in the Hawai'i-Emperor chain (e.g., Lonsdale, 1988; Sharp & Clague, 2002; Koppers *et al*., 2004), and are interpreted as recording changes in Pacific plate motion.

The LSC represents an ideal site to study hotspot-related petrogenetic processes because it is the only other long-lived hotspot trail on the Pacific plate besides the Hawai'i-Emperor seamount chain. As a result, study of the LSC is of critical importance to test models based on the study of the Hawai'i hotspot trail, such as Pacific plate absolute motion (e.g., Wessel & Kroenke, 2008), evolution of ocean island volcanism (e.g., Stearns, 1966; Macdonald, 1968) and genesis of ocean island basalts (OIB). Previous geochemical studies of ocean islands have presented compelling evidence for the presence of compositional heterogeneity in the mantle sources of OIB (e.g., Rhodes & Hart, 1995; Lassiter & Hauri, 1998; Hauri *et al*., 1996; Sobolev *et al*., 2000; Regelous *et*

al., 2003; Devey *et al*., 2003); such heterogeneity is thought to result from recycled oceanic crust, lower continental crust, sediments and/or lithospheric mantle. These recycled materials are generally imagined to be in the form of blobs, streaks or veins (ibid.) within a peridotitic mantle matrix. The matrix in itself is heterogeneous because of the presence of variably aged residues of diverse amounts of partial melting of the mantle, some perhaps dating back to early Earth differentiation before plate tectonics (e.g., Weaver, 1991; Hofmann & White, 1982; Chauvel *et al*., 1992; Pilet *et al*., 2005; Boyet & Carlson, 2006). How much of the range observed in the isotopic composition of Hawai‘ian lavas (the present-day ε_{Nd} value of the Ko‘olau shield-stage lavas alone range from -1.9 to +6.7; Roden *et al*., 1984; 1994; Jackson *et al*., 1999) and other OIB reflects variations in the composition of the mantle source, as opposed to variations in melting conditions, remains uncertain (e.g., Rhodes & Hart, 1995; Lassiter *et al*., 1996; Keller *et al*., 2000; Blichert-Toft *et al*., 2003; Regelous *et al*., 2003; Kurz *et al*., 2004; Ito & Mahoney, 2005a, b; Abouchami *et al*., 2005; Huang *et al*., 2005; Marske *et al*., 2007). One of the factors influencing melting conditions is the thickness of the lithosphere, and hence, the crustal age at the time of the emplacement of ocean islands (e.g., Ito & Mahoney, 2005a). The Louisville volcanoes appear to have been emplaced on oceanic crust of relatively constant age, 40-55 Myr old for much of the chain’s history. Exceptions are seamounts just west of the Wishbone Scarp (see Fig. 4.1), emplaced on 60-Myr-old or older crust, and the westernmost seamounts, emplaced on crust ≤30 Myr old close to the Osbourn Trough fossil spreading center (Lonsdale, 1988; Watts *et al*., 1988; Lyons *et al*., 2000; Worthington *et al*., 2006). This contrasts with the Hawai‘i-Emperor chain, where the age of the crust at the time seamounts were emplaced varies

between the northern (near-ridge) and southeastern seamounts (100 Ma). Detroit Seamount, located at the northern end of the chain, appears to have been emplaced very close to a paleo-spreading centre (e.g., Cottrell & Tarduno, 2003), whereas modern Hawai‘ian volcanoes are emplaced on old, Cretaceous crust (~100 Myr old; e.g., Waggoner, 1993; Müller *et al*., 1997).

The LSC also presents some characteristics that sets it apart from other hotspot chains. Lonsdale (1988) noted that southeast of the 159º W bend (i.e., seamounts younger than ~25 Ma), seamount average size, and therefore, volcanic production rates decline sharply, coupled with a doubling in average spacing between volcanic centers. Magma supply rates prior to 25 Myr appear to have been rather uniform. These characteristics, in combination with evidence from seismic tomography (Montelli *et al*., 2004), indicate that Louisville hotspot activity is waning and that the mantle plume presumed to feed it may be dissipating, or might have already died – possibly the only case worldwide.

The LSC lacks any emergent volcano and, with a ~2500 km section of the chain located in the latitudes of the “roaring forties”, has proven difficult to study. Prior to 2002, chemical analyses existed for only 22 samples, dredged on eleven volcanoes (Hawkins *et al*., 1987). The are overwhelmingly alkalic, consisting of alkalic basalts, basanites, trachybasalts and basaltic trachyandesites with sodic affinity (i.e., hawaiites and mugearites). Strontium and Nd isotopic analyses of 15 samples from six seamounts, and eight Pb isotope analyses, were reported by Cheng *et al*. (1987). The dredge hauls were generally located close to or at the tops of guyots and the summits of non-guyot seamounts, and were taken during four cruises (1961 Monsoon: Menard *et al*., 1964; 1971 Southtow: Hawkins, 1973; 1979 Vema-36-02: Watts *et al*., 1988; 1984 Marathon:

Lonsdale, 1988). Cheng *et al*. (1987) suggested that the Louisville mantle source may have remained extraordinarily homogeneous over more than 60 Myr (nearly its entire history). However, because the rocks were overwhelmingly alkalic and came from the upper parts of seamounts, it was unclear whether sampling was biased and lacked tholeiitic shield-stage lavas. In 2002, additional samples were collected during cruise 167 of the German research vessel F.S. *Sonne*; these rocks are currently being processed (Stoffers *et al*., 2003; Worthington *et al*., 2006).

We dredged samples during Leg 02 of the AMAT expedition of the R.V. *Revelle* of the Scripps Institution of Oceanography in the Spring of 2006. This was a site survey cruise for drilling of the LSC by the Integrated Ocean Drilling Program (IODP proposal #636). Here we present results of a geochemical investigation of major and trace element and Pb-Nd-Sr isotopic compositions of dredged lavas from 19 seamounts (ranging from ~72-24 Ma; Koppers *et al*., 2004), only three of which had been sampled prior to 2002. The aims of the study were to (1) compare the chemical and isotopic differences (if any) between shield phase and post-shield lavas of the Louisville volcanoes, (2) recognize systematic variations in composition, particularly with respect to the "dying end" of the chain, and (3) assess components involved in the mantle source of Louisville magmatism. We use our results to draw comparisons between the LSC and other hotspot tracks, evaluate existing petrogenetic models, and discuss implications for other Pacific hotspots and hotspots elsewhere around the world. We also evaluate a proposed genetic link between the Louisville hotspot and the greater Ontong Java Plateau (OJP) (e.g., Mahoney & Spencer, 1991; Richards *et al*., 1991; Tarduno *et al*., 1991).

SAMPLING

Thirty-three stations were dredged during AMAT Leg 02, targeting 22 seamounts. Specific care was taken to dredge sharply defined landslide scarps and deep incisions on the steep flanks of volcanoes. Our aim was to ensure as representative a sampling of volcanic units as possible by tapping the inner, shield-phase of volcanoes, as opposed to only the alkalic, post-shield carapaces, assuming that Louisville volcanoes follow the Hawai‘ian island evolutionary model of tholeiitic shield to alkalic post-shield to alkalic rejuvenated-stage volcanic development. A few dredge hauls (2D, 3D, 8D, 9D, 18D, 19D, 21D and 23D) targeted parasitic cones or summit pinnacles to sample products of the later phase(s) of activity; in all but one case (19D), these dredge hauls yielded only sedimentary rocks (foraminiferous and nummulitic (9D) limestone), foraminifer ooze, whip and branching corals, and sea stars.

Other dredge hauls recovered a few ~5- to 50-cm-size volcanic rocks of varied mineralogy, which were coated with 1-3 mm (and up to 3 cm) of botryoidal ferromanganese crust. The rocks were sawed and split, and then described onboard using a binocular microscope. Dredge 20D, targeting the steep slopes of a gully on the seamount’s flanks, was by far the most successful, recovering ~50 kg of volcanic rocks from seven visually recognizable lava groups differing in phenocryst assemblage and texture.

The samples were typically fine-grained aphyric or olivine- and clinopyroxene-phyric basaltic rocks. The primary mineral assemblage was olivine, clinopyroxene and plagioclase, which were found in varying amounts and sizes. Phenocrysts, when present, were found to range up to 30% for olivine, 25% for clinopyroxene and 10% for

plagioclase. Phenocryst sizes ranged from 1-18 mm, 1-11 mm and 1-3 mm for olivine, clinopyroxene and plagioclase, respectively.

METHODS

All samples showed varying degrees of alteration. To limit the effects of alteration on our analyses, the least altered, inner cores of samples were preferentially selected for analysis. Major element compositions and some trace element concentrations were determined, respectively, on fused glass disks and pressed powder pellets by X-ray fluorescence (XRF) spectrometry at Washington State University (Norrish & Chappell, 1977; Johnson *et al*., 1999). Powders were prepared using a tungsten carbide mill (Table 4.1). Other trace element concentrations were determined by inductively coupled plasma mass spectrometry (ICP-MS) in the same laboratory (Knaack *et al*., 1994). Analytical precision (2σ) is estimated to be 2-6% based on repeated analyses of standards (ibid.).

Sample preparation and mass spectrometric procedures for Sr, Nd and double-spike Pb isotopic measurements and corresponding parent-daughter isotope-dilution measurements were carried out on a VG Sector multi-collector thermal-ionization mass spectrometer at the University of Hawai‘i following Mahoney *et al*. (1991) and Sheth *et al*. (2003), except that Pb isotopic measurements were carried out by multi-collector dynamic routine rather than static mode. Analyses were performed on splits prepared from small (1-2 mm) rock chips from the interiors of acid-cleaned samples; the chips were picked to avoid alteration and phenocrysts and acid-cleaned prior to dissolution. Although concentrations of Pb, Th, U, Sr, Nd and Sm determined by isotope dilution are

generally in good agreement (≤10%) with ICP-MS data,. Rb shows greater variation. Isotope-dilution values are used only for age correction of the Pb, Sr and Nd isotope ratios because concentrations of picked grains are not strictly representative of the whole-rocks. An exception was made for sample 13D-1; the split of this sample and sample 16D-1 measured by ICP-MS were contaminated with Pb, as shown by anomalously high Pb concentrations of 15.36 and 13.10 ppm, respectively.

RESULTS

Effects of alteration

All samples displayed varying degrees of alteration. Apart from the ferromanganese coating and iddingsitization of olivines, which were found in all samples, visual and binocular microscope examination revealed vesicle fillings of carbonate and phosphate (e.g., 6D-3), hydration and devitrification of volcanic glass (e.g., 10D-5) and replacement of plagioclase and groundmass phases by clay minerals. Some samples also displayed a thin palagonite rind, up to 3 mm in thickness.

Chemically, alteration is expressed in our samples by anomalous peaks and/or troughs in some elements (e.g., Rb, K, U, P, Sr) in primitive-mantle-normalized incompatible element patterns, uncharacteristically high La/Ta ratios (>14, La peak) and/or elevated weight loss on ignition (2.7-11.2 wt%, largely associated with alteration of primary phases to clay minerals) (Fig. 4.2A). More rarely, it is also expressed by elevated CaO and Na_2O (5D-1, 30D-3), and negative Ce anomalies (5D-1, 6D-3, 6D-6, 16D-1, 19D-1, 24D-2, 28D-1, 30D-5, 32D-5). For the purpose of this study, we have classified samples using four categories of alteration (Table 4.1). Samples with “low”

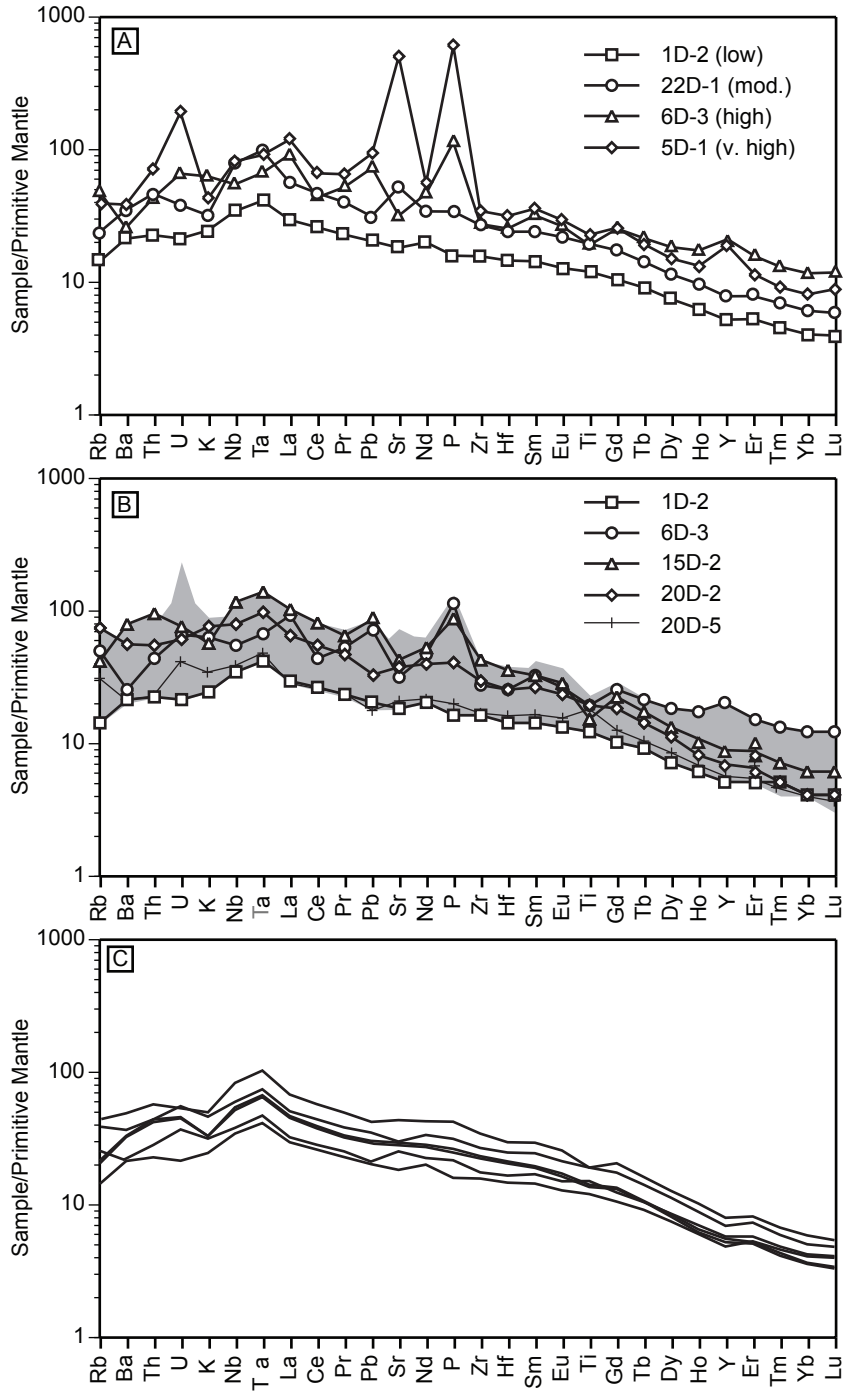

Fig. 4.2: Primitive-mantle-normalized incompatible element patterns of some LSC samples, using primitive mantle values of Sun & McDonough (1989). (A) Effects of alteration on incompatible trace element patterns. (B) Representative patterns showing the range of observed incompatible trace element behavior in the LSC: 1D-2 (squares), 20D-2 (diamonds), 15D-2 (triangles) and 6D-3 (circles). 20D-5 (crosses) is also shown to compare with 20D-2 and illustrates the range of patterns found in the same seamount. Gray field represents the total observed variation among lightly to highly altered samples. (C) Patterns of all samples determined to have undergone low degrees of alteration.

Table 4.1: Major and trace element compositions of Louisville lavas. Major element concentrations are given in wt% of oxide on a volatile-free basis, trace elements in ppm. LOI stands for (weight) loss on ignition at 900°C for 8 hours. "Moderate" alteration is indicated by anomalous peaks and/or troughs in some incompatible-element patterns (e.g., Rb, K, U); "high" is expressed by an anomalously high P concentration as a result of secondary phosphate precipitation, a high relative Sr content, uncharacteristically high La/Ta ratios (>14), and/or elevated LOI (>4). "V. high" (very high) indicates samples for which all of the above geochemical characteristics are observed. CIPW norm is given for samples with low or moderate alteration. † indicates samples for which Pb concentration appears to reflect major Pb contamination of the split analyzed by ICP-MS. Pb isotope dilution value is substituted for sample 13D-1.

Table 4.1: Major and trace element compositions of Louisville lavas

	1D-2	1D-3	5D-1	6D-3	6D-6	7D-1	7D-3	7D-5	7D-6	10D-1	10D-2
Lat. S	27º 30.9'	27º 30.9'	29º 38.1'	35º 50.55'	35º 50.55'	38º 2.3'	38º 2.3'	38º 2.3'	38º 2.3'	38º 10.25'	38º 10.25'
Long. W	174º 20.3'	174º 20.3'	173º 22.8'	169º 53.7'	169º 53.7'	168º 15.8'	168º 15.8'	168º 15.8'	168º 15.8'	168º 39.45'	168º 39.45'
Max. depth (m)	2498	2498	2237	2067	2067	1950	1950	1950	1950	1535	1535
Seamount	27.6	27.6	29.6	35.8	35.8	168.3	168.3	168.3	168.3	168.6	168.6
Alteration	Low	Moderate	V. high	High	High	Moderate	Moderate	Moderate	Moderate	High	High
SiO_2	46.37	47.31	25.32	47.58	46.72	43.71	45.22	46.92	46.07	44.16	45.15
TiO_2	2.39	3.02	4.53	3.80	3.78	3.03	2.91	3.37	3.35	4.39	4.30
Al_2O3	13.68	15.35	12.65	16.00	15.90	11.86	12.76	15.42	15.42	16.87	16.44
FeO*	11.12	11.26	14.58	12.03	11.80	12.57	10.72	11.46	11.82	13.56	10.54
MnO	0.17	0.17	0.16	0.17	0.06	0.19	0.19	0.17	0.16	0.18	0.13
MgO	11.10	6.38	2.79	2.67	3.03	13.78	9.50	5.21	5.20	2.82	2.31
CaO	10.92	11.40	19.57	9.60	10.13	9.97	13.25	11.82	11.77	9.34	10.66
Na_2O	2.12	2.90	1.36	3.49	3.51	2.12	2.46	2.66	2.61	3.57	3.65
K_2O	0.70	1.00	1.22	1.80	2.22	1.00	1.09	1.11	1.14	1.73	2.02
P_2O_5	0.32	0.44	12.29	2.31	2.47	0.54	0.40	0.53	0.57	2.44	2.32
Sum	98.89	99.23	96.02	99.72	99.88	98.77	98.51	98.68	98.13	99.44	97.53
LOI (%)	3.11	1.78	11.21	3.20	3.58	1.40	7.06	2.65	3.24	3.48	3.59
XRF											
Ni	280	76	169	44	41	351	238	75	86	32	21
Cr	692	101	241	72	50	684	665	80	78	4	5
Sc	32	30	22	33	29	23	30	30	30	17	16
V	277	328	283	298	268	259	274	326	334	208	212
Ba	145	190	272	173	217	274	141	216	205	489	475
Rb	9	16	25	30	37	18	26	30	32	22	26
Sr	373	514	10725	645	637	632	375	573	570	1379	1408
Zr	169	223	387	294	265	249	196	235	232	307	300
Y	23	27	86	91	77	23	26	30	29	44	42
Nb	23.2	30.7	57.5	36.7	34.0	43.1	25.6	35.1	34.4	62.5	60.6
Ga	20	25	16	24	23	20	19	24	24	26	27
Cu	92	92	202	69	70	60	51	50	53	30	27
Zn	99	105	247	169	108	113	145	149	167	180	161
ICP-MS											
La	18.9	26.9	76.3	58.8	53.0	34.1	20.0	27.9	27.8	60.1	58.7
Ce	43.1	60.6	110	72.0	64.7	73.4	45.9	62.7	62.3	134	131
Pr	5.74	7.97	16.41	13.10	11.35	9.35	6.23	8.25	8.21	17.66	17.20
Nd	24.7	34.3	69.0	57.4	49.5	38.5	27.6	35.6	35.3	77.4	75.5
Sm	5.79	7.93	14.41	12.81	11.10	8.21	6.84	8.44	8.27	16.90	16.48
Eu	1.95	2.61	4.48	4.03	3.51	2.66	2.33	2.80	2.76	5.57	5.41
Gd	5.66	7.56	13.86	13.68	11.50	7.41	6.71	8.07	8.04	15.36	15.09
Tb	0.89	1.15	1.90	2.11	1.76	1.07	1.04	1.24	1.23	2.09	2.05
Dy	4.97	6.34	10.07	12.27	10.05	5.57	5.81	6.77	6.79	10.56	10.47
Ho	0.92	1.16	1.94	2.54	2.06	1.00	1.06	1.25	1.24	1.84	1.79
Er	2.29	2.82	4.88	6.70	5.23	2.26	2.52	2.99	3.00	4.19	4.07
Tm	0.31	0.37	0.62	0.88	0.70	0.28	0.33	0.39	0.39	0.51	0.51
Yb	1.77	2.08	3.54	5.10	4.00	1.57	1.85	2.26	2.19	2.78	2.71
Lu	0.26	0.31	0.59	0.79	0.63	0.22	0.27	0.32	0.33	0.39	0.39
Ba	133	180	246	160	198	267	128	205	194	471	458
Th	1.78	2.71	5.60	3.40	3.14	3.31	1.89	2.84	2.77	4.82	4.75
Nb	21.7	30.7	45.0	35.8	33.0	43.2	24.0	34.5	34.5	61.1	60.4
Y	22.2	27.5	81.0	92.2	77.3	23.4	25.0	29.8	29.6	44.5	44.5
Hf	4.09	5.43	8.84	7.12	6.52	5.86	4.63	5.82	5.81	7.35	7.10
Ta	1.51	2.11	3.33	2.44	2.30	2.93	1.63	2.37	2.36	4.22	4.13
U	0.43	0.39	3.83	1.32	1.42	0.93	0.59	0.82	0.74	2.51	1.51
Pb	1.41	1.69	6.47	5.03	6.01	1.94	1.26	1.87	1.89	3.56	3.00
Rb	8.38	15.62	24.13	28.07	34.32	18.05	23.79	29.36	31.98	22.37	27.01
Cs	0.33	0.69	0.77	1.58	0.64	0.28	1.25	2.60	2.64	0.74	0.62
Sr	365	508	9325	660	622	650	359	577	576	1394	1422
Sc	33.6	32.6	22.4	35.5	31.5	25.8	31.8	32.6	32.5	18.8	18.7
Zr	157	215	340	274	244	242	176	224	223	298	295
Plagioclase	44	48				31	28	49	48		
Orthoclase	4	6				6	7	7	7		
Nepheline		1				4	8	0	1		
Diopside	22	23				21	35	24	23		
Hypersthene	1										
Olivine	22	13				29	16	10	11		
Ilmenite	5	6				6	6	7	7		
Magnetite	2	2				2	0	2	2		
Apatite	1	1				1	1	1	1		

Table 4.1 (continued): Major and trace element compositions of Louisville lavas

	10D-3	10D-4	13D-1	14D-5	14D-6	14D-11	15D-1A	15D-2	16D-1	17D-1	19D-1
Lat. S	38º 10.25'	38º 10.25'	39º 5.3'	39º 12.8'	39º 12.8'	39º 12.8'	39º 31.1'	39º 31.1'	39º 40.3'	39º 51.8'	40º 25.65'
Long. W	168º 39.45'	168º 39.45'	167º 31.5'	167º 37.1'	167º 37.1'	167º 37.1'	167º 15.0'	167º 15.0'	166º 38.6'	166º 2.65'	165º 41.0'
Max. depth (m)	1535	1535	1920	2335	2335	2335	2318	2318	2462	2439	1262
Seamount	168.6	168.6	167.4	167.4	167.4	167.4	167.3	167.3	166.6	166.1	165.7
Alteration	High	High	Moderate	Moderate	High	High	High	High	V. high	Moderate	High
SiO_2	42.30	42.93	44.80	45.54	43.74	44.53	47.43	46.40	46.36	47.20	42.96
TiO_2	4.69	4.43	4.07	3.68	4.28	4.41	2.88	2.93	4.32	3.26	4.18
Al_2O3	17.91	17.13	16.41	15.14	16.40	15.54	19.14	19.41	15.35	14.94	14.13
FeO*	14.29	14.45	14.42	13.15	13.92	13.78	11.75	12.42	11.36	10.62	15.03
MnO	0.14	0.17	0.21	0.21	0.19	0.17	0.12	0.21	0.14	0.13	0.25
MgO	2.14	2.50	4.29	7.36	3.57	4.71	2.62	2.87	3.94	5.61	9.89
CaO	9.47	10.54	8.40	10.58	10.98	10.95	8.55	8.48	11.08	11.57	8.70
Na_2O	3.24	3.27	3.03	2.78	3.33	2.71	3.66	3.41	3.16	2.87	2.54
K_2O	1.89	1.69	1.69	1.00	1.59	1.14	1.68	1.61	1.49	1.13	0.95
P_2O_5	2.70	2.56	0.81	0.59	1.12	0.67	1.55	1.77	1.10	0.57	0.68
Sum	99.16	100.07	98.14	100.35	99.41	98.62	99.74	99.88	98.30	97.92	99.60
LOI (%)	6.20	5.46	4.52	2.78	6.06	2.72	6.60	8.24	3.58	1.71	8.06
XRF											
Ni	28	30	107	116	34	44	28	58	74	69	232
Cr	5	3	71	311	4	11	8	10	95	139	48
Sc	18	16	25	25	22	25	8	8	25	31	31
V	253	237	382	291	334	381	154	160	374	308	335
Ba	432	432	272	233	280	284	569	564	257	160	285
Rb	29	26	32	17	19	22	25	27	35	41	10
Sr	1380	1501	530	667	740	707	907	910	634	582	493
Zr	324	304	330	287	318	301	471	478	320	197	256
Y	45	43	31	30	36	32	40	40	46	28	30
Nb	65.0	60.9	49.7	43.0	52.0	45.6	80.2	82.3	43.1	26.2	34.1
Ga	26	24	24	24	25	26	29	30	28	20	22
Cu	26	24	72	61	51	70	36	50	102	71	59
Zn	172	164	172	129	135	146	201	213	190	98	187
ICP-MS											
La	61.0	57.8	38.3	34.0	42.4	36.5	65.5	65.5	41.9	23.4	27.0
Ce	136	129	80.4	75.4	86.8	80.5	134	133	84.5	53.8	58.2
Pr	17.98	17.01	10.58	9.77	11.24	10.57	16.44	16.35	11.51	7.35	8.36
Nd	78.9	74.3	44.4	41.6	46.8	45.5	64.9	64.5	49.4	32.5	36.2
Sm	17.06	16.34	10.13	9.61	10.37	10.62	13.43	13.13	11.13	7.84	8.66
Eu	5.65	5.33	3.25	3.13	3.36	3.46	4.30	4.26	3.65	2.70	3.14
Gd	15.75	14.93	9.53	9.02	9.61	9.93	11.74	11.70	11.00	7.92	8.39
Tb	2.14	2.03	1.40	1.33	1.45	1.47	1.73	1.67	1.59	1.17	1.21
Dy	10.79	10.36	7.42	7.05	7.94	7.75	9.01	8.91	8.79	6.35	6.66
Ho	1.88	1.80	1.30	1.23	1.48	1.35	1.61	1.56	1.63	1.17	1.20
Er	4.29	4.06	3.11	2.90	3.45	3.10	3.80	3.71	4.04	2.82	2.88
Tm	0.52	0.50	0.39	0.36	0.46	0.39	0.49	0.48	0.51	0.37	0.37
Yb	2.84	2.67	2.12	2.02	2.60	2.12	2.70	2.73	2.92	2.09	2.11
Lu	0.41	0.39	0.31	0.28	0.39	0.31	0.40	0.39	0.43	0.30	0.31
Ba	406	405	253	217	263	262	537	515	235	151	253
Th	4.94	4.68	3.92	3.36	4.02	3.69	7.44	7.46	4.00	2.25	2.51
Nb	63.4	60.2	49.1	42.4	51.1	45.5	79.1	76.8	41.3	26.8	32.5
Y	46.1	43.9	32.7	29.9	36.8	33.1	40.5	39.6	45.5	28.4	29.2
Hf	7.53	7.07	7.68	6.86	7.35	7.43	9.81	9.78	7.80	4.98	6.02
Ta	4.28	4.04	3.27	2.87	3.52	3.11	5.14	5.05	2.92	1.86	2.23
U	1.57	1.29	1.88	0.87	1.04	0.62	1.17	1.53	0.87	0.62	1.80
Pb	3.14	2.93	2.24†	2.30	3.40	2.39	4.87	5.92	13.10†	1.51	5.13
Rb	29.28	26.44	31.96	16.86	18.32	22.71	23.95	24.95	33.31	40.42	10.97
Cs	1.05	0.98	0.68	0.38	0.23	1.25	0.54	0.48	1.66	3.31	0.34
Sr	1350	1492	542	677	740	732	894	867	624	596	474
Sc	20.1	19.1	26.2	29.2	24.0	27.4	9.1	8.4	26.1	33.0	31.2
Zr	309	293	318	276	301	293	445	437	299	189	233
Plagioclase			51	47						48	
Orthoclase			10	6						7	
Nepheline			1	2						1	
Diopside			9	19						24	
Hypersthene											
Olivine			17	16						10	
Ilmenite			8	7						6	
Magnetite			2	2						2	
Apatite			2	1						1	

Table 4.1 (continued): Major and trace element compositions of Louisville lavas

	20D-1	20D-2	20D-3	20D-5	20D-8	20D-9	20D-15B	20D-17	22D-1	22D-3	22D-4
Lat. S	40º 26.5'	40º 26.5'	40º 26.5'	40º 26.5'	40º 26.5'	40º 26.5'	40º 26.5'	40º 26.5'	40º 44.5'	40º 44.5'	40º 44.5'
Long. W	165º 44.2'	165º 44.2'	165º 44.2'	165º 44.2'	165º 44.2'	165º 44.2'	165º 44.2'	165º 44.2'	165º 27.6'	165º 27.6'	165º 27.6'
Max. depth (m)	2179	2179	2179	2179	2179	2179	2179	2179	1899	1899	1899
Seamount	165.7	165.7	165.7	165.7	165.7	165.7	165.7	165.7	165.4	165.4	165.4
Alteration	High	Moderate	Moderate	Moderate	Moderate	Moderate	Moderate	High	High	Moderate	Moderate
SiO_2	46.51	46.76	47.71	46.63	46.90	47.58	45.09	44.52	44.45	45.78	46.89
TiO_2	4.08	3.83	3.63	3.58	3.45	4.28	3.03	3.02	3.88	3.69	3.70
Al_2O3	15.97	15.64	15.93	15.30	16.63	15.93	14.46	14.65	18.45	17.72	18.09
FeO*	11.34	11.22	11.16	10.84	10.85	8.74	13.87	13.01	13.40	12.71	11.65
MnO	0.15	0.13	0.14	0.15	0.15	0.15	0.19	0.22	0.19	0.19	0.17
MgO	6.27	4.45	4.18	7.25	6.19	3.91	6.10	6.27	3.85	3.68	3.47
CaO	7.72	9.88	10.83	10.45	10.46	12.28	13.27	12.16	10.57	10.25	10.96
Na_2O	3.61	3.57	3.32	3.81	2.89	3.38	2.61	2.73	3.04	3.27	3.26
K_2O	2.02	2.16	1.34	0.97	1.16	1.55	1.10	1.08	0.92	1.31	1.33
P_2O_5	1.04	0.82	0.54	0.40	0.43	0.58	0.56	0.56	0.70	0.61	0.61
Sum	98.71	98.44	98.79	99.39	99.13	98.38	100.61	98.24	99.75	99.47	100.38
LOI (%)	4.73	4.88	1.80	3.71	3.30	3.94	3.86	2.76	3.40	2.44	2.90
XRF											
Ni	69	50	69	119	106	41	182	246	36	23	26
Cr	50	12	79	174	134	31	547	922	3	3	3
Sc	22	19	26	29	23	27	30	33	19	18	18
V	278	273	289	325	292	332	281	334	289	266	263
Ba	329	383	217	144	178	260	240	194	237	257	261
Rb	38	46	29	19	23	36	19	18	14	27	27
Sr	705	781	575	426	573	617	595	667	1058	738	724
Zr	274	317	271	183	228	274	234	213	290	279	277
Y	31	30	32	25	26	34	25	25	35	32	32
Nb	44.0	54.3	42.1	26.0	34.6	42.4	40.4	35.1	53.0	50.5	51.4
Ga	26	27	25	22	24	26	21	20	23	24	26
Cu	46	39	42	77	55	88	96	83	25	22	24
Zn	252	143	124	141	115	103	153	157	135	119	121
ICP-MS											
La	36.9	41.7	31.1	18.0	25.0	31.8	29.0	24.7	36.3	35.0	35.1
Ce	83.1	90.3	69.2	42.5	55.6	71.0	61.9	53.9	78.1	76.2	75.5
Pr	11.13	11.56	9.18	5.97	7.30	9.45	8.03	7.04	10.12	9.85	9.77
Nd	47.8	48.6	39.1	26.6	31.2	40.9	33.7	30.3	42.4	41.3	41.3
Sm	10.57	10.58	9.09	6.60	7.48	9.57	7.60	7.03	9.66	9.53	9.31
Eu	3.69	3.57	3.12	2.35	2.56	3.35	2.59	2.45	3.34	3.18	3.17
Gd	9.80	9.85	8.92	6.70	7.26	9.43	7.32	7.01	9.39	9.02	9.12
Tb	1.38	1.36	1.33	1.01	1.09	1.41	1.08	1.04	1.40	1.34	1.34
Dy	7.30	7.09	7.48	5.59	5.97	7.78	5.83	5.73	7.66	7.37	7.37
Ho	1.26	1.21	1.37	1.00	1.06	1.42	1.03	1.06	1.42	1.36	1.35
Er	2.86	2.82	3.29	2.35	2.57	3.42	2.43	2.50	3.42	3.34	3.37
Tm	0.36	0.34	0.44	0.30	0.34	0.44	0.32	0.33	0.47	0.44	0.43
Yb	1.99	1.92	2.49	1.73	1.93	2.51	1.83	1.83	2.66	2.51	2.54
Lu	0.28	0.27	0.36	0.25	0.27	0.37	0.25	0.27	0.39	0.37	0.36
Ba	304	347	205	135	165	250	222	183	222	246	248
Th	3.34	4.32	2.95	1.76	2.50	3.12	2.99	2.43	3.65	3.58	3.50
Nb	42.4	52.2	41.5	24.8	34.2	41.7	39.7	34.0	52.5	51.0	50.7
Y	30.2	29.9	33.2	23.7	25.9	34.3	25.1	25.4	35.7	33.2	34.0
Hf	6.39	7.12	6.56	4.49	5.41	6.56	5.55	5.12	6.74	6.46	6.43
Ta	2.88	3.54	2.84	1.75	2.33	2.84	2.70	2.31	3.60	3.48	3.43
U	1.02	1.21	0.88	0.82	0.69	1.06	0.99	0.99	0.77	1.01	1.20
Pb	1.81	2.37	1.70	1.22	1.26	1.81	1.55	1.42	2.15	2.00	2.10
Rb	35.85	43.20	28.55	19.26	22.25	34.84	18.97	18.16	13.51	26.19	26.63
Cs	1.55	1.59	0.88	1.50	0.71	1.16	0.31	0.20	0.36	0.94	1.03
Sr	689	768	587	420	571	615	591	678	1063	754	736
Sc	22.8	20.9	28.5	31.9	25.2	29.5	32.5	36.7	20.9	20.3	20.6
Zr	253	296	262	169	214	260	220	203	277	271	269
Plagioclase		41	50	42	53	45	36			54	55
Orthoclase		13	8	6	7	9	7			8	8
Nepheline		5	2	7	1	4	6			3	2
Diopside		20	22	22	17	28	31			15	16
Hypersthene											
Olivine		10	9	13	14	2	11			11	8
Ilmenite		7	7	7	7	8	6			7	7
Magnetite		2	2	2	2	1	2			2	2
Apatite		2	1	1	1	1	1			1	1

Table 4.1 (continued): Major and trace element compositions of Louisville lavas

	24D-2	24D-6	25D-1	26D-1	26D-3	27D-1	27D-7	27D-13	28D-1	30D-2	30D-3
Lat. S	41º 52.6'	41º 52.6'	42º 46.9'	43º 34.45'	43º 34.45'	43º 59.5'	43º 59.5'	43º 59.5'	44º 16.35'	44º 50.4'	44º 50.4'
Long. W	163º 41.7'	163º 41.7'	161º 58.2'	161º 29.1'	161º 29.1'	160º 37.0'	160º 37.0'	160º 37.0'	159º 48.8'	158º 28.35'	158º 28.35'
Max. depth (m)	1390	1390	1525	1514	1514	1435	1435	1435	1685	1504	1504
Seamount	163.6	163.6	162.0	161.5	161.5	160.7	160.7	160.7	159.8	158.5	158.5
Alteration	V. high	Low	V. high	Low	High	Moderate	High	High	High	High	High
SiO_2	42.13	46.91	37.38	46.17	45.55	45.27	44.27	45.58	49.06	47.95	43.21
TiO_2	4.03	3.78	5.19	3.78	3.84	3.16	3.63	3.34	3.86	3.98	3.82
Al_2O3	17.72	16.99	18.06	15.72	17.64	12.51	16.92	15.35	17.31	16.82	16.25
FeO*	13.30	11.44	18.30	12.04	12.00	12.09	13.78	12.77	7.68	8.76	9.86
MnO	0.40	0.17	0.15	0.16	0.13	0.17	0.14	0.27	0.52	0.11	0.18
MgO	3.20	4.69	3.65	4.89	5.11	11.31	4.11	5.04	4.24	4.25	5.29
CaO	11.20	9.07	10.54	10.77	8.71	10.80	10.16	10.72	10.78	11.50	15.67
Na_2O	3.50	3.65	2.69	3.20	3.60	2.51	3.30	3.45	3.66	3.63	2.92
K_2O	1.21	1.42	0.62	1.32	1.31	0.93	1.26	1.35	1.59	1.41	1.89
P_2O_5	2.98	0.86	2.07	0.64	1.03	0.54	1.14	0.79	0.83	0.88	0.90
Sum	100.20	98.99	99.18	98.70	98.94	99.29	98.71	98.66	99.54	99.29	100.30
LOI (%)	4.71	2.27	8.23	1.63	4.06	1.15	3.35	3.17	2.80	4.08	10.23
XRF											
Ni	65	16	191	57	41	317	134	193	179	50	100
Cr	43	3	466	38	3	663	403	391	178	43	50
Sc	17	16	29	24	16	26	24	23	36	29	24
V	292	247	388	330	248	259	349	290	290	308	256
Ba	381	328	272	244	325	238	268	245	239	215	293
Rb	15	27	5	24	24	16	11	23	24	26	53
Sr	2608	878	1948	601	727	623	717	654	604	820	702
Zr	379	367	379	283	366	243	327	298	264	256	300
Y	50	35	39	30	36	26	35	30	52	37	29
Nb	60.0	55.5	55.8	39.5	55.5	37.5	44.0	39.8	33.5	34.7	48.9
Ga	24	27	22	24	26	20	22	23	21	23	24
Cu	30	25	83	31	26	59	55	50	68	51	55
Zn	177	137	192	132	169	117	144	135	184	143	302
ICP-MS											
La	50.0	43.3	42.1	32.4	42.3	29.2	36.6	33.4	35.6	30.5	35.2
Ce	102	95.0	93.2	72.2	90.7	64.2	81.6	74.9	64.3	69.3	75.9
Pr	13.57	12.41	12.55	9.60	11.66	8.39	10.81	9.87	9.67	9.56	9.93
Nd	57.2	52.7	54.3	41.4	49.1	35.9	46.2	42.1	42.5	42.3	41.8
Sm	12.73	11.76	12.76	9.79	11.15	8.44	10.67	9.77	10.23	10.26	9.59
Eu	4.23	3.89	4.30	3.24	3.65	2.81	3.49	3.21	3.40	3.47	3.18
Gd	12.20	11.05	12.15	9.36	10.31	7.88	9.93	8.90	10.53	9.95	8.92
Tb	1.78	1.58	1.70	1.38	1.53	1.17	1.45	1.32	1.61	1.50	1.28
Dy	9.72	8.45	8.73	7.51	8.26	6.26	7.93	7.28	9.39	8.31	6.77
Ho	1.80	1.51	1.48	1.31	1.47	1.09	1.42	1.28	1.79	1.51	1.16
Er	4.44	3.52	3.31	3.16	3.52	2.53	3.44	3.04	4.59	3.66	2.63
Tm	0.57	0.45	0.40	0.40	0.45	0.32	0.43	0.39	0.60	0.47	0.33
Yb	3.27	2.56	2.16	2.19	2.57	1.75	2.48	2.17	3.39	2.65	1.78
Lu	0.47	0.36	0.31	0.32	0.37	0.26	0.37	0.32	0.52	0.39	0.25
Ba	351	311	238	231	293	228	253	229	224	197	261
Th	4.78	4.48	4.37	3.45	4.60	3.16	3.92	3.60	2.95	2.93	3.80
Nb	58.6	55.8	52.4	39.3	51.6	37.8	42.6	39.2	33.2	33.3	43.7
Y	51.6	36.8	39.1	32.2	36.5	26.0	35.8	31.1	54.3	38.6	28.4
Hf	8.61	8.26	8.80	6.91	8.14	5.98	7.76	7.08	6.62	6.22	6.46
Ta	3.93	3.76	3.58	2.72	3.49	2.60	2.94	2.72	2.27	2.30	2.89
U	3.76	1.07	3.32	1.11	0.88	0.68	2.27	0.99	4.73	2.91	2.08
Pb	10.53	2.89	2.84	2.41	3.05	1.81	2.55	2.68	2.87	3.69	2.34
Rb	15.81	26.17	5.29	22.47	22.59	15.67	11.55	22.70	22.63	25.64	52.37
Cs	0.70	1.17	0.14	0.15	1.75	0.28	0.08	0.14	0.24	0.55	2.62
Sr	2572	898	1914	616	707	634	721	664	600	799	659
Sc	18.6	18.7	31.9	24.7	16.2	28.1	26.1	25.0	41.8	32.7	25.3
Zr	366	358	357	273	339	236	315	286	250	244	267
Plagioclase		54		47		35					
Orthoclase		9		8		6					
Nepheline		2		3		3					
Diopside		11		21		24					
Hypersthene											
Olivine		13		11		22					
Ilmenite		7		7		6					
Magnetite		2		2		2					
Apatite		2		2		1					

Table 4.1 (continued): Major and trace element compositions of Louisville lavas

	30D-5	30D-15B	30D-15C	31D-2	31D-5	31D-7	32D-5	33D-1	33D-2	33D-3
Lat. S	44º 50.4'	44º 50.4'	44º 50.4'	45º 22.85'	45º 22.85'	45º 22.85'	46º 13.4'	46º 13.1'	46º 13.1'	46º 13.1'
Long. W	158º 28.35'	158º 28.35'	158º 28.35'	157º 43.75'	157º 43.75'	157º 43.75'	155º 52.75'	155º 52.75'	155º 52.75'	155º 52.75'
Max. depth (m)	1504	1504	1504	1560	1560	1560	1369	1128	1128	1128
Seamount	158.5	158.5	158.5	157.7	157.7	157.7	155.9	155.9	155.9	155.9
Alteration	High	High	V. high	Low	Moderate	Moderate	Moderate	Low	Low	High
SiO_2	46.76	47.86	41.28	46.47	46.31	47.32	45.42	46.13	46.01	42.42
TiO_2	3.42	2.90	4.22	2.99	3.08	2.86	3.66	2.70	2.81	3.39
Al_2O3	15.68	17.34	15.23	15.53	15.97	14.73	15.33	11.86	12.36	14.00
FeO*	13.76	11.69	11.46	10.81	11.15	10.83	14.28	12.31	12.53	14.81
MnO	0.56	0.44	0.62	0.16	0.14	0.16	0.15	0.15	0.16	0.20
MgO	4.84	2.25	5.37	6.02	5.80	7.27	3.91	13.31	12.12	9.44
CaO	8.95	7.07	12.00	13.29	12.73	12.53	9.89	8.77	9.23	11.47
Na_2O	3.21	4.67	4.91	2.50	2.48	2.49	3.48	2.46	2.58	2.29
K_2O	2.08	2.58	0.76	0.90	0.96	0.83	1.86	0.94	0.94	0.97
P_2O_5	1.02	2.48	3.04	0.44	0.52	0.34	0.85	0.50	0.54	0.86
Sum	100.65	99.61	99.18	99.11	99.15	99.36	99.25	99.13	99.28	100.18
LOI (%)	5.75	5.76	9.17	2.50	2.11	1.56	2.75	2.06	2.54	6.69
XRF										
Ni	291	135	226	125	101	118	239	387	364	343
Cr	505	3	12	214	131	226	728	558	560	457
Sc	27	12	20	34	36	35	30	19	22	25
V	326	191	299	378	376	351	313	203	214	270
Ba	273	351	168	145	150	153	296	218	223	231
Rb	36	47	5	16	16	14	38	12	13	11
Sr	559	569	616	512	550	490	708	569	598	569
Zr	251	471	316	187	185	178	301	239	249	256
Y	39	55	49	25	25	24	37	22	23	26
Nb	35.2	64.2	51.2	25.5	25.9	23.8	46.2	34.6	36.5	35.5
Ga	21	27	23	21	23	22	25	20	20	23
Cu	85	54	40	79	79	91	66	42	36	65
Zn	232	358	257	115	119	97	149	125	125	185
ICP-MS										
La	34.7	54.8	49.5	20.6	21.0	20.1	41.8	28.9	29.9	29.3
Ce	67.6	120	110	46.9	47.8	45.6	83.6	62.4	64.8	64.4
Pr	9.45	15.63	15.24	6.34	6.41	6.12	11.27	8.06	8.36	8.54
Nd	40.5	65.7	65.5	27.8	28.3	26.9	47.3	33.7	35.0	37.0
Sm	9.36	15.22	14.23	6.79	6.90	6.59	10.69	7.61	7.81	8.58
Eu	3.18	4.79	4.49	2.28	2.34	2.23	3.52	2.48	2.61	2.85
Gd	8.94	14.25	13.12	6.65	6.82	6.48	10.16	7.04	7.21	8.12
Tb	1.32	2.14	1.84	1.02	1.03	0.98	1.46	1.03	1.04	1.16
Dy	7.40	11.79	9.86	5.69	5.79	5.54	8.02	5.40	5.63	6.14
Ho	1.33	2.16	1.76	1.04	1.04	1.01	1.43	0.95	0.97	1.06
Er	3.24	5.22	4.19	2.49	2.54	2.44	3.46	2.20	2.26	2.40
Tm	0.41	0.68	0.52	0.32	0.33	0.32	0.44	0.28	0.29	0.30
Yb	2.30	3.87	2.85	1.84	1.86	1.79	2.50	1.56	1.59	1.65
Lu	0.35	0.57	0.41	0.27	0.27	0.26	0.36	0.22	0.23	0.23
Ba	251	324	149	139	140	139	280	207	208	203
Th	3.04	6.20	3.71	2.22	2.25	2.15	4.29	3.29	3.42	2.98
Nb	33.9	62.2	45.8	25.1	25.5	24.4	46.6	35.1	36.3	35.1
Y	39.2	55.9	47.1	25.1	25.7	24.4	38.8	23.2	23.9	26.8
Hf	6.04	10.79	6.80	4.64	4.75	4.61	7.60	5.72	5.94	6.10
Ta	2.29	4.12	2.82	1.72	1.76	1.67	3.17	2.37	2.45	2.31
U	2.26	2.96	1.76	0.74	0.81	0.88	2.13	0.90	0.92	1.37
Pb	4.08	5.39	6.92	1.47	1.51	1.44	3.61	2.00	2.10	2.34
Rb	34.55	44.57	5.74	15.90	15.81	14.42	38.90	12.43	12.75	10.24
Cs	0.68	0.69	0.23	0.81	0.70	0.48	0.83	0.45	0.33	0.41
Sr	551	558	585	514	562	498	739	585	607	571
Sc	28.5	13.0	20.5	39.4	39.2	37.6	31.9	22.9	23.3	26.4
Zr	234	443	286	177	177	172	300	232	241	244
Plagioclase				45	48	46	42	40	40	
Orthoclase				5	6	5	11	6	6	
Nepheline				3	2	1	5		1	
Diopside				29	25	27	20	18	19	
Hypersthene										
Olivine				10	11	13	11	29	26	
Ilmenite				6	6	5	7	5	5	
Magnetite				2	2	2	2	2	2	
Apatite				1	1	1	2	1	1	

degrees of alteration do not present any obvious disruption of their incompatible element patterns. Samples with "moderate" alteration display disturbed patterns in the more fluid-mobile elements (e.g., Rb, K, U, Ba; e.g., Humphries & Thompson, 1978; Seyfried & Bischoff, 1979), whereas "highly" altered samples show elevated La/Ta ratios (>14), possibly as a result of marine sediment contamination (e.g., Hole *et al*., 1984), peaks at Sr and P (resulting from precipitates of secondary phosphate and carbonate), and occasional negative Ce anomalies (generally interpreted as evidence of subaerial alteration in oxidizing, low-temperature conditions; e.g., Cotten *et al*., 1995). "Very highly" altered samples show all the signs mentioned above, with pronounced enrichments of P and Sr. In the figures used for interpretation of mantle source and petrogenesis, we do not include data for the highly and very highly altered samples, in order to minimize the alteration signal in our data.

Several of the highly and very highly altered samples that we analyzed isotopically display slightly elevated (>0.7038, vs. 0.7035-0.7039 for most lightly altered samples) age-corrected $(^{87}Sr/^{86}Sr)_t$ relative to $\varepsilon_{Nd}(t)$ (+1.3 to +6.0), which can be attributed to seawater alteration (e.g., Menzies & Seyfried, 1979). In addition, five samples have elevated values of measured and age-corrected $^{207}Pb/^{204}Pb$ and, for some of them, $^{208}Pb/^{204}Pb$, compared to their $^{206}Pb/^{204}Pb$ (6D-3, 10D-3, 14D-11, 16D-3 and 28D-1). This is a common occurrence among highly altered oceanic basalts, as a result of Pb contamination derived from pelagic sediments, ferromanganese crust and/or phosphates, which have Pb concentrations orders of magnitude larger than basement basalts (e.g., De Carlo *et al*., 1987; Ingram *et al*., 1990; Baturin & Yushina, 2007). Out of these five, three (6D-3, 10D-3, 16D-3) have the highest $(^{87}Sr/^{86}Sr)_t$ ratios analyzed, as well as the lowest

(<+4) $\varepsilon_{Nd}(t)$ and $^{206}Pb/^{204}Pb_{(t)}$ (<19.0) values. Although $^{143}Nd/^{144}Nd$ is typically unaffected by moderate levels of seawater alteration (e.g., Mahoney *et al*., 1987; 1998), Cheng *et al*. (1987) noted that some of their most-altered samples had anomalously low ε_{Nd}, and attributed it to rare-earth element (REE) mobility during prolonged low-temperature alteration and/or REE loss during palagonitization of basaltic glass (e.g., Ludden & Thompson, 1979; Staudigel & Hart, 1983).

Major and trace elements

Major element analyses (Table 4.1) show that the majority of samples are nepheline-normative alkalic basalts (Fig. 4.3) and a few are basanites. Our data overlap substantially with those of Hawkins *et al*. (1987). Major element trends (Fig. 4.4) include an increase in Na_2O, K_2O, TiO_2 and Al_2O_3 wt% as MgO wt% decreases, whereas CaO shows no systematic behavior.

Six moderately to lightly altered samples (1D-2, 7D-1, 7D-3, 27D-1, 33D-1, 33D-2) have elevated MgO concentrations (>8 wt%); we henceforth refer to these as the high-MgO group; similar rocks were also observed in Hawkins's *et al*. (1987) sample suite. These rocks are also characterized by the presence of large (4-18 mm) olivine phenocrysts and, in some cases (7D-1, 7D-3), cm-size clinopyroxene, noticeably high values of compatible trace elements (e.g., Cr>400 ppm, Ni>200 ppm), and high MgO/total iron as FeO (FeO*) ratios (0.89-1.10 in the high-MgO group, 0.25-0.67 in other samples). In diagrams of alteration-resistant incompatible vs. compatible trace elements (e.g., Ni vs. Th, Cr vs. Th; Fig. 4.4), the high-MgO group falls off the trend displayed by most of our other samples, which otherwise decrease in compatible element

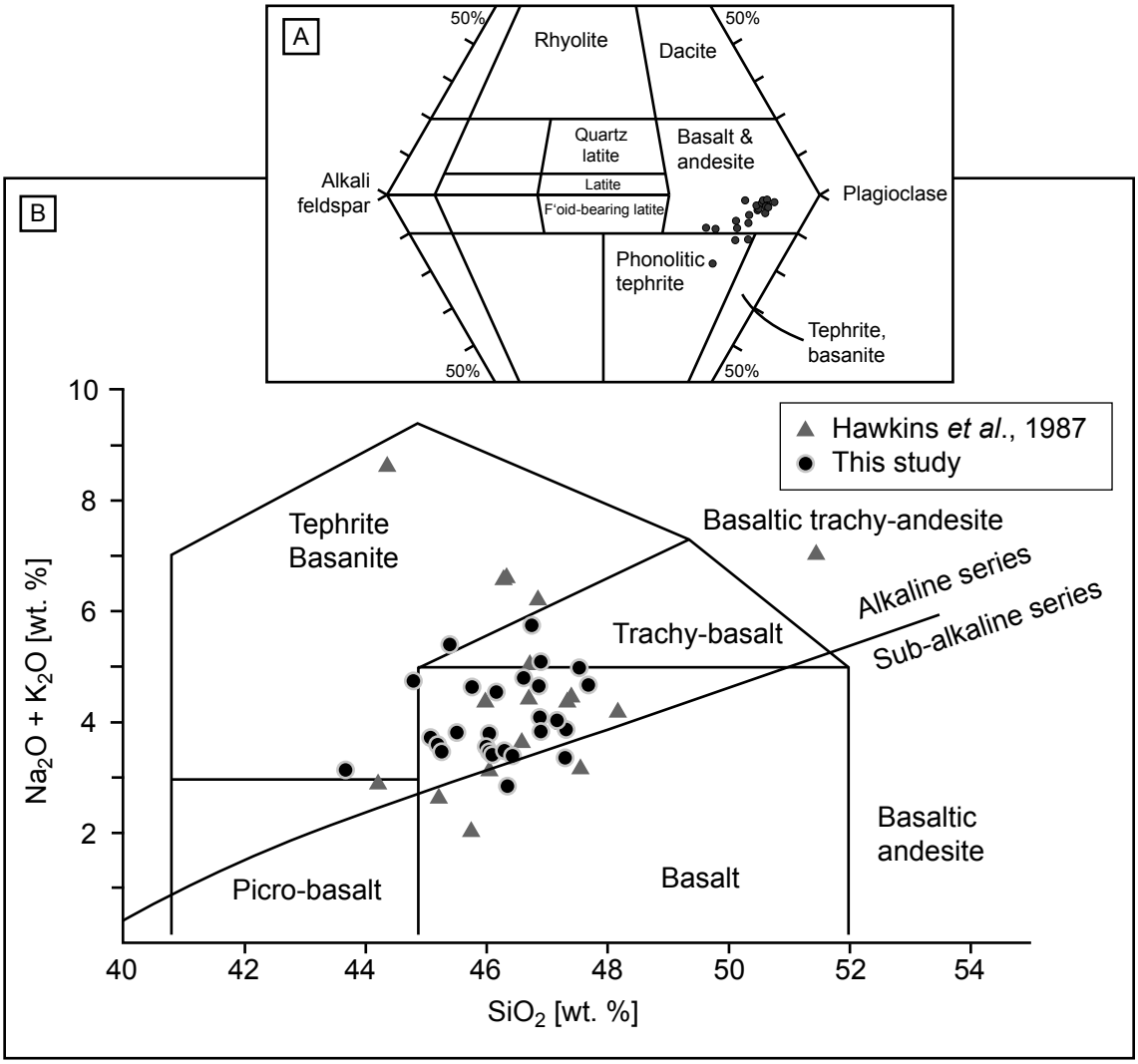

Fig. 4.3: (A) Quartz, alkali feldspar, feldspathoid and plagioclase QAPF classification diagram of Streckeisen (1978), using computed CIPW norms of Louisville samples. (B) Total alkali vs. silica classification diagram (Le Bas *et al*., 1986). Alkaline / sub-alkaline divide line is after Irvine & Baragar (1971). Data for our highly altered samples are not displayed.

concentrations as incompatible element concentrations increase. Interestingly, another group of samples (three among moderately or lightly altered ones: 13D-1, 20D-15B and 32D-5; eleven in total) has, like the previous group, noticeably high Ni concentrations (130-300 ppm). Unlike the high-MgO group, however, it does not have noticeably high MgO concentrations (3.9-6.1 wt%) or MgO/FeO* (0.27-0.44). These rocks often have high (> 350 ppm) Cr concentrations as well, but some do not (e.g., 13D-1 has 71 ppm Cr). Other transitions metals (e.g., FeO*, MnO, Cu, V) do not display any degree of enrichment. This group, termed high-Ni group, is unrepresented in the Hawkins *et al.* (1987) dataset.

Primitive-mantle-normalized incompatible element patterns (Fig. 4.2B) show variations bounded by three extreme compositions. One (e.g., that of sample 1D-2) is characterized by a relatively flat pattern (mantle-normalized $(Nb/Zr)_N < 2.5$ and $(Sm/Lu)_N < 4$) showing modest overall enrichment of incompatible trace elements relative to model primitive-mantle values (e.g., Nb<45, Zr<19 and Lu<4.5 times the primitive mantle estimates of Sun & McDonough, 1989). Another (e.g., 6D-3) has a similarly flat patterns, $(Sm/Lu)_N < 4$, $(Nb/Zr)_N < 2.5$, but greater absolute enrichment (e.g., Lu>9 times primitive mantle estimates). A third (e.g., 15D-2, 20D-2) has more steeply sloping patterns overall, $(Sm/Lu)_N > 5.5$ and $(Nb/Zr)_N > 2.6$. Interestingly, the full range of variation can be observed in a single seamount (e.g., 20D-2 and 20D-5, which have $(Sm/Lu)_N = 6.6$ and 4.5 and Nb = 52 and 25 ppm, respectively; Fig. 4.2B).

In a Zr/Y vs. Nb/Y diagram (Fig. 4.5), the Louisville data define an array, parallel to and within that for Icelandic lavas, that is particularly short and narrow relative to the fields defined by many other hotspot-related island groups and chains. Because Zr and

Fig. 4.4: Variation of some major and trace elements in the LSC. Mg# is defined as (MgO/MgO+FeO*)*100. Arrows indicate the direction of magmatic evolution caused by removal of olivine (ol), clinopyroxene (cpx) and plagioclase (pl), and are based on the mineral analyses of Hawkins et al. (1987). Arrows in the two bottom panels represent model Rayleigh fractionation paths for a mineral assemblage of 30% olivine and 70% clinopyroxene, using K_d values of 10 and 1 for Ni and 1 and 8 for Cr in olivine and cpx, respectively (Duke, 1976), with Th assumed to be extremely incompatible in both minerals (Beattie, 1993). Data for highly altered samples (as defined in the text) are not shown

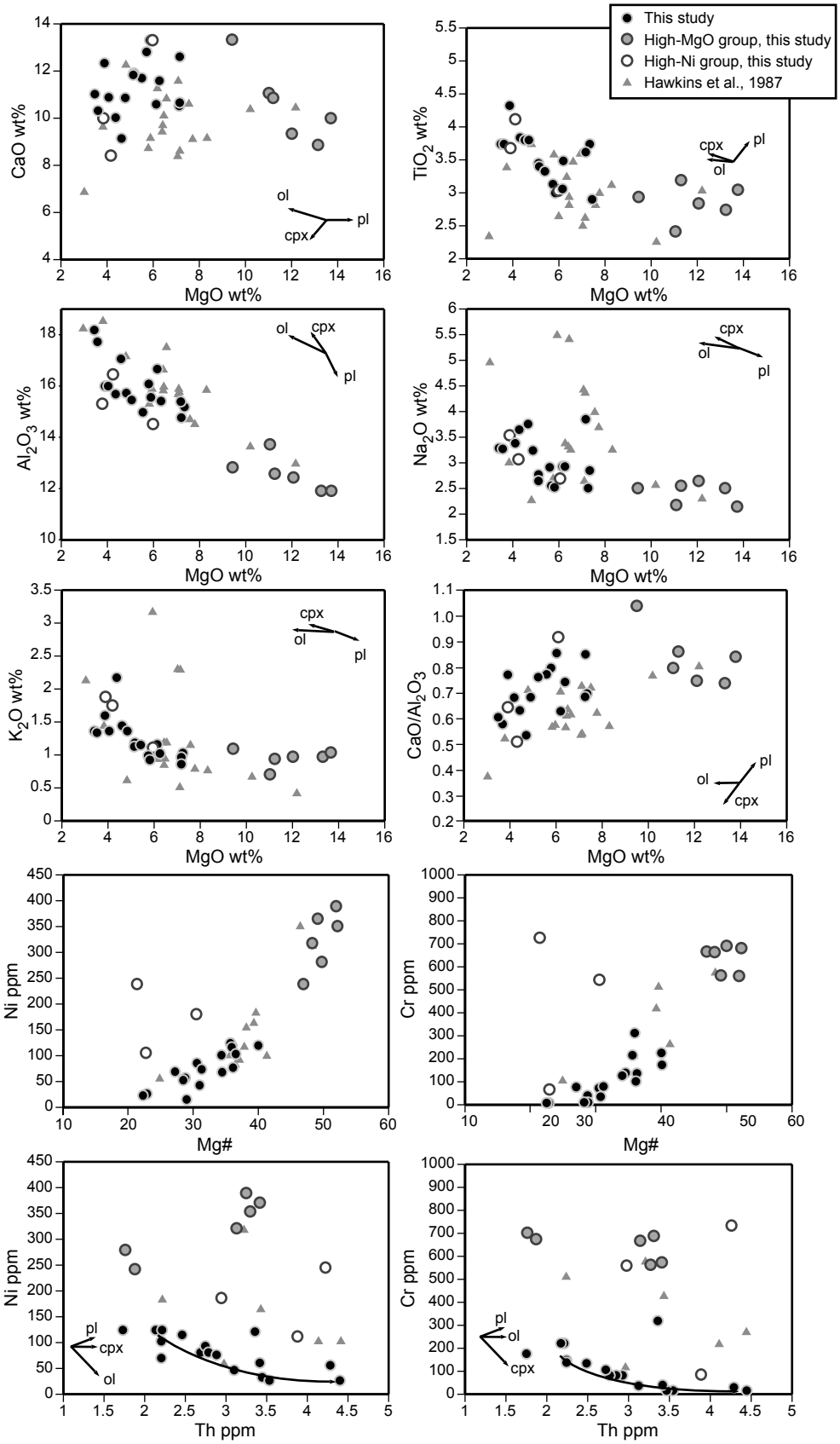
This study
High-MgO group, this study
High-Ni group, this study
Hawkins et al., 1987
CaO wt%
MgO wt%
ol
pl
cpx
TiO2 wt%
Al2O3 wt%
Na2O wt%
K2O wt%
CaO/Al2O3
Ni ppm
Cr ppm
Mg#
Th ppm

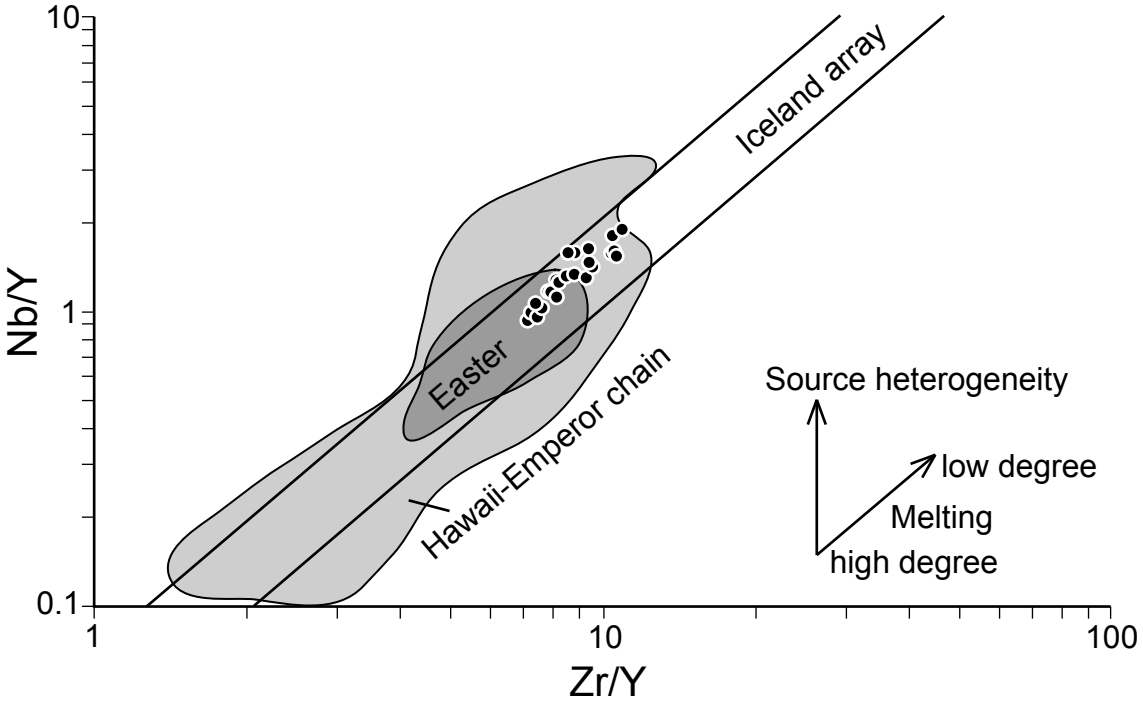

Fig. 4.5: Variation of LSC samples in trace element ratios indicative of the effects of partial melting and source heterogeneity (Fitton *et al*., 1997). Array for Iceland is from Fitton *et al*. (1997); field for the Hawai‘i-Emperor chain is from Edsall (1976), Dalrymple & Clague (1976), Clague & Frey (1980), Stewart *et al*. (1973), Dalrymple *et al*. (1977; 1981), Bence *et al*. (1980), Cambon *et al*. (1980), Regelous *et al*. (2003), Huang *et al*. (2005) and Shafer *et al*. (2005). Field for Easter hotspot trail is from Puzankov & Robrov (1997), Baker *et al*. (1974), Bonatti *et al*. (1977) and Haase *et al*. (1997).

Nb are both highly incompatible elements and behave very similarly during melting of mantle rock compared to Y, varying amounts of partial melting of a single peridotitic source will produce an array approximately parallel to the Icelandic array. Variability of mantle source composition can be expressed by variations in Nb/Zr (Fitton *et al*., 1997). Fractional crystallization, on the other hand, will have little (or no) effect on these ratios as long as the melts are zircon-unsaturated, which is generally the case in basalts (e.g., Hoskin & Schaltegger, 2003; Belousova *et al*., 2002). The restricted field of LSC data thus suggests a homogeneous mantle source and quite limited variation in the amount of partial melting.

Isotopic composition

Despite the fact that the samples represent a nearly 50 Myr span of Louisville hotspot volcanism, their age-corrected isotopic ratios define a narrowly restricted field in all three isotopic systems (Fig. 4.6), overlapping substantially with the data of Cheng *et al*. (1987). For example, excluding the three highly altered samples noted above, our measured $\varepsilon_{Nd}(t)$ ranges from +4.0 to +6.0, whereas theirs ranges from +4.9 to +6.1 (recalculating their ε_{JUV} to ε_{Nd} for a present-day chondritic average of 0.51264). Variation in age-corrected $(^{206}Pb/^{204}Pb)_t$ is only 0.322 (from 19.061 to 19.383) whereas the total range in $(^{87}Sr/^{86}Sr)_t$ is 0.70345 to 0.70427, the higher values likely reflecting greater amounts of seawater alteration. Cheng *et al*.'s (1987) Pb isotope data were not age-corrected but cover a range in measured $^{206}Pb/^{204}Pb$ of 19.128 to 19.452, similar to our present-day values of 19.222-19.606.

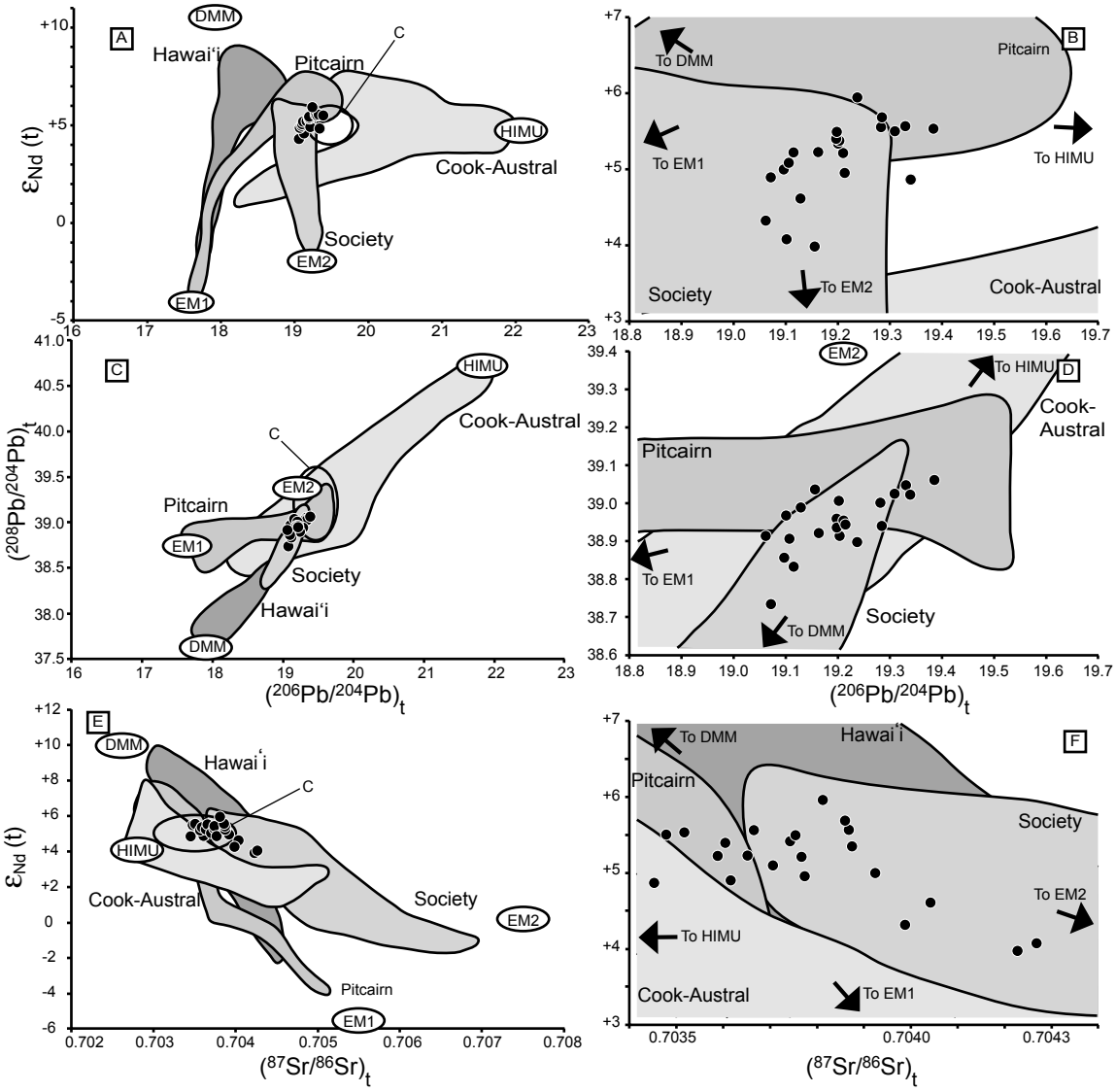

Fig. 4.6: Age-corrected Pb, Nd and Sr isotopic ratios of Louisville samples. The fields in gray represent present-day values for some Pacific hotspot chains. Pitcairn hotspot data from Woodhead & McCulloch (1989), Dupuy *et al*. (1993) and Cotton *et al*. (1995). Cook-Austral from Nakamura & Tatsumoto (1988), Chauvel *et al*. (1997) and Lassiter *et al*. (2003). Society hotspot data from White & Duncan (1996), Devey *et al*. (1990); Cheng *et al*. (1993) and Hemond *et al*. (1994). Hawai'i data from Chen & Frey (1985), West & Leeman (1987), Rhodes & Hart (1995), Reiners & Nelson (1998), Pietruszka & Garcia (1999), Stille *et al*. (1983), Roden *et al*. (1984; 1994), West *et al*. (1987), Chen *et al*. (1990), Frey *et al*. (1994), Chen *et al*. (1996) and Abouchami *et al*. (2000). Boxes and arrows marked DMM, HIMU, EM1, and EM2 indicate the postulated oceanic mantle end-member components of Zindler & Hart (1986), while area for "C" is after Hanan & Graham (1996). Data for highly altered samples are not shown.

The maximum variation in $(^{206}Pb/^{204}Pb)_t$ was observed among five rocks recovered from the same seamount (dredge 20D). There is no apparent isotopic difference between the alkalic basalts and the high-MgO group (Fig. 4.7B), or the basanites (Fig. 4.7C). There is also no systematic variation of isotopic ratios with the amount of enrichment of incompatible trace elements or with indicators of the degree of partial melting (e.g., $(Dy/Yb)_N$, Fig. 4.7D; La/Yb, Fig. 4.8A; Pb and Nd, Fig. 4.8B and C). Indeed, the maximum range in $\varepsilon_{Nd}(t)$ is seen in samples with a very small range in La/Yb of 17-18.

DISCUSSION

The behavior of the major elements is consistent with control by fractional crystallization of olivine and clinopyroxene (Fig. 4.4), as concluded by Hawkins *et al*. (1987). The trend observed in CaO/Al_2O_3 precludes plagioclase from having played an important role in the fractionating assemblage. Using the Rayleigh fractionation equation and Ni, Cr and Th, one can estimate the fractionating mineral assemblage to be ~30% olivine and ~70% clinopyroxene (Fig. 4.4, bottom panels). The high-MgO group of rocks with elevated Cr and Ni concentrations, however, do not fit on the fractionation trend. Rocks of the high-MgO group also have rather elevated concentrations of very incompatible elements (e.g., Nb>35 and Th>3 ppm), which discounts them as being parental to the rest of the rocks. Rather, we interpret the high-MgO samples as evolved basalts with accumulated olivine, which is consistent with their mineralogy. The high-Ni group also falls off fractionation trends (Fig. 4.4). Unlike the high-MgO group, however, the high-Ni samples do not have peculiar mineral abundances, and thus cannot be explained by the accumulation of a mineral phase. Neither can they be explained by

Fig. 4.7: (A) Variation of Zr/Y and $(^{206}Pb/^{204}Pb)_t$ with distance from the inferred hotspot location (assumed to be at the site of dredge MTHN-7D; Lonsdale, 1988). $^{206}Pb/^{204}Pb$ data for samples from dredge 20D are displayed in black. Dotted line represents the approximate location in the LSC east of which seamounts are less voluminous and spaced farther apart (Lonsdale, 1988). (B) Variation of $(^{208}Pb/^{204}Pb)_t$ with degree of magmatic evolution as indicated by Mg number (Mg#), defined as MgO/MgO+FeO*. (C) Pb and Nd isotopic variations in the LSC per rock type. (D) Variation of $(^{208}Pb/^{204}Pb)_t$ with degree of partial melting; $(Dy/Yb)_N$ is used as a proxy for the degree of partial melting (cf. section on modeling of melting in the text). Data for highly altered samples are not included in any of the panels.

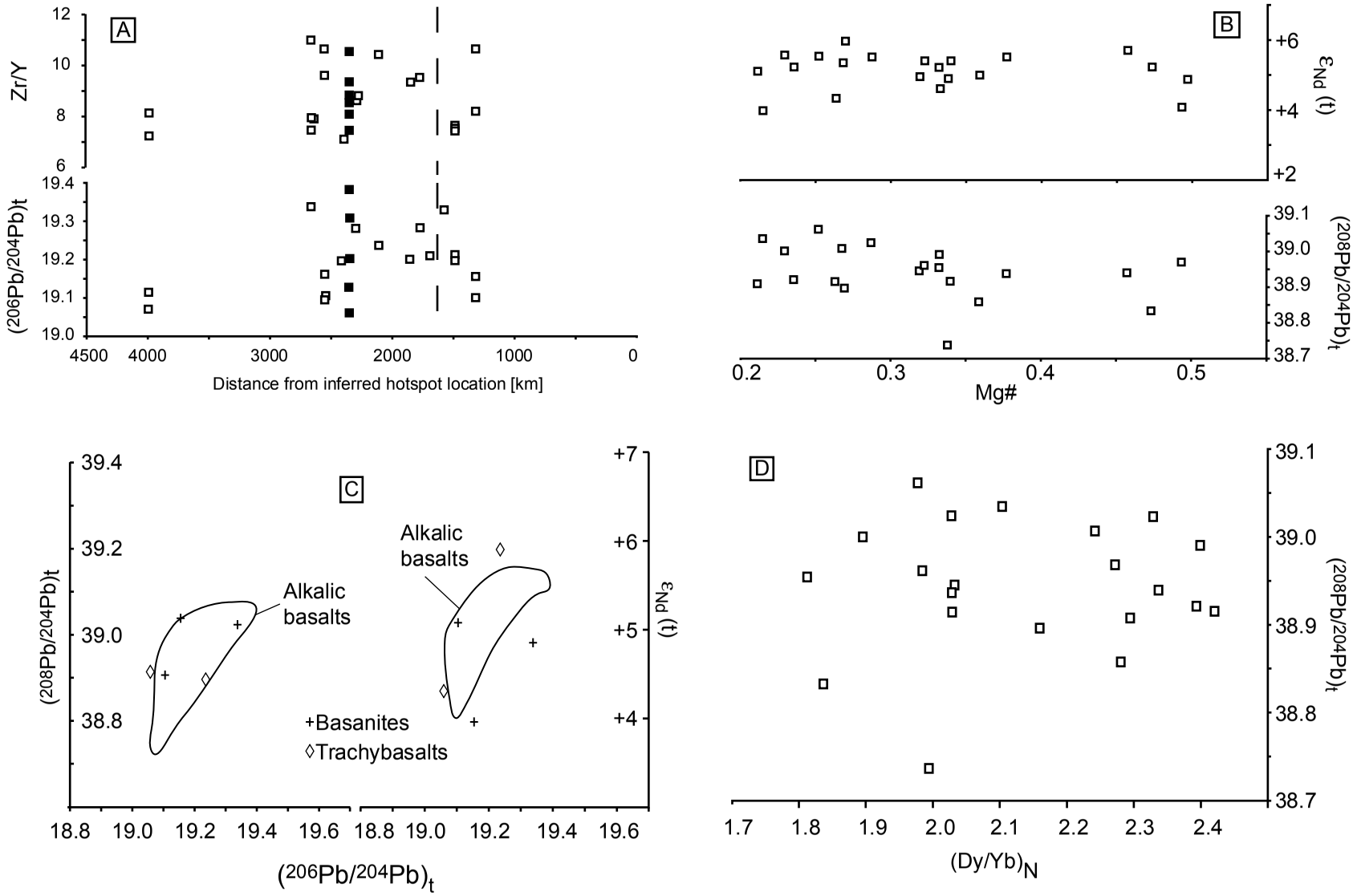
A
Zr/Y
12
10
8
6
(206Pb/204Pb)t
19.4
19.3
19.2
19.1
19.0
4500
4000
3000
2000
1000
0
Distance from inferred hotspot location [km]
B
εNd (t)
+6
+4
+2
(208Pb/204Pb)t
39.1
39.0
38.9
38.8
38.7
0.2
0.3
0.4
0.5
Mg#
C
(208Pb/204Pb)t
39.4
39.2
39.0
38.8
Alkalic basalts
Alkalic basalts
+Basanites
◊Trachybasalts
εNd (t)
+7
+6
+5
+4
18.8
19.0
19.2
19.4
19.6
(206Pb/204Pb)t
D
(208Pb/204Pb)t
39.1
39.0
38.9
38.8
38.7
1.7
1.8
1.9
2.0
2.1
2.2
2.3
2.4
(Dy/Yb)N

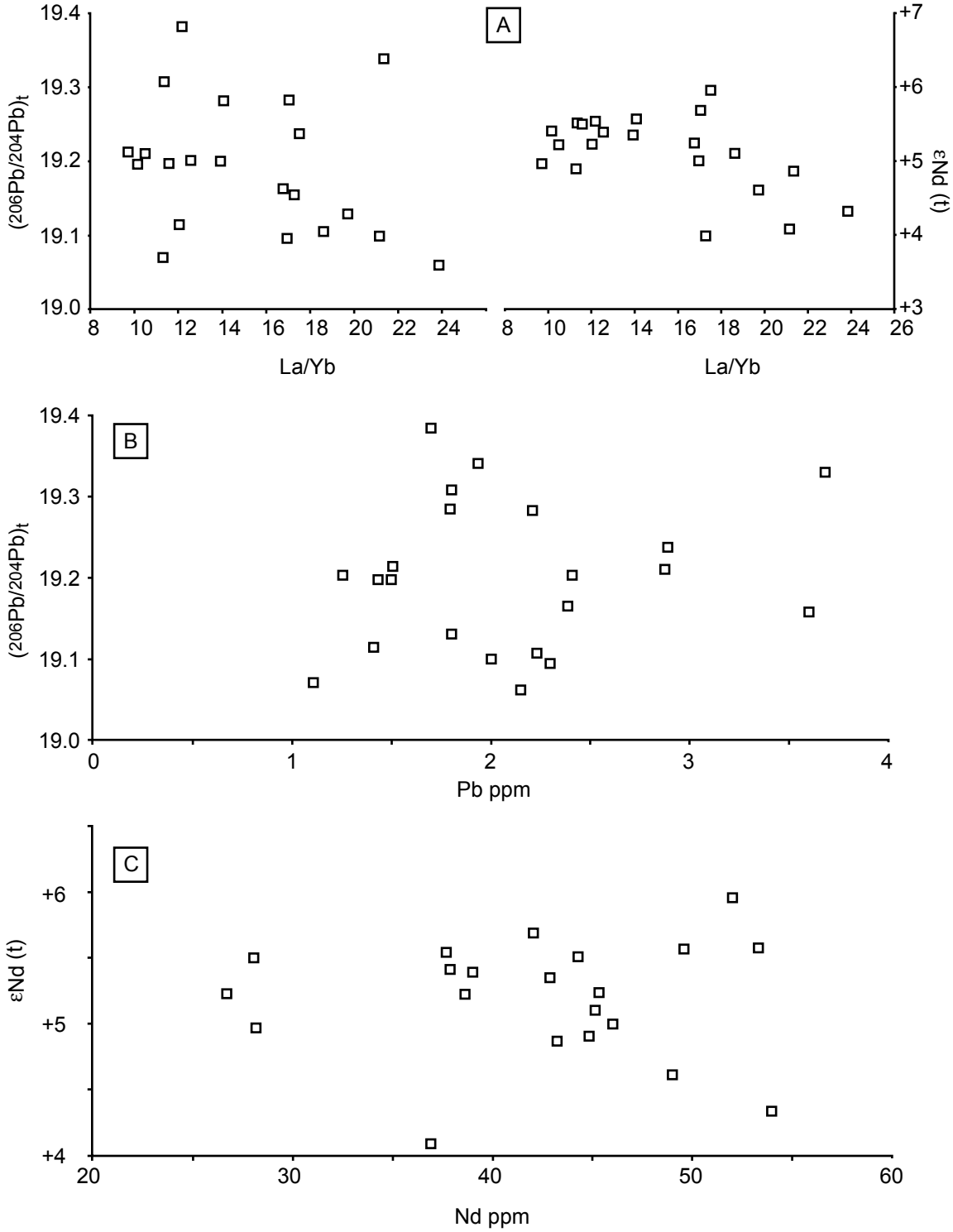

Fig. 4.8: (A) $(^{206}Pb/^{204}Pb)_t$ and $\varepsilon_{Nd}(t)$ variation as a function of La/Yb. (B) and (C) Pb and Nd isotopic variation as a function of Pb and Nd concentration, resp., which shows no systematic variation. Data for highly altered samples are not included in any of the panels.

alteration, as trace element patterns for three of them appear undisturbed, or by contamination by ferromanganese crust, as they have normal MnO, FeO* and P_2O_5 concentrations. A re-analysis of these samples is likely required to rule out analytical problems, and an in-depth study of their mineralogy would help uncover any possible exotic alteration phase. Until then, the origin of the high-Ni samples remains an open question.

A principle component analysis (Fig. 4.9) of major and trace elements of moderately and lightly altered samples confirms the relationships between different elements noted above. This statistical method reduces (i.e., projects) a dataset to its components that display the greatest variance. This analysis shows clusters of elements that behave similarly: Cr, Ni and MgO, which can be related to fractional crystallization of olivine; Ca and Sc, which are compatible in clinopyroxene but not in olivine, and thus record the fractional crystallization of that phase; Si, Cs and V, which are anti-correlated with the MgO-Ni-Cr group and are most affected by olivine fractionation; and a large group of highly to moderately incompatible elements that forms an elongated array resulting from their varying degrees of incompatibility during melting.

As our samples come from 22 seamounts, a single parental mama could not have existed for all of them. The sample showing the least effects from fractionation and no sign of olivine accumulation is 31D-7 (MgO = 7.27 wt%, MgO/FeO* = 0.67, Ni = 118 ppm and Cr = 226 ppm). As such, it is the closest example to potential parental compositions.

Both incompatible element and isotopic ratios hint at the extreme homogeneity of the Louisville mantle source over the course of its history, which isotopically reflect a

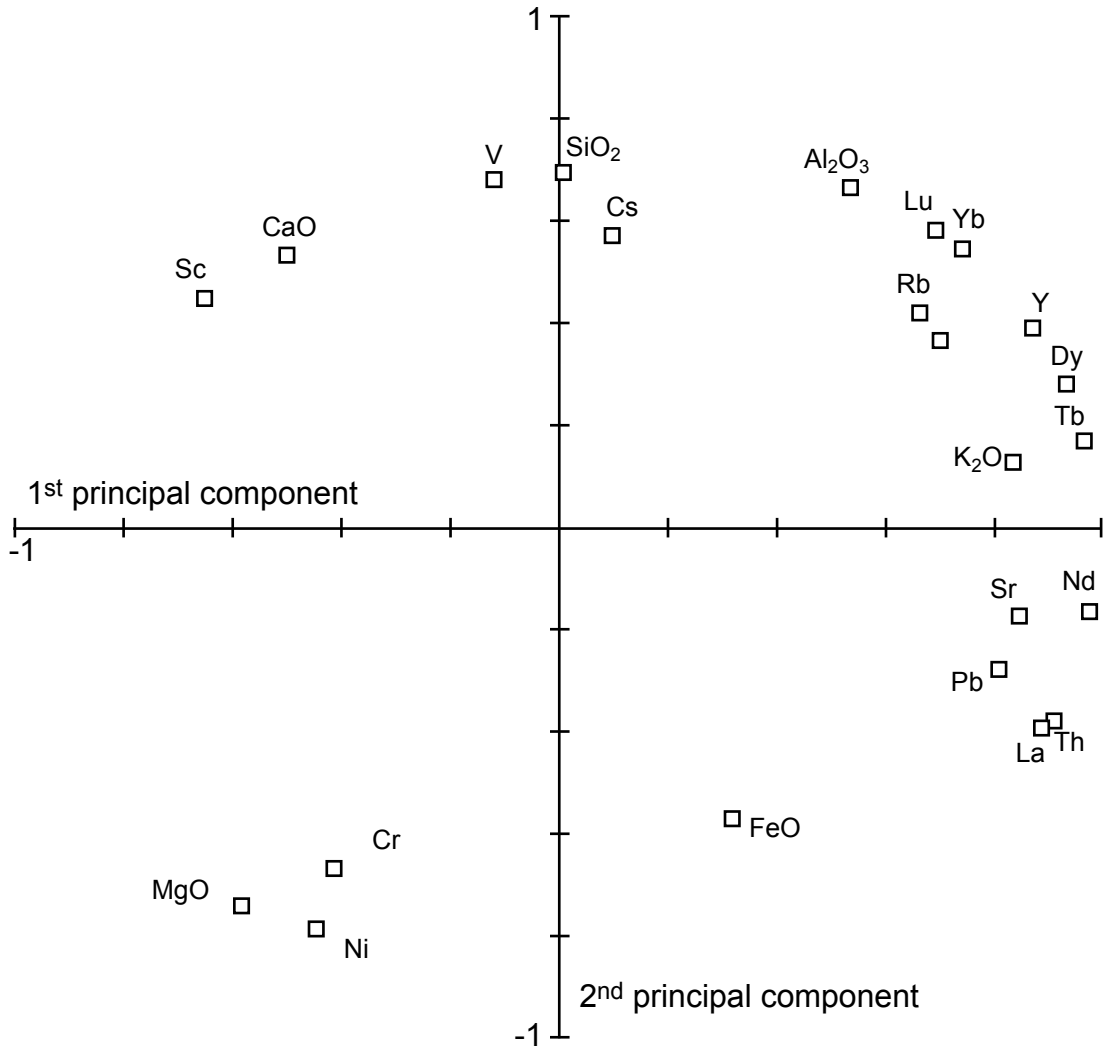

Fig. 4.9: Principle component analysis of moderately and lightly altered samples from the LSC. The 1st principle component reflects the dimension containing the most variation in the dataset and the 2nd principle component the second most variation within the dataset.

broadly "C", or "FOZO" type of mantle-source compositions (e.g., Hart *et al*., 1992; Hanan & Graham, 1996; Stracke *et al*., 2005). Such mantle compositions, argued by Hanan & Graham (1996) to be fed to the upper mantle by deep-sourced mantle plumes, is thought by some workers to represent lower mantle material that underwent some form of depletion early in the Earth's history (e.g., Hart *et al*., 1992; Boyet & Carlson, 2006), although an origin as a highly heterogeneous and well-stirred mixture of recycled oceanic crust has also been proposed (e.g., Kellogg *et al*., 2004). The small variation in isotopic ratios is particularly stunning when the LSC results are compared to data for other Pacific hotspot chains (Fig. 4.6A, B, and C). For comparison, the total observed variation in $(^{206}Pb/^{204}Pb)_t$ (0.324) along the LSC over the ~48 Myr of its history covered by our samples is comparable to the variation (0.302) observed at the Kilauea volcano of Hawai'i since 1917 (Pietruszka & Garcia, 1999).

Nevertheless, small isotopic variations are present along the LSC (Fig. 4.6B and 4.6D). In the coming sections, we will explore hypotheses of the phenomena that may control these small isotopic variations.

Lithospheric thickness at the time of volcanism

To test the hypothesis that the geochemical signature of LSC seamounts was related to variations in melting conditions, it is necessary to estimate the age of the crust upon which each seamount was emplaced, as this determines the thickness of the lithosphere and thus depth of the top of the melting region. We estimated the age of the lithosphere at the time of seamount emplacement and calculated lithospheric thickness at a given age using a simple half-space cooling model, employing the solution of Turcotte & Schubert

(1982) and defining the lithosphere's lower boundary as the 1200ºC isotherm. The age of each seamount was extrapolated from Koppers *et al*. (2004), except for those for which new ^{40}Ar-^{39}Ar ages have been presented (Koppers *et al*., 2007b). The age of the crust to the east of the Wishbone Scarp (dredge stations 24D and higher) was extrapolated from seafloor ages estimated from magnetic anomalies by Lonsdale (1988), Watts *et al*. (1988) and Lyons *et al*. (2000). The origin and history of the Wishbone Scarp and Osbourn Trough are currently matter of debate because of the lack of magnetic anomalies in this region of the seafloor (either unresolved or wholly located in the Cretaceous Long Normal period to the west of the scarp; e.g., Lonsdale, 1997; Billen & Stock, 2000; Mortimer *et al*., 2006; Worthington *et al*., 2006; Downey *et al*., 2007). We accept the interpretation of Lonsdale (1997) that the Osbourn Trough is a paleo-spreading center and the Wishbone Scarp represents a paleo-plate boundary. If this interpretation is found by future workers to be incorrect and the crust west of the Wishbone Scarp formed at the East-Pacific Rise, our estimated lithospheric ages and thicknesses for this part of the LSC would be vastly underestimated; for example, our ~92 Ma estimate for the age of the crust at our oldest dredged seamount would be closer to ~120 Ma (leading to estimated lithospheric thicknesses of 63 km and 97 km at the time of volcanism, respectively). To estimate the age of the crust at the time the Louisville seamounts were emplaced on the Osbourn-Trough-generated oceanic crust, we assume that spreading initiated at 118 Ma and stopped at 86 Ma (Table 4.2), as proposed by Worthington *et al*. (2006).

Melting model

We calculated primitive-mantle-normalized $(Dy/Yb)_N$ and $(Yb/Sm)_N$ for aggregated (accumulated) fractional melts (Shaw, 1970) of a single source for a range (1-15%) of partial melting (Fig. 4.10). These particular elements were chosen because of their moderate incompatibility, resistance to alteration and, in the case of Yb and Dy, compatibility with garnet, which permits a test for the presence of garnet in the source. This differs from the approach of Hawkins *et al*. (1987), who modeled partial melting assuming fractional melting of a garnet lherzolite source to account for their Zr/Nb and Zr/Y data. They estimated a range of 5% to 9% of partial melting.

Two different sets of parameter values (summarized in Appendix B) yielded satisfactory fits to our data. In the model summarized in Fig. 4.10A, we used a source composition with 53% olivine, 30% orthopyroxene (opx), 10% clinopyroxene (cpx) and 7% of variable amounts of garnet and spinel. Phases were assumed to enter the melt in the following proportions: 10% for olivine, 10% for opx, 40% for cpx and 40% for garnet/spinel (both solid and liquid modal abundances are after Janney *et al*., 2000). Melt/solid partition coefficients (K_d) were taken from Salters & Stracke (2004), with the exception of the K_d of Dy in garnet, for which a value of 1.65 was adopted, after Zack *et al*. (1997). The source was assumed to have primitive mantle ratios (Sun & McDonough, 1989) of Dy/Yb = 1.53 and Yb/Sm = 1.09. Results of this model show that our data do not follow a path parallel to a melting curve for any single amount of garnet in the source, indicating that melting likely occurred both in the garnet and spinel stability zones. This result is unexpected considering our estimates of 90- to 120-km-thick lithosphere at the time of emplacement of the majority of seamounts (Table 4.2). If all melting takes place

Table 4.2: Isotopic and isotope-dilution data of Louisville lavas. All isotopic ratios have been age-corrected (subscript t) to seamount formation age. Samples in italics show substantial signs of alteration ("high" or "very high" in Table 1). Seamount formation age is extrapolated from Koppers *et al*. (2004), with the exception of ages noted with an asterisk (*), which are ^{40}Ar-^{39}Ar ages of Koppers *et al.* (2007b). Hotspot location is assumed to be at the site of sample MTHN-7D (50° 26.4' S, 139° 10' W) (Lonsdale, 1988). Current age of the oceanic crust east of the Wishbone Scarp is extrapolated from Lonsdale (1988). Methods of estimating the age of the lithosphere west of the Wishbone Scarp and lithospheric thickness at the time of seamount emplacement are described in the text. Data are reported relative to values of $^{87}Sr/^{86}Sr = 0.710238 \pm 0.000016$ (2σ; n = 39) for standard NBS 987 Sr, $^{143}Nd/^{144}Nd = 0.511843 \pm 0.000009$ (n = 28; 0.2 ε_{Nd} units) for La Jolla Nd. Within-run errors on the Sr and Nd isotopic data are less than or equal to the external uncertainties on these standards. Lead isotope ratios were measured with a double-spike method (Galer, 1999) on 25-50 ng loads of sample. Mean values for 30-40 ng loads of NBS 981 Pb are 16.9406 ± 0.0005, 15.4974 ± 0.0010, and 37.7216 ± 0.0023 for $^{206}Pb/^{204}Pb$, $^{207}Pb/^{204}Pb$ and $^{208}Pb/^{204}Pb$, respectively (2σ, n = 22). Within-run errors on the Pb isotopic ratios are shown below the corresponding ratios. Isotope-dilution concentrations are in ppm. Uncertainties on the isotope-dilution abundances are 0.2% for Sm and Nd, 0.4% for Sr, 1% for Pb, U and Rb and 2% for Th. Total procedural blanks were typically ≤25 pg for Pb, <60 pg for Sr, <10 ng for Nd and ≤2 pg for U and Th. Present day $\varepsilon_{Nd} = 0$ corresponds to $^{143}Nd/^{144}Nd = 0.512640$.

Table 4.2: Isotopic and isotope-dilution data of Louisville lavas

Sample	Dredge site Seamount name	Dredge Conditions	Estimated age (Ma)	Distance from hotspot (km)	Estimated Age of crust (Ma)	Age of crust (Ma) at time of loading	Est. lithosphere thickness (km)
1D-2	27.6	steep slope, guyot	72	3995	92	20	63
1D-3	27.6	steep slope, guyot	72	3995	92	20	63
7D-1	168.3	scarp, guyot	44	2670	108	64	112
13D-1	167.4	scarp, guyot	43	2550	109	66	114
14D-5	167.4	scarp, guyot	43	2550	109	66	114
14D-11	167.4	scarp, guyot	43	2550	109	66	114
17D-1	166.1	scarp, guyot	42	2410	110	68	116
20D-1	165.7	deep gully, guyot	39.8*	2350	111	71.2	119
20D-2	165.7	deep gully, guyot	39.8*	2350	111	71.2	119
20D-3	165.7	deep gully, guyot	39.8*	2350	111	71.2	119
20D-8	165.7	deep gully, guyot	39.8*	2350	111	71.2	119
20D-9	165.7	deep gully, guyot	39.8*	2350	111	71.2	119
22D-4	165.4	flank, guyot	41	2300	113	72.0	119

Table 4.2 (Cont.): Isotopic and isotope-dilution data of Louisville lavas

Sample	$(^{206}Pb/^{204}Pb)_0$	$(^{207}Pb/^{204}Pb)_0$	$(^{208}Pb/^{204}Pb)_0$	$(^{87}Sr/^{86}Sr)_0$	$(^{143}Nd/^{144}Nd)_0$	$^{238}U/^{204}Pb$ (μ)	$(^{206}Pb/^{204}Pb)_t$	$(^{207}Pb/^{204}Pb)_t$	$(^{208}Pb/^{204}Pb)_t$
1D-2	19.339	15.611	39.142	0.70363	0.512880	19.955	19.115	15.600	38.834
	±0.002	±0.003	±0.005				±0.002	±0.003	±0.005
1D-3	19.318	15.613	39.280	0.70371	0.512862	21.997	19.071	15.602	38.738
	±0.002	±0.003	±0.005				±0.002	±0.003	±0.005
7D-1	19.606	15.624	39.291	0.70350	0.512869	38.989	19.339	15.612	39.024
	±0.003	±0.003	±0.006				±0.003	±0.003	±0.006
13D-1	19.348	15.611	39.121	0.70379	0.512883	36.177	19.106	15.600	38.908
	±0.002	±0.002	±0.004				±0.002	±0.002	±0.004
14D-5	19.310	15.610	39.090	0.70399	0.512878	32.072	19.096	15.600	38.859
	±0.002	±0.002	±0.004				±0.002	±0.002	±0.004
14D-11	19.263	15.620	39.136	0.70368	0.512891	14.913	19.163	15.616	38.922
	±0.002	±0.002	±0.004				±0.002	±0.002	±0.004
17D-1	19.369	15.619	39.153	0.70387	0.512902	26.323	19.197	15.611	38.961
	±0.002	±0.003	±0.005				±0.002	±0.003	±0.005
20D-1	19.364	15.613	39.237	0.70411	0.512859	38.101	19.128	15.602	38.991
	±0.002	±0.002	±0.004				±0.002	±0.002	±0.004
20D-2	19.292	15.608	39.178	0.70409	0.512844	37.289	19.061	15.597	38.916
	±0.003	±0.004	±0.007				±0.003	±0.004	±0.007
20D-3	19.593	15.621	39.285	0.70358	0.512908	33.919	19.383	15.611	39.062
	±0.003	±0.004	±0.007				±0.003	±0.004	±0.007
20D-8	19.475	15.607	39.231	0.70368	0.512901	43.977	19.202	15.594	38.916
	±0.003	±0.003	±0.005				±0.003	±0.003	±0.005
20D-9	19.545	15.623	39.264	0.70358	0.512907	38.247	19.308	15.612	39.025
	±0.004	±0.005	±0.009				±0.004	±0.005	±0.009
22D-4	19.568	15.612	39.242	0.70373	0.512908	44.809	19.282	15.598	39.002

Table 4.2 (Cont.): Isotopic and isotope-dilution data of Louisville lavas

Sample	$(^{87}Sr/^{86}Sr)_t$	$\varepsilon_{Nd}(t)$	$(^{143}Nd/^{144}Nd)_t$	Pb ppm	Sr ppm	Rb ppm	Nd ppm	Sm ppm	Th ppm	U ppm
1D-2	0.70359	+5.2	0.512815	1.41	404.3	5.84	26.79	6.09	1.82	0.43
1D-3	0.70362	+4.9	0.512798	1.43	699.1	21.5	44.90	10.02	2.49	0.37
7D-1	0.70345	+4.9	0.512833	1.94	754.6	20.6	43.29	8.97	3.52	1.16
13D-1	0.70371	+5.1	0.512846	2.24	535.2	24.1	45.20	9.83	3.33	1.25
14D-5	0.70393	+5.0	0.512841	2.30	719.2	25.2	46.10	10.10	3.73	1.14
14D-11	0.70365	+5.2	0.512853	2.39	729.4	13.3	45.40	10.16	3.57	0.55
17D-1	0.70374	+5.4	0.512863	1.50	709.7	51.8	37.94	8.87	2.07	0.61
20D-1	0.70404	+4.6	0.512825	1.81	662.9	28.4	49.05	10.56	3.36	1.06
20D-2	0.70399	+4.3	0.512811	2.15	880.4	54.6	54.04	11.42	4.26	1.24
20D-3	0.70352	+5.5	0.512872	1.70	528.1	18.5	37.76	8.52	2.85	0.88
20D-8	0.70361	+5.4	0.512865	1.26	556.5	23.5	39.09	8.95	2.99	0.85
20D-9	0.70348	+5.5	0.512871	1.81	617.6	37.0	44.34	10.11	3.25	1.06
22D-4	0.70367	+5.6	0.512872	2.21	731.3	29.2	49.66	10.92	3.88	1.52

Table 4.2 (Cont.): Isotopic and isotope-dilution data of Louisville lavas

Sample	Dredge site Seamount name	Dredge Conditions	Estimated age (Ma)	Distance from hotspot (km)	Estimated Age of crust (Ma)	Age of crust (Ma) at time of loading	Est. lithosphere thickness (km)
24D-6	163.6	scarp, guyot	37.5	2110	84	46.5	96
26D-1	161.5	scarp, guyot	33.5	1850	77.5	44	94
27D-1	160.7	scarp, guyot	32	1770	75.5	43.5	92
28D-1	159.8	scarp, seamount	31	1695	73.5	42.5	92
30D-4	158.5	steep slope, seamount	26.2*	1575	71	44.8	94
31D-5	157.7	scarp, seamount	27.5	1490	68	40.5	89
31D-7	157.7	scarp, seamount	27.5	1490	68	40.5	89
32D-5	155.9	steep slope, guyot	24	1320	65	41	89
33D-1	155.9	steep slope, guyot	24	1320	65	41	89
6D-3	35.8	steep slope, seamount	46	2990	104	58	107
10D-3	168.6	western scarp, guyot	50.1*	2710	108	57.9	106
16D-3	166.6	landslide scarp, guyot	42.5	2465	110	67.5	115

Table 4.2 (Cont.): Isotopic and isotope-dilution data of Louisville lavas

Sample	$(^{206}Pb/^{204}Pb)_0$	$(^{207}Pb/^{204}Pb)_0$	$(^{208}Pb/^{204}Pb)_0$	$(^{87}Sr/^{86}Sr)_0$	$(^{143}Nd/^{144}Nd)_0$	$^{238}U/^{204}Pb$ (μ)	$(^{206}Pb/^{204}Pb)_t$	$(^{207}Pb/^{204}Pb)_t$	$(^{208}Pb/^{204}Pb)_t$
	±0.002	±0.002	±0.004				±0.002	±0.002	±0.004
24D-6	19.330	15.611	39.087	0.70384	0.512929	16.039	19.237	15.606	38.897
	±0.002	±0.002	±0.003				±0.002	±0.002	±0.003
26D-1	19.358	15.615	39.159	0.70393	0.512901	30.119	19.201	15.607	39.008
	±0.002	±0.002	±0.003				±0.002	±0.002	±0.003
27D-1	19.373	15.609	39.126	0.70388	0.512919	18.022	19.284	15.605	38.941
	±0.002	±0.002	±0.004				±0.002	±0.002	±0.004
28D-1	19.533	15.649	39.055	0.70381	0.512896	66.897	19.210	15.634	38.956
	±0.002	±0.002	±0.003				±0.002	±0.002	±0.003
30D-4	19.507	15.630	39.136	0.70390	0.512915	43.647	19.329	15.622	39.049
	±0.002	±0.002	±0.003				±0.002	±0.002	±0.003
31D-5	19.341	15.613	39.073	0.70381	0.512887	29.910	19.213	15.607	38.946
	±0.002	±0.002	±0.004				±0.002	±0.002	±0.004
31D-7	19.339	15.610	39.076	0.70378	0.512912	33.106	19.197	15.603	38.938
	±0.002	±0.002	±0.003				±0.002	±0.002	±0.003
32D-5	19.253	15.606	39.125	0.70428	0.512834	26.153	19.156	15.602	39.036
	±0.002	±0.002	±0.003				±0.002	±0.002	±0.003
33D-1	19.222	15.593	39.102	0.70429	0.512839	32.499	19.101	15.587	38.970
	±0.002	±0.003	±0.005				±0.002	±0.003	±0.005
6D-3	19.101	15.637	39.034	0.70486	0.512685	15.325	18.991	15.632	38.941
	±0.002	±0.002	±0.003				±0.002	±0.002	±0.003
10D-3	18.914	15.622	38.916	0.70473	0.512746	43.562	18.575	15.606	38.655
	±0.001	±0.002	±0.003				±0.001	±0.002	±0.003
16D-3	19.108	15.647	38.961	0.70449	0.512786	38.980	18.850	15.635	38.817
	±0.002	±0.002	±0.004				±0.002	±0.002	±0.004

Table 4.2 (Cont.): Isotopic and isotope-dilution data of Louisville lavas

Sample	$(^{87}Sr/^{86}Sr)_t$	$\varepsilon_{Nd}(t)$	$(^{143}Nd/^{144}Nd)_t$	Pb ppm	Sr ppm	Rb ppm	Nd ppm	Sm ppm	Th ppm	U ppm
24D-6	0.70381	+6.0	0.512897	2.89	897.6	17.9	52.06	11.28	4.41	0.71
26D-1	0.70388	+5.3	0.512871	2.41	644.6	22.9	42.98	9.76	3.26	1.12
27D-1	0.70386	+5.7	0.512890	1.80	778.2	9.6	42.07	9.55	3.15	0.50
28D-1	0.70377	+5.2	0.512867	2.87	552.1	17.6	38.70	9.01	2.75	2.95
30D-4	0.70387	+5.6	0.512892	3.69	860.1	27.9	53.34	11.95	3.68	2.48
31D-5	0.70377	+5.0	0.512859	1.51	524.3	14.0	28.25	7.31	2.11	0.70
31D-7	0.70376	+5.5	0.512887	1.44	513.8	13.2	28.13	6.59	2.17	0.74
32D-5	0.70423	+4.0	0.512813	3.61	739.3	37.5	45.95	9.93	4.03	1.46
33D-1	0.70427	+4.1	0.512818	2.00	638.9	14.9	37.00	8.02	3.31	1.00
6D-3	0.70482	+1.3	0.512647	5.03	656.5	14.6	60.12	12.46	3.07	1.19
10D-3	0.70468	+2.5	0.512705	3.14	1299.6	33.2	78.49	16.33	4.95	2.13
16D-3	0.70443	+3.2	0.512747	1.37	342.0	11.2	33.03	7.63	1.41	0.83

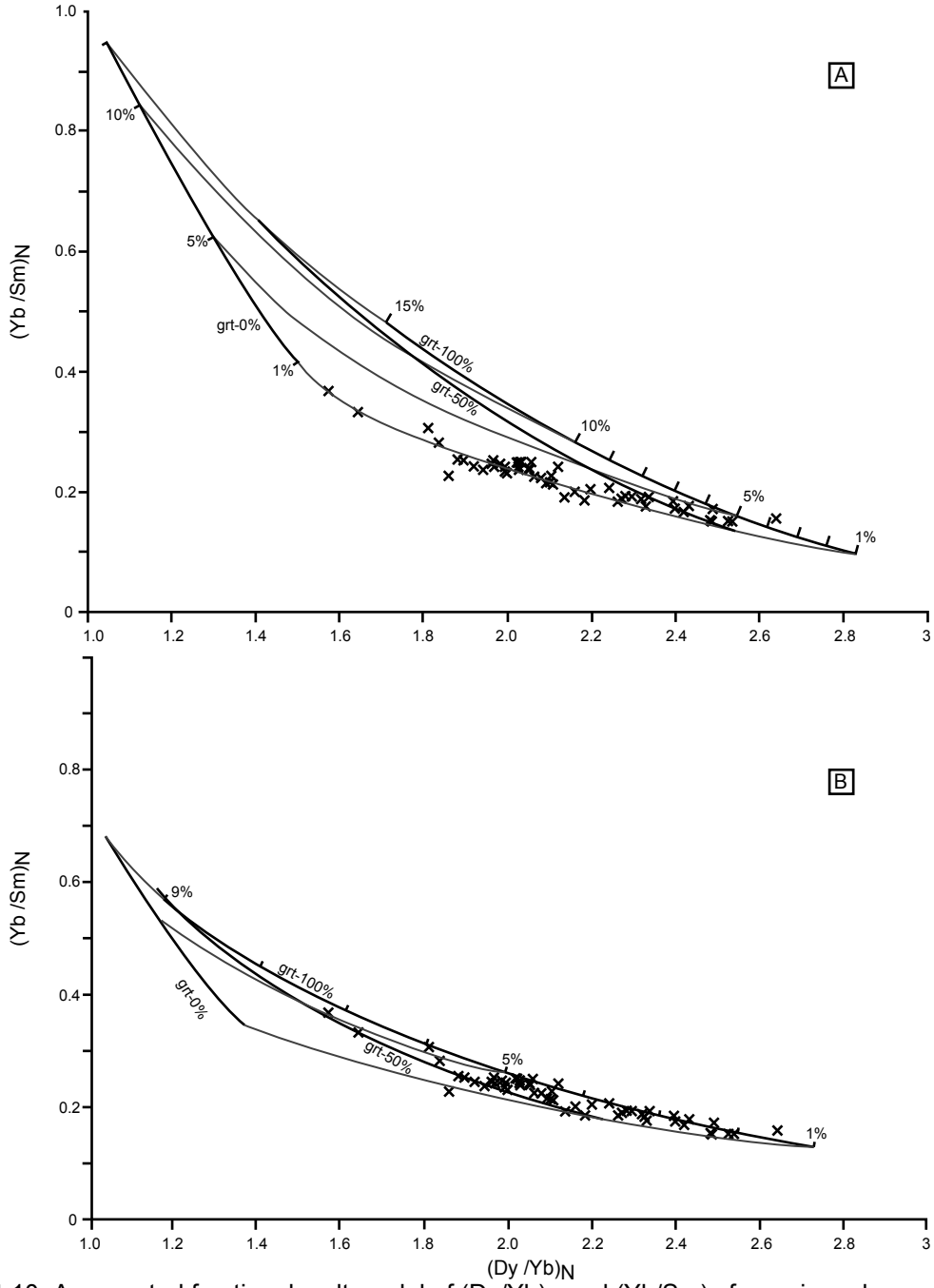

Fig. 4.10: Aggregated fractional melt model of $(Dy/Yb)_N$ and $(Yb/Sm)_N$ for various degrees of partial melting of a peridotitic source. Model parameters are detailed in the text and summarized in Appendix B. Crosses represent our LSC data. (A) Black curves represents 1-15% of partial melting. K_d values are from Salters & Stracke (2004), with the exception of K_d of Dy in garnet, assumed to be 1.65 (Zack *et al*., 1997). Lines labeled grt-0%, grt-50% and grt-100% are modeled assuming 0%, 50% and 100% of garnet as an accessory phase in the unmelted source, respectively. Gray transverse lines represent lines of constant fraction (1%, 5%, 10% and 15%) of partial melting. (B) Black curves represent 1-9% of partial melting, using K_d values of Salters & Stracke (2004) and McKenzie & O'Nions (1991). Lines labeled grt-0%, -50% and -100% are modeled assuming 0%, 1.5% and 3% of garnet in the unmelted source, respectively. Gray transverse curves represent lines of equal degrees (1%, 5% and 9%) of partial melting.

at the base of the lithosphere, melting should occur at pressures of ~2.7-3.6 GPa, squarely in the garnet zone (e.g., O'Hara *et al*., 1971). This consideration would imply that our lithospheric thicknesses are overestimates, perhaps because the lithosphere was thinned by some unknown thermal event prior to passing over the hotspot or by the thermal effect of the Louisville plume – more or less consistently before formation of the magmas represented by our samples. In any case, our estimates of the amount of partial melting with this model are in the 1-5% range, smaller than the estimates of Hawkins *et al*. (1987), who used a simpler batch melting equation.

For the second model, we adopted source modal abundances with less garnet (after Dawson, 2004; Maaløe & Aoki, 1977; Dawson *et al*., 1980), with 57% olivine, 30% opx, 10% cpx and 3% of variable amounts of garnet and spinel. The phases were again assumed to enter the melt in the following proportions: 10% for olivine, 10% for opx, 40% for cpx and 40% for garnet/spinel (Janney *et al*., 2000). We again used K_d values of Salters & Stracke (2004), with the exception of the K_d for Sm (0.22) and Dy (1.06) for garnet, which were from the compilation of McKenzie & O'Nions (1991). The source was assumed to have $(Dy/Yb)_N = 0.91$ and $(Yb/Sm)_N = 0.84$. Although mathematically feasible, this model is geologically improbable. Despite the fact that a $(Dy/Yb)_N$ value of 0.91 is plausible for depleted mantle sources (e.g., the model depleted mid-ocean ridge basalt (MORB) mantle of Workman & Hart (2005) has $(Dy/Yb)_N = 0.91$), processes that would lead to the depletion of Dy relative to Yb are just as likely to deplete Sm relative to Yb, producing $(Yb/Sm)_N > 1$. Thus, it is not clear why a mantle source would have both $(Dy/Yb)_N$ and $(Yb/Sm)_N <1$.

No pyroxenite or eclogite was used in the model source because (a) there is very little isotopic evidence for a two-component source or melting of a recycled oceanic crustal component (though some authors have proposed C-type mantle to be a well-stirred mix of recycled materials; e.g., Kellogg *et al*., 2004) and (b) experimental melts of pyroxenite and eclogite tend to be silica-rich (e.g., O'Hara, 1986; Green *et al*., 1967), which is incompatible with the markedly silica-undersaturated character of the LSC rocks (although Hirschmann *et al*. (2003) obtained alkalic melts from garnet pyroxenite at pressures above 3 GPa).

Systematic geochemical variations

Our data, combined with those of Cheng *et al*. (1987), show that there has been no systematic variation of either chemical or isotopic composition in LSC lavas over a large portion of the hotspot's history (e.g., Fig. 4.7A, in which age is indicated by the present distance of seamounts from the inferred location of the hotspot), despite the abrupt drop in magma productivity over the past 25 Myr. Similarly, there is no observable systematic isotopic variation either with indicators of the degree of magmatic evolution (e.g., Fig. 4.7B) or degree of partial melting (e.g., Fig. 4.7D). These results indicate that the small isotopic variations are more likely to be related to small variations in source composition or, as proposed by Ito & Mahoney (2005a; 2005b), small variations in melting conditions. Analyses of samples from dredge 20D, which were all collected from the same seamount but show a wide range in isotopic compositions (Fig. 4.7A), favor the former hypothesis, as melting conditions are unlikely to vary substantially under a single seamount.

A very rough overall positive correlation can be observed between age-corrected $^{208}Pb/^{204}Pb$ and the age (and thus, thickness) of the lithosphere at the time of a seamount's emplacement (Fig. 4.11A and C). In contrast, Nd, Sr or other Pb isotopic ratios are uncorrelated with lithospheric thickness at the time of volcanism (Fig. 4.11B and D). Similarly, indicators of degree of partial melting (e.g., $(Dy/Yb)_N$, Fig. 4.11E) and ratios of very incompatible elements to moderately incompatible elements (e.g., La/Yb; Fig. 4.11E), which are affected both by degree of partial melting and source heterogeneity (e.g., Fitton *et al.*, 1997), do not show any clear systematic evolution as a function of lithospheric thickness at the time of volcanism.

These results may indicate that (1) although the Louisville source mantle is mostly homogeneous (at the scale of the melting zone), a few relatively small heterogeneities are more or less evenly scattered in the melting region. The wide range of isotopic compositions observed among samples of the same seamount (dredge 20D; Fig. 4.11) offers the best evidence in support of this hypothesis, as lithospheric thickness can be assumed to have remained constant. The weak correlation between the age of the lithosphere at the time of volcanism and $^{208}Pb/^{204}Pb$ could suggest that these heterogeneities cross the solidus at higher pressure, and thus enter the melt phase in greater proportion at higher pressure than at lower pressure, where melting of the volumetrically predominant, more refractory, lower-$^{208}Pb/^{204}Pb$ mantle component prevails. The lack of correlation of lithospheric thickness at the time of seamount emplacement with other isotopic ratios, on the other hand, suggests that lithospheric thickness was not a dominant factor controlling the isotopic composition of the LSC. Furthermore, the range in $(Dy/Yb)_N$ observed in samples of dredge 20D (Fig. 4.11E),

where we can assume the lithospheric thickness to have been constant during construction of the seamount, do not correlate with isotopic ratios, indicating that there was not much difference in fusibility of isotopically different regions of the mantle source. In any case, the quantity of these heterogeneities is small in the Louisville source in comparison to those of other Pacific hotspots, which display a much wider variation in isotopic composition. For comparison, the Cook-Austral volcanoes were emplaced on a ~35 Myr old crust at the time of volcanism; for Pitcairn, ~20 Myr old crust; for Society, a very constant ~65 Myr old crust throughout the chain; for Hawai‘i, volcanoes have been emplaced on crust of extremely varied age, ranging from <10 to ~100 Myr old; and sampled portions of the Easter-Salas y Gomez chain have been built on ~2-15 Myr old crust (Waggoner, 1993; Cottrell & Tarduno, 2003; Müller *et al*., 1997).

Alternatively, (2) the Louisville source mantle is just as heterogeneous as that of any other Pacific hotspot, but the heterogeneities are not expressed prominently in the isotopic signatures of LSC lavas because the consistently thick lithosphere at the time of seamount emplacement along most of the chain has prevented significant melting of the more refractory components in the source mantle. This explanation is unlikely because (a) lavas from seamounts that were emplaced close to a recently active spreading center (Osbourn Seamount at the western end of the chain and the 27.6°S seamount, where we conducted dredge haul 1D) are not isotopically distinct in $(^{87}Sr/^{86}Sr)_t$, $\varepsilon_{Nd}(t)$, or age-corrected $^{206}Pb/^{204}Pb$ or $^{207}Pb/^{204}Pb$ from samples taken at other dredge sites and have only marginally lower $(^{208}Pb/^{204}Pb)_t$. (b) Moreover, volcanoes of some other hotspots, such as the Cook-Austral, Society and Pitcairn, have also been emplaced on crust of

Fig. 4.11: Variation of key geochemical indicators as a function of estimated lithospheric thickness or age at the time of volcanism. (A) Variation of $^{208}Pb/^{204}Pb$ with lithospheric age; variation of (B) $^{206}Pb/^{204}Pb$, (C) $^{208}Pb/^{204}Pb$, (D) $^{87}Sr/^{86}Sr$ and ε_{Nd} and (E) $(Dy/Yb)_N$ and La/Yb as a function of lithospheric thickness at the time of volcano emplacement. Black datapoints are for samples from dredge 20D, white squares represent data for other dredge sites. Data for highly altered samples are not included in any of the panels.

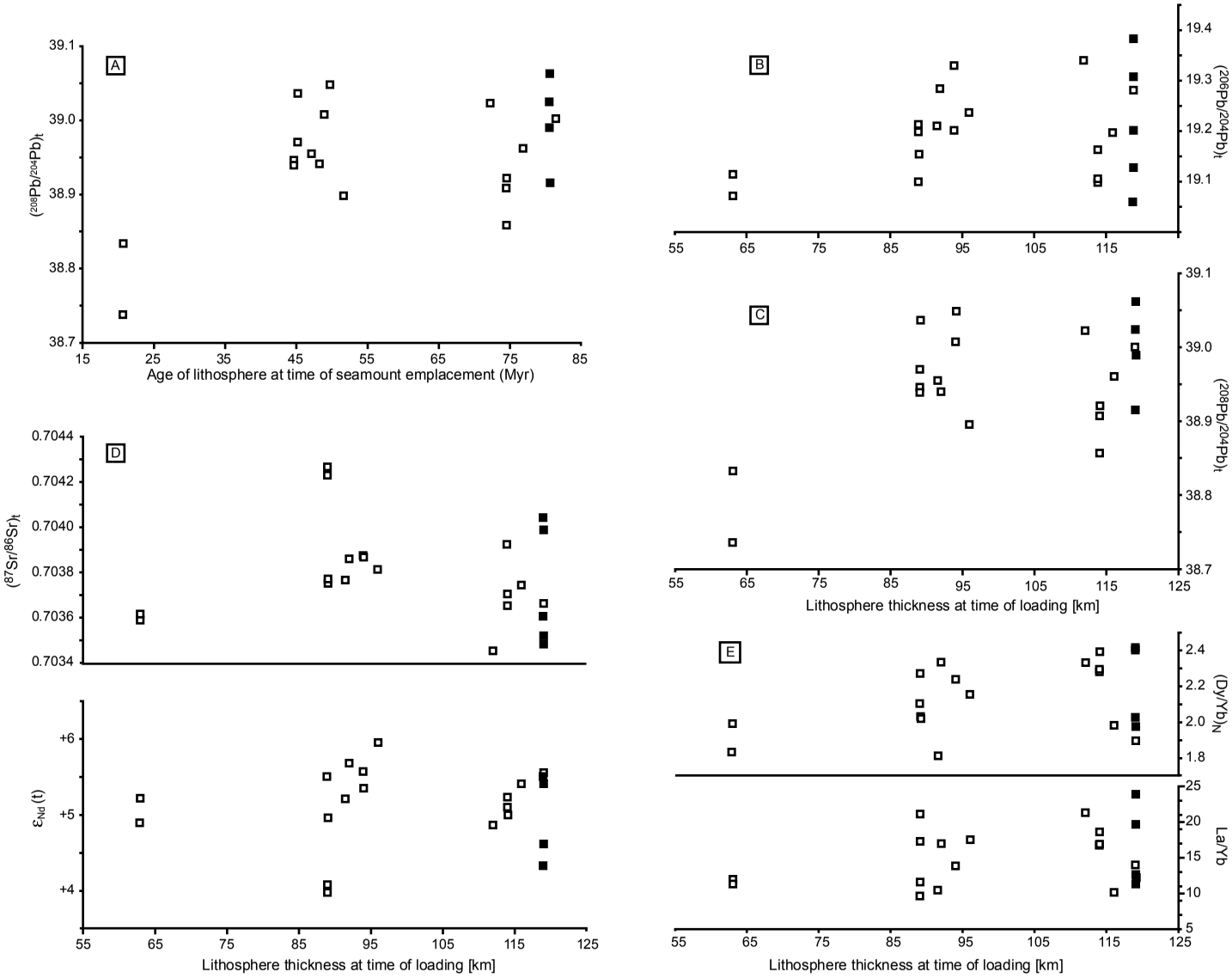
A
B
C
D
E
$(^{208}Pb/^{204}Pb)_t$
$(^{206}Pb/^{204}Pb)_t$
$(^{87}Sr/^{86}Sr)_t$
ε_{Nd} (t)
$(Dy/Yb)_N$
La/Yb
Age of lithosphere at time of seamount emplacement (Myr)
Lithosphere thickness at time of loading [km]

relatively constant age (Müller *et al*., 1997), yet display wide ranges in isotopic compositions.

In summary, our results support the idea that the Louisville source mantle is surprisingly homogeneous, with few scattered heterogeneities in the melting zone. This indicates that, unlike other hotspots, the Louisville plume originates from a well stirred portion of the mantle, for instance, located well above the D" layer (e.g., Courtillot *et al*., 2003; Montelli *et al*., 2004), a region originally proposed by Hart *et al*. (1992) to host FOZO-type compositions.

The Louisville hotspot as the source of the Greater Ontong Java Plateau

The plume head of the Louisville hotspot has been suggested as a possible source for the Ontong Java Plateau (OJP) (e.g., Mahoney, 1987; Mahoney & Spencer, 1991; Tarduno *et al*., 1991; Richards *et al*., 1991) and, by extension, for the Hikurangi and Manihiki plateaus, recently postulated to have originally been part of a single gigantic plateau termed the Greater OJP (Taylor, 2006; Worthington *et al*., 2006). Because portions of the Louisville hotspot trail older than about 80 Myr have been subducted at the Tonga-Kermadec Trench, it is not possible to physically track the hotspot seafloor trace to any specific Early Cretaceous plateau. Most current plate motion models (e.g., Wessel & Kroenke, 2008) fail to place the Louisville hotspot in the vicinity of the OJP at ~120 Ma, although Antretter *et al*. (2004) concluded that the 9° latitudinal discrepancy between the present location of the Louisville hotspot and the inferred source of the OJP at ~120 Ma can be accommodated by allowing for a combination of true polar wander and southward motion of the Louisville hotspot by up to 6° in the past 120 Myr.

Our data for LSC lavas overlap with OJP basalts in age-corrected Nd and Sr isotope ratios. However, the Pb isotopic compositions of 72-24 Myr (Koppers *et al*., 2004; 2007b) LSC lavas are distinct from those of either of the two principal magma types of the ~120 Myr OJP proper (e.g., Mahoney *et al*., 1993; Tejada *et al*., 2004). Isotopic evolution in the LSC mantle source, resulting from radioactive decay of Th and U and ingrowth of radiogenic Pb isotopes, cannot account for or explain these differences (Fig. 4.12). The slope of the age-correction/evolution vector for the LSC data in $^{206}Pb/^{204}Pb$ vs. $^{207}Pb/^{204}Pb$ space (Fig. 4.12) depends upon the present-day $^{238}U/^{235}U$ ratio, 137.88, which is invariant in natural materials in the solar system. This vector not only fails to intersect the OJP data fields, but would also require very high $^{238}U/^{204}Pb$ (=μ) ratios (40-80) in the mantle source in order to explain the difference in age-corrected $(^{206}Pb/^{204}Pb)_t$ between the LSC and OJP rocks. Such μ values are higher than in almost all LSC samples (90% of those presented in Table 4.2 have μ between 15 and 43). Further, because U is more incompatible than Pb (e.g., Tatsumoto, 1988) and the LSC lavas appear to be products of relatively small amounts of partial melting, μ should be lower in the Louisville mantle source than in LSC lavas.

Few isotopic data have been published for the Hikurangi Plateau (Mortimer & Parkinson, 1996), but those that are available are rather similar to those for the Kwaimbaita-type of OJP basalt and thus also distinct from Louisville compositions. The $^{207}Pb/^{204}Pb$ ratio of LSC lavas is also too high to match the compositions measured for Manihiki Plateau samples drilled on DSDP site 317, which are similar to the Singgalo magma type of the OJP. Inter-laboratory measurement bias cannot explain the observed differences between LSC and OJP (*sensu stricto*) lavas, as the great majority of the OJP

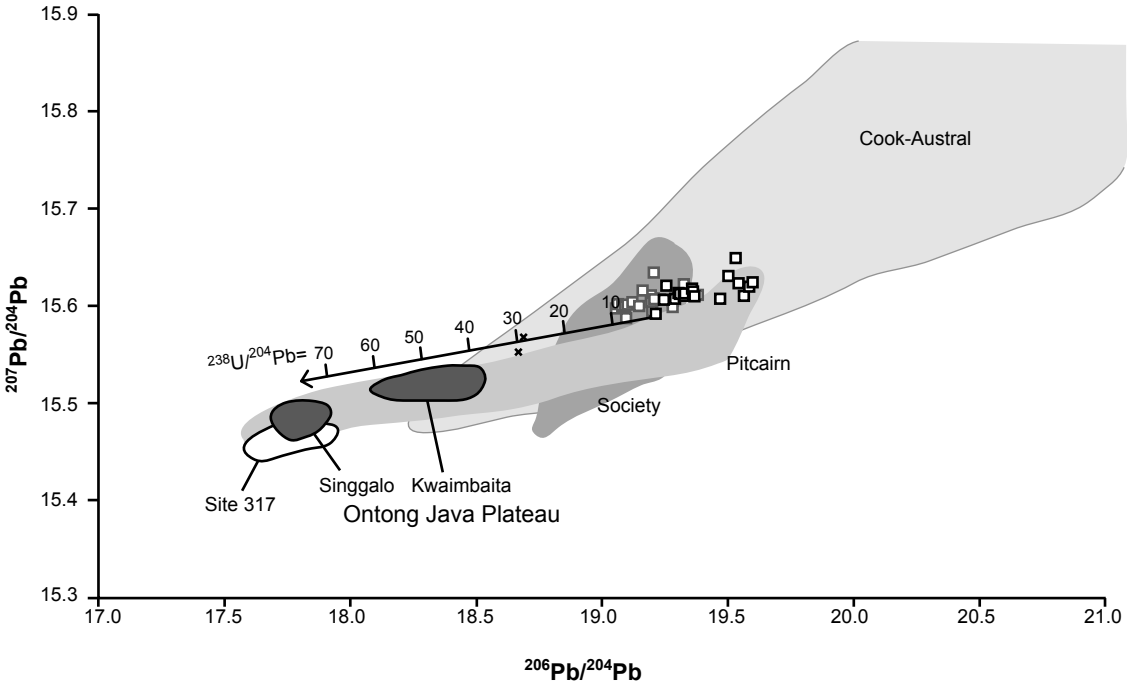

Fig. 4.12: Comparison of LSC $^{207}Pb/^{204}Pb$-$^{206}Pb/^{204}Pb$ values with age-adjusted fields for the two types of OJP basalts (Kwaimbaita and Singgalo magma types) and cored basalts from the Manihiki Plateau from DSDP site 317. Age-corrected values of dredged basalts from the Danger Islands Troughs of the Manihiki Plateau are noted by crosses. Note that interlaboratory bias is not a factor in comparing these data with the LSC results, as the Manihiki data and most of the OJP data were acquired in the UH Isotope Laboratory and many are double-spike measurements. Squares with black borders represent the present-day values of our LSC samples, and squares with gray borders correspond to the age-corrected values. Symbol size is equal to or less than measurement error. The $^{238}U/^{204}Pb$ (μ) vector represents the effect of age-correcting the isotopic ratios to 120 Ma, for different values of μ. Manihiki Plateau data are from Mahoney & Spencer (1991). Ontong Java Plateau data are from Tejada *et al*. (1996; 2002; 2004). Fields for other Pacific hotspot tracks are as in Fig. 4.6.

(and Manihiki) isotopic data were acquired in the same laboratory as that used in the present study, and include a number of double-spike measurements (Tejada *et al*., 2004). On the other hand, data for two glassy samples from a dredge haul in the Danger Islands Troughs of the Manihiki Plateau (Mahoney & Spencer, 1991) fall exactly on the LSC age-correction vector in Fig. 4.12. This implies that a LSC-like composition exists in some parts of the Greater OJP, but has so far been found only in a deeply dissected part of the Manihiki Plateau and remains to be discovered in the OJP proper. As a result, a genetic link between the Louisville hotspot and the OJP can therefore not be ruled out. A shift in isotopic composition between a plume-head and plume-tail stage would also not be entirely unexpected considering the very high degrees of partial melting estimated for OJP basalts (18-30%; e.g., Mahoney *et al*., 1993; Tejada *et al*., 1996; Neal *et al*., 1997), which could have swamped any Louisville-like isotopic signal through the melting of refractory, volumetrically dominant, mantle components.

CONCLUSIONS

Study of the major element, trace element and isotopic composition of samples dredged from seamounts of the Louisville hotspot trail reveals that Louisville lavas are typically undersaturated in silica. By selecting dredge sites on steep slopes, landslide scarps, and in deep incisions in the volcanic edifices, we attempted to reach the inner, shield-stage lavas. Our new sample suite is similar to most of those described by Hawkins *et al*. (1987), which were mostly collected on pinnacles, peaks or parasitic cones that dot many of the seamounts' summits and that, from their morphology, appear to have formed late in the history of the volcanoes. Our dataset, combined with that of Hawkins'

et al. (1987), indicates either that (1) despite our best attempts, shield-stage lavas were not recovered or (2) the Louisville volcanoes do not follow the textbook, Hawai‘ian style of evolution characterized by geochemically distinct shield and post-shield stages. Overall, samples collected on the flanks of the volcanoes are geochemically indistinguishable from those collected on late-stage peaks (Hawkins *et al*., 1987; Cheng *et al*., 1987), suggesting that phases in the life of LSC volcanoes are geochemically identical. This issue, however, cannot be entirely resolved until the Louisville seamounts are drilled.

Major and compatible trace elements show patterns consistent with the fractionation of an olivine-dominated mineral assemblage. Some samples with anomalous MgO and Ni show clear chemical and mineralogical indications of having accumulated olivine. Incompatible trace elements indicate that the melts were at least partly formed in the garnet stability zone by the partial melting of 1-7% of a peridotitic source with a C-like isotopic composition. As suspected by Cheng *et al*. (1987), the Louisville mantle source appears to have remained extraordinarily homogeneous over the last ~70 Myr. Magma fluxes from the hotspot have decreased sharply in the past 25 Myr (e.g., Lonsdale, 1988; Montelli *et al*., 2004), which has been interpreted as evidence for a waning mantle plume. Surprisingly, this decline of hotspot activity has not been accompanied by any change in chemical or isotopic composition of Louisville lavas, indicating that the mantle source and melting conditions have both remained much the same. The lack of systematic variation along the chain is epitomized by the fact that nearly the entire range of geochemical characteristics (alkalinity, isotopic ratios, degree of magmatic evolution, partial melting) can be observed in a single seamount.

Small isotopic variations appear unrelated either to the degree of partial melting or magmatic evolution. Correlation between lithospheric thickness at the time of volcanism and $^{208}Pb/^{204}Pb$ is crude, at best, and absent from other isotopic systems. Rather, the entire range of degrees of partial melting and isotopic variability can be observed in a single seamount (dredge 20D). This suggests that isotopic variability was not controlled by changes in melting conditions, but instead by the amount of isotopically distinct heterogeneities present in the melting zone. The absence of correlation between degree of partial melting and isotopic ratios also implies that isotopically different regions of the mantle source had similar fusibility. In any case, the range of isotopic compositions observed along the LSC remains small, a characteristic which sets it apart from other Pacific hotspot tracks.

The isotopic signature of the Louisville lavas is absent in OJP basalts (as well as in the few Hikurangi Plateau lavas for which analyses have been published). We cannot completely discount that the Louisville hotspot was the source of these Cretaceous Pacific plateaus, but it would require a shift in mantle source composition between the plume head and plume tail stages of the hotspot's activity. This change would be particularly striking in light of the homogeneity of Louisville lavas for the past ~70 Myr (cf. Mahoney, 1987). Alternatively, the isotopic differences may be attributed to the vastly different degrees of partial melting inferred for LSC (1-9%) and OJP (18-30%) lavas, such that more-refractory mantle components are not expressed at the LSC. Lastly, the Pb isotopes age-correction vector of the Louisville seamounts, as well as the range of their Sr and Nd isotopic ratios, appear to match the values of some lavas of the Manihiki Plateau dredged in the Danger Islands Troughs, but to be dissimilar to values for

Manihiki basalts cored at DSDP site 317. Because the Manihiki Plateau has been postulated to originally have been part of the OJP (Taylor, 2006), the evidence of a LSC-like mantle source for at least some Manihiki Plateau lavas may indicate a stronger link between the Louisville hotspot and the OJP than suggested by most recent plate motion models.

ACKNOWLEDGMENTS

We thank Captain D. Murline, B. Eakins, R. Comer and the technicians and crew of the R.V. *Revelle* for their invaluable work during the AMAT expedition, and D. Pyle for laboratory assistance and for his extensive review of the manuscript. R. Workman, S. Ingle, T. Bianco, E. Mittelstaedt and M. Garcia offered many helpful comments. The authors gratefully acknowledge the support of the National Science Foundation (grants OCE04-52127 and OCE03-51512).

CHAPTER 5

CONCLUSIONS

Our geochemical study of volcanic rocks from the Louisville Seamount Chain (LSC) and the Deccan Traps of India has both regional and global implications for understanding hotspot initiation and activity, which I will summarize in the present chapter. In addition, the discussion will be broadened to consider outstanding questions regarding these volcanic provinces and models for their origin, along with future avenues for research.

DIKES OF THE DECCAN TRAPS

Our study of the geochemical signature of dikes of the Deccan Traps enabled us to correlate dikes with flow formations and place constraints on the locations of active dike swarm systems feeding the lava pile at different stages of the flood basalt event. In turn, we recognized multiple stages in feeder dike swarm activity: (1) Probable feeder dikes to the lower and middle formations were found in the Narmada-Tapi swarm system, and were emplaced when the two grabens were actively undergoing N-S extension. Five probable N-S-striking feeder dikes for the lower and middle formations were also identified as much as 300 km farther south. (2) Inferred feeder dikes for the three main upper formations (Poladpur, Ambenali and Mahabaleshwar) were found in all three swarms, but in greater numbers within the Nasik-Pune swarm where they do not display a strong preferred orientation. Geochemical similarities among several dikes of the Narmada-Tapi swarm and lavas of the northern and northeastern Deccan suggest that,

perhaps simultaneously, the Narmada-Tapi swarm acted as a feeder system for flows found in those areas. (3) North-south-striking tholeiitic dikes chemically similar to the Thakurvadi formation found along the west coast are isotopically distinct from any lava flow of the Deccan Traps yet analyzed and thus, cannot be considered as feeders to the lava pile. This fact strengthens the observations of Hooper & Widdowson (submitted), who documented that these dikes cross-cut flows and probable feeder dikes of the upper formations. This implies the existence of a tholeiitic, late-stage of Deccan volcanism controlled by E-W extension along the coast. (4) Dikes of diverse acidic and alkalic compositions, striking N-S, are also found along the west coast, documenting an even later phase of Deccan volcanism and, according to Hooper & Widdowson (submitted), a syn-rift phase of magmatism.

The main implications of my research are: (1) rifting models (e.g., White & McKenzie, 1989) generally fail to account for the scattered orientations of the inferred feeders of the upper lava formations, which are considered by several authors to represent the volumetric peak of Deccan volcanism (e.g., Self *et al*., 2006); and (2) the main phase of volcanism preceded the main phase of rifting along the Indian west coast, which eventually led to the splitting of the Seychelles Bank from mainland India (e.g., Collier *et al*., 2008). These findings favor a plume-head model (e.g., Campbell & Griffiths, 1990) for the origin of the Deccan Traps. Although plume-head models alone do not predict tectonic control during emplacement of the lower- and middle-formation feeder dikes, tectonic control could be explained if active rifting occurred contemporaneously along the Narmada and Tapi grabens, which indeed had been active well prior to the onset of Deccan volcanism. The outstanding weakness of the plume-head model is the apparent

absence of evidence for a pre-volcanic uplift that the model predicts (e.g., Sheth, 1999; 2007).

Numerous aspects about the Traps' feeder system remain open and offer future perspectives for research in the province.

* The submarine section of the province is poorly studied, in part because the thickness of the Indus sediment fan makes imaging or accessing the basement in the Arabian Sea difficult, and in part because much of India's continental shelf is under concession for oil exploration and drilling and thus, available geophysical and well-logging data are proprietary. Recently, Collier *et al*. (2008) imaged substantial volumes of seaward-dipping reflectors along the Indian continental margin and its conjugate margin on the Seychelles Plateau. Besides the obvious importance of the offshore portion of the province for understanding the Deccan's original volume and spatial extent, and the timing of rifting along the west coast relative to the main phase of volcanism, the offshore sequence holds the answers to at least two questions regarding the feeder dike systems and the locus of the Deccan's main vents. (1) How much of the feeder system lies offshore? Could the paucity of likely feeder dikes for the lower and middle formations found on land mean that the majority of such dikes are now underwater? (2) Considering that roughly 40% of the dikes analyzed for Pb-Nd-Sr isotope ratios have compositions distinct from those of lavas found anywhere in the Deccan, how many of these dikes are hypabyssal and how many actually fed flows that now lay offshore? Did the phase of volcanism that produced the late-stage chemically Thakurvadi-like dikes along the west coast also produce associated lava flows that are now underwater?

* A few dikes with chemical similarities to the lava flows of the northern and northeastern Deccan have been found in the Narmada-Tapi swarm, but abundant feeders for these flows remain to be found. Future efforts should focus on locating the feeder systems for the geochemically distinct flows of the northern and northeastern reaches of the province, such as recent work by Sheth *et al*. (submitted) on an eastern section of the Narmada-Tapi swarm system, near Pachmarhi.

* Unlike the better-studied complexes of Katchchh and the Narmada-Tapi grabens (Mundwara, Barmer, Rajpipla and Amba Dongar; e.g., Mahoney *et al*., 1985; Simonetti *et al*., 1995; 1998), the alkalic rocks of the west coast are comparatively less well-characterized isotopically, particularly for the Pb system (e.g., Melluso *et al*., 2002). Nd and Sr isotopic data seem to indicate that alkalic rocks, and more specifically lamprophyric rocks, bear some isotopic affinity with a Réunion-like mantle source. This is of no small importance considering that a Réunion-like isotopic signature is absent from other Deccan-related rocks, with but a few exceptions (cf. Peng & Mahoney, 1995; Mahoney *et al*., 2002). Continued studies of the alkalic rocks of the province may yield critical information regarding the inferred link between the Réunion hotspot and the Deccan Traps, and the evolution of the mantle source during the transition from the plume-head to plume-tail phases of volcanism.

THE LOUISVILLE SEAMOUNT CHAIN

Study of the major element, trace element and isotopic composition of samples dredged from seamounts of the Louisville hotspot trail reveal that Louisville lavas are typically undersaturated in silica and alkalic. When comparing the geochemical data for our samples, thought to mostly represent the inner, shield-stages of the seamounts, with those of Hawkins *et al*. (1987), thought to represent the post-shield stages of volcanism, we find no measurable chemical or isotopic difference between the samples. Based on their geochemical signature, LSC lavas can be interpreted as having been generated at least partly in the garnet stability zone by the partial melting of 1-7% of a peridotitic source with a C-like isotopic composition, melts which then evolved by fractional crystallization of an assemblage dominated by olivine and clinopyroxene.

Our isotopic data show that the LSC mantle source is distinct from the sources that produced Ontong Java Plateau (OJP) and Hikurangi Plateau lavas and lavas of the Manihiki Plateau drilled by the Deep Sea Drilling Project at Site 317. Although these data do not rule out the Louisville hotspot as the source of the OJP, a shift in isotopic composition between magmas produced during the plume head and plume tail stages of the hotspot is required to explain the discrepancy in Pb isotopes between the LSC and OJP data (e.g., Mahoney, 1987). Such a shift could be attributed, for instance, to the vastly different degrees of partial melting of the mantle source inferred for the LSC (1-7%) and OJP (18-30%) (e.g., Mahoney *et al*., 1993; Tejada *et al*., 1996; Neal *et al*., 1997). Our data also shows that the LSC source is isotopically similar to the source of two Manihiki lavas dredged in the Danger Islands Troughs (Mahoney & Spencer, 1991). If Taylor's (2006) hypothesis that the Manihiki, OJP and Hikurangi plateaus were once a

single plateau is correct, these two samples suggest that a shift in isotopic composition of the hotspot source between the plume head and tail stages may no longer be required. The implication would be that a LSC-like composition exists in some parts of the Greater OJP, but has so far been found only in a deeply dissected part of the Manihiki Plateau and remains to be discovered in the OJP proper.

Our isotopic data, combined with those of Cheng *et al*. (1987), also show that the Louisville mantle source appears to have remained extraordinarily homogeneous over the last ~70 Myr, despite a sharp decrease in magma fluxes from the hotspot in the past 25 Myr (e.g., Lonsdale, 1988). The absence of systematic variation in isotopic composition, estimates of the amount of partial melting or incompatible element ratios indicative of source heterogeneity as a function of distance along the chain, alkalinity, or thickness of the lithosphere at the time of volcanism suggest either that heterogeneities are absent from the mantle source or that heterogeneities are present in the source but are not melting. Considering that the Cook-Austral and Society hotspot chains were emplaced on crust roughly the same age as the LSC, but display a much wider range of isotopic compositions (e.g., Devey *et al*., 1990; Hemond *et al*., 1994; Chauvel *et al*., 1997; Lassiter *et al*., 2003), the former hypothesis has to be preferred.

The main outstanding question is, of course, why is the LSC markedly more homogeneous than other Pacific hotspots? The simple answer – heterogeneities are simply not present in the mantle source – leads to further hypotheses and conjectures that can be stated but might prove difficult to test. One such hypothesis is that no significant heterogeneity is present at the root of the Louisville mantle plume and thus no heterogeneity can be entrained by the plume on its way to the surface. Another

hypothesis is that heterogeneities are present at the base of the plume, but fail to be entrained in the plume; for instance, because of density contrasts. Studies of the topography of the core-mantle boundary from seismic tomography suggest that there is no substantial difference either in density or seismic velocity between the root of a possible deep-seated Louisville mantle plume and the roots of other South Pacific hotspots (e.g., Boschi & Dziewonski, 2000; Yoshida, 2008). One would therefore not expect drastic differences in the major element composition of source materials at the roots of Pacific plumes, thus favoring the second hypothesis. Recent numerical and experimental modeling of thermo-chemical plumes (e.g., Lin & van Keken, 2006; Harris *et al*., 2007) has shown that small viscosity and density contrasts can lead to radically different chemical structures in model plumes and that, depending on conditions, dense heterogeneities present at the plume root may not be entrained at all. These studies show that it is not an unreasonable hypothesis to explain the observed >70-Myr homogeneity of the Louisville mantle source. Finally, it is possible that the Louisville plume does not originate from the core-mantle boundary, but rather from a well stirred region of the lower mantle located well above the D" layer. The FOZO-like compositions observed at the LSC fit well with this hypothesis, as FOZO compositions have been originally hypothesized by Hart *et al*. (1992) to be hosted in a well stirred region of the lower mantle.

Future research on the LSC would greatly benefit from the drilling program outlined in IODP proposal #636. Not only would it help resolve outstanding geochemical questions regarding the differences between shield, post-shield and rejuvenated phases of volcanism and further test whether such small isotopic variability persists throughout the

full growth history of Louisville seamounts, but it would also allow more accurate dating of the bends observed in the chain and of the chain itself, thus impacting models of plate motion and hotspot fixity (e.g., Koppers *et al*., 2004; 2007b). Future research should also focus on the young end of the chain. In recent years, estimates of the exact location of the Louisville hotspot have varied by as much as 200 km depending on the authors (e.g., Lonsdale, 1988; Koppers *et al*., 2004; Wessel & Kroenke, 2008). The issue can only be resolved by detailed geophysical and bathymetric surveying, coupled with sampling of the seamounts and any recent lava flow-fields on the seafloor in this area for geochemical and geochronological work. In the same area, the geochemical and structural effects of the proximity of the Eltanin Fracture Zone system and Hollister Ridge should also be studied. Hollister Ridge, the mid-ocean spreading center located at the boundary between the Pacific and Antarctic plates, is of particular interest, as it displays structural evidence of migrating towards the Louisville hotspot (Small, 1995), and geochemical evidence of contribution of the Louisville plume in the magmas produced at the mid-ocean ridge (e.g., Vlastélic & Dosso, 2005).

Appendix A: Major element (wt%) and trace element (ppm) compositions of Deccan dikes. Relative uncertainty on major and minor element concentrations is ~1%, 0.5% for SiO_2. For trace elements, relative uncertainties are 1-5% for most elements (relative errors as two standard deviations range from 1.4% for Sr to 7.0% for Gd), based on repeatability of standards analyzed as unknowns. An indication of accuracy is given by measured and recommended values of the BHVO-1 rock standard (Jenner *et al*., 1990; Govindaraju, 1994; Eggins *et al*., 1997). The row labeled "lab" indicates in what laboratory the analyses where performed. "WSU" indicates Washington State University, where both major and trace element (Sc to Li) concentrations were acquired by XRF. Additional trace elements (La to U) where acquired on selected samples by ICP-MS, with the exception of samples BO-31, BO-32 and DH-27, which were measured by ICP-AES (inductively coupled plasma-atomic emission spectrometry) at Royal Holloway College, UK. Walsh (1992) reports a precision of ±2% using this method. "UH" indicates analyses acquired at the University of Hawai'i. Major elements were measured by XRF and trace elements by ICP-MS. All major element values are recalculated to 100% on a water-free basis, with totals ranging from 98.81 to 101.68 wt%. Pre-normalization totals and loss on ignition (LOI) are also reported when available. "SIO" indicates a sample analyzed at the Scripps Institute of Oceanography. For this sample, major elements are water-free electron microprobe analyses, with the exception of Rb and Sr, which were determined by isotope dilution. See Mahoney (1984) for details. Strike is reported in degrees of azimuth from the north. Dike thickness at sampling site is in meters. Cases indicated by an asterisk (*) represent minimum estimated thickness when one or both edges of a dike could not be observed. "DFA result" indicates the formational assignment of the discriminant-function analysis; formation names are abbreviated to save space (Amb = Ambenali, Thak = Thakurvadi, etc.). The second-best match is indicated in parentheses if the squared Mahalanobis distance of the second-best

Appendix A: Major element (wt%) and trace element (ppm) compositions of Deccan dikes.

Sample	AL82-12	ALI-6	DDH-009	DDH-010	DDH-011	DDH-015	DDH-017	DDH-018	DDH-019	DDH-022	DDH-029	DDH-030	DDH-033	DDH-034	DDH-036	DDH-037	DDH-038	DDH-039
Swarm	Coast	Coast	Coast	Coast	Coast	Coast	Coast	Coast	Coast	Coast	Coast	Coast	Coast	Coast	Coast	Coast	Coast	Coast
Strike		20	20	0	20	0	0	8	0	10	5	15	17	170	5	0		170
Thickness (m)		8	0.5	0.5	0.5	2	0.5	0.25	25	20	100*	8*	8	18	5			8
DFA result	Amb	Amb (Bhima)	Thak (Pol)	Thak (Pol)	Thak (Pol)				Neral	Pol (amb)	Mahab (Neral)	Mahab (Amb)			Bushe		Khand (Thak)	Amb (Mahab)
Mahalanobis distance	3.458	3.11	7.35	6.89	4.81				17.28	4.74	21.95	7.66			3.77		8.75	7.81
Lab	SIO	WSU	WSU	WSU	WSU	WSU	WSU	WSU	WSU	WSU	WSU	WSU	WSU	WSU	WSU	WSU	WSU	WSU
SiO_2	48.55	48.26	50.28	50.68	50.28	46.05	49.49	49.37	51.20	50.98	50.12	50.22	50.33	46.27	52.09	48.88	48.87	49.96
TiO_2	2.42	2.55	1.95	1.88	1.95	3.31	2.23	2.71	3.73	2.51	3.18	2.84	2.27	1.12	1.17	3.41	1.32	2.99
Al_2O_3	13.92	13.96	13.54	13.10	13.63	10.35	11.17	11.67	13.66	12.93	12.96	13.56	14.90	7.74	14.56	14.47	16.89	13.58
FeO (t)	15.81	14.39	12.15	11.67	12.07	12.70	12.07	12.47	13.70	15.26	14.68	14.07	11.26	12.66	10.52	13.86	12.47	14.17
MnO	0.21	0.25	0.19	0.19	0.20	0.20	0.24	0.20	0.19	0.19	0.23	0.21	0.18	0.19	0.18	0.20	0.18	0.22
MgO	6.23	6.77	8.29	8.45	8.08	12.06	12.38	10.15	4.41	5.07	5.42	5.88	6.48	22.93	7.74	5.76	7.10	5.83
CaO	10.74	11.28	10.61	11.23	10.78	10.33	9.21	9.79	8.29	9.86	9.94	10.36	11.12	7.79	11.09	9.54	10.43	9.87
Na_2O	2.39	2.24	2.51	2.31	2.51	2.53	2.35	2.54	3.63	2.46	2.42	2.09	2.59	0.99	2.22	2.73	2.31	2.49
K_2O	0.20	0.08	0.27	0.28	0.29	1.78	0.62	0.79	0.83	0.52	0.69	0.49	0.66	0.21	0.33	0.79	0.29	0.60
P_2O_5	0.23	0.22	0.21	0.20	0.21	0.69	0.25	0.31	0.37	0.23	0.37	0.29	0.22	0.10	0.10	0.36	0.13	0.29
Total																		
LOI																		
Sc		37	38	35	37	30	29	31	26	37	36	34	32	25	35	33	35	36
V	448	424	295	303	300	264	263	275	429	410	443	432	325	212	297	349	249	410
Cr		93	233	493	252	793	884	925	118	88	140	110	219	1638	386	102	64	103
Co		43	41	39	44	48	47	44	39	45	42	41	37	56	30	41	36	43
Ni	99	86	154	190	169	304	497	311	52	47	67	60	111	984	134	102	141	68
Cu		251	151	138	157	110	100	105	35	241	320	270	216	97	143	329	143	309
Zn		114	100	95	105	109	109	112	140	122	142	131	94	85	81	118	104	129
Ga		23	20	17	19	16	19	18	28	25	24	26	23	11	18	27	18	24
Rb	5.64	1	4	5	6	37	11	12	18	13	25	9	17	5	23	18	5	17
Sr	195.5	212	310	297	309	1291	395	442	321	200	218	194	324	114	147	309	213	210
Y	34	31	24	21	23	27	20	24	37	36	41	35	25	14	23	36	23	35
Zr	142	139	130	123	129	334	151	216	213	158	212	170	150	67	90	211	96	174
Nb	11	11	15	14	13	97	34	31	22	13	24	16	21	4	7	29	6	16
Cs																		
Ba	31	4	114	117	88	805	157	186	232	87	139	88	124	0	66	149	130	110
Li		10	10	9	9	19	14	16	12	9		7	8	6	8	9	10	9
La					15	119	30	30		14	22	17	18	5			11	17
Ce					33	219	59	66		31	48	37	38	11			23	37
Pr					4.2	23	6.9	8.5		4.2	6.3	4.8	4.8	1.6			2.9	5.0
Nd					19	87	28	37		20	29	23	21	8			13	24
Sm					5.2	14.7	6.2	8.0		6.3	8.2	6.9	5.7	2.6			4.0	7.1
Eu					1.7	4.0	1.9	2.3		2.2	2.5	2.2	1.9	0.94			1.5	2.3
Gd					5.4	10	5.6	6.8		7.1	8.9	7.5	5.6	2.9			4.6	7.9
Tb					0.85	1.3	0.84	0.97		1.2	1.5	1.3	0.93	0.50			0.82	1.3
Dy					5.0	6.4	4.8	5.5		7.7	9.3	8.1	5.5	3.0			5.2	8.1
Ho					0.94	1.1	0.91	0.99		1.5	1.8	1.6	1.0	0.58			1.1	1.6
Er					2.5	2.5	2.3	2.5		3.9	4.8	4.2	2.7	1.5			2.9	4.1
Tm					0.34	0.32	0.31	0.33		0.54	0.67	0.58	0.37	0.19			0.42	0.58
Yb					2.0	1.8	1.8	1.9		3.3	4.0	3.4	2.2	1.1			2.5	3.4
Lu					0.29	0.27	0.28	0.29		0.50	0.60	0.54	0.33	0.17			0.39	0.52
Hf					3.3	7.7	3.9	5.4		4.4	6.1	4.9	4.0	1.7			2.7	5.0
Ta					0.78	5.7	2.0	1.9		0.80	1.4	1.0	1.2	0.26			0.32	0.97
Pb					2.0	8.5	2.6	2.8		2.0	2.5	2.4	2.4	0.79			2.6	2.4
Th					1.2	11	2.6	2.4		2.1	2.6	2.0	2.2	0.71			1.0	2.0
U					0.28	2.3	0.62	0.59		0.48	0.57	0.41	0.48	0.16			0.17	0.44

Appendix A (continued): Major element (wt%) and trace element (ppm) compositions of Deccan dikes.

Sample	DDH-040	DDH-042	DDH-043	DDH-044	DDH-045	DDH-047	DDH-095	DDH-100	DDH-102	DDH-103	DDH-112	DDH-116	DDH-117	DDH-119	DDH-120	DDH-121	DDW-001
Swarm	Coast	Coast	Coast	Coast	Coast	Coast	Coast	Coast	Coast	Coast	Coast	Coast	Coast	Coast	Coast	Coast	Coast
Strike	5	5	5	160	160	17	20	10	15	165	0	15	15	5	0	0	23
Thickness (m)	1.5	26	26	30	30	10	30	1.5	19	4	10	4	4	2	3	3	20*
DFA result	Amb (Mahab)			Amb (Thak)	Pol (Khand)	Amb (Pol)	Pol (Khand)	Bushe	Mahab (Thak)	Pol (Amb)		Amb (Bhima)	Amb (Pol)	Thak (Neral)	Thak (Pol)	Thak (Pol)	
Mahalanobis distance	16.74			15.57	10.45	8.51	6.15	6.39	18.32	15.14		1.71	15.63	10.12	9.46	14.72	
Lab	WSU	WSU	WSU	WSU	WSU	WSU	WSU	WSU	WSU	WSU	WSU	WSU	WSU	WSU	WSU	WSU	WSU
SiO_2	50.36	49.50	49.89	49.50	52.06	50.46	51.12	52.64	53.90	50.18	49.38	49.36	50.06	49.99	49.35	49.97	52.43
TiO_2	3.33	3.02	3.02	2.81	2.34	2.11	2.55	1.34	1.50	3.05	3.13	2.46	2.60	1.31	1.75	1.61	0.92
Al_2O_3	12.86	13.34	14.44	14.23	13.38	13.85	13.36	14.33	13.74	13.40	13.61	13.83	14.52	12.84	13.86	13.21	13.77
FeO (t)	14.26	14.72	13.78	13.21	13.84	13.44	13.95	11.31	10.54	13.79	14.56	14.07	13.45	12.06	12.31	11.93	12.52
MnO	0.22	0.22	0.17	0.20	0.21	0.21	0.22	0.19	0.15	0.21	0.22	0.22	0.22	0.14	0.19	0.18	0.22
MgO	5.66	5.69	4.97	6.19	5.24	6.34	5.36	6.75	6.58	5.64	5.75	6.42	5.09	11.94	9.58	9.41	6.58
CaO	9.78	9.83	10.24	10.52	9.49	10.86	9.94	10.58	10.04	10.56	9.91	10.90	11.20	8.31	9.67	11.36	10.73
Na_2O	2.53	2.58	2.48	2.54	2.70	2.25	2.59	2.23	2.46	2.57	2.44	2.37	2.36	2.49	2.60	1.99	2.11
K_2O	0.66	0.77	0.69	0.51	0.50	0.30	0.67	0.52	0.92	0.30	0.69	0.15	0.27	0.76	0.46	0.16	0.59
P_2O_5	0.33	0.33	0.30	0.28	0.24	0.18	0.25	0.11	0.17	0.30	0.30	0.22	0.22	0.16	0.23	0.17	0.14
Total																	
LOI																	
Sc	37	36	36	36	35	41	38	40	33	37	37	38	41	31	35	40	43
V	441	334	362	383	371	384	404	321	277	466	368	406	419	246	286	281	310
Cr	161	108	117	235	141	116	114	131	319	119	99	94	104	1110	952	950	48
Co	40	43	42	39	39	40	40	38	37	43	43	41	43			42	36
Ni	82	73	85	91	79	69	77	74	114	65	75	84	100	280	302	235	44
Cu	324	284	277	287	230	213	228	131	146	342	270	244	258	152	106	140	153
Zn	140	119	122	112	114	106	117	90	81	119	119	118	123	86	94	94	99
Ga	25	24	26	22	21	22	26	19	21	23	28	26	20	19	21	21	15
Rb	19	21	17	14	33	8	21	14	26	15	16	5	5	11	6	2	11
Sr	213	305	318	247	239	205	212	122	341	228	302	208	210	306	291	244	180
Y	40	33	32	32	34	27	35	27	19	38	31	30	33	20	25	22	23
Zr	189	198	186	167	170	119	170	95	125	185	182	136	141	100	139	102	83
Nb	22	31	28	20	15	11	14	8	11	20	28	11	12	12	16	14	11
Cs																	
Ba	84	172	160	69	161	42	84	74	193	48	114	34	10	252	98	58	191
Li	9	9	7	9	7	8	10	8	9	8	9	13	8			11	6
La																	
Ce																	
Pr																	
Nd																	
Sm																	
Eu																	
Gd																	
Tb																	
Dy																	
Ho																	
Er																	
Tm																	
Yb																	
Lu																	
Hf																	
Ta																	
Pb																	
Th																	
U																	

Appendix A (continued): Major element (wt%) and trace element (ppm) compositions of Deccan dikes.

Sample	DDW-002	DDW-003	DDW-004	DDW-005	DDW-047	DDW-052	DDG-001	DH-23	DH-24	DH-31	DH-41	DH-43	DH-47	DH-49	DH-50	DN-01B	DN-05
Swarm	Coast	Coast	Coast	Coast	Coast	Coast	Coast	Coast	Coast	Coast	Coast	Coast	Coast	Coast	Coast	Coast	Coast
Strike	16		10	20	7	14	25?	10	8	20	0	0	160	0	170	165	165
Thickness (m)	8		20	1	7	10	sill?										
DFA result	Mahab (Amb)			Thak (Amb)	Pol (Amb)			Bushe	Thak (Pol)	Pol (Bushe)		Khand (Pol)	Thak (Pol)	Khand (Thak)	Khand	Bhima (Amb)	Pol (Khand)
Mahalanobis distance	9.70			8.46	3.23			12.90	5.15	10.30		2.88	7.32	11.66	8.79	12.57	8.86
Lab	WSU	WSU	WSU	WSU	WSU	WSU	WSU	WSU	WSU	WSU	WSU	WSU	WSU	WSU	WSU	WSU	WSU
SiO_2	50.34	50.72	53.59	50.15	50.11	51.82	50.38	54.13	49.68	51.78	52.73	51.57	50.05	52.17	51.66	49.33	51.87
TiO_2	2.55	1.36	2.01	2.56	2.49	0.80	2.32	0.98	1.78	1.89	1.93	1.70	2.02	1.81	3.48	2.41	2.83
Al_2O_3	14.14	8.92	13.83	14.34	13.52	14.44	14.43	15.48	14.94	14.32	14.38	14.84	15.31	15.15	12.68	12.99	12.48
FeO (t)	13.33	11.02	13.65	12.40	14.76	11.24	12.01	9.73	11.62	12.45	10.62	11.61	11.83	11.06	14.86	14.49	13.88
MnO	0.21	0.19	0.19	0.19	0.23	0.20	0.20	0.17	0.19	0.20	0.20	0.19	0.19	0.15	0.21	0.23	0.22
MgO	5.70	13.12	4.30	6.18	5.47	7.25	6.33	5.84	7.37	5.95	5.70	6.35	6.37	5.93	4.58	6.92	5.75
CaO	10.69	12.77	8.93	11.20	10.54	11.80	10.17	9.96	11.87	10.09	10.51	10.40	13.09	10.16	8.56	10.93	9.20
Na_2O	2.29	1.43	2.30	2.32	2.43	1.91	2.97	2.59	2.21	2.49	2.72	2.47	0.70	2.24	2.57	2.25	2.50
K_2O	0.53	0.35	0.88	0.42	0.22	0.42	0.92	1.02	0.19	0.65	1.02	0.67	0.23	1.15	1.00	0.27	0.98
P_2O_5	0.24	0.12	0.31	0.24	0.23	0.12	0.27	0.11	0.15	0.18	0.19	0.18	0.21	0.20	0.39	0.19	0.30
Total																	
LOI																	
Sc	36	43	33	35	36	44	32	36	40	35	32	38	40	34	31	39	39
V	395	370	413	360	418	304	331	212	323	359	341	334	315	260	424	484	394
Cr	143	1754	55	288	95	119	285	128	367	153	196	172	645	749	69	115	164
Co	36	41	31	43	39	36	37										
Ni	60	205	27	100	61	71	64	30	139	81	66	96	51	74	43	82	52
Cu	256	82	269	203	283	134	143	45	175	200	68	174	105	123	313	233	261
Zn	113	75	125	112	119	85	105	78	83	102	86	94	98	94	136	111	121
Ga	19	13	23	23	24	15	23	16	16	20	20	21	38	24	29	21	20
Rb	13	9	17	6	5	8	18	44	4	20	29	18	11	44	25	6	28
Sr	212	179	252	258	194	160	430	141	266	210	222	211	45	141	207	200	202
Y	31	19	30	29	33	19	27	29	22	29	28	27	26	27	45	29	42
Zr	150	89	144	152	150	68	172	111	95	129	160	126	127	119	255	124	200
Nb	15	8	21	17	13	7	17	8	8	11	10	8	9	9	21	9	16
Cs																	
Ba	128	64	275	71	49	107	289	179	14	106	142	174	12	157	163	41	120
Li	7	12	10	5	9	5	10										
La																	
Ce																	
Pr																	
Nd																	
Sm																	
Eu																	
Gd																	
Tb																	
Dy																	
Ho																	
Er																	
Tm																	
Yb																	
Lu																	
Hf																	
Ta																	
Pb																	
Th																	
U																	

Appendix A (continued): Major element (wt%) and trace element (ppm) compositions of Deccan dikes.

Sample	DN-10	DN-11	DN-12	DN-16	DN-22	DN-24	DN-32	DN-36	DN-38	DN-39	DN-43	DN-49	DN-50	JH-29	JH-32	JH-35	JH-36	JH-40
Swarm	Coast	Coast	Coast	Coast	Coast	Coast	Coast	Coast	Coast	Coast	Coast	Coast	Coast	Coast	Coast	Coast	Coast	Coast
Strike	0	165	0	5	8	10	0		4	4	165	0	8	0	0	5	10	175
Thickness (m)																		
DFA result	Pol (Thak)	Pol (Thak)	Bushe		Pol (Bushe)	Pol (Igat-Jaw)	Bhima (Thak)		Bushe		Thak (Khand)	Pol (Mahab)	Bhima (Thak)		Amb (Thak)	Bhima (Amb)	Amb (Pol)	Bhima
Mahalanobis distance	6.75	5.25	12.50		8.55	11.33	16.71		17.39		7.48	5.37	5.73		14.49	14.24	3.77	23.42
Lab	WSU	WSU	WSU	WSU	WSU	WSU	WSU	WSU	WSU	WSU	WSU	WSU	WSU	WSU	WSU	WSU	WSU	WSU
SiO_2	51.34	52.00	52.40	51.29	52.60	50.98	52.48	49.34	52.44	49.34	51.93	52.26	50.29	52.81	49.58	49.34	50.08	49.87
TiO_2	2.06	1.89	1.20	3.02	2.00	2.56	1.83	3.77	1.25	3.77	2.08	2.02	2.40	1.46	1.52	2.07	2.59	3.20
Al_2O_3	14.61	14.44	15.32	13.43	14.21	13.35	14.18	13.05	14.58	13.05	14.28	14.47	15.14	14.00	15.25	14.35	13.30	12.05
FeO (t)	12.21	11.01	10.90	13.96	11.78	14.59	10.95	14.21	11.99	14.21	12.84	10.91	12.25	12.55	11.85	12.97	14.39	17.48
MnO	0.19	0.18	0.19	0.19	0.19	0.22	0.21	0.22	0.20	0.22	0.20	0.17	0.17	0.21	0.19	0.20	0.22	0.26
MgO	5.92	6.43	6.29	4.96	5.89	5.35	6.68	5.83	6.09	5.83	5.38	6.27	5.63	5.74	7.53	7.11	6.16	4.83
CaO	11.04	10.66	10.66	8.95	9.96	9.77	11.22	10.09	10.34	10.09	9.78	10.37	10.97	9.67	11.43	11.26	10.39	9.03
Na_2O	2.22	2.39	2.34	1.99	2.75	2.47	2.07	2.56	2.38	2.56	2.51	2.67	2.31	2.58	2.32	2.28	2.34	2.52
K_2O	0.23	0.81	0.57	1.91	0.41	0.48	0.19	0.58	0.59	0.58	0.81	0.64	0.61	0.81	0.22	0.26	0.30	0.53
P_2O_5	0.18	0.19	0.13	0.33	0.21	0.25	0.19	0.36	0.13	0.36	0.19	0.21	0.23	0.17	0.12	0.16	0.23	0.24
Total																		
LOI																		
Sc	36	37	39	30	35	31	36	38	42	38	36	37	38	40	39	38	36	36
V	363	328	311	368	351	389	305	430	336	430	357	338	353	354	339	382	424	582
Cr	130	263	105	148	155	70	299	157	123	157	94	245	199	126	204	232	127	56
Co																		
Ni	72	96	53	87	74	56	84	64	54	64	58	95	79	68	133	125	64	38
Cu	190	183	138	220	191	246	112	303	177	303	183	203	215	203	137	189	270	287
Zn	99	90	86	121	92	121	93	140	93	140	103	87	104	97	84	102	116	139
Ga	20	22	21	20	23	27	22	29	19	29	22	23	29	18	23	24	23	26
Rb	8	20	19	36	10	12	1	14	19	14	22	16	11	27	5	6	6	13
Sr	273	229	153	233	238	211	417	261	146	261	244	218	279	135	211	196	206	206
Y	27	29	26	37	29	36	23	36	30	36	28	30	32	35	20	26	33	36
Zr	128	130	93	189	146	174	133	190	100	190	139	148	149	116	86	106	148	153
Nb	9	9	7	18	11	14	12	25	9	25	12	12	12	12	8	8	11	12
Cs																		
Ba	53	133	131	532	103	68	97	104	119	104	122	112	111	123	12	14	38	63
Li																		
La																		
Ce																		
Pr																		
Nd																		
Sm																		
Eu																		
Gd																		
Tb																		
Dy																		
Ho																		
Er																		
Tm																		
Yb																		
Lu																		
Hf																		
Ta																		
Pb																		
Th																		
U																		

Appendix A (continued): Major element (wt%) and trace element (ppm) compositions of Deccan dikes.

Sample	JH-47	JH-48	JH-49	JH-50	JH-51	JH-55	JH-57	JH-67	JH-69	JH-72	JW-06	JW-07	JW-29	JW-30	JW-32	KVS-302
Swarm	Coast	Coast	Coast	Coast	Coast	Coast	Coast	Coast	Coast	Coast	Coast	Coast	Coast	Coast	Coast	Coast
Strike	0	0	10	10	10	170	5	0	10	10	0	160	165	0	0	165
Thickness (m)											5.5	2	10	2.5	15	
DFA result	Pol (Amb)	Bushe (Pol)	Pol (Bhima)	Pol (Amb)	Amb	Khand (Thak)	Bhima (Neral)	Igat-Jaw (Khand)	Pol (Khand)	Bushe	Thak (Bushe)	Igat-Jaw (Neral)	Thak	Thak (Mahab)	Thak (Pol)	Bushe
Mahalanobis distance	4.91	8.87	8.61	13.70	20.41	9.70	19.56	15.83	8.19	12.53	14.57	19.87	6.56	5.75	3.09	22.02
Lab	WSU	WSU	WSU	WSU	WSU	WSU	WSU	WSU	WSU	WSU	WSU	WSU	WSU	WSU	WSU	WSU
SiO_2	51.05	52.45	50.56	50.52	49.91	51.77	49.51	52.28	50.69	52.73	51.40	50.59	52.12	50.73	51.53	52.90
TiO_2	2.46	2.01	3.14	2.80	2.86	3.75	2.52	2.69	2.64	1.25	1.98	2.98	1.69	2.01	1.95	1.32
Al_2O_3	12.88	14.07	12.47	13.34	12.86	12.61	14.29	13.45	13.64	14.38	13.99	13.14	14.64	14.23	13.87	14.05
FeO (t)	14.96	12.36	15.57	14.23	15.30	14.46	14.39	13.18	14.44	11.57	13.18	15.23	10.69	11.27	11.31	12.23
MnO	0.24	0.20	0.23	0.23	0.24	0.21	0.18	0.19	0.22	0.21	0.21	0.22	0.16	0.18	0.16	0.21
MgO	5.50	5.60	5.19	5.78	5.91	4.39	6.45	5.08	5.26	6.49	5.66	4.52	7.23	7.44	7.36	5.97
CaO	9.73	9.84	9.39	9.87	9.83	8.44	9.03	8.50	9.91	10.35	9.64	9.02	10.05	11.08	10.70	10.08
Na_2O	2.36	2.41	2.42	2.40	2.38	2.45	2.44	2.99	2.28	2.32	2.41	2.40	2.63	2.25	2.30	2.41
K_2O	0.60	0.88	0.70	0.58	0.48	1.50	0.95	1.39	0.68	0.57	1.34	1.61	0.59	0.59	0.61	0.69
P_2O_5	0.22	0.19	0.32	0.26	0.23	0.42	0.24	0.25	0.24	0.12	0.19	0.29	0.21	0.22	0.21	0.14
Total																
LOI																
Sc	39	36	36	34	38	33	30	33	37	39	34	35	34	37	38	39
V	437	361	472	426	439	423	339	379	409	355	386	436	305	326	317	356
Cr	84	110	72	102	108	76	238	77	98	145	131	82	273	391	383	100
Co																
Ni	58	70	53	72	75	49	78	30	58	68	59	35	82	139	128	44
Cu	241	170	293	258	251	322	116	118	247	171	217	184	60	138	88	182
Zn	123	100	133	120	125	144	117	115	118	93	107	113	92	97	94	95
Ga	27	24	24	22	27	29	27	22	22	16	26	21	21	28	20	18
Rb	16	27	18	16	13	47	25	40	25	20	35	45	26	15	14	20
Sr	191	228	194	204	205	197	253	254	214	118	190	231	337	307	308	115
Y	35	30	42	36	34	50	30	34	37	28	31	36	23	26	25	32
Zr	150	138	198	173	163	266	163	188	166	93	135	194	133	133	130	104
Nb	11	10	15	14	12	22	15	15	13	8	11	18	10	14	14	8
Cs																
Ba	67	112	96	94	43	169	163	227	104	91	140	255	159	130	149	124
Li																
La																
Ce																
Pr																
Nd																
Sm																
Eu																
Gd																
Tb																
Dy																
Ho																
Er																
Tm																
Yb																
Lu																
Hf																
Ta																
Pb																
Th																
U																

Appendix A (continued): Major element (wt%) and trace element (ppm) compositions of Deccan dikes.

Sample	KVS-303	KVS-305	KVS-309	KVS-311	KVS-312	KVS-314	KVS-315	R.5.7	R.6.1	R.9.2	R.9.30	R.9.32	UDD-04	UDD-05	UDD-06	UDD-07
Swarm	Coast	Coast	Coast	Coast	Coast	Coast	Coast	Coast	Coast	Coast	Coast	Coast	Coast	Coast	Coast	Coast
Strike	165	160	175	160	5	160	160	0	0	0	0	0	175	177.5	0	0
Thickness (m)								2.5	3		1	1	15	25	25	
DFA result		Thak (Pol)	Amb (Thak)	Bhima (Thak)		Pol (Khand)	Pol (Khand)	Thak (Mahab)	Pol (Thak)	Bhima (Thak)	Khand Pol)	Igat-Jaw (Khand)	Khand		Bushe	Khand
Mahalanobis distance		3.58	15.78	18.08		15.93	17.45	5.21	5.07	5.24	6.14	12.26	13.70		17.50	23.71
Lab	WSU	WSU	WSU	WSU	WSU	WSU	WSU	WSU	WSU	WSU	WSU	WSU	UH	UH	UH	UH
SiO_2	52.60	51.47	50.56	51.36	52.86	50.65	50.98	50.38	51.66	52.15	51.34	51.28	51.59	51.65	52.44	51.71
TiO_2	2.27	2.24	2.01	2.18	1.31	3.29	3.44	2.49	2.08	2.07	2.47	2.80	3.02	3.16	1.31	2.82
Al_2O_3	12.92	13.30	13.93	14.44	14.07	12.45	12.46	14.08	14.82	14.24	13.97	13.05	12.95	12.79	14.39	13.73
FeO (t)	11.91	11.88	12.55	12.16	12.16	15.71	15.20	12.42	10.83	11.88	13.99	14.75	14.32	14.98	12.31	13.72
MnO	0.17	0.19	0.20	0.18	0.20	0.23	0.24	0.19	0.17	0.17	0.20	0.24	0.20	0.21	0.20	0.19
MgO	6.60	7.28	6.76	5.97	5.96	4.80	4.90	6.33	6.65	6.22	4.89	4.71	4.99	4.36	6.05	4.77
CaO	10.18	11.76	10.92	10.78	9.85	9.60	9.44	11.07	10.90	9.96	9.99	9.37	9.05	8.60	10.35	9.28
Na_2O	2.07	1.21	2.25	2.27	2.33	2.55	2.59	2.32	2.33	2.43	2.54	2.55	2.49	2.61	2.14	2.51
K_2O	1.06	0.45	0.63	0.43	1.12	0.39	0.42	0.48	0.37	0.68	0.35	0.95	1.03	1.18	0.66	0.92
P_2O_5	0.22	0.22	0.18	0.23	0.14	0.32	0.34	0.24	0.20	0.21	0.26	0.29	0.34	0.46	0.14	0.35
Total													100.23	100.47	100.36	101.10
LOI																
Sc	34	36	36	34	41	38	37	35	37	34	33	33	35	32	44	33
V	357	364	373	315	364	448	453	337	352	300	392	414				
Cr	224	321	155	227	105	71	65	275	306	216	80	79	102	36	117	101
Co													42	43	43	41
Ni	85	108	75	72	48	40	41	93	118	82	61	53	50	40	59	49
Cu	244	183	191	188	183	274	276	192	216	170	205	239	284	270	159	294
Zn	97	94	101	96	95	138	144	110	84	96	118	128	140	158	85	139
Ga	17	20	22	22	17	27	28	23	21	24	26	25				
Rb	31	18	14	10	27	21	23	12	7	19	26	24	35	40	20	30
Sr	688	261	208	422	112	207	201	253	241	294	306	265	214	216	125	221
Y	28	27	26	27	32	42	43	28	29	27	33	37	48	58	34	48
Zr	144	128	114	149	103	212	217	148	139	140	173	193	241	315	108	203
Nb	12	12	7	15	10	18	17	15	11	13	13	16	17	22	7.7	16
Cs													0.26	0.60	0.19	0.31
Ba	111	47	55	83	117	93	92	100	84	101	186	259	202	222	137	160
Li																
La													22	29	11	22
Ce													52	67	24	51
Pr													7.0	8.9	3.1	7.0
Nd													31	39	13	31
Sm													7.8	9.7	3.4	7.9
Eu													2.2	2.6	1.1	2.2
Gd													8.2	9.8	4.1	8.0
Tb													1.3	1.6	0.77	1.3
Dy													7.9	9.5	5.0	7.9
Ho													1.5	1.8	1.1	1.5
Er													4.2	5.1	3.2	4.3
Tm													0.62	0.77	0.51	0.64
Yb													3.6	4.4	3.1	3.6
Lu													0.53	0.65	0.48	0.53
Hf													6.0	7.7	2.7	5.3
Ta													1.1	1.4	0.5	1.0
Pb													3.2	4.0	2.3	3.5
Th													4.3	5.7	2.7	4.2
U													1.0	1.4	0.64	1.0

Appendix A (continued): Major element (wt%) and trace element (ppm) compositions of Deccan dikes.

Sample	UDD-07B	UDD-08	ADS-02	AM-02	AM-26	AM-30	BH-75	BH-76	BH-81	BH-81*	BH-87	BH-89	BH-89*	BH-91	BH-91*	BO-31
Swarm	Coast	Coast	Nasik-Pune	Nasik-Pune	Nasik-Pune	Nasik-Pune	Nasik-Pune	Nasik-Pune	Nasik-Pune	Nasik-Pune	Nasik-Pune	Nasik-Pune	Nasik-Pune	Nasik-Pune	Nasik-Pune	Nasik-Pune
Strike	10	170	25	115	80	65	0	20	90	90	105	55	55	115	115	80
Thickness (m)	23	7.5	6	3	7*	18*	6	3	6	6	4	6	6	7.5	7.5	5
DFA result	Khand		Amb (Pol)	Pol (Amb)	Khand (Thak)	Neral (Thak)	Thak (Pol)	Amb (Bhima)	Amb (Pol)	Amb (Pol)	Pol (Khand)	Khand (Bhima)	Khand (Bhima)	Pol (Amb)	Pol (Amb)	Pol (Khand)
Mahalanobis distance	22.21		10.54	6.26	14.07	10.86	2.97	5.83	11.15	14.14	4.73	14.67	9.76	6.25	7.46	13.78
Lab	UH	UH	WSU	WSU	WSU	WSU	WSU	WSU	WSU	WSU	WSU	WSU	WSU	WSU	WSU	WSU
SiO_2	51.85	52.72	50.41	50.55	50.08	50.23	50.87	50.96	49.89	50.00	51.07	50.55	50.54	50.38	50.61	51.06
TiO_2	2.74	1.83	2.70	2.31	0.99	1.65	2.04	2.21	2.54	2.55	2.64	3.12	3.08	2.43	2.37	3.23
Al_2O_3	13.23	13.60	13.48	13.68	13.95	12.75	13.81	14.16	13.74	13.71	13.17	13.60	13.50	13.29	13.03	12.57
FeO (t)	13.92	15.60	14.61	12.60	11.22	11.36	11.61	12.50	13.14	13.12	14.61	13.70	13.89	14.11	14.06	15.21
MnO	0.21	0.24	0.23	0.20	0.19	0.19	0.16	0.19	0.21	0.20	0.22	0.20	0.20	0.22	0.23	0.23
MgO	5.12	4.14	5.46	6.44	10.04	10.29	7.53	6.44	6.60	6.58	5.31	5.50	5.52	5.94	6.00	4.96
CaO	9.24	8.23	10.05	11.09	11.40	10.56	11.41	10.51	11.10	11.04	9.94	10.07	9.99	10.70	10.70	9.51
Na_2O	2.40	2.68	2.54	2.61	1.86	1.74	1.99	2.33	2.39	2.39	2.51	2.58	2.59	2.40	2.43	2.54
K_2O	0.95	0.73	0.28	0.32	0.16	1.10	0.40	0.52	0.17	0.18	0.30	0.38	0.38	0.34	0.37	0.38
P_2O_5	0.32	0.24	0.24	0.21	0.11	0.15	0.17	0.19	0.22	0.22	0.24	0.30	0.30	0.21	0.21	0.32
Total	100.68	100.87														
LOI																
Sc	34	41	35	44	40	38	37	37	37	39	36	34	35	38	39	34
V			436	378	266	310	353	361	383	368	422	387	392	405	422	429
Cr	110	15	74	135	677	723	500	238	223	236	88	222	225	112	85	67
Co	41	47		42	42	43										58
Ni	50	24	42	97	234	185	162	87	86	88	59	83	83	57	51	40
Cu	273	251	285	238	133	79	162	152	222	226	233	266	275	220	231	282
Zn	137	121	139	125	91	90	86	97	104	104	113	116	117	112	118	142
Ga			28	24	18	21	23	28	22	25	24	25	24	23	25	26
Rb	30	20	14	9	7	39	12	15	8	8	13	17	18	7	7	24
Sr	216	148	240	206	154	238	239	249	219	216	240	263	264	215	208	204
Y	47	45	34	32	20	23	25	26	31	30	34	37	36	31	31	42
Zr	231	156	161	134	73	107	117	124	144	145	159	191	192	137	133	209
Nb	16	16	11	11	5	8	11	11	14	15	12	18	17	11	10	17
Cs	0.26	0.17														
Ba	171	172	82	59	101	181	58	66	2	17	38	121	115	22	63	105
Li				8	9	12										12
La	21	17			8.2	15										23
Ce	49	37			17	33										45
Pr	6.6	4.6			2.1	4.5										
Nd	29	19			9.6	22										38
Sm	7.4	4.6			2.9	6.7										9.3
Eu	2.1	1.5			1.0	2.3										2.5
Gd	7.6	5.5			3.4	7.4										
Tb	1.3	0.99			0.62	1.3										
Dy	7.5	6.5			4.0	7.6										7.9
Ho	1.5	1.4			0.84	1.5										
Er	4.1	4.2			2.3	3.7										
Tm	0.62	0.69			0.33	0.50										
Yb	3.5	4.2			2.0	2.9										4.1
Lu	0.52	0.65			0.31	0.43										
Hf	5.8	3.8			1.9	4.6										
Ta	1.0	1.0			0.21	0.75										
Pb	3.3	2.5			1.9	2.3										
Th	4.2	3.4			0.80	2.0										
U	2.0	3.0			0.12	0.45										

Appendix A (continued): Major element (wt%) and trace element (ppm) compositions of Deccan dikes.

Sample	BO-32	BO-32*	BO-38	BO-40	BO-40*	BOR-012	BOR-013	BOR-014	BOR-020	BOR-029	BOR-046	CAT-107	CAT-113	CAT-150	CAT-156	CAT-158
Swarm	Nasik-Pune	Nasik-Pune	Nasik-Pune	Nasik-Pune	Nasik-Pune	Nasik-Pune	Nasik-Pune	Nasik-Pune	Nasik-Pune	Nasik-Pune	Nasik-Pune	Nasik-Pune	Nasik-Pune	Nasik-Pune	Nasik-Pune	Nasik-Pune
Strike	80	80	50	0	0		98	85	95	20	75	0	120		40	20
Thickness (m)	3	3	2	13.5	13.5		3	3	2	4	2.5	2	2	6	4.5	2
DFA result	Pol (Khand)	Pol (Khand)	Khand (Igat-Jaw)	Mahab (Bhima)	Bhima (Mahab)	Mahab			Amb (Mahab)	Bhima (Amb)	Pol (Khand)	Amb (Pol)	Amb	Pol (Amb)	Pol (Khand)	
Mahalanobis distance	17.45	15.93	5.95	6.88	4.86	21.50			16.64	6.12	4.06	3.65	19.44	2.25	6.43	
Lab	WSU	WSU	WSU	WSU	WSU	WSU	WSU	WSU	WSU	WSU	WSU	WSU	WSU	WSU	WSU	WSU
SiO_2	50.98	50.65	50.01	52.29	51.93	48.39	49.59	49.38	49.83	50.86	51.98	50.51	50.31	50.94	51.38	49.57
TiO_2	3.44	3.29	2.66	2.17	2.11	3.52	3.35	3.31	2.96	2.61	2.29	2.38	3.48	2.04	2.88	3.19
Al_2O_3	12.46	12.45	14.31	14.79	14.84	14.01	13.48	13.48	13.91	13.69	14.24	14.00	12.60	13.95	13.06	13.34
FeO (t)	15.20	15.71	14.62	10.95	11.63	15.67	15.20	15.47	13.11	14.06	12.93	13.65	15.23	13.06	14.52	14.76
MnO	0.24	0.23	0.20	0.19	0.18	0.36	0.22	0.23	0.21	0.22	0.21	0.22	0.24	0.20	0.21	0.22
MgO	4.90	4.80	4.71	5.52	5.53	5.08	4.88	5.28	6.42	5.60	5.38	6.06	5.18	6.07	5.09	5.71
CaO	9.44	9.60	9.46	10.43	10.31	10.44	9.78	9.66	10.34	9.88	9.68	10.36	9.70	10.85	9.26	9.72
Na_2O	2.59	2.55	2.59	2.65	2.50	1.96	2.55	2.53	2.41	2.42	2.68	2.34	2.58	2.34	2.48	2.71
K_2O	0.42	0.39	1.18	0.80	0.75	0.20	0.62	0.33	0.50	0.44	0.39	0.26	0.33	0.37	0.84	0.46
P_2O_5	0.34	0.32	0.28	0.22	0.21	0.36	0.33	0.33	0.30	0.24	0.22	0.22	0.35	0.18	0.28	0.32
Total																
LOI																
Sc	37	38	32	34	32	38	36	35	38	36	35	32	34	38	36	31
V	453	448	391	323	326	428	416	400	369	426	378	422	441	367	428	365
Cr	65	71	55	143	142	151	137	133	239	75	103	96	140	127	80	170
Co	52					45	44	44	41	41	46	31	40	37	36	40
Ni	41	40	41	75	72	56	57	58	87	50	48	66	59	80	51	83
Cu	276	274	181	57	123	370	366	326	282	227	233	251	383	178	271	300
Zn	144	138	125	97	94	158	159	136	119	118	125	136	180	128	151	166
Ga	28	27	29	24	26	27	25	29	20	20	21	22	24	22	22	24
Rb	23	21	30	23	22	3	16	11	14	7	19	4	10	12	33	17
Sr	201	207	289	292	296	238	234	242	231	241	237	216	249	208	194	311
Y	43	42	37	27	26	41	39	38	33	31	31	31	40	29	40	34
Zr	217	212	184	145	144	208	194	195	171	156	153	137	204	123	185	196
Nb	17	18	15	14	14	25	25	24	21	13	12	11	21	8	15	29
Cs																
Ba	92	93	240	151	135	80	132	121	85	65	125	40	104	68	119	147
Li	13					17	18	17	17	16	16	6	9	8	10	10
La	23						21	22	17	14	17					
Ce	47						46	47	37	32	37					
Pr							6.0	6.2	4.8	4.4	4.7					
Nd	38						28	29	23	21	22					
Sm	9.5						8.1	8.3	6.8	6.5	6.3					
Eu	2.6						2.6	2.7	2.3	2.2	2.1					
Gd							8.7	9.0	7.3	7.2	6.9					
Tb							1.5	1.5	1.2	1.2	1.2					
Dy	8.2						8.9	9.2	7.4	7.4	7.1					
Ho							1.7	1.8	1.4	1.4	1.4					
Er							4.4	4.5	3.7	3.6	3.5					
Tm							0.60	0.62	0.50	0.49	0.49					
Yb	4.2						3.6	3.7	3.0	2.8	2.9					
Lu							0.54	0.56	0.44	0.42	0.43					
Hf							5.7	5.8	4.7	4.5	4.5					
Ta							1.4	1.4	1.2	0.72	0.77					
Pb							2.7	2.7	2.0	2.1	3.6					
Th							2.6	2.7	2.0	2.0	3.1					
U							0.59	0.60	0.45	0.44	0.74					

Appendix A (continued): Major element (wt%) and trace element (ppm) compositions of Deccan dikes.

Sample	CAT-191	CAT-197	CAT-213	CAT-215	CAT-216	CAT-218	CAT-284	CAT-376	DDG-002	DDG-003	DDG-004	DDH-005	DDH-013	DDH-016	DDH-023	DDH-023A2
Swarm	Nasik-Pune	Nasik-Pune	Nasik-Pune	Nasik-Pune	Nasik-Pune	Nasik-Pune	Nasik-Pune	Nasik-Pune	Nasik-Pune	Nasik-Pune	Nasik-Pune	Nasik-Pune	Nasik-Pune	Nasik-Pune	Nasik-Pune	Nasik-Pune
Strike	90						20	60	18	9	90	67	137	80	22.5	22.5
Thickness (m)	3.5						5	10	5	5*	18	3	3	2		
DFA result	Pol (Amb)	Bushe				Bhima (Amb)	Pol (Thak)	Pol (Thak)	Mahab			Amb (Pol)	Amb (Bhima)	Pol (Bushe)	Bushe (Thak)	Bushe
Mahalanobis distance	5.06	20.93				7.69	5.34	2.60	18.63			6.57	7.78	12.70	11.72	23.33
Lab	WSU	WSU	WSU	WSU	WSU	WSU	WSU	WSU	WSU	WSU	WSU	WSU	WSU	WSU	WSU	WSU
SiO_2	50.31	51.28	48.61	49.12	48.48	49.63	50.60	51.30	49.66	49.73	50.86	49.76	49.13	50.68	55.24	55.65
TiO_2	1.96	0.73	3.39	3.31	3.55	2.24	1.90	2.07	3.40	3.42	2.90	2.51	2.44	1.69	1.550	1.580
Al_2O_3	13.90	18.19	14.05	14.34	13.95	15.69	14.07	14.01	12.86	12.56	13.05	13.63	13.65	14.43	13.78	13.99
FeO (t)	13.41	8.93	15.19	14.99	15.66	12.32	12.76	11.73	15.61	15.76	14.47	13.63	14.33	11.45	9.77	9.70
MnO	0.21	0.15	0.23	0.22	0.24	0.19	0.21	0.19	0.24	0.24	0.22	0.22	0.24	0.20	0.147	0.150
MgO	6.47	6.86	5.50	4.96	5.24	6.06	6.51	6.86	5.19	5.31	5.24	6.22	6.54	7.35	6.59	6.38
CaO	11.05	11.09	9.51	9.70	9.45	10.91	11.27	10.75	9.64	9.62	9.76	10.97	10.92	11.51	8.53	8.22
Na_2O	2.33	2.27	2.65	2.59	2.61	2.35	2.33	2.40	2.69	2.65	2.59	2.53	2.34	2.42	3.40	3.37
K_2O	0.19	0.41	0.53	0.46	0.47	0.39	0.19	0.49	0.37	0.36	0.69	0.32	0.22	0.13	0.81	0.78
P_2O_5	0.17	0.08	0.34	0.34	0.36	0.22	0.17	0.19	0.35	0.35	0.24	0.22	0.20	0.14	0.18	0.18
Total																
LOI																
Sc	34	30	32	27	28	36	37	34	36	34	35	37	41	44	30	30
V	374	177	374	359	395	346	377	365	420	426	447	412	444	367	268	273
Cr	122	375	146	154	162	137	128	267	151	147	78	160	181	254	303	341
Co							39	38	44	46	42	40	47	38	32	32
Ni	69	163	77	71	80	91	75	93	67	67	50	86	100	99	116	154
Cu	222	73	389	384	343	241	215	215	334	344	247	236	239	192	107	105
Zn	144	78	167	165	146	118	116	98	138	140	129	111	113	94	79	78
Ga	17	22	23	25	25	19	20	22	28	26	25	23	23	22	20	20
Rb	6	13	21	15	19	5	5	13	15	16	22	12	7	3	18	18
Sr	213	171	309	317	298	237	214	206	238	231	207	225	205	147	263	267
Y	28	18	37	35	37	30	27	29	39	39	34	30	30	29	23	23
Zr	120	74	207	202	218	136	117	133	201	200	167	139	129	99	133	132
Nb	9	5	30	27	32	13	10	10	22	24	15	14	11	7	10	11
Cs																
Ba	26	55	158	145	176	73	33	59	120	89	77	48	38	29	184	220
Li							6	9	9	9	11	7	7	7	9	9
La												12	9.2	7.4		
Ce												27	22	17		
Pr												3.6	3.0	2.3		
Nd												18	15	12		
Sm												5.6	5.2	4.1		
Eu												2.0	1.9	1.5		
Gd												6.4	6.1	5.2		
Tb												1.1	1.0	0.97		
Dy												6.7	6.4	6.2		
Ho												1.3	1.2	1.2		
Er												3.2	3.2	3.4		
Tm												0.44	0.44	0.48		
Yb												2.6	2.6	2.8		
Lu												0.39	0.39	0.42		
Hf												3.9	3.4	2.8		
Ta												0.82	0.60	0.40		
Pb												1.6	1.4	1.4		
Th												1.3	1.1	1.0		
U												0.30	0.26	0.24		

Appendix A (continued): Major element (wt%) and trace element (ppm) compositions of Deccan dikes.

Sample	DDH-025	DDH-026	DDH-027	DDH-028	DDH-031	DDH-032	DDH-035	DDH-048	DDH-049	DDH-051	DDH-053	DDH-054	DDH-055	DDH-056	DDH-057	DDH-059
Swarm	Nasik-Pune	Nasik-Pune	Nasik-Pune	Nasik-Pune	Nasik-Pune	Nasik-Pune	Nasik-Pune	Nasik-Pune	Nasik-Pune	Nasik-Pune	Nasik-Pune	Nasik-Pune	Nasik-Pune	Nasik-Pune	Nasik-Pune	Nasik-Pune
Strike	120	140	25	25	107	110	87	50	35	95	20	15	110	10	100	65
Thickness (m)	2	1	15	25	8*	5*	3	15	18	3	2	7	1.5	5	1	3
DFA result	Mahab (Amb)	Mahab	Amb (Pol)	Pol (Amb)	Pol (Amb)	Pol (Amb)	Pol (Khand)	Pol (Khand)	Khand	Mahab (Neral)	Amb (Pol)		Mahab			Pol (Igat-Jaw)
Mahalanobis distance	21.86	12.44	5.53	3.29	4.84	8.55	11.08	9.87	11.97	16.56	4.56		23.68			10.10
Lab	WSU	WSU	WSU	WSU	WSU	WSU	WSU	WSU	WSU	WSU	WSU	WSU	WSU	WSU	WSU	WSU
SiO_2	49.65	49.47	50.19	50.66	50.19	50.14	52.02	51.12	51.33	49.96	49.46	49.98	49.54	50.04	49.72	51.29
TiO_2	3.32	3.42	2.48	2.17	2.34	2.38	2.35	2.91	3.61	3.19	2.34	2.60	3.36	2.64	3.40	2.88
Al_2O_3	12.87	12.96	14.25	13.59	13.83	13.71	13.37	12.75	12.54	12.98	13.78	14.83	12.86	14.60	12.69	13.10
FeO (t)	15.43	15.76	13.25	13.69	12.79	12.84	13.90	14.81	15.19	15.24	14.14	12.62	15.71	12.69	15.67	14.21
MnO	0.23	0.23	0.20	0.22	0.20	0.20	0.21	0.22	0.21	0.23	0.22	0.19	0.24	0.17	0.24	0.23
MgO	5.46	5.27	5.90	5.78	6.54	6.58	5.25	5.27	4.36	5.22	6.45	6.17	5.16	6.19	5.23	5.24
CaO	9.85	9.81	10.81	11.01	11.15	11.10	9.42	9.52	8.60	9.57	10.85	10.30	9.67	10.14	9.66	9.52
Na_2O	2.51	2.36	2.32	2.35	2.45	2.54	2.69	2.46	2.64	2.63	2.37	2.64	2.74	2.61	2.66	2.52
K_2O	0.35	0.38	0.39	0.33	0.31	0.31	0.56	0.66	1.11	0.64	0.18	0.43	0.37	0.65	0.37	0.75
P_2O_5	0.33	0.34	0.22	0.19	0.21	0.21	0.24	0.29	0.40	0.34	0.20	0.25	0.35	0.26	0.35	0.28
Total																
LOI																
Sc	37	39	36	38	38	36	36	38	31	38	37	33	38	34	34	38
V	412	430	401	400	386	384	381	440	414	399	400	311	424	317	422	450
Cr	154	160	148	78	139	133	97	111	96	109	181	237	170	245	146	92
Co	44	45	40	42	42	39	41	40	40	42	42	38	45	38	46	40
Ni	65	70	85	70	86	83	60	71	61	55	101	99	77	102	61	49
Cu	324	331	263	222	239	231	231	298	324	331	251	223	355	241	340	265
Zn	132	141	119	109	108	112	118	123	136	139	116	108	143	112	139	122
Ga	24	28	24	23	23	23	20	25	25	21	20	22	25	22	24	23
Rb	6	9	10	5	7	7	33	19	37	14	8	13	16	14	19	27
Sr	247	246	210	197	207	205	235	196	210	245	200	328	237	329	236	198
Y	39	38	32	32	31	30	34	41	48	39	29	26	39	27	40	38
Zr	194	202	142	135	136	136	171	191	263	198	130	164	202	168	205	186
Nb	22	23	14	11	12	13	14	16	23	23	12	23	24	25	25	15
Cs																
Ba	94	130	53	75	40	31	148	127	177	145	10	147	105	139	133	97
Li	9	9	9	9	7	7	8	10	13	10	7	9	9	9	8	9
La					11	11										
Ce					25	26										
Pr					3.5	3.6										
Nd					17	17										
Sm					5.5	5.6										
Eu					1.9	1.9										
Gd					6.2	6.4										
Tb					1.1	1.1										
Dy					6.7	6.7										
Ho					1.3	1.3										
Er					3.4	3.3										
Tm					0.46	0.46										
Yb					2.7	2.6										
Lu					0.40	0.40										
Hf					3.8	3.9										
Ta					0.77	0.78										
Pb					1.2	1.4										
Th					1.1	1.2										
U					0.26	0.28										

Appendix A (continued): Major element (wt%) and trace element (ppm) compositions of Deccan dikes.

Sample	DDH-060	DDH-061	DDH-062	DDH-063	DDH-064	DDH-065	DDH-066	DDH-067	DDH-070	DDH-071	DDH-072	DDH-073	DDH-074	DDH-075	DDH-076	DDH-077
Swarm	Nasik-Pune	Nasik-Pune	Nasik-Pune	Nasik-Pune	Nasik-Pune	Nasik-Pune	Nasik-Pune	Nasik-Pune	Nasik-Pune	Nasik-Pune	Nasik-Pune	Nasik-Pune	Nasik-Pune	Nasik-Pune	Nasik-Pune	Nasik-Pune
Strike	45	130	27	50	50	135	20	25	65	50	5	38	120	48	40	50
Thickness (m)	6	6	3	6	5*	2	11	7	wide	3	5	6	7	5	6	15
DFA result	Pol (Mahab)	Pol (Amb)	Igat-Jaw (Pol)	Pol (Amb)	Thak	Pol (Thak)	Pol (Thak)			Mahab (Amb)	Pol (Amb)	Pol (Khand)	Pol (Amb)	Pol (Mahab)	Pol (Khand)	Pol (Amb)
Mahalanobis distance	10.71	1.85	12.95	8.20	23.82	10.75	5.89			9.09	6.53	9.74	7.99	11.98	8.17	7.30
Lab	WSU	WSU	WSU	WSU	WSU	WSU	WSU	WSU	WSU	WSU	WSU	WSU	WSU	WSU	WSU	WSU
SiO_2	51.25	50.43	51.77	50.08	50.18	50.18	51.19	49.28	46.35	50.04	49.83	51.22	50.02	50.86	51.00	50.03
TiO_2	2.85	2.08	2.26	2.33	2.30	2.36	2.07	3.16	0.83	3.16	2.41	2.71	2.30	2.84	2.85	2.66
Al_2O_3	13.06	13.98	13.51	13.98	14.04	14.03	14.16	13.55	6.80	13.20	13.78	13.10	13.78	13.12	12.94	13.33
FeO (t)	14.47	13.87	13.95	12.86	12.59	12.77	11.44	14.86	13.79	14.19	14.18	14.41	12.94	14.80	14.48	14.60
MnO	0.21	0.23	0.21	0.20	0.20	0.21	0.19	0.21	0.20	0.22	0.22	0.22	0.20	0.21	0.22	0.23
MgO	5.19	5.85	5.47	6.43	6.48	6.23	6.94	5.75	24.72	5.59	6.11	5.36	6.59	5.12	5.27	5.99
CaO	9.50	10.71	9.23	11.41	11.42	11.44	11.18	9.75	6.38	10.20	10.53	9.93	11.47	9.78	9.93	10.33
Na_2O	2.46	2.48	2.64	2.37	2.40	2.41	2.40	2.63	0.73	2.53	2.54	2.50	2.37	2.48	2.64	2.42
K_2O	0.73	0.20	0.76	0.14	0.18	0.16	0.25	0.49	0.11	0.54	0.19	0.31	0.13	0.52	0.40	0.19
P_2O_5	0.28	0.18	0.22	0.20	0.20	0.21	0.19	0.32	0.09	0.32	0.22	0.25	0.20	0.27	0.28	0.24
Total																
LOI																
Sc	37	38	37	39	40	37	36	33	22	40	37	37	37	38	34	35
V	431	390	367	386	363	381	377	360	156	436	426	443	378	421	417	413
Cr	114	89	106	126	140	130	297	201	1556	111	110	79	139	152	108	169
Co	39	41	37	36	40	40	37	43	61	44	46	40	41	39	41	41
Ni	69	82	63	81	85	82	114	101	749	58	82	60	80	88	69	94
Cu	291	186	160	209	214	212	217	309	55	296	276	265	224	280	282	266
Zn	125	106	112	107	105	109	93	126	92	141	112	128	107	118	122	123
Ga	24	22	21	21	21	20	22	22	9	22	20	25	23	19	25	23
Rb	23	4	21	6	8	6	9	13	5	13	6	15	5	24	18	7
Sr	200	220	230	212	210	216	212	317	110	231	220	247	215	203	206	232
Y	38	31	32	30	28	30	28	34	11	37	31	33	29	36	38	34
Zr	184	127	157	132	132	137	129	196	61	181	141	164	133	182	185	160
Nb	17	10	13	13	18	14	12	29	7	19	13	12	13	17	16	14
Cs																
Ba	111	56	142	22	24	0	58	130	1	67	27	98	36	97	94	41
Li	10	7	9	7	7		7	10	8	8	8	8	7	8	8	9
La																
Ce																
Pr																
Nd																
Sm																
Eu																
Gd																
Tb																
Dy																
Ho																
Er																
Tm																
Yb																
Lu																
Hf																
Ta																
Pb																
Th																
U																

Appendix A (continued): Major element (wt%) and trace element (ppm) compositions of Deccan dikes.

Sample	DDH-078	DDH-079	DDH-080	DDH-081	DDH-083	DDH-084	DDH-085	DDH-086	DDH-087	DDH-088	DDH-089	DDH-090	DDH-091	DDH-092	DDH-093	DDH-094
Swarm	Nasik-Pune	Nasik-Pune	Nasik-Pune	Nasik-Pune	Nasik-Pune	Nasik-Pune	Nasik-Pune	Nasik-Pune	Nasik-Pune	Nasik-Pune	Nasik-Pune	Nasik-Pune	Nasik-Pune	Nasik-Pune	Nasik-Pune	Nasik-Pune
Strike	120	45	90	65	50	60	50	90	33	25	125	130	15	12	170	125
Thickness (m)	1.25	8	2	2.5	5	4	2	2	6.5	0.5	2	1	1.5	2.5	4	6*
DFA result	Amb (Thak)	Amb (Pol)	Pol (Amb)	Pol (Amb)	Pol (Bushe)	Khand (Pol)	Bhima (Amb)		Thak (Pol)	Thak (Pol)	Thak (Pol)	Thak (Pol)	Thak (Pol)	Pol (Thak)	Thak	Amb (Thak)
Mahalanobis distance	12.74	9.70	3.96	7.24	9.96	7.95	6.08		4.87	7.96	3.86	5.78	5.55	6.05	22.56	7.86
Lab	WSU	WSU	WSU	WSU	WSU	WSU	WSU	WSU	WSU	WSU	WSU	WSU	WSU	WSU	WSU	WSU
SiO_2	50.27	50.75	51.16	50.86	52.72	52.42	49.63	50.87	50.59	50.09	50.56	50.38	51.06	51.64	48.93	49.29
TiO_2	2.53	2.60	2.66	2.58	1.96	2.28	2.68	2.74	1.89	2.15	1.95	1.94	2.13	2.17	0.85	2.81
Al_2O_3	13.72	13.53	13.12	13.48	14.21	13.77	14.26	13.95	13.27	14.71	13.51	13.39	14.64	14.25	14.88	13.42
FeO (t)	12.87	14.15	14.27	14.13	12.34	13.10	13.60	13.07	10.71	11.75	11.06	11.28	11.88	11.94	10.42	14.25
MnO	0.20	0.22	0.22	0.22	0.21	0.20	0.20	0.20	0.16	0.19	0.18	0.18	0.19	0.18	0.18	0.22
MgO	6.62	5.63	5.48	5.48	5.33	5.12	5.73	5.53	9.38	6.87	8.55	8.68	6.02	6.02	8.82	6.17
CaO	10.89	10.06	10.00	10.14	10.02	9.70	10.52	10.14	11.49	11.84	11.87	11.77	11.21	10.80	13.81	10.55
Na_2O	2.36	2.51	2.57	2.56	2.71	2.70	2.52	2.85	1.97	2.08	2.01	2.08	2.42	2.49	1.80	2.48
K_2O	0.32	0.33	0.28	0.33	0.33	0.49	0.60	0.36	0.39	0.13	0.14	0.15	0.25	0.31	0.23	0.57
P_2O_5	0.22	0.23	0.24	0.22	0.19	0.23	0.26	0.29	0.16	0.19	0.16	0.16	0.19	0.20	0.08	0.25
Total																
LOI																
Sc	38	35	35	35	36	34	36	34	39	37	41	37	34	35	51	39
V	404	416	430	427	355	348	405	359	336	356	332	330	330	328	307	419
Cr	253	102	90	100	75	98	174	127	535	240	515	518	221	220	373	136
Co	38	40	38	40	36	39	39	38	38	36	38	38	37	37	34	44
Ni	103	71	65	67	50	63	87	59	220	97	180	179	92	88	148	87
Cu	231	227	250	234	175	187	252	206	172	182	179	186	167	174	133	274
Zn	110	115	121	116	104	113	117	126	81	94	83	90	94	96	67	121
Ga	22	25	24	22	22	24	26	27	20	25	21	18	22	23	17	26
Rb	6	11	14	7	19	26	12	10	10	3	5	4	11	16	5	15
Sr	212	245	242	246	250	242	256	294	215	272	245	245	268	264	121	230
Y	30	31	34	32	28	34	33	32	24	26	22	24	26	27	20	32
Zr	142	154	161	153	138	166	162	171	109	133	109	112	133	139	56	155
Nb	14	11	12	12	10	12	12	22	9	12	11	12	13	13	7	17
Cs																
Ba	24	72	54	78	99	202	108	144	70	27	38	18	61	85	62	53
Li	7	7	7	7	8	8	8	9	7	8	10	10	7	7	6	8
La																
Ce																
Pr																
Nd																
Sm																
Eu																
Gd																
Tb																
Dy																
Ho																
Er																
Tm																
Yb																
Lu																
Hf																
Ta																
Pb																
Th																
U																

Appendix A (continued): Major element (wt%) and trace element (ppm) compositions of Deccan dikes.

Sample	DDH-096	DDH-097	DDH-098	DDH-099	DDH-101	DDH-104	DDH-105	DDH-106	DDH-107	DDH-108	DDH-109	DDH-110	DDH-111	DDH-113	DDH-114	DDH-115
Swarm	Nasik-Pune	Nasik-Pune	Nasik-Pune	Nasik-Pune	Nasik-Pune	Nasik-Pune	Nasik-Pune	Nasik-Pune	Nasik-Pune	Nasik-Pune	Nasik-Pune	Nasik-Pune	Nasik-Pune	Nasik-Pune	Nasik-Pune	Nasik-Pune
Strike	85	85	40	30	25	130	20	20	30	5	0	20	155	25	25	30
Thickness (m)	2.5	5.5	2	30*	2.5	1.5	12	18	13	1.5	20*	4	2	4	4*	6
DFA result	Thak (Pol)	Khand (Thak)	Pol (Khand)	Pol (Amb)	Thak	Pol (Bhima)	Neral (Igat-Jaw)	Khand (Neral)	Bushe	Pol (Khand)	Khand	Pol (Khand)		Pol (Mahab)	Pol (Thak)	Thak (Khand)
Mahalanobis distance	3.30	5.76	7.25	3.59	19.28	5.28	9.98	12.65	3.99	10.75	14.55	9.52		6.81	5.28	9.62
Lab	WSU	WSU	WSU	WSU	WSU	WSU	WSU	WSU	WSU	WSU	WSU	WSU	WSU	WSU	WSU	WSU
SiO_2	50.82	49.46	51.26	50.44	51.05	50.24	50.51	51.17	54.43	51.28	51.52	50.85	49.33	51.45	52.05	50.67
TiO_2	1.52	1.04	2.88	2.14	2.55	1.81	3.27	3.26	1.06	2.92	3.73	2.74	3.12	1.79	1.75	1.35
Al_2O_3	13.33	14.98	12.85	13.44	14.65	14.05	12.73	12.53	15.09	12.91	12.52	13.40	13.36	14.45	14.26	12.11
FeO (t)	11.24	11.15	14.78	14.31	13.31	12.93	15.30	15.22	9.61	14.69	14.69	13.94	14.84	11.66	11.29	11.24
MnO	0.18	0.18	0.22	0.23	0.19	0.20	0.24	0.24	0.16	0.22	0.21	0.22	0.22	0.18	0.18	0.20
MgO	9.34	9.72	4.93	5.99	4.86	6.79	4.77	4.63	5.97	4.90	4.51	5.65	5.60	6.45	6.56	12.46
CaO	10.85	10.94	9.83	10.57	9.13	11.38	9.57	9.28	10.10	9.50	8.72	10.04	9.97	10.76	10.62	9.27
Na_2O	2.25	2.04	2.63	2.49	3.03	2.27	2.42	2.51	2.59	2.56	2.53	2.33	2.49	2.43	2.46	2.03
K_2O	0.32	0.38	0.34	0.20	0.93	0.18	0.87	0.85	0.88	0.75	1.15	0.57	0.76	0.64	0.66	0.52
P_2O_5	0.16	0.12	0.29	0.19	0.30	0.16	0.32	0.33	0.11	0.29	0.41	0.26	0.32	0.18	0.18	0.16
Total																
LOI																
Sc	35	36	37	35	31	38	37	37	36	37	34	38	35	35	38	31
V	285	262	417	398	335	347	427	438	270	420	447	426	352	325	318	259
Cr	536	504	70	73	73	137	66	71	180	58	69	168	90	246	231	1103
Co	38	41	41	42	42	42	41	40	34	39	43	39	43	36	38	46
Ni	196	221	46	60	72	79	34	35	70	35	42	93	57	84	82	328
Cu	110	100	260	226	139	185	281	289	121	267	338	264	300	161	164	86
Zn	85	87	127	106	121	91	140	136	77	128	140	120	125	92	91	92
Ga	23	20	21	21	22	20	28	20	20	26	26	24	25	20	22	20
Rb	10	8	13	9	25	6	28	27	32	24	34	10	12	15	20	10
Sr	218	175	212	211	364	224	200	201	165	203	211	206	313	232	228	212
Y	22	21	39	30	29	25	41	42	24	40	49	36	33	26	27	23
Zr	111	82	191	130	185	113	210	217	99	196	261	177	192	129	126	106
Nb	9	6	16	10	22	9	18	19	7	17	23	15	30	10	10	9
Cs																
Ba	103	128	102	51	253	49	107	130	127	136	166	92	157	112	148	128
Li	11	7	8	7	10	6	11	10	9	10	13	8	9	9	8	13
La																
Ce																
Pr																
Nd																
Sm																
Eu																
Gd																
Tb																
Dy																
Ho																
Er																
Tm																
Yb																
Lu																
Hf																
Ta																
Pb																
Th																
U																

Appendix A (continued): Major element (wt%) and trace element (ppm) compositions of Deccan dikes.

Sample	DDH-118	DDH-122	DDH-123	DDH-124	DDH-125	DDH-126	DDH-127	DDH-128
Swarm	Nasik-Pune	Nasik-Pune	Nasik-Pune	Nasik-Pune	Nasik-Pune	Nasik-Pune	Nasik-Pune	Nasik-Pune
Strike	35	50	95	5	85	85	45	160
Thickness (m)	5	50*	30	25	10	Wide	12	10
DFA result	Amb (Bhima)	Neral (Khand)	Pol (Amb)	Pol (Khand)	Pol (Amb)	Bhima (Pol)	Neral (Khand)	Thak (Pol)
Mahalanobis distance	3.28	11.98	8.07	11.99	6.24	2.14	7.93	4.50
Lab	WSU	WSU	WSU	WSU	WSU	WSU	WSU	WSU
SiO_2	49.56	51.06	50.15	51.03	49.95	50.38	49.99	50.38
TiO_2	2.47	3.27	2.34	3.22	2.13	2.39	3.21	1.89
Al_2O_3	13.75	12.47	13.80	12.93	14.90	14.26	13.39	13.38
FeO (t)	13.91	15.21	12.97	15.29	12.38	13.02	14.83	11.09
MnO	0.22	0.24	0.20	0.20	0.19	0.20	0.20	0.18
MgO	6.55	4.88	6.56	4.91	6.04	6.16	4.97	9.42
CaO	10.72	9.45	11.05	8.82	11.56	10.76	9.61	11.31
Na_2O	2.35	2.28	2.41	2.43	2.32	2.34	2.65	2.01
K_2O	0.26	0.82	0.32	0.84	0.33	0.26	0.80	0.19
P_2O_5	0.21	0.33	0.21	0.32	0.20	0.23	0.35	0.16
Total								
LOI								
Sc	38	35	39	34	40	36	37	38
V	412	427	361	420	363	378	367	329
Cr	93	79	129	76	217	249	130	572
Co	41	43	42	42	37	40	42	40
Ni	77	35	80	41	73	93	50	242
Cu	256	285	233	279	212	217	245	162
Zn	119	136	110	134	107	108	135	77
Ga	24	27	22	22	22	26	27	21
Rb	6	22	6	18	6	15	28	7
Sr	200	227	205	195	216	262	287	236
Y	30	44	31	43	29	29	38	24
Zr	134	215	137	211	127	148	211	111
Nb	12	18	14	19	13	12	22	10
Cs								
Ba	25	169	33	110	46	66	211	36
Li	9	10	8	9	10	9	13	9
La								
Ce								
Pr								
Nd								
Sm								
Eu								
Gd								
Tb								
Dy								
Ho								
Er								
Tm								
Yb								
Lu								
Hf								
Ta								
Pb								
Th								
U								

Appendix A (continued): Major element (wt%) and trace element (ppm) compositions of Deccan dikes.

Sample	DDH-129	DDH-130	DDH154	DDH154SP	DDH-158	DDH-161	DDW-038	DDW-040	DH-27	DH-39	DN-27	DN-29	DN-33	DN-44	IGA-006	IGA-013	IGA-019
Swarm	Nasik-Pune	Nasik-Pune	Nasik-Pune	Nasik-Pune	Nasik-Pune	Nasik-Pune	Nasik-Pune	Nasik-Pune	Nasik-Pune	Nasik-Pune	Nasik-Pune	Nasik-Pune	Nasik-Pune	Nasik-Pune	Nasik-Pune	Nasik-Pune	Nasik-Pune
Strike	180	25	115	115	100	70	140	90	30	115	25	150	25	110	0	20	10
Thickness (m)	1.5	15	85 (sill?)	85 (sill?)	2.5	0.5	5									2	6
DFA result	Pol (Khand)	Pol (Neral)	Thak (Pol)				Mahab	Amb (Bhima)	Thak (Bushe)	Thak (Mahab)	Pol (Thak)	Khand (Thak)	Thak (Bhima)	Bushe	Igat-Jaw (Khand)	Bhima (Amb)	Thak (Pol)
Mahalanobis distance	6.81	19.64	16.96				8.20	2.28	8.75	9.39	5.50	7.11	9.12	6.57	5.61	2.58	3.46
Lab	WSU	WSU	WSU	WSU	WSU	WSU	WSU	WSU	WSU	WSU	WSU	WSU	WSU	WSU	WSU	WSU	WSU
SiO_2	51.14	50.86	51.94	51.25	57.02	53.13	49.69	49.71	51.25	50.66	50.94	51.54	49.88	51.77	50.67	50.51	52.89
TiO_2	2.86	2.90	2.93	3.73	1.733	2.100	3.58	2.31	1.90	1.91	1.86	3.44	2.00	0.99	2.96	2.36	1.43
Al_2O_3	12.90	12.78	13.11	11.08	16.22	14.33	12.78	14.15	13.75	16.11	14.32	12.53	15.92	15.84	13.70	14.44	14.07
FeO (t)	14.72	15.19	14.20	17.83	9.11	12.55	15.14	13.74	11.41	11.59	11.68	14.91	11.37	10.14	14.99	12.91	10.57
MnO	0.23	0.22	0.21	0.28	0.153	0.194	0.22	0.21	0.17	0.16	0.19	0.22	0.18	0.18	0.24	0.20	0.17
MgO	5.06	5.12	4.43	3.19	2.69	4.15	5.36	6.47	7.13	5.04	7.02	4.58	6.05	6.78	4.55	6.30	7.43
CaO	9.54	9.46	8.12	8.23	6.04	6.69	9.94	10.64	12.29	10.93	10.86	8.40	11.90	11.57	9.14	10.51	10.45
Na_2O	2.50	2.46	3.75	2.78	4.13	4.40	2.40	2.37	1.44	2.62	2.44	2.70	2.34	2.22	2.62	2.31	2.17
K_2O	0.76	0.73	0.96	0.97	2.43	2.11	0.53	0.18	0.50	0.79	0.52	1.26	0.21	0.42	0.87	0.24	0.65
P_2O_5	0.29	0.29	0.36	0.67	0.47	0.34	0.36	0.21	0.16	0.19	0.18	0.42	0.15	0.10	0.28	0.23	0.16
Total																	
LOI																	
Sc	37	35	34	34	22	28	35	34	38	35	41	34	37	42	32	33	34
V	427	421	277	166	145	340	432	396	350	341	332	404	380	257	431	352	273
Cr	61	65	47	10	23	30	136	136	266	200	289	97	249	268	70	233	343
Co	39	42					45	43	38						39	40	43
Ni	37	45	30	0	16	16	69	91	66	68	99	64	104	80	42	86	84
Cu	260	276	259	586	225	233	301	256	95	95	190	305	196	132	263	223	94
Zn	128	130	134	194	102	116	143	118	98	96	94	136	96	74	172	109	89
Ga	23	25	22	27	24	21	24	24	24	24	21	27	22	20	21	25	22
Rb	21	20	26	35	61	42	9	7	33	23	15	45	4	13	15	10	11
Sr	206	193	289	216	370	372	243	215	149	256	282	207	230	132	265	255	281
Y	40	40	41	68	34	29	38	29	27	28	28	46	23	24	36	30	20
Zr	192	196	226	357	215	179	206	131	115	140	125	249	100	80	193	145	109
Nb	16	19	22	37	34	29	24	11	7	11	9	22	8	6	16	12	9
Cs																	
Ba	116	148	170	222	621	506	108	28	51	151	81	193	0	78	201	83	187
Li	8	12					9	8	10						15	16	18
La									16						24	15	16
Ce									31						49	32	32
Pr															6.4	4.3	3.8
Nd									26						29	20	16
Sm									6.6						8.2	6.0	4.2
Eu									1.9						2.6	2.1	1.4
Gd															8.7	6.5	4.4
Tb															1.4	1.1	0.71
Dy									5.5						8.4	6.6	4.2
Ho															1.6	1.3	0.82
Er															4.0	3.2	2.1
Tm															0.55	0.42	0.29
Yb									2.6						3.2	2.5	1.7
Lu															0.48	0.49	0.37
Hf															5.8	5.8	4.1
Ta															1.1	1.0	0.72
Pb															3.1	3.3	1.9
Th															3.4	3.5	2.0
U															0.75	0.79	0.47

Appendix A (continued): Major element (wt%) and trace element (ppm) compositions of Deccan dikes.

Sample	JEB-008	JEB-016	JEB-153D	JEB-176D	JEB-182D	JEB-201	JEB-207D	JEB-233D	JEB-245D	JEB-257D	JEB-273D	JEB-278D	JEB-284D	JEB-320D	JEB-321D
Swarm	Nasik-Pune	Nasik-Pune	Nasik-Pune	Nasik-Pune	Nasik-Pune	Nasik-Pune	Nasik-Pune	Nasik-Pune	Nasik-Pune	Nasik-Pune	Nasik-Pune	Nasik-Pune	Nasik-Pune	Nasik-Pune	Nasik-Pune
Strike	160	160	45	175	120		50		30	35	175	170	155	10	30
Thickness (m)															15
DFA result	Bhima (Thak)	Khand	Pol (Thak)	Amb (Bhima)	Mahab	Amb	Pol (Igat-Jaw)	Khand (Thak)	Pol (Igat-Jaw)	Pol (Bhima)	Thak (Pol)	Khand (Pol)	Khand (Igat-Jaw)	Thak (Pol)	Igat-Jaw (Pol)
Mahalanobis distance	11.06	4.32	7.88	3.15	17.23	23.65	5.48	6.56	4.68	8.08	11.36	10.74	1.59	16.14	7.18
Lab	WSU	WSU	WSU	WSU	WSU	WSU	WSU	WSU	WSU	WSU	WSU	WSU	WSU	WSU	WSU
SiO_2	49.90	51.44	50.28	49.96	50.00	49.02	51.49	49.45	51.28	50.08	51.24	49.58	51.85	51.10	51.21
TiO_2	2.13	2.61	2.31	2.36	3.39	3.64	2.82	1.06	2.54	3.00	2.58	2.93	2.61	2.73	2.61
Al_2O_3	16.41	14.15	13.67	13.87	12.93	13.29	13.04	15.43	13.27	13.18	13.42	13.81	13.70	13.04	13.25
FeO (t)	11.84	14.03	12.93	14.20	15.23	15.02	14.36	11.47	14.45	15.10	12.37	15.25	13.48	14.67	14.00
MnO	0.19	0.20	0.20	0.21	0.24	0.23	0.20	0.19	0.21	0.23	0.18	0.24	0.19	0.20	0.22
MgO	5.40	4.78	6.42	5.95	5.15	5.59	5.18	8.87	5.11	4.94	6.83	5.12	4.98	5.29	5.30
CaO	11.09	9.41	11.40	10.36	9.82	10.06	9.44	11.10	9.49	9.64	10.13	9.84	9.33	9.69	9.59
Na_2O	2.43	2.64	2.42	2.55	2.61	2.47	2.46	2.10	2.78	2.83	2.39	2.62	2.74	2.47	2.80
K_2O	0.40	0.49	0.17	0.32	0.30	0.34	0.74	0.22	0.61	0.68	0.60	0.35	0.85	0.57	0.76
P_2O_5	0.20	0.27	0.21	0.21	0.34	0.35	0.28	0.13	0.26	0.32	0.26	0.27	0.27	0.25	0.26
Total															
LOI															
Sc	35	34	36	32	35	40	35	32	31	34	31	34	34	37	36
V	329	347	366	402	416	453	414	257	392	412	400	434	395	428	412
Cr	102	46	156	95	138	147	75	484	83	84	382	141	59	173	95
Co	36	41	48	47	53	55	45	46	47	44	43	49		72	48
Ni	62	40	93	66	55	86	44	206	49	52	193	90	44	202	55
Cu	199	226	274	244	347	370	141	130	229	298	269	286	167	216	393
Zn	101	131	142	114	146	151	133	102	122	142	114	128	130	118	194
Ga	25	27	21	26	26	24	21	18	20	24	24	25	25	25	21
Rb	10	24	6	9	7	11	26	8	20	15	15	16	22	15	20
Sr	243	274	210	215	252	214	197	184	267	204	246	219	269	241	252
Y	26	36	29	31	40	43	38	22	35	42	34	38	36	35	34
Zr	128	184	133	132	199	207	186	84	175	200	164	180	179	164	172
Nb	13	15	13	10	24	21	15	4	14	19	15	14	14	13	14
Cs															
Ba	64	256	14	44	125	122	112	130	141	122	103	71	259	100	136
Li	15	16	6	8	6	6	6	5	9	9	7	6		11	11
La	12	23		11	24		18	26	20		17	17	24	15	19
Ce	27	47		25	52		39	54	44		36	39	47	34	42
Pr	3.6	6.0		3.5	6.7		5.2	6.8	5.6		5.0	5.3	6.3	4.6	5.4
Nd	17	27		17	31		25	30	26		24	25	29	23	25
Sm	5.2	7.7		5.6	8.9		7.4	8.2	7.3		7.0	7.6	8.1	6.9	7.2
Eu	1.8	2.5		2.0	2.9		2.4	2.7	2.4		2.4	2.5	2.6	2.4	2.4
Gd	5.8	8.2		6.4	9.7		8.2	8.3	7.9		7.7	8.6	8.8	7.6	7.7
Tb	0.98	1.4		1.1	1.6		1.4	1.3	1.3		1.3	1.4	1.4	1.3	1.3
Dy	6.0	8.1		6.7	9.6		8.4	7.8	7.7		7.5	8.7	8.4	7.6	7.6
Ho	1.2	1.6		1.3	1.9		1.6	1.5	1.5		1.5	1.7	1.6	1.4	1.5
Er	3.0	4.0		3.4	4.9		4.2	3.8	3.8		3.7	4.3	4.1	3.7	3.7
Tm	0.41	0.54		0.46	0.66		0.58	0.51	0.52		0.49	0.58	0.56	0.49	0.50
Yb	2.4	3.2		2.7	3.9		3.4	3.0	3.0		2.9	3.4	3.2	2.9	2.9
Lu	0.26	0.47		0.40	0.59		0.51	0.45	0.45		0.42	0.51	0.49	0.42	0.44
Hf	3.0	5.3		3.8	6.2		5.3	5.7	5.1		4.6	5.3	5.4	4.5	4.8
Ta	0.53	0.83		0.67	1.5		0.93	1.9	0.93		0.90	0.93	0.84	0.74	0.85
Pb	4.7	4.0		1.4	2.9		2.6	2.9	3.3		2.1	2.2	4.0	2.3	3.2
Th	3.2	3.1		1.2	2.9		2.9	3.3	2.9		2.1	2.3	3.1	2.0	2.6
U	0.89	0.58		0.29	0.66		0.66	0.75	0.68		0.52	0.58	0.60	0.46	0.59

Appendix A (continued): Major element (wt%) and trace element (ppm) compositions of Deccan dikes.

Sample	JEB-322D	JEB-325	JEB-327D	JEB-332D	JEB-333D	JEB-336D	JEB-393D	JEB-396D	JEB-397D	JEB-426D	JEB-436D	JEB-438D	JEB-440D	JEB-442D	JEB-443D	JEB-453D
Swarm	Nasik-Pune	Nasik-Pune	Nasik-Pune	Nasik-Pune	Nasik-Pune	Nasik-Pune	Nasik-Pune	Nasik-Pune	Nasik-Pune	Nasik-Pune	Nasik-Pune	Nasik-Pune	Nasik-Pune	Nasik-Pune	Nasik-Pune	Nasik-Pune
Strike	163	180	100	160	75	100	60	130	50	95	175	40	125	45	30	80
Thickness (m)	4															
DFA result	Khand	Khand (Pol)	Khand	Pol (Amb)	Khand	Pol (Khand)	Pol (Neral)	Mahab			Amb (Pol)	Pol (Khand)	Pol (Khand)	Thak (Pol)	Pol (Khand)	Thak (Pol)
Mahalanobis distance	5.48	18.44	3.64	7.64	8.40	3.32	10.24	19.83			6.81	3.20	7.14	3.74	7.07	3.21
Lab	WSU	WSU	WSU	WSU	WSU	WSU	WSU	WSU	WSU	WSU	WSU	WSU	WSU	WSU	WSU	WSU
SiO_2	51.80	50.54	51.49	50.95	49.88	52.13	50.60	49.79	50.26	49.53	50.26	51.04	51.99	51.31	52.30	53.59
TiO_2	2.64	3.26	2.71	2.66	1.05	2.29	3.03	3.40	2.63	3.38	1.90	2.96	2.29	2.01	2.29	2.34
Al_2O_3	13.76	12.26	13.43	13.03	14.79	13.36	12.63	12.64	14.30	12.93	14.66	12.73	13.33	13.31	13.29	13.47
FeO (t)	13.30	15.84	14.32	14.62	11.54	13.90	15.24	15.72	12.78	15.16	11.97	14.78	14.07	11.13	13.72	12.32
MnO	0.21	0.24	0.21	0.23	0.18	0.21	0.23	0.24	0.20	0.23	0.19	0.23	0.21	0.17	0.21	0.18
MgO	4.99	4.74	4.59	5.32	8.96	5.25	4.96	5.06	6.04	5.45	6.75	4.87	5.19	8.26	5.30	5.22
CaO	9.66	9.65	9.53	10.03	11.13	9.53	9.75	9.67	10.31	9.61	11.44	9.73	9.58	11.05	9.34	8.88
Na_2O	2.92	2.48	2.91	2.63	2.13	2.69	2.77	2.76	2.77	2.78	2.33	2.61	2.72	2.10	2.66	2.74
K_2O	0.44	0.67	0.53	0.29	0.22	0.42	0.49	0.37	0.44	0.58	0.32	0.75	0.40	0.47	0.67	1.02
P_2O_5	0.28	0.33	0.29	0.24	0.13	0.23	0.31	0.35	0.26	0.35	0.17	0.31	0.24	0.18	0.22	0.26
Total																
LOI																
Sc	35	36	33	38	36	31	37	35	33	33	37	39	34	35	35	33
V	399	424	374	420	276	397	417	434	336	369	336	413	421	350	406	355
Cr	75	73	67	105	478	98	87	141	240	162	168	75	104	439	102	82
Co	47	48	48	50	48	47	50	53	50	53	50	54	50	44	48	45
Ni	52	39	47	70	197	55	52	61	97	71	87	43	56	180	54	58
Cu	344	460	382	299	136	221	280	374	243	314	187	320	233	187	215	141
Zn	186	224	200	153	107	122	142	169	124	133	104	149	123	95	113	104
Ga	24	26	24	23	19	22	23	26	26	25	23	25	22	21	23	24
Rb	18	22	27	18	6	21	24	16	16	17	10	17	18	12	21	28
Sr	269	229	275	243	184	238	207	241	333	308	214	209	239	239	235	293
Y	37	46	37	32	23	32	42	39	27	36	26	42	33	25	35	29
Zr	177	215	187	160	83	156	200	202	165	211	112	199	157	120	157	167
Nb	14	17	14	12	4	12	18	23	22	31	9	17	12	12	14	16
Cs																
Ba	238	165	263	68	143	150	109	124	142	151	49	98	120	58	133	185
Li	10	11	9	9	9	9	13	9	9	10	56?	17	13	12	90?	13
La	22	21	24	15	10		20	21	20	25	9.5	21	17	12	18	21
Ce	45	46	49	33	20		43	46	41	52	21	44	37	25	39	44
Pr	5.6	6.1	6.2	4.4	2.5		5.7	5.9	5.2	6.6	2.9	5.8	4.7	3.4	5.0	5.5
Nd	26	29	28	22	11		26	28	23	30	14	27	22	17	23	24
Sm	7.3	8.4	7.9	6.6	3.2		7.8	8.0	6.3	8.0	4.4	7.9	6.3	5.0	6.6	6.6
Eu	2.4	2.6	2.5	2.3	1.2		2.5	2.6	2.1	2.6	1.6	2.5	2.1	1.8	2.2	2.1
Gd	7.8	9.4	8.5	7.4	3.8		8.6	8.7	6.4	8.2	5.1	8.7	6.8	5.6	7.2	6.7
Tb	1.3	1.6	1.4	1.2	0.68		1.5	1.5	1.0	1.3	0.87	1.5	1.2	0.92	1.2	1.1
Dy	7.7	9.5	8.4	7.4	4.3		8.8	8.7	6.0	7.7	5.3	9.0	6.9	5.5	7.5	6.4
Ho	1.5	1.9	1.6	1.4	0.90		1.7	1.7	1.2	1.5	1.0	1.7	1.4	1.0	1.4	1.2
Er	3.8	4.8	4.1	3.7	2.4		4.5	4.4	2.9	3.7	2.7	4.5	3.5	2.7	3.7	3.1
Tm	0.52	0.66	0.57	0.49	0.35		0.62	0.60	0.40	0.51	0.37	0.62	0.48	0.35	0.52	0.42
Yb	3.0	3.9	3.3	2.9	2.1		3.7	3.6	2.3	3.0	2.2	3.7	2.8	2.1	3.1	2.5
Lu	0.45	0.58	0.49	0.43	0.33		0.55	0.54	0.35	0.45	0.33	0.55	0.42	0.31	0.46	0.38
Hf	5.0	6.0	5.3	4.4	2.2		5.8	5.6	4.5	5.7	3.0	5.7	4.4	3.4	4.6	4.7
Ta	0.76	1.0	0.83	0.68	0.24		1.1	1.4	1.4	1.8	0.64	1.1	0.76	0.65	0.81	0.98
Pb	3.7	3.2	3.9	2.2	2.3		2.9	2.6	2.3	2.7	1.2	2.8	3.5	1.5	3.6	4.1
Th	2.7	3.7	3.1	1.7	0.9		3.3	2.4	2.4	2.9	0.89	3.4	2.9	1.5	3.1	3.8
U	0.49	0.83	0.55	0.40	0.12		0.81	0.51	0.47	0.61	0.22	0.91	0.72	0.38	0.75	0.97

Appendix A (continued): Major element (wt%) and trace element (ppm) compositions of Deccan dikes.

Sample	JEB-455D	JH-12	JH-14	JH-20	JH-22	JH-25	JH-27	JH-28	JH-30	JW-12	JW-13	JW-14	R.6.3	R.6.7	RED-1	TRM-34
Swarm	Nasik-Pune	Nasik-Pune	Nasik-Pune	Nasik-Pune	Nasik-Pune	Nasik-Pune	Nasik-Pune	Nasik-Pune	Nasik-Pune	Nasik-Pune	Nasik-Pune	Nasik-Pune	Nasik-Pune	Nasik-Pune	Nasik-Pune	Nasik-Pune
Strike	20	170	0	0	145	10	0	0	100	10	15	10	45	100		10
Thickness (m)										1.5	15	2	4.5			2
DFA result	Pol (Amb)	Igat-Jaw (Khand)	Bhima (Thak)	Neral	Mahab (Khand)	Igat-Jaw (Thak)	Thak (Bhima)	Amb (Pol)	Pol (Amb)	Bhima (Khand)	Bhima (Thak)	Khand (Igat-Jaw)	Khand		Pol (Amb)	Thak (Mahab)
Mahalanobis distance	7.31	9.32	12.50	16.71	15.49	9.39	11.74	2.67	5.22	8.77	21.57	9.40	21.54		6.91	1.91
Lab	WSU	WSU	WSU	WSU	WSU	WSU	WSU	WSU	WSU	WSU	WSU	WSU	WSU	WSU	WSU	WSU
SiO_2	51.28	51.22	50.91	50.78	51.15	51.36	49.93	50.03	50.13	49.79	49.93	50.92	50.26	51.94	50.69	52.59
TiO_2	2.63	3.70	2.63	3.72	2.67	2.26	1.78	2.17	2.16	3.071	2.259	3.135	1.17	0.92	2.01	1.91
Al_2O_3	12.95	12.68	13.50	12.60	13.32	13.91	14.64	14.34	14.44	13.13	17.13	12.85	14.61	14.13	14.48	14.01
FeO (t)	14.56	14.58	14.34	14.79	14.29	12.84	12.89	13.24	12.18	15.31	12.02	15.22	12.26	12.50	13.19	11.19
MnO	0.22	0.22	0.21	0.22	0.22	0.20	0.20	0.21	0.20	0.226	0.175	0.230	0.21	0.23	0.21	0.17
MgO	5.32	4.62	5.22	4.58	5.16	5.87	6.78	6.33	6.70	5.26	3.96	4.90	6.79	7.03	5.68	6.39
CaO	9.92	8.69	9.53	8.42	9.88	9.62	10.55	10.84	11.46	10.01	10.73	9.18	11.99	9.65	10.48	10.35
Na_2O	2.61	2.47	2.33	2.12	2.32	2.68	2.15	2.35	2.28	2.53	2.81	2.39	2.28	2.86	2.59	2.42
K_2O	0.28	1.39	1.08	2.37	0.75	1.05	0.92	0.31	0.26	0.38	0.76	0.86	0.31	0.61	0.50	0.79
P_2O_5	0.24	0.42	0.24	0.40	0.25	0.21	0.16	0.19	0.19	0.30	0.22	0.32	0.12	0.14	0.18	0.20
Total																
LOI																
Sc	33	32	37	31	33	32	36	37	39	35	31	38	42	44	35	33
V	436	439	429	433	416	371	338	395	377	417	285	422	339	339	377	301
Cr	78	79	100	107	85	106	128	117	208	127	53	86	163	51	83	139
Co	53															
Ni	46	47	67	64	54	57	105	82	94	56	43	48	79	52	58	55
Cu	238	310	233	312	235	55	183	224	215	288	148	278	207	156	214	123
Zn	123	138	115	135	112	102	93	96	97	131	100	132	85	100	106	91
Ga	23	26	21	28	27	25	21	24	24	25	26	22	18	17	21	22
Rb	17	40	27	57	19	28	20	7	6	14	12	25	8	15	10	15
Sr	247	196	233	203	231	255	210	216	220	273	343	199	159	194	217	242
Y	35	47	35	47	34	30	26	28	28	37	27	42	26	23	30	24
Zr	160	247	161	242	169	162	111	124	124	187	155	209	80	85	125	129
Nb	11	21	13	21	14	14	9	11	10	15	17	17	6	10	10	12
Cs																
Ba	93	171	88	270	127	201	55	51	24	127	149	140	89	223	66	166
Li	9															
La	15															
Ce	35															
Pr	4.7															
Nd	22															
Sm	6.8															
Eu	2.3															
Gd	7.6															
Tb	1.3															
Dy	7.6															
Ho	1.4															
Er	3.7															
Tm	0.50															
Yb	2.9															
Lu	0.43															
Hf	4.6															
Ta	0.76															
Pb	2.3															
Th	2.0															
U	0.47															

Appendix A (continued): Major element (wt%) and trace element (ppm) compositions of Deccan dikes.

Sample	TRM-59	TRM-59	JH-63	JH-66	JH-66*	JH-71	KVS-307	R.11.9	R.11.6	R.11.7	DD-01	DD-02	DD-03	DD-05	DD-06
Swarm	Nasik-Pune	Nasik-Pune	Nasik-Pune	Nasik-Pune	Nasik-Pune	Nasik-Pune	Nasik-Pune	Nasik-Pune	Nasik-Pune	Nasik-Pune	Narmada-Tapi	Narmada-Tapi	Narmada-Tapi	Narmada-Tapi	Narmada-Tapi
Strike	135	135	25	90	90	35?	110	140	45	45	80	90	80	145	40
Thickness (m)	2	2						5	2	2	15	5	2	5	10
DFA result			Igat-Jaw (Bhima)	Thak (Mahab)	Igat-Jaw (Khand)	Khand (Pol)	Thak (Bhima)	Bushe	Mahab (Neral)	Pol (Khand)					Thak (Bhima)
Mahalanobis distance			6.10	9.80	10.22	7.00	4.59	18.79	16.99	12.85					11.41
Lab	WSU	WSU	WSU	WSU	WSU	WSU	WSU	WSU	WSU	WSU	UH	UH	UH	UH	UH
SiO_2	52.26	52.36	51.31	52.02	52.21	52.05	53.39	54.86	49.36	51.16	53.62	50.34	52.09	54.39	50.19
TiO_2	1.28	1.20	2.63	2.65	2.59	2.25	2.02	1.17	3.16	2.49	1.19	3.05	2.21	3.47	2.24
Al_2O_3	14.17	14.91	13.33	13.19	13.35	13.91	13.56	15.12	13.37	13.22	15.28	12.66	14.80	11.76	14.29
FeO (t)	12.92	12.13	14.20	13.38	13.13	13.13	11.46	9.94	14.71	14.33	9.70	15.09	11.06	15.26	11.50
MnO	0.22	0.21	0.21	0.20	0.19	0.19	0.18	0.16	0.23	0.22	0.15	0.22	0.16	0.21	0.19
MgO	5.88	5.68	5.35	5.00	5.03	5.40	5.96	5.55	5.62	5.48	6.24	5.23	5.51	3.13	7.03
CaO	9.96	10.18	9.32	9.56	9.33	10.09	9.98	9.90	10.35	10.12	9.93	9.94	9.61	6.84	11.78
Na_2O	2.31	2.45	2.49	2.63	2.77	2.30	2.22	2.46	2.11	2.27	2.26	2.39	2.79	2.96	2.13
K_2O	0.85	0.77	0.90	1.12	1.15	0.48	1.03	0.73	0.76	0.50	1.39	0.69	1.34	1.46	0.42
P_2O_5	0.15	0.13	0.26	0.27	0.25	0.21	0.21	0.12	0.34	0.22	0.24	0.39	0.44	0.53	0.23
Total											100.40	100.77	100.44	100.65	100.48
LOI															
Sc	40	40	33	35	31	34	31	32	40	36	33	35	26	29	28
V	357	337	411	363	383	360	319	255	451	392					
Cr	77	72	87	85	81	91	117	220	88	126	55	98	136	75	295
Co											40	41	38	29	38
Ni	43	40	54	38	31	65	48	97	57	61	46	67	36	18	111
Cu	175	161	233	168	153	176	124	121	296	201	67	236	41	209	94
Zn	102	90	122	111	108	107	97	81	143	113	75	130	98	134	103
Ga	20	17	24	26	26	27	16	21	24	25					
Rb	20	22	25	28	30	20	34	26	20	11	54	24	38	36	4.9
Sr	134	118	246	230	234	257	361	259	218	233	233	289	356	431	307
Y	31	30	34	35	34	32	26	25	40	30	30	45	30	49	29
Zr	101	95	174	173	172	157	140	116	195	154	143	222	174	252	137
Nb	8	10	16	18	13	12	10	9	19	12	12	16	17	26	11
Cs											0.32	1.07	0.18	0.15	0.02
Ba	140	109	129	195	213	194	184	133	123	83	248	141	273	379	161
Li															
La											25	24	26	32	19
Ce											47	51	55	71	41
Pr											5.2	6.3	7.1	9.5	5.3
Nd											21	29	29	40	22
Sm											5.0	8.3	6.3	9.9	5.2
Eu											1.3	2.2	1.8	2.6	1.6
Gd											4.8	7.6	6.5	9.6	5.2
Tb											0.81	1.4	0.94	1.6	0.87
Dy											4.6	8.1	5.0	9.0	4.9
Ho											0.93	1.6	0.98	1.8	0.94
Er											2.5	4.2	2.5	4.7	2.4
Tm											0.37	0.61	0.34	0.69	0.33
Yb											2.6	3.9	2.2	4.2	2.1
Lu											0.39	0.57	0.33	0.64	0.32
Hf											3.6	6.1	4.4	7.2	3.6
Ta											0.78	0.97	0.98	1.6	0.65
Pb											5.2	3.3	4.4	4.7	3.5
Th											8.3	4.2	4.1	6.3	2.8
U											1.8	1.0	0.88	1.5	0.70

Appendix A (continued): Major element (wt%) and trace element (ppm) compositions of Deccan dikes.

Sample	DD-07	DD-08	DD-09	DD-10	DD-11	DD-12	DD-13	DD-14	DD-15	DD-16	DD-17	DD-18	DD-19
Swarm	Narmada-Tapi	Narmada-Tapi	Narmada-Tapi	Narmada-Tapi	Narmada-Tapi	Narmada-Tapi	Narmada-Tapi	Narmada-Tapi	Narmada-Tapi	Narmada-Tapi	Narmada-Tapi	Narmada-Tapi	Narmada-Tapi
Strike	135	65	65	150	55	75	70	75	70	70	75	55	
Thickness (m)	10	5	30	5	10	6	5	5	2	5	5	5	10
DFA result				Bhima (Thak)		Khand (Bhima)	Thak (Khand)		Bushe	Bushe		Neral (Khand)	
Mahalanobis distance				10.49		8.53	15.13		10.72	11.84		17.54	
Lab	UH	UH	UH	UH	UH	UH	UH	UH	UH	UH	UH	UH	UH
SiO_2	51.65	49.88	50.83	51.15	49.15	51.12	50.29	52.68	51.96	52.28	52.57	51.31	51.63
TiO_2	1.95	2.43	2.54	2.31	3.13	3.12	2.02	1.65	1.45	1.47	1.53	3.07	1.46
Al_2O_3	14.52	16.42	14.59	13.70	13.96	12.69	13.87	14.02	14.87	14.55	13.74	12.37	14.53
FeO (t)	11.43	12.21	13.38	12.40	14.41	15.44	12.77	12.90	11.95	12.04	14.32	15.74	13.24
MnO	0.18	0.16	0.19	0.18	0.21	0.21	0.20	0.19	0.19	0.19	0.21	0.22	0.20
MgO	6.62	4.78	5.16	6.52	5.24	4.90	6.77	5.28	5.99	5.90	4.95	4.56	5.77
CaO	9.98	9.95	8.99	10.52	9.06	9.19	11.16	9.70	10.72	10.58	8.84	8.71	10.02
Na_2O	2.55	2.59	3.14	2.50	2.97	2.49	2.33	2.49	2.11	2.10	2.39	2.59	2.60
K_2O	0.89	1.35	0.89	0.46	1.53	0.51	0.35	0.78	0.62	0.72	1.21	1.03	0.32
P_2O_5	0.23	0.23	0.30	0.25	0.35	0.33	0.23	0.31	0.15	0.16	0.24	0.39	0.22
Total	100.38	100.77	100.58	100.66	100.65	100.82	100.63	100.51	100.98	100.78	100.33	100.61	100.83
LOI													
Sc	33	28	33	33	32	36	37	36	42	40	39	35	37
V													
Cr	146	100	121	259	129	60	207	34	156	160	38	52	65
Co	40	37	39	43	40	42	47	45	41	41	45	39	46
Ni	54	34	54	97	44	56	95	41	75	74	53	46	70
Cu	70	117	126	143	128	238	163	149	169	178	178	243	154
Zn	92	104	110	106	121	134	106	108	91	93	113	134	97
Ga													
Rb	28	50	37	41	56	23	12	20	26	36	43	41	12
Sr	445	305	422	336	481	282	273	319	192	182	272	275	439
Y	30	29	35	32	36	43	33	27	36	38	32	46	32
Zr	156	82		162	148	203	131	120	115	129	132	218	113
Nb	9.3	14	11	13	18	17	11	12	8.6	8.7	14	18	9.9
Cs	0.45	0.52	1.03	2.74	0.41	0.18	0.20	0.09	0.67	0.70	0.45	0.29	0.19
Ba	231	226	208	163	317	131	111	292	159	176	295	197	123
Li													
La	20	23	21	20	28	24	14	24	16	17	27	26	19
Ce	41	46	47	40	56	50	30	45	32	32	48	53	36
Pr	4.5	5.4	5.9	4.8	6.9	6.1	3.6	4.9	3.4	3.5	5.3	6.8	3.8
Nd	20	24	25	22	31	28	17	20	15	16	21	31	16
Sm	5.0	6.0	5.8	5.7	7.9	7.3	4.6	4.3	4.2	4.2	5.3	8.2	4.4
Eu	1.6	1.7	1.8	1.7	2.1	2.1	1.5	1.4	1.2	1.3	1.4	2.2	1.2
Gd	5.2	5.7	6.5	5.5	7.6	7.5	4.6	4.7	4.4	4.7	5.0	8.2	4.4
Tb	0.87	0.90	1.0	0.95	1.2	1.4	0.87	0.74	0.85	0.91	0.78	1.5	0.80
Dy	5.0	5.0	5.7	5.5	6.5	7.9	5.3	4.3	5.6	5.9	4.8	8.4	5.0
Ho	0.95	0.92	1.1	1.0	1.2	1.5	1.1	0.87	1.2	1.3	0.98	1.6	0.99
Er	2.5	2.2	2.8	2.7	3.0	4.0	3.0	2.3	3.3	3.5	2.8	4.2	2.8
Tm	0.36	0.29	0.38	0.36	0.39	0.55	0.41	0.34	0.48	0.53	0.41	0.58	0.40
Yb	2.3	1.9	2.5	2.4	2.5	3.5	2.7	2.3	3.3	3.5	2.8	3.8	2.6
Lu	0.36	0.29	0.35	0.35	0.36	0.53	0.40	0.36	0.50	0.54	0.46	0.58	0.42
Hf	3.8	2.4		4.2	4.0	5.3	3.3	3.0	2.9	3.3	3.1	5.9	3.0
Ta	0.51	0.76	0.68	0.74	1.0	0.96	0.63	0.65	0.52	0.53	0.75	1.0	0.57
Pb	3.0	4.1	3.5	2.6	4.5	3.5	2.0	3.1	4.0	5.4	5.1	4.0	4.9
Th	2.8	4.0	3.7	3.3	4.5	3.9	1.4	3.6	3.4	3.8	4.7	4.1	4.7
U	0.55	0.60	0.73	0.79	0.77	0.86	0.30	0.85	0.70	0.86	1.0	0.97	0.94

Appendix A (continued): Major element (wt%) and trace element (ppm) compositions of Deccan dikes.

Sample	DD-20	DD-21	DD-22	DD-23	DHD-01	DHD-02	DHD-03	DHD-05	DHD-06	DHD-07	DHD-08	DHD-09	DHD-10
Swarm	Narmada-Tapi	Narmada-Tapi	Narmada-Tapi	Narmada-Tapi	Narmada-Tapi	Narmada-Tapi	Narmada-Tapi	Narmada-Tapi	Narmada-Tapi	Narmada-Tapi	Narmada-Tapi	Narmada-Tapi	Narmada-Tapi
Strike	65	50	70	70	70	70	85	130	70	60	80	80	50
Thickness (m)	10	5	10	15	10	10	50	3.5	20	5	5	5	5
DFA result											Amb (Mhaba)		
Mahalanobis distance											16.29		
Lab	UH	UH	UH	UH	UH	UH	UH	UH	UH	UH	UH	UH	UH
SiO_2	52.30	56.19	49.25	51.22	51.25	53.04	50.17	50.25	51.85	49.79	49.99	49.94	51.99
TiO_2	1.51	2.70	1.76	2.37	2.55	1.55	1.49	2.55	1.05	2.19	2.24	2.23	1.06
Al_2O_3	15.09	14.63	14.38	13.33	13.93	13.60	14.09	13.58	13.45	13.70	13.86	13.86	13.65
FeO (t)	12.08	10.63	13.32	13.97	13.86	14.39	13.04	13.53	13.23	13.17	13.32	13.17	13.22
MnO	0.18	0.25	0.20	0.21	0.17	0.21	0.19	0.17	0.22	0.20	0.20	0.20	0.22
MgO	5.46	3.64	6.90	5.66	5.46	4.91	7.31	6.63	6.95	7.10	6.78	6.85	6.71
CaO	9.32	8.27	11.22	10.22	9.23	9.09	11.25	11.05	11.05	11.39	11.32	11.23	10.85
Na_2O	2.48	2.04	2.64	2.21	2.05	2.08	2.11	1.56	1.57	1.91	1.91	2.03	1.71
K_2O	1.32	1.15	0.14	0.50	1.24	0.88	0.19	0.46	0.49	0.33	0.20	0.28	0.45
P_2O_5	0.26	0.50	0.18	0.30	0.26	0.26	0.14	0.22	0.14	0.21	0.20	0.22	0.15
Total	100.60	100.11	100.76	100.94	100.16	100.33	99.85	100.72	100.38	100.76	99.96	100.73	100.22
LOI					1.24	1.76	2.76	2.72	0.79	0.67	0.87	0.78	0.83
Sc	35	21	38	34	33	45	46	40	53	42	42	41	53
V													
Cr	126	52	125	118	76	18	138	187	54	220	198	209	53
Co	37	29	46	42	45	50	49	49	52	49	49	48	54
Ni	64	10	86	74	60	62	90	113	74	95	86	78	71
Cu	169	33	149	199								223	
Zn	88	115	100	114	103	108	91	88	97	99	98	106	95
Ga													
Rb	51	33	4.5	18	36	18	5.9	7.0	17	8.0	4.0	6.5	16
Sr	255	1574	353	278	250	184	238	254	118	183	197	195	95
Y	37	42	30	41	34	28	28	28	32	32	31	31	33
Zr		284	75	183	296	181	168	332	144	202	117	99	305
Nb	9.6	39	11	14	14	15	7.3	9.2	8.3	11	11	11	8.7
Cs	0.25	2.27	0.07	0.31	0.36	0.16	0.09	0.02	0.25	0.10	0.04	0.08	0.19
Ba	232	346	60	149	240	303	78	128	111	80	75	77	116
Li													
La	19	43	13	22	20	23	9	12	8	10	10	11	9
Ce	39	91	26	46	45	46	19	29	17	25	25	26	18
Pr	4.5	13	3.0	5.6	5.7	5.3	2.5	4.0	2.0	3.5	3.5	3.8	2.3
Nd	17	50	14	26	27	22	12	20	9	18	18	17	10
Sm	4.3	10.1	3.7	5.9	6.5	4.6	3.5	5.4	2.5	5.0	4.9	4.9	2.7
Eu	1.3	2.7	1.3	2.0	1.9	1.4	1.3	1.9	0.86	1.8	1.7	1.6	1.0
Gd	4.7	10.4	4.0	6.7	6.5	4.8	4.1	5.5	3.3	5.4	5.3	5.3	3.7
Tb	0.86	1.4	0.78	1.2	1.1	0.78	0.76	0.93	0.67	0.97	0.93	0.91	0.73
Dy	5.5	7.2	4.9	7.2	6.0	4.7	4.8	5.4	4.6	5.8	5.5	5.5	5.0
Ho	1.2	1.4	1.0	1.4	1.2	0.99	1.0	1.0	1.1	1.2	1.1	1.1	1.2
Er	3.2	3.6	2.7	3.7	3.1	2.8	2.8	2.7	3.2	3.2	3.0	3.0	3.4
Tm	0.45	0.50	0.39	0.53	0.47	0.46	0.44	0.40	0.56	0.50	0.47	0.44	0.59
Yb	3.0	3.2	2.5	3.3	2.7	2.8	2.6	2.3	3.4	2.9	2.7	2.7	3.7
Lu	0.47	0.48	0.36	0.50	0.41	0.45	0.40	0.33	0.55	0.44	0.41	0.39	0.58
Hf		7.8	2.2	4.8	4.9	3.0	2.6	3.8	2.0	3.8	3.6	2.7	2.1
Ta	0.56	2.7	0.64	0.84	1.1	1.1	0.66	0.87	0.65	0.89	0.91	0.74	0.69
Pb	4.4	9.9	1.7	3.2	3.7	3.8	3.0	2.1	2.1	1.4	1.5	1.4	2.1
Th	4.2	11	1.6	3.5	4.7	4.2	1.9	1.8	2.2	1.2	1.1	1.1	2.1
U	0.78	2.6	0.32	0.85	1.2	1.0	0.43	0.41	0.59	0.29	0.27	0.23	0.51

Appendix A (continued): Major element (wt%) and trace element (ppm) compositions of Deccan dikes.

Sample	DHD-11	DND-01	DND-02	DND-03	DND-04	DND-05	DND-06	DND-07	NBD-01	NBD-01B	NBD-02	NBD-03	NBD-03B
Swarm	Narmada-Tapi	Narmada-Tapi	Narmada-Tapi	Narmada-Tapi	Narmada-Tapi	Narmada-Tapi	Narmada-Tapi	Narmada-Tapi	Narmada-Tapi	Narmada-Tapi	Narmada-Tapi	Narmada-Tapi	Narmada-Tapi
Strike	70	10	45	85	85	105	80	95	85	95	75	75	75
Thickness (m)	5	8	8.5	6.5	10			12.5	5.4	24	3	10	42
DFA result		Khand	Khand		Pol (Khand)	Pol (Amb)	Pol (Thak)	Khand (Thak)			Pol (Bhima)	Neral (Khand)	Pol (Khand)
Mahalanobis distance		18.84	11.19		19.48	9.18	10.20	9.42			10.63	13.39	7.74
Lab	UH	UH	UH	UH	UH	UH	UH	UH	UH	UH	UH	UH	UH
SiO_2	50.33	51.69	51.71	49.86	49.75	49.93	50.12	53.23	52.43	52.45	50.01	49.60	49.34
TiO_2	2.45	2.30	2.19	3.34	1.91	1.95	2.05	2.09	0.93	0.94	2.55	2.60	2.22
Al_2O_3	13.46	14.17	14.29	12.89	13.84	14.45	14.05	14.94	15.35	15.54	13.30	13.60	13.24
FeO (t)	14.36	13.35	13.06	15.25	13.45	12.85	13.23	10.93	10.61	10.60	14.72	14.30	14.12
MnO	0.21	0.20	0.20	0.22	0.20	0.20	0.21	0.16	0.18	0.17	0.23	0.22	0.21
MgO	5.99	5.29	5.43	5.35	7.23	6.80	6.45	5.55	6.92	6.74	5.90	6.54	7.79
CaO	10.42	9.89	10.09	9.94	11.43	11.42	11.27	9.81	10.85	10.71	10.19	10.28	10.45
Na_2O	2.11	2.40	2.37	2.09	1.81	1.92	1.96	2.01	1.82	1.96	2.34	2.03	1.90
K_2O	0.42	0.48	0.42	0.69	0.20	0.31	0.47	1.03	0.77	0.76	0.49	0.55	0.47
P_2O_5	0.24	0.25	0.23	0.37	0.17	0.17	0.19	0.24	0.14	0.13	0.25	0.29	0.25
Total	100.32	100.37	100.39	100.95	100.30	100.38	100.43	100.22	99.82	98.93	100.31	100.20	100.47
LOI	1.35												
Sc	37	33	33	37	37	35	36	29	40	40	42	40	41
V													
Cr	59	68	75	86	156	160	167	169	94	82	66	92	173
Co	49	47	47	49	55	50	52	39	42	44	49	49	55
Ni	73	67	71	71	107	101	105	65	57	61	52	77	109
Cu		185	173	291	183	179	184	88	105	108	214	268	240
Zn	103	126	114	159	103	104	106	99	67	70	133	129	122
Ga													
Rb	10	24	21	19	7.7	7.4	7.8	26	20	22	12	15	13
Sr	215	248	249	219	218	200	207	249	165	176	201	202	198
Y	34	36	34	42	28	27	28	29	24	24	39	39	34
Zr	106	192	175	189	132	122	130	157	129	128	160	169	160
Nb	11	11	10	19	8.1	7.7	8.0	12	7.4	7.3	14	15	13
Cs	0.04	0.63	0.84	0.41	0.30	0.08	0.08	0.29	0.24	0.34	0.14	0.22	0.18
Ba	107	219	209	168	70	64	67	222	228	228	112	141	124
Li													
La	14	20	18	19	9	8	8	20	15	15	13	15	13
Ce	32	44	41	45	23	20	21	43	30	30	33	36	31
Pr	4.6	5.8	5.4	6.4	3.4	3.0	3.1	5.5	3.7	3.6	4.6	5.1	4.4
Nd	23	25	24	29	16	14	15	23	15	14	21	23	20
Sm	6.1	6.3	5.9	7.6	4.5	4.2	4.3	5.5	3.2	3.2	5.6	6.0	5.2
Eu	2.2	1.9	1.8	2.2	1.5	1.4	1.5	1.7	1.0	1.0	1.8	1.8	1.6
Gd	6.8	6.6	6.2	7.8	4.9	4.5	4.7	5.8	3.8	3.8	6.1	6.4	5.6
Tb	1.1	1.1	1.0	1.3	0.82	0.77	0.81	0.91	0.63	0.62	1.0	1.1	0.94
Dy	6.9	6.4	6.0	7.6	4.9	4.7	4.8	5.2	3.8	3.8	6.3	6.4	5.6
Ho	1.4	1.2	1.2	1.5	0.96	0.91	0.96	0.99	0.82	0.81	1.3	1.3	1.1
Er	3.6	3.4	3.2	4.1	2.6	2.5	2.6	2.7	2.4	2.3	3.6	3.6	3.2
Tm	0.55	0.51	0.49	0.60	0.40	0.37	0.38	0.40	0.38	0.37	0.55	0.55	0.49
Yb	3.4	3.0	2.8	3.6	2.3	2.2	2.2	2.4	2.3	2.3	3.2	3.2	2.8
Lu	0.48	0.45	0.41	0.53	0.34	0.32	0.33	0.34	0.36	0.35	0.48	0.48	0.42
Hf	3.9	4.9	4.5	5.0	3.4	3.2	3.3	4.1	3.1	3.1	4.2	4.3	4.0
Ta	0.94	0.69	0.64	1.2	0.52	0.50	0.50	0.78	0.48	0.45	0.91	0.96	0.83
Pb	2.3	4.0	3.8	2.9	1.1	1.1	1.0	2.7	6.1	4.6	1.7	2.0	1.9
Th	1.8	3.5	3.3	2.1	1.2	1.0	1.0	5.4	3.0	2.8	1.5	1.8	1.6
U	0.40	0.71	0.66	0.44	0.32	0.22	0.23	1.2	0.79	0.73	0.37	0.43	0.38

Appendix A (continued): Major element (wt%) and trace element (ppm) compositions of Deccan dikes.

Sample	NBD-04	NBD-05	NBD-06	NBD-07	NBD-08	NBD-09	NBD-10	NBD-11	NBD-12	NBD-13	NBD-14	NBD-15	NBD-16
Swarm	Narmada-Tapi	Narmada-Tapi	Narmada-Tapi	Narmada-Tapi	Narmada-Tapi	Narmada-Tapi	Narmada-Tapi	Narmada-Tapi	Narmada-Tapi	Narmada-Tapi	Narmada-Tapi	Narmada-Tapi	Narmada-Tapi
Strike	65	95	60	100	80	76	80	90	78	80	60	80	83
Thickness (m)	3.8	18			62	23	11	11	20	8	4	20	20
DFA result	Bushe	Khand	Thak					Bushe (Khand)		Khand (Pol)			Pol (Amb)
Mahalanobis distance	20.34	20.68	9.37					18.46		12.91			8.35
Lab	UH	UH	UH	UH	UH	UH	UH	UH	UH	UH	UH	UH	UH
SiO_2	51.95	52.34	51.65	51.50	50.34	51.88	50.53	51.49	49.63	49.78	52.21	51.35	50.21
TiO_2	1.30	0.91	0.92	1.59	2.92	1.97	2.53	1.84	2.74	2.66	1.39	2.18	2.33
Al_2O_3	14.37	15.71	16.46	16.19	12.90	13.59	14.10	14.86	13.25	13.60	14.37	16.33	13.57
FeO (t)	11.91	10.32	9.72	12.11	15.08	13.88	13.61	13.39	14.76	14.21	12.92	11.43	14.30
MnO	0.19	0.17	0.16	0.19	0.22	0.22	0.20	0.20	0.22	0.21	0.19	0.18	0.22
MgO	6.78	6.82	6.68	4.79	5.79	5.63	5.75	4.88	6.05	6.14	5.81	4.40	6.10
CaO	10.17	10.99	11.62	10.41	9.68	9.43	9.60	9.82	10.43	10.45	10.12	10.50	10.52
Na_2O	1.83	1.72	1.97	2.35	2.18	2.25	2.40	2.11	2.17	2.05	1.94	2.60	2.06
K_2O	1.34	0.88	0.69	0.67	0.54	0.87	0.98	1.22	0.44	0.64	0.81	0.70	0.47
P_2O_5	0.14	0.14	0.13	0.20	0.34	0.28	0.30	0.19	0.31	0.28	0.22	0.32	0.22
Total	99.47	100.32	100.03	100.48	100.57	100.37	99.46	100.18	100.41	98.81	99.63	100.38	100.95
LOI													
Sc	44	32	38	38	42	33	31	42	36	44	45	28	39
V													
Cr	143	155	169	45	88	116	67	53	117	91	35	101	80
Co	45	38	42	39	51	33	41	41	38	55	46	31	50
Ni	71	120	66	37	12	57	38	43	61	78	46	42	62
Cu	167	103	85	202		191	93	211	206	268	207	223	216
Zn	87	69	69	97	5.2	102	102	99	110	146	92	102	122
Ga													
Rb	34	31	16	22	12	31	29	35	33	19	21	27	12
Sr	135	212	252	163	209	204	264	150	218	247	135	338	204
Y	33	24	18	37	45	38	31	38	41	41	33	40	32
Zr	117	84	92	100	263	155	137	143	157	191	121	190	147
Nb	8.9	6.6	7.1	9.3	16	17	13	9.7	17	17	11	15	9.3
Cs	0.20	0.19	0.11	0.25	0.16	0.31	0.85	0.40	0.35	0.17	0.15	0.20	0.26
Ba	144	225	193	182	149	204	204	180	218	116	154	187	96
Li													
La	12	16	12	12	16	21	20	13	22	15	13	19	10
Ce	25	32	24	27	40	44	44	28	44	36	27	44	25
Pr	3.2	3.7	3.0	3.5	5.6	5.1	5.8	3.6	5.2	5.1	3.4	5.8	3.6
Nd	13	14	12	15	26	21	25	16	22	23	14	26	17
Sm	3.5	2.8	2.7	4.1	6.7	4.9	6.1	4.2	5.2	6.2	3.4	6.6	4.7
Eu	1.1	1.0	1.0	1.3	2.0	1.5	1.8	1.4	1.6	1.9	1.1	2.1	1.6
Gd	4.2	3.4	3.2	4.8	6.8	5.5	6.2	5.0	6.1	6.6	4.1	7.0	5.2
Tb	0.76	0.54	0.51	0.86	1.2	0.96	0.97	0.90	1.0	1.1	0.75	1.1	0.90
Dy	4.9	3.5	2.9	5.6	7.2	6.2	5.4	5.8	6.4	6.7	4.8	6.9	5.3
Ho	1.1	0.77	0.62	1.2	1.4	1.3	1.0	1.2	1.4	1.3	1.0	1.4	1.1
Er	3.2	2.1	1.7	3.5	4.0	3.7	2.7	3.5	3.9	3.6	3.1	3.5	2.9
Tm	0.51	0.33	0.27	0.55	0.61	0.56	0.39	0.56	0.58	0.54	0.51	0.50	0.43
Yb	3.1	2.1	1.7	3.2	3.5	3.6	2.3	3.3	3.8	3.1	3.1	3.3	2.5
Lu	0.47	0.35	0.25	0.49	0.53	0.58	0.33	0.50	0.59	0.46	0.47	0.52	0.36
Hf	2.9	2.1	2.3	2.7	6.5	3.8	3.7	3.7	4.0	4.8	3.0	4.9	3.8
Ta	0.57	0.39	0.39	0.61	1.0	0.88	0.85	0.64	0.90	1.1	0.71	0.84	0.59
Pb	2.7	5.3	2.8	3.0		3.6	2.3	2.7	3.9	1.5	2.3	2.8	1.9
Th	2.9	2.6	1.6	2.9	2.1	3.7	3.9	3.1	3.7	1.7	2.9	2.1	1.5
U	0.74	0.66	0.36	0.69	0.48	0.74	0.81	0.73	0.76	0.42	0.71	0.50	0.29

Appendix A (continued): Major element (wt%) and trace element (ppm) compositions of Deccan dikes.

Sample	NBD-17	NBD-18	NBD-19	NBD-20	NBD-21	NBD-22	NBD-23	NBD-24	NBD-25	NBD-26	NBD-27	NBD-28	NBD-29
Swarm	Narmada-Tapi	Narmada-Tapi	Narmada-Tapi	Narmada-Tapi	Narmada-Tapi	Narmada-Tapi	Narmada-Tapi	Narmada-Tapi	Narmada-Tapi	Narmada-Tapi	Narmada-Tapi	Narmada-Tapi	Narmada-Tapi
Strike	83	85	85	110	70	75	87.5	83	80	90	85	90	90
Thickness (m)	20	6	7	3.5	5.5		8.5	62	7.5		4	4.5	15
DFA result	Khand (Pol)		Bhima (Khand)	Khand	Mahab	Igat-Jaw (Khand)	Neral (Bhima)		Bushe	Khand (Amb)	Khand		
Mahalanobis distance	13.40		3.51	12.26	17.93	13.44	7.00		25.32	18.92	10.54		
Lab	UH	UH	UH	UH	UH	UH	UH	UH	UH	UH	UH	UH	UH
SiO_2	50.00	50.30	50.10	51.53	49.21	49.91	49.10	49.26	51.90	49.79	51.16	50.90	52.76
TiO_2	2.72	3.15	2.54	2.23	3.34	2.77	3.04	3.56	1.03	2.75	2.44	1.99	1.25
Al_2O_3	13.06	12.79	14.41	14.00	13.28	13.69	13.56	14.10	14.53	13.43	13.86	13.60	14.38
FeO (t)	14.79	15.69	13.26	13.44	15.51	13.96	14.18	14.34	12.01	14.34	13.97	14.59	11.83
MnO	0.23	0.23	0.20	0.19	0.22	0.21	0.21	0.21	0.20	0.22	0.20	0.23	0.19
MgO	6.17	5.20	5.88	5.67	5.40	6.34	6.30	5.12	6.58	5.93	5.46	5.37	6.38
CaO	10.09	9.69	10.71	10.12	9.85	10.19	10.63	10.23	11.65	10.62	9.85	9.52	9.99
Na_2O	2.09	2.16	2.18	2.16	2.28	2.10	2.12	2.19	1.71	2.15	2.30	1.80	2.29
K_2O	0.54	0.40	0.47	0.42	0.56	0.56	0.53	0.56	0.26	0.48	0.49	1.73	0.78
P_2O_5	0.30	0.37	0.25	0.24	0.34	0.28	0.32	0.44	0.12	0.28	0.26	0.26	0.15
Total	100.16	100.70	99.96	99.92	100.37	99.66	100.44	100.42	100.88	100.45	100.12	100.23	100.12
LOI													
Sc	45	34	32	31	38	41	39	35	48	38	34	43	37
V													
Cr	88	140	195	136	95	83	135	81	143	69	64	35	245
Co	50	41	39	39	50	49	48	44	44	49	47	47	38
Ni	67	74	84	84	69	82	83	63	67	68	67	45	101
Cu	265	110	186	149	306	236	302	342	160	229	185	226	168
Zn	136	76	113	105	158	127	331	148	76	126	118	111	90
Ga													
Rb	14	30	15	31	15	16	14	14	8	12	13	39	37
Sr	195	248	292	296	228	232	213	250	122	231	250	179	208
Y	41	25	36	35	41	37	40	46	30	35	38	41	37
Zr	186	204	163	165	183	177	195	179	89	157	190	148	105
Nb	14	7.2	14	9.9	20	13	19	19	5.4	15	12	19	8.1
Cs	0.15	0.47	0.13	1.87	0.20	0.13	0.20	0.21	1.87	0.17	0.62	0.39	0.30
Ba	138	234	120	207	130	133	127	144	110	111	232	198	158
Li													
La	14	17	16	20	17	13	16	19	9	13	20	18	15
Ce	35	34	38	43	41	33	39	47	18	33	44	38	32
Pr	4.9	3.8	5.1	5.4	5.7	4.6	5.4	6.7	2.2	4.7	5.8	4.9	3.8
Nd	22	15	23	23	26	21	24	30	9	21	25	20	15
Sm	5.9	4.0	5.5	5.5	6.8	5.5	6.2	7.9	2.6	5.6	6.2	4.9	3.9
Eu	1.8	1.0	1.7	1.8	2.1	1.7	1.9	2.3	0.9	1.8	1.9	1.5	1.2
Gd	6.2	3.8	5.8	6.0	7.0	5.8	6.5	7.9	3.3	5.8	6.5	5.5	4.4
Tb	1.1	0.59	1.0	0.99	1.1	1.0	1.1	1.3	0.63	0.99	1.1	0.96	0.83
Dy	6.5	3.8	5.8	5.7	6.8	6.0	6.6	7.7	4.3	5.8	6.2	6.1	5.5
Ho	1.3	0.80	1.2	1.1	1.3	1.2	1.3	1.5	0.93	1.1	1.2	1.3	1.2
Er	3.6	2.3	3.1	2.9	3.5	3.3	3.6	4.0	2.8	3.1	3.3	3.7	3.4
Tm	0.56	0.34	0.43	0.42	0.53	0.50	0.54	0.59	0.46	0.45	0.50	0.59	0.53
Yb	3.3	2.3	2.6	2.7	3.0	2.9	3.1	3.4	2.7	2.6	2.9	3.6	3.4
Lu	0.49	0.37	0.42	0.40	0.44	0.43	0.46	0.49	0.41	0.39	0.42	0.55	0.54
Hf	4.8	5.0	4.2	4.1	4.7	4.5	5.0	4.7	2.3	4.1	4.7	3.7	2.8
Ta	0.90	0.40	0.84	0.55	1.3	0.86	1.2	1.2	0.36	0.94	0.71	1.1	0.52
Pb	2.1	5.2	1.9	4.1	1.8	1.9	2.1	2.2	2.4	1.5	3.9	3.1	4.0
Th	1.8	2.9	1.8	3.3	1.8	1.7	2.1	2.0	2.1	1.6	3.2	2.9	3.5
U	0.41	0.71	0.41	0.66	0.40	0.40	0.51	0.43	0.49	0.38	0.63	0.66	0.76

Appendix A (continued): Major element (wt%) and trace element (ppm) compositions of Deccan dikes.

Sample	NBD-30	NBD-31	NBD-32	NBD-33	NBD-34	NBD-35	NBD-36	NBD-37	NBD-38	NBD-39	NBD-40	NBD-41	NBD-42
Swarm	Narmada-Tapi	Narmada-Tapi	Narmada-Tapi	Narmada-Tapi	Narmada-Tapi	Narmada-Tapi	Narmada-Tapi	Narmada-Tapi	Narmada-Tapi	Narmada-Tapi	Narmada-Tapi	Narmada-Tapi	Narmada-Tapi
Strike	85	85	90	82.5	77.5	75	85	85	85	90	90	90	55
Thickness (m)	30	10	20	13	45	8	8	8	12	12.5	13	7	8
DFA result		Bushe	Bhima	Khand (Neral)						Thak (Neral)	Neral (Khand)		Khand
Mahalanobis distance		8.81	20.81	11.24						8.99	9.23		18.57
Lab	UH	UH	UH	UH	UH	UH	UH	UH	UH	UH	UH	UH	UH
SiO_2	53.58	53.45	49.91	49.79	53.55	49.34	51.52	51.41	50.11	51.87	50.98	51.33	51.40
TiO_2	2.17	0.78	2.06	3.02	2.63	2.76	1.66	2.55	3.54	1.88	2.62	2.09	2.81
Al_2O_3	13.55	15.56	19.24	13.60	13.57	13.47	14.11	13.52	12.83	14.14	13.13	13.44	13.21
FeO (t)	14.42	9.88	10.15	14.09	12.56	14.82	10.97	13.23	14.95	11.15	14.40	14.84	14.85
MnO	0.21	0.16	0.15	0.21	0.20	0.22	0.17	0.19	0.23	0.17	0.21	0.23	0.21
MgO	4.09	6.63	4.32	5.77	4.82	5.87	7.89	5.75	5.17	6.82	5.50	5.28	4.79
CaO	7.85	10.33	10.84	10.39	8.23	10.26	10.84	9.76	9.67	11.16	10.23	9.62	9.60
Na_2O	2.72	2.01	2.65	2.27	2.44	2.17	1.92	2.52	2.36	2.01	1.98	2.14	2.34
K_2O	1.00	1.10	0.41	0.54	1.66	0.83	0.75	0.78	0.68	0.56	0.68	0.75	0.45
P_2O_5	0.42	0.10	0.26	0.30	0.33	0.25	0.17	0.29	0.47	0.22	0.28	0.29	0.32
Total	100.20	100.36	100.29	100.09	100.15	100.21	100.16	100.03	99.29	100.14	100.55	100.31	100.58
LOI													
Sc	37	38	24	38	30	38	35	32	37	33	39	37	34
V													
Cr	10	199	68	146	42	78	298	198	97	331	82	99	78
Co	39	42	36	47	36	50	44	45	44	44	46	38	45
Ni	24	90	73	83	27	69	106	68	54	66	56	57	48
Cu	340	89	207	259	44	265	72	189	351	63	238	217	216
Zn	124	60	92	140	104	132	76	119	150	97	131	115	136
Ga													
Rb	36	38	10	14	47	18	21	22	17	7.4	16	25	23
Sr	180	138	283	232	266	229	175	249	244	302	182	222	256
Y	48	23	32	39	36	38	23	32	53	26	35	42	43
Zr	106	91	154	203	81	187		75	275	125	162	166	222
Nb	26.8	5.8	13	17	13	13	9.0	14	22	8.3	15	19	14
Cs	0.84	0.53	0.11	0.17	0.32	0.18	0.38	0.27	0.14	0.03	0.10	0.25	1.25
Ba	241	154	104	121	304	101	199	193	168	178	141	217	305
Li													
La	27	14	12	16	25	12	12	20	22	16	15	22	24
Ce	57	28	30	38	55	30	27	44	55	36	36	45	53
Pr	6.9	3.2	4.2	5.3	7.1	4.4	3.6	5.8	7.8	4.7	4.9	5.5	6.9
Nd	28	12	19	24	29	21	15	25	36	20	22	23	30
Sm	6.1	2.7	5.0	6.3	6.9	5.8	3.9	6.1	9.2	4.8	5.5	5.7	7.3
Eu	1.8	0.8	1.7	1.9	2.0	1.9	1.3	1.9	2.6	1.5	1.7	1.7	2.2
Gd	7.1	3.2	5.3	6.4	7.0	6.1	4.3	6.3	9.2	5.1	5.8	6.2	7.6
Tb	1.1	0.55	0.88	1.1	1.1	1.1	0.71	1.0	1.5	0.80	0.96	1.1	1.2
Dy	7.1	3.4	5.3	6.4	6.3	6.4	4.0	5.7	9.0	4.6	5.8	6.7	7.3
Ho	1.5	0.73	1.0	1.2	1.2	1.3	0.79	1.1	1.7	0.87	1.1	1.4	1.4
Er	4.4	2.2	2.8	3.4	3.2	3.5	2.1	2.8	4.8	2.4	3.2	4.0	3.9
Tm	0.69	0.35	0.42	0.51	0.47	0.52	0.31	0.41	0.71	0.35	0.49	0.61	0.58
Yb	4.1	2.1	2.4	3.0	2.7	3.0	1.8	2.3	4.0	2.0	2.9	3.9	3.3
Lu	0.63	0.33	0.36	0.43	0.40	0.44	0.27	0.33	0.59	0.29	0.44	0.62	0.49
Hf	2.8	2.3	3.9	5.1	2.5	4.8	2.4	2.4	6.9	3.3	4.2	4.2	5.5
Ta	1.6	0.41	0.85	1.1	0.86	0.84	0.61	0.88	1.4	0.55	1.0	1.0	0.85
Pb	3.5	5.2	1.5	2.0	3.6	1.3	1.6	2.9	1.6	2.7	2.2	2.6	4.5
Th	4.1	5.2	1.4	1.9	6.2	1.3	2.5	3.1	2.4	2.4	2.4	3.2	3.5
U	0.77	1.2	0.34	0.44	1.3	0.34	0.52	0.55	0.59	0.45	0.53	0.71	0.66

Appendix A (continued): Major element (wt%) and trace element (ppm) compositions of Deccan dikes.

Sample	SDPD-1	SDPD-2	DND-08	UDD-01	UDD-02	UDD-09	BHVO-1	BHVO-1
Swarm	Narmada-Tapi	Narmada-Tapi	Nasik-Pune	Nasik-Pune	Nasik-Pune	Nasik-Pune	measured	recommended
Strike	90	90	1	90	90	25		
Thickness (m)	7	6.5	24		20	7		
DFA result	Igat-Jaw (Neral)	Khand	Khand		Khand	Bushe		
Mahalanobis distance	13.58	23.19	10.96		22.98	5.67		
Lab	UH	UH	UH	UH	UH	UH	UH	
SiO_2	49.74	52.58	51.79	52.05	51.75	52.93	49.36	49.59
TiO_2	3.13	1.98	3.19	2.75	2.95	1.04	2.71	2.69
Al_2O_3	12.90	14.77	12.73	13.67	13.13	14.16	13.72	13.70
FeO (t)	15.44	12.40	14.98	13.27	14.17	10.53	12.35	12.39
MnO	0.22	0.19	0.20	0.20	0.20	0.18	0.16	0.17
MgO	5.27	4.94	4.53	5.03	4.86	8.03	7.22	7.22
CaO	9.92	10.12	8.83	9.37	8.96	10.66	11.32	11.32
Na_2O	2.11	2.29	2.31	2.51	2.56	1.79	2.39	2.24
K_2O	0.93	0.53	1.06	0.82	1.03	0.60	0.50	0.52
P_2O_5	0.33	0.21	0.37	0.32	0.38	0.08	0.27	0.27
Total	101.48	100.22	100.67	101.68	99.61	100.04		
LOI								
Sc	37	32	34	34	36	37	32	31.8
V								317
Cr	71	72	43	101	118	397	286	289
Co	49	42	44	41	42	48	45	45
Ni	56	44	42	49	42	144	117	120
Cu	267	126	270	268	252	114	146	136
Zn	158	101	154	127	126	75	123	105
Ga								21
Rb	19	13	34	24	30	19	10	9.5
Sr	223	241	204	227	224	116	401	396
Y	42	32	51	46	47	24	28	27.6
Zr	208	172	250	174	211	83	183	180
Nb	17	9.9	18	16	17	4.7	20	19.5
Cs	0.18	0.76	0.43	0.25	0.25	0.25	0.12	0.10
Ba	128	188	222	171	190	92	140	133
Li								4.9
La	16	17	25	21	24	9.0	16	15.8
Ce	39	39	59	50	55	20	39	38
Pr	5.6	5.0	7.9	6.7	7.4	2.5	5.6	5.45
Nd	26	21	34	30	33	11	25	25.2
Sm	6.8	5.2	8.6	7.5	8.3	2.8	6.2	6.17
Eu	2.1	1.6	2.4	2.2	2.3	0.93	2.0	2.06
Gd	7.0	5.5	8.8	7.6	8.2	3.6	6.3	6.22
Tb	1.2	0.91	1.4	1.3	1.3	0.63	0.98	0.96
Dy	7.1	5.4	8.5	7.6	8.0	3.9	5.3	5.25
Ho	1.4	1.1	1.7	1.5	1.5	0.81	0.98	0.99
Er	3.8	2.9	4.6	4.0	4.2	2.2	2.5	2.56
Tm	0.56	0.44	0.70	0.60	0.63	0.35	0.36	0.33
Yb	3.2	2.6	4.0	3.5	3.6	2.1	2.1	2.02
Lu	0.48	0.38	0.59	0.51	0.51	0.32	0.30	0.278
Hf	5.3	4.4	6.3	4.7	5.2	2.2	4.6	4.38
Ta	1.1	0.63	1.2	1.1	1.1	0.35	1.2	1.23
Pb	1.7	4.2	4.4	3.2	3.4	3.6	2.0	2.10
Th	1.8	3.9	4.7	4.4	3.7	2.6	1.3	1.26
U	5.0	6.0	1.2	1.0	0.91	4.0	0.45	0.42

Appendix B: model parameters used to estimate degrees of partial melting at the LSC in chapter 4

Model 1

	Olivine	Cpx	Opx	Garnet	Spinel
K_d - Sm	0.001	0.15	0.02	0.23	
K_d - Tb	0.02	0.25	0.08	5.5	
K_d - Dy	0.0027	0.17	0.065	1.65	
Proportion in source	0.53	0.1	0.3	0.07	(0.07-grt)
Proportion entering the melt	0.1	0.4	0.1	0.4	(0.4-grt)

	Sm	Yb	Dy
Unmelted source starting concentrations (ppm)	0.406	0.441	0.674

Model 2

	Olivine	Cpx	Opx	Garnet	Spinel
K_d - Sm	0.001	0.15	0.02	0.22	
K_d - Tb	0.02	0.25	0.08	5.5	
K_d - Dy	0.0027	0.17	0.065	1.06	
Proportion in source	0.57	0.1	0.3	0.03	(0.03-grt)
Proportion entering the melt	0.1	0.4	0.1	0.4	(0.4-grt)

	Sm	Yb	Dy
Unmelted source starting concentrations (ppm)	0.4	0.365	0.505

APPENDIX C

PRINCIPLES OF DISCRIMINANT FUNCTION ANALYSES

The aim of this appendix is to present the basic principles of discriminant function analyses, a statistical method used in chapter 2 to discriminate between groups of Deccan Traps lavas on the basis of their major and trace element compositions.

Discriminant function analysis (DFA) is a statistical tool with two common usages: (1) determine which variables discriminate between two or more naturally occurring groups and (2) predictive classification. In a sense, DFA is a reversed multivariate analysis of variance (MANOVA) because, unlike for MANOVA, the independent variables in the DFA are considered as the predictors and the dependent variables as the groups.

Discriminant function analysis can be broken into a two-step process: (1) testing significance of a set of discriminant functions, and (2) classification. The first step determines whether or not two or more groups are statistically significantly different from one another with respect to the mean of a particular variable. Computationally speaking, matrices of variances and covariances are calculated both across the dataset and within each group. The matrices are then compared via multivariate F tests in order to determine whether or not there are any significant differences (with regard to all variables) between groups. The multivariate tests are performed first and, if statistically significant, the analysis proceeds to determine which of the variables have significantly different means across the groups. Once group means are found to be significantly different statistically,

the DFA classifies the variables. The DFA calculates a set of functions called discriminant functions (or canonical roots or functions) representing optimal combinations of variables (in which variables are weighed by discriminant coefficients) so that the first function provides the most overall discrimination between groups, the second provides second most, and so on. In our case, eight canonical functions were calculated. The first function encompasses the most variation, the second function covers the greatest part of the remaining unexplained variation, etc.

Classification is possible from the canonical functions. For each sample, the discriminant score is calculated by applying the discriminant function formula to the sample's data. This score is also called "Z score" if data is standardized, which it is in our particular case (i.e., the discriminant coefficients are determined to weigh the *relative* classifying importance of variables). The mean discriminant score for each group is called the group centroid, and the distance (in a n-dimensional space defined by n variables) between a sample's score and a group centroid is called Mahalanobis distance. A sample will be classified as belonging to the group to which its Mahalanobis distance is shortest. The shorter the Mahalanobis distance, the higher the probability that a sample belongs to a group.

In our case, group centroids were calculated for nine different groups, each representing a lava flow formation (with the exception of the Igatpuri and Jawhar formations, which form a single group), from a standard set of 624 lava flow analyses from the Deccan "type" sections of the Western Ghats. SiO_2, Al_2O_3, TiO_2, CaO, K_2O, P_2O_5, Ni, Ba, Sr, Zr, Y and Nb were chosen as our predictor variables.

Appendix D: Measurements of standards by ICP-MS. Legend as in Appendix A.

Standard	K-1919	K-1919	K-1919	K-1919	K-1919
Lab	UH-Quadrupole	UH-Quadrupole	UH-Quadrupole	UH-Quadrupole	UH-Quadrupole
Date	12/22/2005	12/22/2005	12/22/2005	06/17/2006	06/17/2006
Sc	35	32	34	35	36
Cr	290	287	288	285	333
Co	51	48	50	51	47
Ni	112	109	111	113	112
Cu	135	132	135	140	138
Zn	103	103	104	109	109
Rb	13	12	13	14	14
Sr	424	413	420	425	434
Y	28	27	27	27	27
Zr	185	181	185	183	182
Nb	20	20	20	20	19
Cs	0.12	0.10	0.11	0.10	0.10
Ba	177	176	178	208	203
La	19	19	19	18	18
Ce	42	42	42	43	44
Pr	5.4	5.4	5.4	5.6	5.4
Nd	26	26	26	26	26
Eu	2.0	1.9	2.0	2.0	2.0
Gd	6.0	5.9	6.0	6.3	6.1
Tb	0.96	0.92	0.95	1.0	0.97
Dy	5.2	5.1	5.2	5.4	5.4
Ho	0.97	0.98	0.97	1.0	0.98
Er	2.3	2.4	2.4	2.5	2.5
Tm	0.42	0.41	0.41	0.37	0.37
Yb	2.0	2.0	2.0	2.2	2.1
Lu	0.29	0.30	0.30	0.32	0.30
Hf	4.5	4.5	4.5	4.4	4.4
Ta	1.4	1.4	1.4	1.4	1.4
Pb	1.1	1.1	1.1	1.3	1.3
Th	1.6	1.6	1.6	1.3	1.4
U	0.54	0.56	0.54	0.45	0.47

Appendix D (Cont.): Measurements of standards by ICP-MS. Legend as in Appendix A.

Standard	K-1919	K-1919	K-1919	K-1919	K-1919	K-1919
Lab	UH-Element2	UH-Element2	UH-Element2	UH-Element2	UH-Element2	UH-Element2
Date	11/20/2006	11/20/2006	11/20/2006	11/20/2006	11/20/2006	11/20/2006
Li	4.8	4.7	4.8	4.8	5.0	4.9
Sc	35	35	36	36	43	37
Cr	280	279	281	281	342	281
Co	56	56	56	56	56	56
Ni	112	112	112	112	111	112
Cu	163	160	159	160	158	158
Zn	137	130	132	132	128	130
Rb	11	11	11	11	11	11
Sr	435	438	440	443	439	442
Y	31	31	31	31	31	31
Zr	203	186	203	190	207	203
Nb	22	21	22	22	22	22
Cs	0.12	0.12	0.12	0.12	0.12	0.12
Ba	154	152	152	152	149	149
La	17	17	17	17	17	17
Ce	44	43	42	42	42	42
Pr	6.2	6.1	6.0	6.0	6.0	5.9
Nd	28	28	27	27	27	27
Sm	7.0	6.9	6.7	6.7	6.6	6.6
Eu	2.2	2.2	2.2	2.2	2.1	2.1
Gd	7.0	6.7	6.8	6.7	6.5	6.5
Tb	1.1	1.1	1.1	1.0	1.0	1.0
Dy	6.0	5.8	5.8	5.7	5.6	5.6
Ho	1.1	1.1	1.1	1.1	1.0	1.0
Er	2.9	2.8	2.8	2.7	2.7	2.7
Tm	0.41	0.40	0.39	0.38	0.38	0.38
Yb	2.4	2.3	2.2	2.2	2.1	2.1
Lu	0.34	0.32	0.32	0.32	0.31	0.31
Hf	5.2	4.7	5.0	4.8	5.2	5.0
Ta	1.5	1.5	1.5	1.5	1.5	1.4
Pb	1.0	1.1	1.0	1.1	1.1	1.0
Th	1.4	1.4	1.4	1.4	1.4	1.4
U	0.50	0.48	0.48	0.48	0.48	0.47

Appendix D (Cont.): Measurements of standards by ICP-MS. Legend as in Appendix A.

Standard	K-1919	K-1919	K-1919	K-1919	K-1919	K-1919
Lab	UH-Element2	UH-Element2	UH-Element2	UH-Element2	UH-Element2	UH-Element2
Date	11/20/2006	11/20/2006	11/20/2006	11/20/2006	11/20/2006	11/20/2006
Li	4.8	4.9	4.9	4.4	4.9	5.0
Sc	37	37	37	33	35	36
Cr	280	276	275	253	272	275
Co	55	55	55	51	54	55
Ni	111	100	110	102	108	109
Cu	158	119	153	146	148	156
Zn	130	107	130	119	118	128
Rb	11	11	11	11	11	11
Sr	444	437	439	412	435	441
Y	31	31	31	29	31	31
Zr	204	191	200	191	210	206
Nb	22	21	22	20	21	22
Cs	0.12	0.12	0.12	0.11	0.12	0.12
Ba	149	148	149	141	147	150
La	17	17	17	16	17	17
Ce	42	42	42	39	41	42
Pr	5.9	5.9	5.9	5.6	5.8	6.0
Nd	27	26	27	25	26	27
Sm	6.6	6.5	6.5	6.2	6.5	6.6
Eu	2.1	2.1	2.1	2.0	2.1	2.1
Gd	6.5	6.5	6.5	6.2	6.4	6.5
Tb	1.0	1.0	1.0	1.0	1.0	1.0
Dy	5.6	5.6	5.6	5.4	5.6	5.7
Ho	1.0	1.0	1.0	1.0	1.0	1.1
Er	2.7	2.6	2.7	2.5	2.6	2.7
Tm	0.38	0.37	0.37	0.36	0.37	0.38
Yb	2.2	2.1	2.1	2.1	2.1	2.2
Lu	0.31	0.30	0.31	0.29	0.30	0.31
Hf	5.0	4.9	5.0	4.7	5.3	5.2
Ta	1.5	1.5	1.5	1.3	1.5	1.5
Pb	1.0		1.0	1.1		1.1
Th	1.4	1.4	1.4	1.3	1.4	1.4
U	0.47	0.48	0.47	0.45	0.47	0.48

Appendix D (Cont.): Measurements of standards by ICP-MS. Legend as in Appendix A.

Standard	K-1919	K-1919	BHVO-1	BIR-1	BCR-2
Lab	UH-Element2	UH-Element2	UH-Element2	UH-Element2	WSU
Date	11/20/2006	11/20/2006	11/20/2006	11/20/2006	10/19/2006
Li	4.9	5.0	4.7	3.1	
Sc	36	35	32	44	33
Cr	275	273	286	367	
Co	55	54	45	50	
Ni	109	108	117	164	
Cu	154	155	146	115	
Zn	128	131	123	64	
Rb	11	11	10	1.0	45
Sr	439	440	401	111	334
Y	31	31	28	16	35
Zr	198	199	183	26	172
Nb	21	22	20	0.89	11
Cs	0.12	0.12	0.12	0.02	1.1
Ba	150	151	140	11	673
La	17	17	16	0.76	25
Ce	42	42	39	2.3	53
Pr	6.0	6.0	5.6	0.45	6.9
Nd	27	27	25	2.5	29
Sm	6.6	6.7	6.2	1.1	6.8
Eu	2.1	2.2	2.0	0.51	2.1
Gd	6.6	6.7	6.3	1.8	6.9
Tb	1.0	1.0	1.0	0.36	1.1
Dy	5.7	5.8	5.3	2.5	6.9
Ho	1.0	1.0	1.0	0.56	1.4
Er	2.7	2.7	2.5	1.6	3.8
Tm	0.39	0.38	0.36	0.26	0.54
Yb	2.2	2.2	2.1	1.6	3.3
Lu	0.32	0.31	0.30	0.25	0.51
Hf	4.9	4.9	4.6	0.81	4.9
Ta	1.4	1.4	1.2	0.05	0.78
Pb	1.1	1.0	2.0	4.4	6.0
Th	1.4	1.4	1.3	0.03	11
U	0.47	0.48	0.45	0.01	1.7

Appendix D (Cont.): Measurements of standards by ICP-MS. Legend as in Appendix A.

Standard	BCR-2	AGV-2	AGV-2	BHVO-2	BHVO-2
Lab	WSU	WSU	WSU	WSU	WSU
Date	10/19/2006	10/19/2006	10/19/2006	10/19/2006	10/19/2006
Sc	33	12	12	31	31
Rb	45	64	64	9	9
Sr	332	632	635	383	382
Y	35	19	19	26	25
Zr	171	211	212	159	157
Nb	11	13	13	17	17
Cs	1.1	1.1	1.1	0.11	0.10
Ba	668	1105	1111	133	130
La	25	38	38	16	15
Ce	52	68	69	38	37
Pr	6.9	8.1	8.2	5.4	5.3
Nd	29	30	30	25	24
Sm	6.7	5.7	5.7	6.3	6.1
Eu	2.1	1.6	1.6	2.2	2.2
Gd	6.9	4.7	4.7	6.4	6.3
Tb	1.1	0.66	0.67	0.99	0.99
Dy	7.1	3.7	3.8	5.7	5.6
Ho	1.4	0.71	0.70	1.1	1.0
Er	3.7	1.8	1.8	2.5	2.5
Tm	0.53	0.26	0.26	0.33	0.33
Yb	3.2	1.5	1.6	1.9	1.9
Lu	0.50	0.24	0.25	0.28	0.28
Hf	5.0	5.1	5.1	4.4	4.3
Ta	0.76	0.81	0.82	1.1	1.1
Pb	6.1	6.2	6.3	1.4	1.3
Th	11	13	13	2.6	2.5
U	1.7	1.9	1.9	0.46	0.43

REFERENCES

Abouchami, W., Galer, S. J. G. & Hofmann, A. W. (2000). High precision lead isotope systematics of lavas from the Hawaiian scientific drilling project. *Chemical Geology* **169**, 187-209.

Abouchami, W., Hofmann, A. W., Galer, S. J. G., Frey, F. A., Eisele, J. & Feigenson, M. (2005). Lead isotopes reveal bilateral asymmetry and vertical continuity in the Hawaiian mantle plume. *Nature* **434**, 851-856.

Agashe, L. V. & Gupte, R. B. (1972). Mode of eruption of Deccan Trap basalts. *Bulletin of Volcanology* **35**, 591-601.

Agrawal, J. K. & Rama, F. A. (1976). Chronology of Mesozoic volcanics of India. *Proceedings of the Indian Academy of Science* **84A**, 157-179.

Allègre, C. J., Birck, J. L., Capmas, F. & Courtillot, V. (1999). Age of the Deccan traps using ^{187}Re-^{187}Os systematics. *Earth and Planetary Science Letters* **170**, 197-204.

Anderson, D. L. (1994). The sublithospheric mantle as the source of continental flood basalts: the case against the continental lithosphere and plume head reservoirs. *Earth and Planetary Science Letters* **123**, 269-280.

Antretter, M., Riisager, P., Hall, S., Zhao, X. & Steinberger, B. (2004), Modeled paleolatitudes for the Louisville hotspot and the Ontong Java Plateau. In: Fitton, J. G. et al. (eds.) *Origin and evolution of the Ontong Java Plateau*. *Geological Society of London Special Publications* **229**, 21-30.

Auden, J. B. (1949). Dykes in western India – a discussion of their relationship with the Deccan Traps. *Transactions of the National Institute of Science, India* **3**, 123-157.

Backman, J. & Duncan, R. A. (1987). New studies of the Indian Ocean. *Nature* **329**, 586-587.

Baker, P. E., Buckley, F. & Holland, J. G. (1974). Petrology and geochemistry of Easter Island. *Contributions to Mineralogy and Petrology* **44**, 85-100.

Baksi, A. K. (1994). Geochronological studies on whole-rock basalts, Deccan Traps, India: evaluation of the timing of volcanism relative to the K-T boundary. *Earth and Planetary Science Letters* **121**, 43-56.

Baksi, A. K. (2007). A quantitative tool for detecting alteration in undisturbed rocks and minerals—II: Application to argon ages related to hotspots. In: Foulger, G. R. & Jurdy, D. M. (eds.) *Plates, plumes and planetary processes. Geological Society of America Special Paper* **430**, 305-333.

Basu, D. N., Banerjee, A. & Tanshane, D. M. (1982). Facies distribution and petroleum geology of the Bombay offshore basin, India. *Journal of Petroleum Geology* **5**, 51-57.

Basu, D. N., Renne, P. R., DasGupta, D. K., Teichmann, F. & Poreda, R. J. (1993). Early and late alkali igneous pulses and a high-^{3}He origin for the Deccan flood basalts. *Science* **261**, 902-906.

Baturin, G. & Yushina, I. (2007). Rare earth elements in phosphate-ferromanganese crusts on Pacific seamounts. *Lithology and Mineral Resources* **42** (2), 101-117.

Beane, J. E. (1988). Flow stratigraphy, chemical variation and petrogenesis of Deccan flood basalts from the Western Ghats, India. Ph.D. dissertation, Washington State University, pp. 576.

Beane, J. E., Turner, C. A., Hooper, P. R., Subbarao, K. V. & Walsh, J. N. (1986). Stratigraphy, composition and form of the Deccan basalts, Western Ghats, India. *Bulletin of Volcanology* **48**, 61-83.

Beattie, P. (1993). Uranium-thorium disequilibria and partitioning on melting of garnet peridotite. *Nature* **363**, 63-65.

Belousova, E., Griffin, W., O'Reilly, S. Y. & Fisher, N. (2002). Igneous zircon: trace element composition as an indicator of source rock type. *Contributions to Mineralogy and Petrology* **143** (5), 602-622.

Bence, A. E., Taylor, S. R. & Fisk, M. (1980). Major and trace-element geochemistry of basalts from Ojin, Nintoku, and Suiko seamounts of the Emperor seamount chain, DSDP-IPOD leg 55. *Initial Report of the Deep Sea Drilling Project* **55**, 599-605.

Bhattacharji, S., Chatterjee, J. M., Wampler, J. M., Nayak, P. N. & Deshmukh, S. S. (1996). Indian intraplate and continental margin rifting, lithospheric extension, and mantle upwelling in Deccan flood basalt volcanism near the K/T boundary: Evidence from mafic dike swarms. *Journal of Geology* **104**, 379-398.

Billen, M. I. & Stock, J. (2000). Morphology and origin of the Osbourn Trough. *Journal of Geophysical Research* **105** (B6), 13481-13489.

Biswas, S. K. (1987). Regional tectonic framework, structure and evolution of the western marginal basins of India. *Tectonophysics* **135**, 307-327.

Blichert-Toft, J., Weis, D., Maerschalk, C., Agranier, A. & Albarède, F. (2003). Hawaiian hot spot dynamics as inferred from the Hf and Pb isotope evolution of Mauna Kea volcano. *Geochemistry Geophysics Geosystems* **4** (2), 8704.

Bonatti, E. (1990). Not so hot “hot spots” in the oceanic mantle. *Science* **250** (4977), 107-111.

Bonatti, E., Harrison, C. G. A., Fisher, D. E., Honnorez, J., Schilling, J.-G., Stipp, J. J. & Zentilli, M. (1977). Easter volcanic chain (Southeast Pacific): a mantle hot line. *Journal of Geophysical Research* **82**, 2457-2478.

Bondre, N. R., Hart, W. K. & Sheth, H. C. (2006). Geology and geochemistry of the Sangamner mafic dike swarm, western Deccan volcanic province, India: implications for regional stratigraphy. *Journal of Geology* **114**, 155-170.

Boschi, L. & Dziewonski, A. M. (2000). Whole Earth tomography from delay times of P, PcP, and PKP phases: Lateral heterogeneities in the outer core or radial anisotropy in the mantle? *Journal of Geophysical Research* **105**, 13675-13696.

Bose, M. K. (1973). Petrology and geochemistry of the igneous complex of Mount Girnar, Gujarat, India. *Contributions to Mineralogy and Petrology* **39**, 247-266.

Boyet, M. & Carlson, R. W. (2006). A new geochemical model for the Earth's mantle inferred from ^{146}Sm-^{142}Nd systematics. *Earth and Planetary Science Letters* **250**, 254-268.

Burke, K. C. & Dewey, J. F. (1973). Plume-generated triple junctions: key indicators in

applying plate tectonics to old rocks. *Journal of Geology* **81**, 406-433.

Cambon, P., Joron, J.-L., Bougault, H. & Treuil, M. (1980). Leg 55, Emperor seamounts: trace elements in transitional tholeiities, alkali basalts and hawaiites – mantle homogeneity or heterogeneity and magmatic processes. *Initial Report of the Deep Sea Drilling Project* **55**, 585-597.

Campbell, I. H. (1998). The mantle's chemical structure: insights from the melting products of mantle plumes. In: Jackson, I. (ed.) *The Earth's mantle: Composition, structure and evolution*. Cambridge University Press, 259-310.

Campbell, I. H. & Griffiths, R. W. (1990). Implications of mantle plume structure for the evolution of flood basalts. *Earth and Planetary Science Letters* **99**, 79-93.

Chandrasekharam, D. (1985). Structure and evolution of the western continental margin of India deduced from gravity, seismic, geomagnetic and geochronological studies. *Physics of the Earth and Planetary Interiors* **41**, 186-198.

Chandrasekharam, D., Mahoney, J. J., Sheth, H. C. & Duncan, R. A. (1999). Elemental and Nd-Sr-Pb isotope geochemistry of flows and dikes from the Tapi rift, Deccan flood basalt province, India. *Journal of Volcanology and Geothermal Research* **93**, 111-123.

Chauvel, C., McDonough, W. F., Guille, G., Maury, R. & Duncan, R. A. (1997).

Contrasting old and young volcanism in Rurutu island, Austral chain. *Chemical Geology* **139**, 125-143.

Chauvel, C., Hofmann, A.W. & Vidal, P. (1992). HIMU–EM; the French Polynesian connection. *Earth and Planetary Science Letters* **110**, 99-119.

Chen, C.-Y. & Frey, F. A. (1985). Trace element and isotopic geochemistry of lavas from Haleakala volcano, East Maui, Hawaii: Implications for the origin of Hawaiian basalts. *Journal of Geophysical Research* **90** (B10), 8743-8768.

Chen, C.-Y., Frey, F. A. & Garcia, M. O. (1990). Evolution of alkalic lavas at Haleakala volcano, East Maui, Hawaii: major, trace element, and isotopic constraints. *Contributions to Mineralogy and Petrology* **105**, 197-218.

Chen, C.-Y., Frey, F. A., Rhodes, J. M. & Easton, R. M. (1996). Temporal geochemical evolution of Kilauea volcano: comparison of Hilina and Puna basalt. In: Basu, A. & Hart, S. R. (eds.) *Earth Processes: Reading the Isotopic Code*. *Geophysical Monograph, American Geophysical Union* **95**, 161-181.

Chenet, A.-L., Quidelleur, X., Fluteau, F. & Courtillot, V. (2007). ^{40}K-^{40}Ar Dating of the main Deccan large igneous province: Further evidence of KTB age and short duration. *Earth and Planetary Science Letters* **263**, 1-15.

Chenet, A.-L., Fluteau, F., Courtillot, V., Gérard, M. & Subbarao, K. V. (2008). Determination of rapid Deccan eruptions across the KTB using paleomagnetic secular variation: (I) Results from a 1200m-thick section in the Mahabaleshwar escarpment. *Journal of Geophysical Research* **113**, B04101, pp. 27.

Cheng, Q., Park, K.-H., Macdougall, J. D., Zindler, A., Lugmair, G. W., Staudigel, H., Hawkins, J. & Lonsdale, P. (1987). Isotopic evidence for a hotspot origin of the Louisville seamount chain. In: Keating, B. H. et al. (eds.) *Seamounts, Islands, and Atolls*. *Geophysical Monograph, American Geophysical Union* **43,** 283-296.

Cheng, Q. C., Macdougall, J. D. & Lugmair, G. W. (1993). Geochemical studies of Tahiti and Mehetia, Society island chain. *Journal of Volcanology and Geothermal Research* **55**, 155-184.

Clague, D. A. & Jarrard, R. D. (1973). Tertiary plate motion deduced from the Hawaii-Emperor chain. *The Geological Society of America Bulletin* **84**, 1135-1154.

Clague, D. A. & Frey, F. A. (1980). Trace-element geochemistry of tholeiitic basalts from site 433C, Suiko seamount. *Initial Report of the Deep Sea Drilling Project* **55**, 559-569.

Collier, J. S., Sansom, V., Ishizuka, O., Taylor, R. N., Minshull, T. A. & Whitmarsh, R. B. (2008). Age of Seychelles-India breakup. *Earth and Planetary Science Letters* **272** (1-2), 264-277.

Cotten, J., Le Dez, A., Bau, M., Caroff, M., Maury, R. C., Dulski, P., Fourcade, S., Bohn, M. & Brousse, R. (1995). Origin of anomalous rare-earth element and yttrium enrichments in subaerially exposed basalts: evidence from French Polynesia. *Chemical Geology* **119**, 115-138.

Cottrell, R. D. & Tarduno, J. A. (2003). A Late cretaceous pole for the Pacific plate: Implications for apparent and true polar wander and the drift of hotspots. *Tectonophysics* **362**, 321-333.

Courtillot, V., Besse, J., Vandamme, D., Montigny, R., Jaeger, J.-J. & Cappetta, H. (1986). Deccan flood basalts at the Cretaceous/Tertiary boundary? *Earth and Planetary Science Letters* **80**, 361-374.

Courtillot, V., Féraud, G., Maluski, H., Vandamme, D., Moreau, M. G. & Besse, J. (1988). Deccan flood basalts and the Cretaceous/Tertiary boundary. *Nature* **333**, 843-846.

Courtillot, V., Gallet, Y., Rocchia, R., Féraud, G., Robin, E., Hofmann, C., Bhandari, N. & Ghevariya, Z. G. (2000). Cosmic markers, $^{40}Ar/^{39}Ar$ dating and paleomagnetism of the

KT sections in the Anjar Area of the Deccan large igneous province. *Earth and Planetary Science Letters* **182**, 137-156.

Courtillot, V., Davaille, A., Besse, J. & Stock, J. (2003). Three distinct types of hotspots in the Earth's mantle. *Earth and Planetary Science Letters* **205**, 295-308.

Courtney, R. C. & White, R. S. (1986). Anomalous heat flow and geoid across the Cape Verde Rise: Evidence for dynamic support from a thermal plume in the mantle. *Geophysical Journal of the Royal Astronomical Society* **87**, 815-867.

Cox, K. G. & Hawkesworth, C. J. (1984). Relative Contribution of crust and mantle to flood basalt magmatism, Mahabaleshwar area, Deccan Traps. *Philosophical Transactions of the Royal Society of London* **310**, 627-641.

Cox, K. G. & Hawkesworth, C. J. (1985). Geochemical stratigraphy of the Deccan Traps at Mahabaleshwar, Western Ghats, India, with implications for open system magmatic processes. *Journal of Petrology* **26** (2), 355-377.

Creaser, R. A., Erdmer, P., Stevens, R. A. & Grant, S. L. (1997). Tectonic affinity of Nisutlin and Anvil assemblage strata from Teslin tectonic zone, northern Canadian Cordillera: Constraints from neodymium isotope and geochemical evidence. *Tectonics* **16,** 107-121.

Crookshank, H. (1936). Geology of the northern slopes of the Satpuras between the Morand and the Sher Rivers. *Memoirs of the Geological Survey of India* **66** (2), 173-381.

Dalrymple, G. B. & Clague, D. A. (1976). Age of the Hawaiian-Emperor bend. *Earth and Planetary Science Letters* **31**, 313-329.

Dalrymple, G. B., Clague, D. A. & Lanphere, M. A. (1977). Revised age for Midway volcano, Hawaiian volcanic chain. *Earth and Planetary Science Letters* **37**, 107-116.

Dalrymple, G. B., Clague, D. A., Garcia, M. O. & Bright, S. W. (1981). Petrology and K-Ar ages of dredged samples from Laysan Island and Northampton Bank volcanoes, Hawaiian ridge, and evolution of the Hawaiian-Emperor chain. *The Geological Society of America Bulletin* **92** (6), II 884-II 933.

Davis, J. C. (2002). *Statistics and data analysis in geology, 3rd edition*. John Wiley & Sons, New York, pp. 656.

Davis, A. S., Gray, L. B., Clague, D. A. & Hein, J. R. (2002). The Line Islands revisited: New $^{40}Ar/^{39}Ar$ geochronologic evidence for episodes of volcanism due to lithospheric extension. *Geochemistry Geophysics Geosystems* **3** (3), 10.

Dawson, J. B., Smith, J. V. & Hervig, R. L. (1980). Heterogeneity in upper-mantle lherzolites and harzburgites. *Philosophical Transactions of the Royal Society of London*

A 297, 323-331.

De Carlo, E. H., McMurtry, G. M. & Kim, K. H. (1987). Geochemistry of ferromanganese crusts from the Hawaiian Archipelago — I. Northern survey areas. *Deep Sea Research* **34** (3), 441-467.

Delaney, P. T. & Gartner, A. E. (1997). Physical processes of shallow mafic dike emplacement near the San Rafael Swell, Utah. *The Geological Society of America Bulletin* **109** (9), 1177-1192.

Delaney, P. T., Pollard, D. D., Ziony, J. I. & McKee, E. H. (1986). Field relations between dikes and joints: emplacement processes and paleostress analysis. *Journal of Geophysical Research* **91**, 4920-4938.

Deshmukh, S. S. & Sehgal, M. N. (1988). Mafic dyke swarms in Deccan volcanic province of Madhya Pradesh and Maharashtra. In: Subbarao, K. V. (ed.) *Deccan flood basalts. Memoir of the Geological Society of India* **10**, 323-340.

Dessai, A. G. & Bertrand, H. (1995). The 'Panvel Flexure' along the western Indian continental margin: an extensional fault structure related to Deccan magmatism. *Tectonophysics* **241**, 165-178.

Dessai, A. G. & Viegas, A. A. A. A. (1995). Multi-generation mafic dyke-swarm related to Deccan magmatism, south of Bombay: Implications on the evolution of the western Indian continental margin. *Memoir of the Geological Society of India* **33**, 435-451.

Devey, C. W. & Lightfoot, P. C. (1986). Volcanological and tectonic control of stratigraphy and structure in the western Deccan Traps. *Bulletin of Volcanology* **48**, 195-207.

Devey, C. W. & Stephens, W. E. (1991). Tholeiitic dykes in the Seychelles and the original spatial extent of the Deccan. *Journal of the Geological Society of London* **148**, 979-983.

Devey, C. W., Albarède, F., Cheminée, J.-L., Michard, A., Mühe, R. & Stoffers, P. (1990). Active submarine volcanism on the Society hotspot swell (west Pacific): A geochemical study. *Journal of Geophysical Research* **95**, 5049–5066.

Devey, C. W., Lackschewitz, K. S., Mertz, D. F., Bourdon, B., Cheminée, J.-L., Dubois, J., Guivel, C., Hékinian, R., Stoffers, P. (2003). Giving birth to hotspot volcanoes: Distribution and composition of young seamounts from the seafloor near Tahiti and Pitcairn islands. *Geology* **31**, 395-398.

Duncan, R. A. (1990). The volcanic record of the Réunion hot-spot. In: Duncan, R. A., Backman, J., Peterson, L. C. et al. (eds.) *Proceedings of the Ocean Drilling Program, Initial Reports* **115**. College Station, Texas (Ocean Drilling Program), 3-10.

Duncan, R. A. & Pyle, D. G. (1988). Rapid eruption of the Deccan flood basalts at the Cretaceous/Tertiary boundary. *Nature* **333**, 841-843.

Dupuy, C., Vidal, P., Maury, R. C. & Guille, G. (1993). Basalts from Mururoa, Fangataufa, and Gambier islands (French Polynesia); geochemical dependence on the age of the lithosphere. *Earth and Planetary Science Letters* **117**, 89-100.

Duke, J. M. (1976). Distribution of the period four transition elements among olivine, calcic clinopyroxene and mafic silicate liquid; experimental results. *Journal of Petrology* **17** (4), 499-521.

Dyment, J. (1998). Evolution of the Carlsberg Ridge between 60 and 45 Ma: ridge propagation, spreading asymmetry, and the Deccan Reunion hotspot. *Journal of Geophysical Research* **103***,* 24067-24084.

Eales, H. V., Marsh, J. S. & Cox, K. G. (1984). The Karoo igneous province: an introduction. *Special Publication of the Geological Society of South Africa* **13**, 1-26.

Eason, D. & Sinton, J. (2006). Origin of high-Al N-MORB by fractional crystallization in

the upper mantle beneath the Galápagos Spreading Center. *Earth and Planetary Science Letters* **252**, 423-436.

Edsall, D. W. (1976). Trace elements in tephra as indicator of magmatic composition in the Aleutian arc. *The Geological Society of America Bulletin* **87**, 1269-1272.

Eggins, S. M., Woodhead, J. D., Kinsley, L. P. J., Mortimer, G. E., Sylvester, P., McCulloch, M. T., Hergt, J. M. & Handler, M. R. (1997). A simple method for the precise determination of 40 trace elements in geological samples by ICP-MS using enriched isotope internal standardisation. *Chemical Geology* **134**, 311-326.

Eldholm, O. & Coffin, M. F. (2000). Large igneous provinces and plate tectonics. In: Richards, M. A., Gordon, R. G. & van der Hilst, R. D. (eds.) *The History and Dynamics of Global Plate Motions*. *Geophysical Monograph, American Geophysical Union* **121**, 309-326.

Epp, D. (1978). Age and tectonic relationships among volcanic chains on the Pacific plate. Ph.D. dissertation, University of Hawai‘i, Honolulu.

Ernst, R. E. & Buchan, K. L. (1997). Giant radiating dyke swarms: Their use in identifying pre-Mesozoic large igneous provinces and mantle plumes. In: Mahoney, J. J. & Coffin, M. F. (eds.) *Large Igneous Provinces: Continental, Oceanic, and Planetary Flood Volcanism. Geophysical Monograph, American Geophysical Union* **100**, 297-333.

Ernst, R. E., Grosfils, E. B. & Mege, D. (2001). Giant dyke swarms on Earth, Venus, and Mars. *Annual Reviews of Earth and Planetary Sciences* **29**, 489-534.

Fisk, M. R., Upton B. G. J., Ford C. E. & White W. M. (1988). Geochemical and experimental study of the genesis of magmas of Réunion Island, Indian Ocean. *Journal of Geophysical Research* **B93**, 4933-4950.

Fitton, J. G., Saunders, A. D., Norry, M. J., Hardarson, B. S. & Taylor, R. N. (1997). Thermal and chemical structure of the Iceland plume. *Earth and Planetary Science Letters* **153** (3-4), 197-208.

Foulger, J. R. & Anderson, D. L. (2005). A cool model for the Iceland hotspot. *Journal of Volcanology and Geothermal Research* **141**, 1-22.

Frey, F. A., Garcia, M. O. & Roden, M. F. (1994). Geochemical characteristics of Koolau volcano, implications of intershield geochemical differences among Hawaiian volcanoes. *Geochimica et Cosmochimica Acta* **58**, 1441-1462.

Galer, S. J. G. (1999). Optimal double and triple spiking for high precision lead isotopic measurement. *Chemical Geology* **157** (3-4), 255-274.

Govindaraju, K. (1994). 1994 compilation of working values and sample descriptions for

383 geostandards. *Geostandards Newsletter* **18**, 1-158.

Green, T. H., Green, D. H. & Ringwood, A. E. (1967). The origin of high-alumina basalts and their relationships to quartz tholeiites and alkali basalts. *Earth and Planetary Science Letters* **2**, 41-51.

Gudmundsson, A. & Marinoni, L. B. (2002). Geometry, emplacement, and arrest of dykes. *Annales Tectonicae* **13**, 71-92.

Gwalani, L. G., Rock, N. M. S., Chang, W.-J., Fernandez, S., Allègre, C. J. & Prinzhofer, A. (1993). Alkaline and carbonatites of Amba Dongar and adjacent areas, Deccan igneous province, Gujarat, India. 1. Geology, petrography and petrochemistry. *Mineralogy and Petrology* **47**, 219-253.

Gwalani, L. G., Fernandez, S., Karanth, R. V., Demény, A., Chang, W.-J. & Avasia, R. K. (1995). Alkaline and tholeiitic dyke swarm associated with Amba Dongar and Phenai Mata complexes, Chhota Udaipur alkaline sub-province, Western India. *Memoir of the Geological Society of India* **33**, 391-423.

Haase, K. M., Stoffers, P. & Garbe-Schönberg, C. D. (1997). The petrogenetic evolution of lavas from Easter Island and neighbouring seamounts, near-ridge hotspot volcanoes in the SE Pacific. *Journal of Petrology* **38**, 785-813.

Hall, L. S., Mahoney, J. J., Sinton, J. M. & Duncan, R. A. (2006). Spatial and temporal distribution of a C-like asthenospheric component in the Rano Rahi seamount field, East Pacific Rise, 15º-19ºS. *Geochemistry Geophysics Geosystems* **7**, Q03009.

Hanan, B. B. & Graham, D. W. (1996). Lead and helium isotope evidence from oceanic basalts for a common deep source of mantle plumes. *Science* **272**, 991-995.

Harris, A. C., Kincaid, C. & Kelley, K. A. (2007). Constraints on structure and melting of heterogeneous plumes from laboratory experiments with three components. *Eos Transactions, American Geophysical Union,* **88** (52), Fall Meeting Supplement, Abstract U14A-02.

Hart, S. R., Hauri, E. H., Oschmann, L. A. & Whitehead, J. A. (1992). Mantle plumes and entrainment: isotopic evidence. *Science* **256**, 517-520.

Hauri, E. H., Lassiter, J. C. & DePaolo, D. J. (1996). Osmium isotope systematics of drilled lavas from Mauna Loa, Hawaii. *Journal of Geophysical Research* **101**, 11793-11806.

Hawkins, J. W. (1973). Louisville ridge. *Eos, Transactions, American Geophysical Union* **54**, 1212.

Hawkins, J. W., Lonsdale, P. F. & Batiza, R. (1987). Petrologic evolution of the Louisville seamount chain. In: Keating, B. H. et al. (eds.) *Seamounts, Islands, and Atolls*. *Geophysical Monograph, American Geophysical Union* **43**, 235-254.

Hayes, D. E. & Ewing, M. (1971). The Louisville ridge – A possible extension of the Eltanin fracture zone. In: Reid, J. L. (ed.) *Antarctic Oceanology I, Antarctic Research, American Geophysical Union* **15**, 223-228.

Hemond, C., Devey, C. W. & Chauvel, C. (1994). Source compositions and melting processes in the Society and Austral plumes (South Pacific Ocean); element and isotope (Sr, Nd, Pb, Th) geochemistry. *Chemical Geology* **115**, 7-45.

Herzberg, C. (2004). How Many Hotspots are on Present-day Earth, and are all Plumes hot? *Eos Transactions, American Geophysical Union,* **85** (47), Fall Meeting Supplement, Abstract V43G-04.

Hirschmann, M. M., Kogiso, T., Baker, M. B. & Stolper, E. M. (2003). Alkalic magmas generated by partial melting of garnet pyroxenite. *Geology* **31** (6), 481-484.

Hofmann, A. W. & White, W. M. (1982). Mantle plumes from ancient oceanic crust. *Earth and Planetary Science Letters* **57**, 421-436.

Hofmann, A. W., Jochum, K. P., Seufert, H. M. & White W. M. (1986). Nb and Pb in oceanic basalts: new constraints on mantle evolution. *Earth and Planetary Science Letters* **79**, 33-45.

Hofmann, C., Féraud, G. & Courtillot, V. (2000). $^{40}Ar/^{39}Ar$ dating of mineral separates and whole rocks from the Western Ghats lava pile: further constraints on duration and age of the Deccan traps. *Earth and Planetary Science Letters* **180**, 13-27.

Hole, M. J., Saunders, A. D., Marriner, G. F. & Tarney, J. (1984). Subduction of pelagic sediments: implications for the origin of Ce-anomalous basalts from the Mariana Islands. *Journal of the Geological Society of London* **141** (3), 453-472.

Hooper, P. R. (1990). The timing of crustal extension and the eruption of continental flood basalts. *Nature* **345**, 246-249.

Hooper, P. R. (1997). The Columbia River flood basalt province: Current status. In: Mahoney, J. J. & Coffin, M. F. (eds.) *Large igneous provinces: continental, oceanic, and planetary flood volcanism. Geophysical Monograph, American Geophysical Union* **100**, 1-27.

Hooper, P. R. (1999). The Deccan Traps. In: Subbarao, K. V. (ed.) *Deccan Volcanic Province. Memoir of the Geological Society of India* **43**, 153-165.

Hooper, P. R. & Widdowson, M. (submitted). West Coast dike-flow correlation and the timing of the final phases of the Deccan flood basalt province, India. *Journal of the Mineralogical Society of India*.

Hoskin, P. W. O. & Schaltegger, U. (2003). The composition of zircon and igneous and metamorphic petrogenesis. *Reviews in Mineralogy and Geochemistry* **53**, 27-62.

Huang, S., Regelous, M., Thordarson, T. & Frey, F. A. (2005). Petrogenesis of lavas from Detroit seamount: Geochemical differences between Emperor chain and Hawaiian volcanoes. *Geochemistry Geophysics Geosystems* **6**, Q01L06.

Humphries, S. E. & Thompson, G. (1978). Hydrothermal alteration of oceanic basalts by seawater. *Geochimica et Cosmochimica Acta* **42**, 107-125.

Ida, Y. (1999). Effects of the crustal stress on the growth of dykes: Conditions of intrusion and extrusion of magma. *Journal of Geophysical Research* **104**, 17897-17909.

Ingle, S., Mahoney, J. J., Sato, H., Coffin, M. F., Kimura, J.-I., Hirano, N. & Nakanishi, M. (2007). Depleted mantle wedge and sediment fingerprint in unusual basalts from the Manihiki Plateau, central Pacific Ocean. *Geology* **35** (7), 595-598.

Ingram, B. L., Hein, J. R. & Farmer, G. L. (1990). Age determinations and growth rates of Pacific ferromanganese deposits using strontium isotopes. *Geochimica et Cosmochimica Acta* **54**, 1709-1721.

Irvine, T. N. & Baragar, W. R. A. (1971). A guide to the chemical classification of the common volcanic rocks. *Canadian Journal of Earth Sciences* **8**, 523-548.

Ito, G. & Mahoney, J. J. (2005a). Flow and melting of a heterogeneous mantle: 1. Method and importance to the geochemistry of ocean island and mid-ocean ridge basalts. *Earth and Planetary Science Letters* **230** (1-2), 29-46.

Ito, G. & Mahoney, J. J. (2005b). Flow and melting of a heterogeneous mantle: 2. Implications for a chemically nonlayered mantle. *Earth and Planetary Science Letters* **230** (1-2), 47-63.

Jackson, M. C., Frey, F. A., Garcia, M. O. & Wilmoth, R. A. (1999). Geology and geochemistry of basaltic lava flows and dikes from the Trans-Koolau tunnel, Oahu, Hawaii. *Bulletin of Volcanology* **60**, 381-401.

Janney, P. E., Macdougall, J. D., Natland, J. H. & Lynch, M. A. (2000). Geochemical evidence from the Pukapuka volcanic ridge system for a shallow enriched mantle domain beneath the South Pacific superswell. *Earth and Planetary Science Letters* **181**, 47-60.

Jay, A. E. & Widdowson, M. (2008). Stratigraphy, structure and volcanology of the SE Deccan continental flood basalt province: implications for eruptive extent and volumes. *Journal of the Geological Society* **165**, 177-188.

Jenner, G. A., Longerich, H. P., Jackson, S. E. & Fryer, B. J. (1990). ICP-MS — A powerful tool for high-precision trace-element analysis in earth sciences: Evidence from analysis of selected USGS reference samples. *Chemical Geology* **83**, 133-148.

Jerram, D. A. & Widdowson, M. (2005). The anatomy of continental flood basalt provinces: geological constraints on the processes and products of flood volcanism. *Lithos* **79** (3-4), 385-405.

Johnson, D. M., Hooper, P. R. & Conrey, R. M. (1999). XRF analysis of rocks and minerals for major and trace elements on a single low dilution Li-tetraborate fused bead. In: Clemens, B. et al. (eds.) *Advances in X-ray analysis - Proceedings of the Denver X-ray conference* **41**, 843-867.

Jourdan, F., Féraud, G., Bertrand, H., Watkeys, M. K., Kampunzu, A. B. & Le Gall, B. (2006). Basement control on dyke distribution in large igneous provinces: Case study of the Karoo triple junction. *Earth and Planetary Science Letters* **241**, 307-322.

Jurdy, D. M. (1978). An alternative model for early Tertiary absolute plate motions. *Geology* **6**, 469-472.

Kaila, K. L. (1988). Mapping the thickness of Deccan Trap flows in India from DSS studies and inferences about a hidden Mesozoic basin in the Narmada-Tapti region. In: Subbarao, K. V. (ed.) *Deccan Flood Basalts. Memoir of the Geological Society of India* **10**, 91-116.

Keller, R. A., Fish, M. R. & White, W. M. (2000). Isotopic evidence for Late Cretaceous plume-ridge interaction at the Hawaiian hotspot. *Nature* **405**, 673-676.

Kellogg, J. B., Jacobsen, S. B. & O'Connell, R. J. (2004). Mantle isotopic heterogeneity: The FOZO's in the pudding. *Eos Transactions, American Geophysical Union* **85** (17), Joint Assembly Supplement, Abstract V43A-12.

Kent, R. W., Pringle, M. S., Müller, R. D., Saunders, A. D. & Ghose, N. C. (2002). $^{40}Ar/^{39}Ar$ geochronology of the Rajmahal basalts, India, and their relationship to the Kerguelen Plateau. *Journal of Petrology* **43**, 1141-1153.

King, S. D. & Anderson, D. L. (1995). An alternative mechanism of flood basalt formation. *Earth and Planetary Science Letters* **136**, 269-279.

Knaack, C., Cornelius, S. B. & Hooper, P. R. (1994). Trace element analyses of rocks and minerals by ICP-MS. *Technical notes, GeoAnalytical Lab, Washington State University*. Pullman, USA.

Koppers, A. A. P., Duncan, R. A. & Steinberger, B. (2004). Implications of a nonlinear $^{40}Ar/^{39}Ar$ age progression along the Louisville seamount trail for models of fixed and moving hot spots. *Geochemistry Geophysics Geosystems* **5**, Q06L02.

Koppers, A. A. P., Staudigel, H., Phipps Morgan, J. & Duncan, R. A. (2007a). Nonlinear $^{40}Ar/^{39}Ar$ age systematics along the Gilbert Ridge and Tokelau Seamount Trail and the timing of the Hawaii-Emperor Bend. *Geochemistry Geophysics Geosystems* **8,** Q06L13.

Koppers, A. A. P., Staudigel, H. & Konter, J. (2007b). Constraining absolute plate motion by $^{40}Ar/^{39}Ar$ Age dating and geochemical fingerprinting of linear volcanic chains. *Eos, Transactions, American Geophysical Union* **88** (52), Fall Meeting Supplement, Abstract U13A-0869.

Krishnamacharlu, T. (1972). Dykes around Dadiapada, Broach district, Gujarat. In: Aswathanarayana, U. (ed.) *Proceedings of symposium on Deccan Trap and other flood eruptions (Sagar, India). Bulletin of Volcanology* **35**, 947-956.

Krishnamurthy, P. & Cox, K. G. (1977). Picrite basalts and related lavas from the Deccan Traps of Western India. *Contributions to Mineralogy and Petrology* **62** (1), 53-75.

Krishnamurthy, P. & Cox, K. G. (1980). A potassium-rich alkalic suite from the Deccan Traps, Rajpipla, India. *Contributions to Mineralogy and Petrology* **73**, 179-189.

Kurz, M. D., Curtice, J., Lott III, D. E. & Solow, A. (2004). Rapid helium isotopic variability in Mauna Kea shield lavas from the Hawaiian Scientific Drilling Project. *Geochem. Geophys. Geosystems* **5**, Q04G14.

Larson, R. L. & Chase, C. E. (1972). Late Mesozoic evolution of the western Pacific Ocean. *The Geological Society of America Bulletin* **83**, 3627-3644.

Lassiter, J. C. & Hauri, E. H. (1998). Osmium-isotope variations in Hawaiian lavas: Evidence for recycled oceanic lithosphere in the Hawaiian plume. *Earth and Planetary Science Letters* **164**, 483-496.

Lassiter, J. C., DePaolo, D. J. & Tatsumoto, M. (1996). Isotopic evolution of Mauna Kea Volcano: results from the initial phase of the Hawaii Scientific Drilling Project. *Journal of Geophysical Research* **101**, 11769-11780.

Lassiter, J. C., Blichert-Toft, J., Hauri, E. H. & Barsczus, H. G. (2003). Isotope and trace element variations in lavas from Raivavae and Rapa, Cook-Austral islands: constraints on the nature of HIMU- and EM-mantle and the origin of mid-plate volcanism in French Polynesia. *Chemical Geology* **202**, 115-138.

Le Bas, M. J., Le Maitre, R. W., Streckeisen, A. & Zanettin, B. (1986). A chemical classification of volcanic rocks on the total alkali–silica diagram. *Journal of Petrology* **27**, 745-750.

Lightfoot, P. C. & Hawkesworth, C. J. (1988). Origin of Deccan Trap lavas: evidence from combined trace element and Sr-, Nd- and Pb-isotope studies. *Earth and Planetary Science Letters* **91**, 89-104.

Lightfoot, P. C., Hawkesworth, C. J. & Sethna, S. F. (1987). Petrogenesis of rhyolites and trachytes from the Deccan Trap: Sr, Nd and Pb isotope and trace element evidence. *Contributions to Mineralogy and Petrology* **95**, 44-54.

Lightfoot, P. C., Hawkesworth, C. J., Devey, C. W., Rogers, N. W. & Van Calsteren, P. W. C. (1990). Source and differentiation of Deccan Trap lavas: implications of geochemical and mineral chemical variations. *Journal of Petrology* **31** (5), 1165-1200.

Lin, S.-C. & van Keken, P. E. (2005). Multiple volcanic episodes of flood basalts caused by thermochemical mantle plumes. *Nature* **436**, 250-252.

Lin, S.-C. & van Keken, P. E. (2006). Dynamics of thermochemical plumes: 2. Complexity of plumes structures and implications for the mapping of mantle plumes. *Geochemistry Geophysics Geosystems* **7**, Q03003.

Lonsdale, P. (1988). Geography and history of the Louisville hotspot chain in the Southwest Pacific. *Journal of Geophysical Research* **93** (B4), 3078-3104.

Lonsdale, P. (1997). An incomplete geologic history of the south-west Pacific Basin. *The Geological Society of America Abstracts with Programs* **29** (5), 4574.

Ludden, J. N. & Thompson, G. (1979). An evaluation of the behavior of the rare earth elements during the weathering of seafloor basalt. *Earth and Planetary Science Letters* **43**, 85-92.

Lyons, S. N., Sandwell, D. T. & Smith, W. H. F. (2000). Three-dimensional estimation of elastic thickness under the Louisville Ridge. *Journal of Geophysical Research* **105** (B6), 13239-13252.

Macdonald, G. A. (1968). Composition and origin of Hawaiian lavas. *The Geological Society of America Memoir* **116**, 477-522.

Mahoney, J. J. (1984). Isotopic and chemical studies of the Deccan and Rajmahal traps, India: mantle sources and petrogenesis. Ph.D. dissertation. University of California, San Diego.

Mahoney, J. J. (1987). An isotopic survey of Pacific oceanic plateaus: Implications for their nature and origin. In: Keating, B. H. et al. (eds.) *Seamounts, Islands, and Atolls*. *Geophysical Monograph, American Geophysical Union* **43,** 207-220.

Mahoney, J. J. (1988). Deccan Traps. In: Macdougall, J. D. (ed.) *Continental Flood Basalts*. Kluwer Academic Publishers, 151-194.

Mahoney, J. J. & Spencer, K. J. (1991). Isotopic evidence for the origin of the Manihiki and Ontong Java oceanic plateaus. *Earth and Planetary Science Letters* **104**, 196-210.

Mahoney, J. J., Macdougall, J. D., Lugmair, J. W., Murali, A. V., Sankar Das, M. & Gopalan, K. (1982). Origin of the Deccan Trap flows at Mahabaleshwar inferred from Nd and Sr isotopic and chemical evidence. *Earth and Planetary Science Letters* **60**, 47-60.

Mahoney, J. J., Macdougall, J. D., Lugmair, G. W., Gopalan, K. & Krishnamurthy, P. (1985). Origin of contemporaneous tholeiitic and K-rich alkalic lavas: a case study from the northern Deccan Plateau, India. *Earth and Planetary Science Letters* **72**, 39-53.

Mahoney, J. J., Natland, J. H., White, W. M., Poreda, R., Bloomer, S. H., Fisher, R. L. & Baxter, A. N. (1989). Isotopic and geochemical provinces of the western Indian Ocean spreading centers. *Journal of Geophysical Research* **94**, 4033-4052.

Mahoney, J. J., Nicollet, C. & Dupuy, C. (1991). Madagascar basalts: tracking oceanic and continental sources. *Earth and Planetary Science Letters* **104**, 350-363.

Mahoney, J. J., Storey, M., Duncan, R. A., Spencer, K. J. & Pringle, M. S. (1993). Geochemistry and age of the Ontong Java Plateau. In: Pringle, M. S. et al. (eds.) *The Mesozoic Pacific. Geology, tectonics, and volcanism. Geophysical Monograph, American Geophysical Union* **77**, 233-261.

Mahoney, J. J., Frei, R., Tejada, M. L. G., Mo, X. X., Leat, P. T. & Nägler, T. F. (1998). Tracing the Indian Ocean mantle domain through time: Isotopic results from old West Indian, East Tethyan, and South Pacific seafloor. *Journal of Petrology* **39** (7), 1285-1306.

Mahoney, J. J., Sheth, H. C., Chandrasekharam, D. & Peng, Z. X. (2000). Geochemistry of flood basalts of the Toranmal section, Northern Deccan Traps, India: Implications for regional Deccan stratigraphy. *Journal of Petrology* **41** (7), 1099-1120.

Mahoney, J. J., Duncan, R. A., Khan, W., Gnos, E. & McCormick, G. R. (2002). Cretaceous volcanic rocks of the South Tethyan suture zone, Pakistan: implications for the Réunion hotspot and Deccan Traps. *Earth and Planetary Science Letters* **203** (1), 295-310.

Mahoney, J. J., Duncan, R. A., Tejada, M. L. G., Sager, W. W. & Bralower, T. J. (2005). Jurassic-Cretaceous boundary age and mid-ocean-ridge–type mantle source for Shatsky Rise. *Geology* **33** (3), 185-188.

Maaløe, S. & Aoki, K.-I. (1977). The major element composition of the upper mantle estimated from the composition of lherzolites. *Contributions to Mineralogy and Petrology* **63** (2), 161-173.

Marske, J. P., Pietruszka, A. J., Weis, D., Garcia, M. O. & Rhodes, J. M. (2007). Rapid passage of a small-scale mantle heterogeneity through the melting regions of Kilauea and Mauna Loa Volcanoes. *Earth and Planetary Science Letters* **259**, 34-50.

Matsuhisa, Y., Bhattacharya, S. K., Gopalan, K., Mahoney, J. J. & Macdougall, J. D. (1986). Oxygen isotope evidence for crustal contamination in Deccan basalts. *Terra Cognita* **6**, 181.

McKenzie, D. & Sclater, J. G. (1971). The evolution of the Indian Ocean since the Late Cretaceous. *Geophysical Journal International* **24** (5), 437-528.

McKenzie, D. & O'Nions, R. K. (1991). Partial melt distributions from inversion of rare Earth element concentrations. *Journal of Petrology* **32**, 1021-1091.

Melluso, L., Beccaluva, P., Brotzu, A., Gregnanin, A., Gupta, A. K., Morbidelli, L. & Traversa, G. (1995). Constraints on the mantle sources of the Deccan Traps from the petrology and geochemistry of the basalts of Gujarat state (Western India). *Journal of Petrology* **36**, 1393-1432.

Melluso, L., Sethna, S. F., Morra, V., Khateeb, A. & Javeri, P. (1999). Petrology of the mafic dyke swarm of the Tapti River in the Nandurbar area (Deccan volcanic province). In: Subbarao, K. V. (ed.) *Deccan Volcanic Province. Memoir of the Geological Society of India* **43**, 735-755.

Melluso, L., Sethna, S. F., D'Antonio, M., Javeri, P. & Bennio, L. (2002). Geochemistry and petrogenesis of sodic and potassic mafic alkaline rocks in the Deccan Volcanic Province, Mumbai Area (India). *Mineralogy and Petrology* **74**, 323-342.

Menard, H. W. (1964). *Marine geology of the Pacific*. McGraw-Hill, New York, pp. 271.

Menard, H. W., Smith, S. M. & Chase, T. E. (1964). Guyots in the Southwestern Pacific basin. *The Geological Society of America Bulletin* **75**, 145-148.

Menzies, M. A. & Seyfried, W. E. (1979). Basalt-seawater interaction: trace element and strontium isotopic variations in experimentally altered glassy basalt. *Earth and Planetary Science Letters* **44**, 463-472.

Mitchell, C. & Widdowson, M. (1991). A geological map of the southern Deccan Traps, India and its structural implications. *Journal of the Geological Society of London* **148**, 495-505.

Mohan, M. (1985). Geohistory analysis of Bombay High region. *Marine and Petroleum Geology* **2**, 350-360.

Molnar, P. T., Atwater, T., Mammerickx, J. & Smith, S. M. (1975). Magnetic anomalies, bathymetry and the tectonic evolution of the South Pacific since the Late Cretaceous. *Geophysical Journal of the Royal Astronomical Society* **40**, 383-420.

Montelli, R., Nolet, G., Dahlen, F. A., Masters, G., Engdahl, E. R. & Hung, S.-H. (2004). Finite-Frequency Tomography Reveals a Variety of Plumes in the Mantle. *Science* **303**, 338-343.

Morgan, W. J. (1971). Convection plumes in the lower mantle. *Nature* **230**, 42-43.

Morgan, W. J. (1972). Plate motions and deep mantle convection. *Geological Society of America Memoir* **132**, 7-22.

Morgan, W. J. (1981). Hotspot tracks and the opening of the Atlantic and Indian oceans. In: Emiliani, C. (ed.) *The Sea*, *vol. 7. The Oceanic Lithosphere*. Wiley-Interscience, New York, 443-487.

Mortimer, N. & Parkinson, D. (1996). Hikurangi Plateau: a Cretaceous large igneous province in the southwest Pacific Ocean. *Journal of Geophysical Research* **101**, 687-696.

Mortimer, N., Hoernle, K., Hauff, F., Palin, J. M., Dunlap, W. J., Werner, R. & Faure, K. (2006). New constraints on the age and evolution of the Wishbone Ridge, southwest Pacific Cretaceous microplates, and Zealandia–West Antarctica breakup. *Geology* **34** (3), 185-188.

Müller, R. D., Roest, W. R., Royer, J.-Y., Gahagan, L. M., Sclater, J. G. (1997). Digital isochrons of the world's ocean floor. *Journal of Geophysical Research* **102** (B2), 3211-3214.

Murali, A. V., Sankar Das, M. & Aswathanarayana, U. (1976). Mount Girnar complex, western India, as a possible continental analog of Iceland. *25th International Geological Congress, Sydney, Section* **10**, 423.

Nakamura, Y. & Tatsumoto, M. (1988). Pb, Nd, and Sr isotopic evidence for a multicomponent source for rocks of Cook-Austral islands and heterogeneities of mantle plumes. *Geochimica et Cosmochimica Acta* **52**, 2909-2924.

Neal, C. R. (2001). The Interior of the Moon: the presence of garnet in the primitive, deep lunar mantle. *Journal of Geophysical Research* **106**, 27865-27885.

Neal, C. R., Mahoney, J. J., Kroenke, L. W., Duncan, R. A. & Petterson, M. G. (1997). The Ontong Java Plateau. In: Mahoney, J. J. & Coffin, M. F. (eds.) *Large igneous provinces: Continental, oceanic, and planetary flood volcanism. Geophysical Monograph, American Geophysical Union* **100**, 183-216.

Newsom, H. E., White, W. M., Jochum K. P. & Hofmann, A. W. (1986). Siderophile and chalcophile element abundances in oceanic basalts, Pb isotope evolution and growth of the Earth's core. *Eearth and Planetary Science Letters* **80**, 299-313.

Norrish, K. & Chappell, B. W. (1977). X-ray Fluorescence spectrometry. In: Zussman, J. (ed.) *Physical Methods in Determinative Mineralogy*, *2nd edition*. Academic Press, New York, 201-272.

Norrish, K. & Hutton, J. (1977). An accurate X-ray spectrographic method for the analysis of a wide range of geological samples. *Geochimica et Cosmochimica Acta* **33**, 431-441.

O'Hara, M. J. (1968). The bearing of phase equilibria studies in synthetic and natural systems on the origin and evolution of basic and ultrabasic rocks. *Earth-Science Reviews* **4**, 69-134.

O'Hara, M. J., Richardson, S. W. & Wilson, G. (1971). Garnet-peridotite stability and occurrence in crust and mantle. *Contributions to Mineralogy and Petrology* **32** (1), 48-68.

Pal, P. C. & Bhimasankaran, V. L. S. (1976). Tectonics of the Narmada-Son-Brahmaputra Lineament. *Miscellaneous Publications of the Geological Survey of India* **34** (2), 133-140.

Pallister, J. S. (1981). Structure of the sheeted dike complex of the Samail ophiolite near Ibra, Oman. *Journal of Geophysical Research* **86** (B4), 2661-2672.

Pande, K. (2002). Age and duration of the Deccan Traps, India: a review of radiometric and paleomagnetic constraints. *Proceedings of the Indian Academy of Sciences (Earth and Planetary Sciences)* **111**, 115-123.

Pande, K., Pattanayak, S. K., Subbarao, K. V., Navaneethakrishnan, P. & Venkatesan, T. R. (2004). ^{40}Ar-^{39}Ar age of a lava flow from the Bhimashankar Formation, Giravali Ghat, Deccan Traps. *Proceedings of the Indian Academy of Sciences (Earth and Planetary Sciences)* **113** (4), 755-758.

Paul, D. K., Potts, R. J., Rex, D. C. & Beckinsale, R. D. (1977). Geochemical and petrological study of the Girnar igneous complex, Deccan volcanic province, India. *The Geological Society of America Bulletin* **88**, 227-234.

Paul, D. K., Ray, A., Das, B., Patil, S. K. & Biswas, S. A. (2008). Petrology, geochemistry and paleomagnetism of the earliest magmatic rocks of Deccan Volcanic Province, Kutch, Northwest India. *Lithos* **102** (1-2), 237-259.

Peate, D. W. (1997). The Paraná-Etendeka Province. In: Mahoney, J. J. & Coffin, M. F. (eds.) *Large Igneous Provinces: Continental, Oceanic, and Planetary Flood Volcanism. Geophysical Monograph, American Geophysical Union* **100**, 217-245.

Peccerillo, A. & Taylor, S. R. (1976). Geochemistry of Eocene calc-alkaline volcanic rocks from the Kastamonu area, Northern Turkey. *Contributions to Mineralogy and Petrology* **58**, 63-81.

Peng, Z. X. (1998). Geochemical studies of the northwestern, central, and northeastern Deccan Traps, India: Sources, petrogenesis, and relations to southwestern Deccan stratigraphy. Ph.D. dissertation, University of Hawai‘i, Honolulu.

Peng, Z. X. & Mahoney, J. J. (1995). Drillhole lavas from the northwestern Deccan Traps, and the evolution of Réunion hotspot mantle. *Earth and Planetary Science Letters* **134**, 169-185.

Peng, Z. X., Mahoney, J. J., Hooper, P., Harris, C. & Beane, J. (1994). A role for lower continental crust in flood basalt genesis? Isotopic and incompatible element study of the

lower six formations of the Western Ghats Traps. *Geochimica et Cosmochimica Acta* **58**, 267-288.

Peng, Z. X., Mahoney, J. J., Hooper, P. R., Macdougall, J. D. & Krishnamurthy, P. (1998). Basalts of the northeastern Deccan Traps, India: Isotopic and elemental geochemistry and relation to southwestern Deccan stratigraphy. *Journal of Geophysical Research* **103** (B12), 29843-29865.

Pietruszka, A. P. & Garcia, M. O. (1999). A rapid fluctuation in the mantle source and melting history of Kilauea volcano inferred from the geochemistry of its historical summit lavas (1790-1982). *Journal of Petrology* **40**, 1321-1342.

Pilet, S., Hernandez, J., Sylverster, P. & Poujol, M. (2005). The metasomatic alternative for ocean island basalt heterogeneity. *Earth and Planetary Science Letters* **236**, 148-166.

Powar, K. B. (1981). Lineament fabric and dyke pattern in the western part of the Deccan Volcanic Province. *Memoir of the Geological Society of India* **3**, 45-57.

Puzankov, Y. M. & Bobrov, V. A. (1997). Geochemistry of the volcanic rocks from Easter and Sala y Gomez islands. *Geochemistry International* **35**, 609-619.

Pyle, D. G., Christie, D. M., Mahoney, J. J. & Duncan, R. A. (1995). Geochemistry and geochronology of ancient southeast Indian and southwest Pacific seafloor. *Journal of Geophysical Research* **100** (B11), 22261-22282.

Radhakrishna, T., Dallmeyer, R. D. & Joseph, M. (1994). Palaeomagnetism and ^{36}Ar=^{40}Ar vs. ^{39}Ar=^{40}Ar isotope correlation ages of dyke swarms in central Kerala, India: Tectonic implications. *Earth and Planetary Science Letters* **121**, 213-226.

Raja Rao, C. S., Sahasrabudhe, Y. S., Deshmukh, S. S. & Raman, R. (1978). Distribution, structure and petrography of the Deccan Trap, India. *Report of the Geological Survey of India*, pp. 43.

Raju, A. T. R. (1968). Geological evolution of Assam and Cambay Tertiary basins of India. *American Association of Petroleum Geologists Bulletin* **52**, 2422-2437.

Raval, U. & Veeraswamy, K. (2003). India-Madagascar separation: Breakup along a pre-existing mobile belt and chipping of the craton. *Gondwana Research* **6**, 467-485.

Ravizza, G. & Peucker-Ehrenbrink, B. (2003). Chemostratigraphic evidence of Deccan volcanism from the marine osmium isotope record. *Science* **302**, 1392-1395.

Ray, J. S. & Shuckla, P. N. (2004). Trace element geochemistry of Amba Dongar carbonatite complex, India: Evidence for fractional crystallization and silicate-carbonate melt immiscibility. *Journal of Earth System Science* **113** (4), 519-531.

Ray, R., Sheth, H. C. & Mallik, J. (2007). Structure and emplacement of the Nandurbar-Dhule mafic dyke swarm, Deccan Traps, and the tectonomagmatic evolution of flood basalts. *Bulletin of Volcanology* **69** (5), 537-551.

Ray, R., Shukla, A. D., Sheth, H. C., Ray, J. S., Duraiswami, R. A., Vanderkluysen, L., Rautela, C. M. & Mallik, J. (2008). Highly heterogeneous Precambrian basement under the central Deccan Traps, India: Direct evidence from xenoliths in dykes. *Gondwana Research* **13**, 375-385.

Regelous, M., Hofmann, A. W., Abouchami, W. & Galer, S. J. G. (2003). Geochemistry of lavas from the Emperor seamounts, and geochemical evolution of Hawaiian magmatism from 85 to 42 Ma. *Journal of Petrology* **44**, 113-140.

Reiners, P. W. & Nelson, B. K. (1998). Temporal-compositional-isotopic trends in rejuvenated-stage magmas of Kauai, Hawaii, and implications for mantle melting processes. *Geochimica et Cosmochimica Acta* **62**, 2347-2368.

Rhodes, J. M. & Hart, S. R. (1995). Episodic trace element and isotopic variations in historical Mauna Loa lavas: implications for magma and plume dynamics. In: Rhodes, J.

M & Lockwood, J. P. (eds.) *Mauna Loa revealed*. *Geophysical Monograph, American Geophysical Union* **92**, 263-288.

Richards, M. A., Duncan, R. A. & Courtillot, V. E. (1989). Flood basalts and hotspot tracks: Plume heads and tails. *Science* **246**, 103-107.

Richards, M. A., Jones, D. L., Duncan, R. A. & DePaolo, D. J. (1991). A mantle plume initiation model for the formation of Wrangelia and other oceanic flood basalt plateaus. *Science* **254**, 263-266.

Roden, M. F., Frey, F. A. & Clague, D. A. (1984). Geochemistry of tholeiitic and alkalic lavas from the Koolau range, Oahu, Hawaii: Implications for Hawaiian volcanism. *Earth and Planetary Science Letters* **69**, 141-158.

Roden, M. F., Trull, T. W., Hart, S. R. & Frey, F. A. (1994). New He, Nd, Pb, and Sr isotopic constraints on the constitution of the Hawaiian plume; results from Koolau volcano, Oahu, Hawaii, USA. *Geochimica et Cosmochimica Acta* **58**, 1431-1440.

Salters, V. J. M. & Stracke, A. (2004). Composition of the depleted mantle. *Geochemistry Geophysics Geosystems* **5**, Q05B07.

Salters, V. J. M., Longhi, J. E. & Bizimis, M. (2002). Near mantle solidus trace element partitioning at pressures up to 3.4 GPa. *Geochemistry Geophysics Geosystems* **3** (7), 1038.

Saunders, A. D., Fitton, J. G., Kerr, A. C., Norry, M. J. & Kent, R. W. (1997). The North Atlantic igneous province. In: Mahoney, J. J. & Coffin, M. F. (eds.) *Large igneous provinces: continental, oceanic, and planetary flood volcanism. Geophysical Monograph, American Geophysical Union* **100**, 45-93.

Schilling, J.-G., Bergeron, M. B., Evans, R. & Smith, J. V. (1980). Halogens in the Mantle Beneath the North Atlantic. *Philosophical Transactions of the Royal Society of London* **A 297** (1431), 147-178.

Self, S., Widdowson, M., Thordarson, T. & Jay, A. E. (2006). Volatile fluxes during flood basalt eruptions and potential effects on global environment: A Deccan perspective. *Earth and Planetary Science Letters* **248**, 518-532.

Sen, G. (1995). A simple petrologic model for the generation of Deccan Traps magmas. *International Geological Review* **37**, 825-850.

Sen, G. (2001). Generation of Deccan Trap magmas. *Proceedings of the Indian Academy of Science (Earth and Planetary Science)* **110** (4), 409-431.

Sen, G., Bizimis, M., Das, R., Paul, D. K. & Ray, A. (submitted). Deccan Plume, lithosphere rifting, and volcanism in Kutch, India. *Earth and Planetary Science Letters*.

Sen, N. (1991). The Narmada-Son-Brahmaputra transform: a Mesozoic fracture zone in Gondwanic India. *Tectonophysics* **186**, 359-364.

Sethna, S. F. & Battiwala, H. K. (1977). Chemical classification of the intermediate and acid rocks (Deccan Trap) of Salsette Island, Bombay. *Journal of the Geological Society of India* **18**, 323–330.

Sethna, S. F. & Battiwala, H. K. (1980). Major element geochemistry of the intermediate and acidic rocks associated with the Deccan Traps basalts. *Proceedings of the 3rd Indian Geological Congress, Poona*, 281-295.

Sethna, S. F. & D'Sa, C. P. R. (1991). Occurrence of ijolite with veinlets of carbonatite in the Deccan Trap at Murud-Janjira, Maharashtra, India. *Journal of the Geological Society of India* **37**, 257-263.

Sethna, S. F., Khateeb, A. & Javeri, P. (1996). Petrology of the basic intrusives in the Deccan Province south of Tapti valley and their comparison with those along the west coast. *Gondwana Geological Magazine Special Publications* **2**, 225-232.

Seyfried, W. E. & Bischoff, J. L. (1979). Low temperature basalt alteration by seawater:

an experimental study at 70°C and 150°C. *Geochimica et Cosmochimica Acta* **43**, 1937-1947.

Shafer, J. T., Neal, C. R. & Regelous, M. (2005). Petrogenesis of Hawaiian postshield lavas: Evidence from Nintoku seamount, Emperor seamount chain. *Geochemistry Geophysics Geosystems* **6**, Q05L09.

Sharma, M. (1997). Siberian Traps. In: Mahoney, J. J. & Coffin, M. F. (eds.) *Large Igneous Provinces: Continental, Oceanic, and Planetary Flood Volcanism. Geophysical Monograph, American Geophysical Union* **100**, 273-295.

Sharp, W. D. & Clague, D. A. (2002). An older, slower Hawaii-Emperor bend. *Eos, Transactions, American Geophysical Union* **83** (47), Fall Meeting Supplement, Abstract T61C-04.

Shaw, D. M. (1970). Trace element fractionation during anatexis. *Geochimica et Cosmochimica Acta* **34**, 237-243.

Sheth, H. C. (1998). A reappraisal of the coastal Panvel flexure, Deccan Traps, as a listric-fault-controlled reverse drag structure. *Tectonophysics* **294** (1-2), 143-149.

Sheth, H. C. (1999). A historical approach to continental flood basalt volcanism: insights into pre-volcanic rifting, sedimentation, and early alkaline magmatism. *Earth and*

Planetary Science Letters **168**, 19-26.

Sheth, H. C. (2005). Were the Deccan flood basalts derived in part from ancient oceanic crust within the Indian continental lithosphere? *Gondwana Research* **8** (2), 109-127.

Sheth, H. C. (2007). Plume-related regional prevolcanic uplift in the Deccan Traps: Absence of evidence, evidence of absence. In: Foulger, G. R. & Jurdy, D. M. (eds.) *Plates, plumes and planetary processes. Geological Society of America Special Paper* **430**, 785-814.

Sheth, H. C. & Ray, J. S. (2002). Rb/Sr - $^{87}Sr/^{86}Sr$ variations in Bombay trachytes and rhyolites (Deccan Traps): Rb-Sr isochron, or AFC process? *International Geology Review* **44** (7), 624-638.

Sheth, H. C., Pande, K. & Bhutani, R. (2001). ^{40}Ar-^{39}Ar Ages of Bombay trachytes: Evidence for a Palaeocene phase of Deccan volcanism. *Geophysical Research Letters* **28** (18), 3513-3516.

Sheth, H. C., Ray, J. S., Ray, R., Vanderkluysen, L., Mahoney, J. J., Saini, A. K., Shukla, A. D., Jana, B., Das, P. & Adhikari, S. (submitted). Geology and geochemistry of Deccan Trap intrusions in the Satpura Gondwana Basin around Pachmarhi, central India: Correlations with Deccan lavas, and eruptive models. *Contributions to Mineralogy and Petrology*.

Simonetti, A., Bell, K. & Viladkar, S. G. (1995). Isotopic data from the Amba Dongar carbonitite complex, west-central India: evidence for an enriched mantle source. *Chemical Geology (Isotope Geoscience Section)* **122**, 185-198.

Simonetti, A., Goldstein, S. L., Schmidberger, S. S. & Viladkar, S. G. (1998). Geochemical and Nd, Pb, and Sr isotope data from Deccan alkaline complexes—Inferences for mantle sources and plume–lithosphere Interaction. *Journal of Petrology* **39** (11-12), 1847-1864.

Sinha-Roy, S. & Radhakrishna, T. (1983). Geochemistry and petrogenesis of basic dykes of Agali area, Palghat district, Kerala. *Journal of the Geological Society of India* **24**, 628-638.

Sinton, J., Grönvold, K. & Sæmundsson, K. (2005). Eruptive history of the Western Volcanic Zone, Iceland. *Geochemistry Geophysics Geosystems* **6**, Q12009.

Small, C. (1995). Observations of ridge-hotspot interactions in the Southern Ocean. *Journal of Geophysical Research* **100**, 17931-17946.

Smith, A. D. (1993). The continental mantle as a source for hotspot volcanism. *Terra Nova* **5**, 452-460.

Smith, A. D. & Lewis, C. (1999). The planet beyond the plume hypothesis. *Earth-Science Reviews* **48**, 135-182.

Sobolev, A., Hofmann, A. W. & Nikogosian, I. K. (2000). Recycled oceanic crust observed in 'ghost plagioclase' within the source of Mauna Loa lavas. *Nature* **404**, 986-990.

Sreenivasa Rao, M., Ramasubbareddy, N., Subbarao, K. V., Prasad, C. V. R. K. & Radhakrishnamurthy, C. (1985). Chemical and magnetic stratigraphy of parts of Narmada region, Deccan basalt province. *Journal of the Geological Society of India* **26** (9), 617-639.

Staudigel, H. & Hart, S.R. (1983). Alteration of basaltic glasses: Mechanisms and significance for the oceanic crust-seawater budget. *Geochimica et Cosmochimica Acta* **47**, 337-350.

Stearns, H. (1966). *Geology of the State of Hawaii*. Pacific Books, Palo Alto, CA, pp. 266.

Stewart, R. J., Natland, J. H. & Glassey, W. E. (1973). Petrology of volcanic rocks recovered on DSDP leg 19 from the north Pacific Ocean and the Bering Sea. *Initial Report of the Deep Sea Drilling Project* **19**, 615-627.

Stille, P., Unruh, D. M. & Tatsumoto, M. (1983). Pb, Sr, Nd, and Hf isotopic evidence of multiple sources for Oahu, Hawaii basalts. *Nature* **304**, 25-29.

Stoffers, P., Worthington, T. & 17 others (2003). Cruise Report Sonne 167: Louisville. *Christian-Albrechts-Universität zu Kiel. Institut für Geowissenschaften, Berichte-Reports* **20**, pp. 276.

Storey, M., Mahoney, J. J., Saunders, A. D., Duncan, R. A., Kelley, S. P. & Coffin, M. F. (1995). Timing of hot-spot related volcanism and the breakup of Madagascar and India. *Science* **267**, 852-855.

Stracke, A., Hofmann, A. W. & Hart, S. R. (2005). FOZO, HIMU, and the rest of the mantle zoo. *Geochemistry Geophysics Geosystems* **6**, Q05007.

Streckeisen, A. L. (1978). IUGS Subcommission on the Systematics of Igneous Rocks. Classification and Nomenclature of Volcanic Rocks, Lamprophyres, Carbonatites and Melilite Rocks. Recommendations and Suggestions. *Neues Jahrbuch für Mineralogie, Abhandlungen* **141**, 1-14.

Subbarao, K. V., Chandrasekharam, D., Navaneethakrishnan, P. & Hooper, P. R. (1994). Stratigraphy and structure of parts of the central Deccan basalt province: eruptive models. In: Subbarao, K. V. (ed.) *Volcanism*. Wiley Eastern, New Delhi, 321-332.

Subrahmanya, K. R. (1998). Tectono-magmatic evolution of the west coast of India. *Gondwana Research* **1** (3-4), 319-328.

Sukheswala, R. N. & Avasia, R. K. (1972). Carbonitite-alkalic complex of Panwad-Kawant, Gujarat, and its bearing on the structural characteristics of the area. *Bulletin of Volcanology* **35**, 563-578.

Sun, S.-S. & McDonough, W. F. (1989). Chemical and isotopic systematics of oceanic basalts: implications for mantle composition and processes. In: Saunders, A. D. & Norry, M. J. (eds.) *Magmatism in the Ocean Basins. Geological Society of London Special Publications* **42**, 313-345.

Sutton, A. J., Elias, T. & Kauahikaua, J. (2003). Lava-effusion rates for the Pu‘u ‘Ō‘ō-Kūpaianaha eruption derived from SO_2 emissions and very low frequency (VLF) measurements. In: Heliker, C. et al. (eds.) *The Pu‘u ‘Ō‘ō-Kūpaianaha eruption of Kilauea Volcano, Hawai‘i: The first 20 years. United States Geological Survey Professional Paper* **1676**, 137-148.

Tarduno, J. A., Sliter, W. V., Kroenke, L., Leckie, M., Mayer, H., Mahoney, J. J., Musgrave, R., Storey, M. & Winterer, E. L. (1991). Rapid formation of Ontong Java Plateau by Aptian mantle plume volcanism. *Science* **254**, 399-403.

Tatsumoto, M. (1988). U, Th and Pb abundances in Hawaiian xenoliths. Conf. Origin of the Earth. Lunar Planet. Inst., 89-90.

Taylor, B. (2006). The single largest oceanic plateau: Ontong Java–Manihiki–Hikurangi. *Earth and Planetary Science Letters* **241**, 372-380.

Tejada, M. L. G., Mahoney, J. J., Duncan, R. A. & Hawkins, M. P. (1996). Age and geochemistry of basement and alkalic rocks of Malaita and Santa Isabel, Solomon Islands, southern margin of Ontong Java Plateau. *Journal of Petrology* **37**, 361-394.

Tejada, M. L. G., Mahoney, J. J., Neal, C. R., Duncan, R. A. & Petterson, M. G. (2002). Basement geochemistry and geochronology of central Malaita, Solomon Islands, with implications for the origin and evolution of the Ontong Java Plateau. *Journal of Petrology* **43**, 449-484.

Tejada, M. L. G., Mahoney, J. J., Castillo, P. R., Ingle, S. P., Sheth, H. C. & Weis, D. (2004). Pin-pricking the elephant: Evidence on the origin of the Ontong Java Plateau from Pb-Sr-Hf-Nd isotopic characteristics of ODP Leg 192 basalts. In: Fitton, J. G. et al. (eds.) *Origin and evolution of the Ontong Java Plateau*. *Geological Society of London Special Publications* **229**, 133-150.

Todt, W., Cliff, R. A., Hanser, A. & Hofmann, A. W. (1996). Evaluation of a ^{202}Pb + ^{205}Pb double spike for high-precision lead isotopic analyses. In: Basu, A. & Hart, S. (eds.)

Earth Processes: Reading the Isotopic Code. Geophysical Monograph, American Geophysical Union **95**, 429-437.

Turcotte, D. L. & Schubert, G. (1982). *Geodynamics: Applications of Continuum Physics to Geological Problems*. John Wiley & Sons, New York, pp. 450.

Vandamme, D., Courtillot, V., Besse, J. & Montigny, R. (1991). Paleomagnetism and the age determinations of the Deccan Traps (India): results of a Nagpur-Bombay traverse and review of earlier work. *Reviews of Geophysics* **29** (2), 159-190.

Venkatesan, T.R., Pande, K. & Gopalan, K. (1993). Did Deccan volcanism pre-date the Cretaceous/Tertiary transition? *Earth and Planetary Science Letters* **119**, 181-189.

Venkatesan, T.R., Pande, K. & Ghevariya, Z. G. (1996). ^{40}Ar-^{39}Ar ages of lava flows from Anjar, western Deccan Province, India and its relation to the Cretaceous-Tertiary boundary events. *Current Science* **70**, 990-996.

Vlastélic, I. & Dosso, L. (2005). Initiation of a plume-ridge interaction in the South Pacific recorded by high-precision Pb isotopes along Hollister Ridge. *Geochemistry Geophysics Geosystems* **6**, Q05011.

Vogt, P., Lowrie, A., Bracey, D. R. & Hey, R. N. (1976). Subduction of aseismic ridges: Effects on shape, seismicity, and other characteristics of consuming plate boundaries. *Geological Society of America Special Paper* **172**, pp. 59.

Wadia, D. N. (1975). *Geology of India*. Tata McGraw-Hill, New Delhi, pp. 508.

Waggoner, D. G. (1993). The age and alteration of central Pacific oceanic crust near Hawaii, site 843. In: Wilkens, R. H., Firth, J., Bender, J et al. (eds.) *Proceedings of the Ocean Drilling Program, Initial Reports* **136**. College Station, Texas (Ocean Drilling Program), 119-132.

Walker, G. P L. (1971). Compound and simple lava flows and flood basalts. *Bulletin of Volcanology* **35** (3), 579-590.

Walsh, J. N. (1992). Use of multiple internal standards for high-precision, routine analysis of geological samples by inductively coupled plasma-atomic emission spectrometry. *Chemical Geology* **95** (1-2), 113-121.

Watts, A. B., Weissel, J. K., Duncan, R. A. & Larson, R. L. (1988). Origin of the Louisville ridge and its relationship to the Eltanin fracture zone system. *Journal of Geophysical Research* **93**, 3051-3077.

Watts, A. B. & Cox, K. G. (1989). The Deccan Traps: an interpretation in terms of progressive lithospheric flexure in response to a migrating load. *Earth and Planetary Science Letters* **93**, 85-97.

Weaver, B.L. (1991). The origin of ocean island end-member compositions: trace element and isotopic constraints. *Earth and Planetary Science Letters* **104**, 381-397.

Wessel, P. & Kroenke, L. W. (2008). Pacific absolute plate motion since 145 Ma: An assessment of the fixed hot spot hypothesis. *Journal of Geophysical Research* **113**, B06101.

West, H. B. & Leeman, W. P. (1987). Isotopic evolution of lavas from Haleakala crater, Hawaii. *Earth and Planetary Science Letters* **84**, 211-225.

West, H. B., Gerlach, D. C., Leeman, W. P. & Garcia, M. O. (1987). Isotopic constraints on the origin of Hawaiian lavas from the Maui volcanic complex, Hawaii. *Nature* **330**, 216-220.

West, W. D. (1959). The source of the Deccan Trap flows. *Journal of the Geological Society of India* **1**, 44-52.

White, R. & McKenzie, D. (1989). Magmatism at rift zones: The generation of volcanic continental margins and flood basalts. *Journal of Geophysical Research* **94** (B6), 7685-7729.

White, W. M. & Duncan, R. A. (1996). Geochemistry and geochronology of the Society islands: new evidence for deep mantle recycling. In: Basu, A. & Hart, S. R. (eds.) *Earth Processes: Reading the Isotopic Code*. *Geophysical Monograph, American Geophysical Union* **95**, 183-206.

Widdowson, M. & Mitchell, C. (1992). A geological map of the southern Deccan Traps, India: Reply to Kale, V. S. et al. *Journal of the Geological Society of London* **149**, 475-478.

Widdowson, M., Pringle, M. S. & Fernandez, O. A. (2000). A post K–T boundary (Early Palaeocene) age for Deccan-type feeder dykes, Goa, India. *Journal of Petrology* **41** (7), 1177-1194.

Wilson, J. T. (1963). A possible origin of the Hawaiian Islands. *Canadian Journal of Physics* **41**, 863-870.

Woodhead, J. D. & McCulloch, M. T. (1989). Ancient seafloor signals in Pitcairn Island lavas and evidence for large amplitude, small length-scale mantle heterogeneities. *Earth and Planetary Science Letters* **94**, 257-273.

Workman R. K. & Hart S. R. (2005). Major and trace element composition of the depleted MORB mantle (DMM). *Earth and Planetary Science Letters* **231**, 53-72.

Worthington, T. J., Hekinian, R., Stoffers, P., Kuhn, Th. & Hauff, F. (2006). Osbourn Trough: Structure, geochemistry and implications of a mid-Cretaceous paleospreading ridge in the South Pacific. *Earth and Planetary Science Letters* **245**, 685-701.

Yoshida, M. (2008). Core-mantle boundary topography estimated from numerical simulations of instantaneous mantle flow. *Geochemistry Geophysics Geosystems* **9** (7), Q07002.

Zack, T., Foley, S. F. & Jenner, G. A. (1997). A consistent partition coefficient set for clinopyroxene, amphibole and garnet from laser ablation microprobe analysis of garnet pyroxenites from Kakanui, New Zealand. *Neues Jahrbuch für Mineralogie, Abhirchen* **172** (1), 23-41.

Zindler, A. & Hart, S. (1986). Chemical Geodynamics. *Annual Review of Earth and Planetary Sciences* **14**, 493-571.